MODULATION OF HIGH ENERGY COSMIC RAYS IN THE HELIOSPHERE

by

Damian Lindsay Hall, B.Sc., (Hons.)

A thesis submitted in fulfilment of the requirements for the degree of Doctor of Philosophy in the University of Tasmania

March, 1995

DECLARATIONS

I certify that this thesis does not incorporate without acknowledgment any material previously submitted for a degree or diploma in any university; and to the best of my knowledge and belief it does not contain any material previously published or written by another person where due reference is not made in the text.

Damian Lindsay Hall

This thesis may be made available for loan and limited copying in accordance with the *Copyright Act 1968*.

Damian Lindsay Hall

ABSTRACT

The distribution of galactic cosmic ray particles in the heliosphere is influenced (modulated) by the Sun's interplanetary magnetic field (IMF) and the solar wind. The particles diffuse inward, convect outward and have drifts in the motion of their gyro-centres. They are also scattered from their gyro-orbits by irregularities in the IMF. These processes are the components of solar modulation and produce streaming (anisotropies) of particles in the heliosphere. The anisotropies can be investigated at Earth by examining the count rates of cosmic ray detectors. The anisotropic streams appear as diurnal and semi-diurnal variations in the count rates of cosmic ray recorders in solar and sidereal time. Theoretical models of solar modulation predict effects which are dependent on the polarity of the Sun's magnetic dipole ($A>0$ or $A<0$). The solar diurnal and North-South anisotropy can be used to test these predictions.

The yearly averaged solar and sidereal diurnal variations in data recorded by seven neutron monitors and ten muon telescopes for the period 1957 to 1990 have been deduced by Fourier analysis methods. The rigidities of the galactic cosmic rays to which these instruments respond encompass the range 10 to 1400 Giga volts (GV). The rigidity spectrum of the solar diurnal anisotropy has been inferred to have a mean spectral index extremely close to zero and an idealised upper limiting rigidity of 100 ± 25 GV. This is in good agreement with previous determinations. It is shown that this upper limit has a temporal variation between 50 GV and 180 GV and is correlated with the magnitude of the IMF. The rigidity spectrum is likely to be dependent on the polarity of the Sun's magnetic dipole, the spectral index being determined as positive in the $A>0$ magnetic polarity state and negative in the $A<0$ polarity state. It is also shown that the amplitude of the anisotropy varies with an 11-year variation and the time of maximum varies with 22-year variation. Both of these variations are shown to be independent of any change in the rigidity spectrum.

The solar diurnal anisotropy is also used as a tool to calculate the modulation parameters $\overline{\lambda_{\parallel} G_r}$ (the product of the parallel mean-free path and radial density gradient) and $G_{|z|}$ (an indicator of the symmetric latitudinal density gradient). $\overline{\lambda_{\parallel} G_r}$ is found to have a 22-year variation at all rigidities studied and furthermore to only have rigidity dependence when the heliosphere is in the $A>0$ magnetic polarity state. It is unlikely that $\overline{\lambda_{\parallel} G_r}$ has any rigidity dependence in the $A<0$ polarity state. $G_{|z|}$ indicates that below 50 GV the symmetric latitudinal density gradient behaves in accordance with the predictions of current modulation theories. Between 50 and 195 GV however, the predicted behaviour is only observed when the rigidity spectrum of the solar diurnal anisotropy is assumed to be flat, static and have an upper limiting rigidity of 100 GV.

The sidereal diurnal variation in the data recorded by the instruments has been deduced and used to study the North-South anisotropy. The results indicate that this anisotropy has only a small variation in amplitude. There is strong evidence for heliospheric asymmetric modulation (with respect to above and below the neutral sheet) of a galactic anisotropy in the sense proposed by Nagashima et al. (1982) and that this modulation may have a 22-year variation. From the examination of the North-South anisotropy the radial density gradients (G_r) at 1 AU of 17 to 195 GV particles were determined. The gradient is slightly smaller

around times of solar minimum. No magnetic polarity dependence of the radial gradient was observed, in direct conflict with conventional theoretical predictions.

The modulation parameters have been used to determine the parallel mean-free path ($\lambda_{||}$) of galactic cosmic rays with rigidities between 17 and 195 GV near the Earth. It was found that this parameter depends on magnetic polarity at all the rigidities examined and has a linear relationship with rigidity. Perpendicular diffusion has been examined and shown to have very little contribution to the values of the modulation parameters except for years near solar minimum.

ACKNOWLEDGMENTS

In any project of this magnitude there are always many people without whose help the project would have been impossible. It is my hope that I can thoughtfully thank all those who have helped me during the last four years.

In May of 1991 I was fortunate to be sitting in on a postgraduate lecture about cosmic ray physics given by Dr. Marc Duldig from the Australian Antarctic Division and Dr. John Humble from the Physics Department in the University of Tasmania. After the lecture I approached Dr. Humble with the idea of doing my Ph.D. under his supervision. I am indebted to Dr. Humble and Dr. Duldig for giving me the opportunity to work under their joint supervision and for their continual encouragement while undertaking this degree.

For the first half of my tenure I had the pleasure of sharing an office with Dr. Chris Baker. His assistance in introducing me to the Physics Department, Hobart and cosmic ray physics has been invaluable. I thank him for many helpful discussions about modulation theory and his continual barrage of jokes brought back from those mysterious FTP sites.

I would like to express my thanks to the postgraduate students and other personnel in the Physics Department who have helped me during my time there. Special thanks go to Jenny Cramp, Dr. Edward King and Jim Lovell who have always tried to answer any of my queries and I would especially like to thank Judy Whelan for her almost flawless ability to perform any task for me.

I wish to thank the Australian Antarctic Division for allowing me the opportunity to visit Mawson Station for 14 weeks during the southern Summer of 1992–93 to service and modify the cosmic ray telescopes there. I also thank the Australian Antarctic Division, the National Science Foundation of the United Sates and the University of Tasmania for giving me the chance to participate in the joint neutron monitor survey of the Southern Ocean for three weeks during the southern Summer of 1994–95. It was during this time that I was able discuss parts of Chapter 5 with Professor Paul Evenson from the Bartol Institute. I am grateful for his advice towards this thesis, especially his suggestions about treating skew errors and his patient attempts to explain magnetic helicity to me. I thank the Australian Institute of Physics (Tasmanian Branch), the Physics Department of the University of Tasmania, the Astronomical Society of Australia and the Donovan Trust for their financial support in attending interstate and international conferences.

I must also thank Professor Derek Swinson for allowing me to use his data from the Embudo and Socorro underground muon telescopes and for sending me the analysed data promptly. Similarly, I wish to extend my gratitude to Dr. Sue Gussenhoven for providing me with polar rain data which allowed me to extend some of the analyses up to the end of 1990. To Dr. Glen McPherson of the Mathematics Department, I thank him for his help in the error treatment in Chapter 3.

I have been in receipt of an Australian Postgraduate Research Award for most of my candidature, for which I am very grateful. I also extend my gratitude to the Australian

Antarctic Division for allowing me to use their word-processing facilities when writing this thesis.

On a personal note I would like to thank my good friends Marc Duldig, Tim Rossiter and Judy Whelan for their moral support over the years. Their assistance has been truly invaluable and will never be forgotten.

Finally, but most importantly I thank my parents Gay and Brian Hall for their devotion to me over the years. They have supported every goal I have ever had and made many sacrifices in order to help me achieve them. They have been an inspiration to me. Without their support this work would have never been possible. Thankyou Mum and Dad.

PREFACE

I dedicate this thesis with love and appreciation to my parents Leslie G. Hall and Brian L. Hall.

TABLE OF CONTENTS

CHAPTER 1

INTRODUCTION

Galactic cosmic ray particles are high energy nuclei and exist in roughly the same relative galactic abundances as their corresponding atomic elements. Thus most of the galactic cosmic rays are protons. The energies of galactic cosmic rays range from about 10^8 eV to 10^{21} eV but the accelerating mechanisms of the highest energy galactic cosmic rays are not understood.

The heliosphere is the region of space where the interplanetary magnetic field (IMF) of the Sun dominates the galactic magnetic field. Outside the heliosphere, in the local inter-stellar region the distribution of galactic particles is considered almost isotropic in space and time. Due to random motion and collisions these particles cross the boundary and enter the heliosphere. They will gyrate around the IMF but due to small scale irregularities in the IMF the particles are scattered from their gyro-orbits. The overall motion of the particles will be seen as diffusion from the boundary towards the Sun. Along their diffusive journey the particles will also undergo gradient and curvature drifts in the IMF according to first order orbit theory (Isenberg and Jokipii 1979). The Sun also emits a solar wind plasma radially from its surface with the IMF *frozen* into it and convects particles back toward the heliospheric boundary. The overall result of these processes is the solar modulation within the heliosphere of the galactic distribution of cosmic ray particles (Forman and Gleeson 1975).

Solar modulation causes gradients in the number density of particles. Proof of the existence and knowledge of the magnitudes of these density gradients of particles are key elements in discussing the validity of solar modulation models. Up to rigidities (relativistic momentum per unit charge) of 10 GV, modulation models predict 11 and 22 year cycles in the radial density gradient (G_r), and 22 year cycles in a latitudinal density gradient (G_θ), related to solar activity and solar magnetic cycles (for example – Jokipii and Kopriva 1979, Jokipii 1984, Potgeiter and Moraal 1985, Jokipii 1989). These solar cycles are presented in Figure 1.1.

Particle-streaming results from solar modulation in the heliosphere. This produces an anisotropy (ξ) of the galactic distribution. The streaming in the inner heliosphere can be decomposed into components in and perpendicular to the ecliptic plane. (For the sake of argument the ecliptic plane is taken to be approximately the solar equatorial plane). A galactic cosmic ray particle in the background or anisotropic flux in the heliosphere is called a primary cosmic ray. Secondary cosmic ray particles are produced by nuclear interactions at the top of the Earth's atmosphere between incoming primary particles and atmospheric nuclei. Secondaries can be divided into three components. These are the electromagnetic (soft) component, meson (hard) component and the nucleonic component. All the secondary particles are the result of a nuclear disintegration; the most common nucleon being the neutron and the most common meson being the pion. The neutral pion decays into two photons producing an electron-photon cascade, while the positive and negative pions decay into muons of the same charge. The muons (being relativistic) are able to survive a time-

dilated journey to sea level if their energy is greater than about 2 GeV, and thus be recorded. At the Earth, primaries streaming in the ecliptic plane are recorded by a cosmic ray telescope or monitor as a diurnal variation in its counting rate in solar time (Solar Diurnal Variation) superposed onto a large isotropic component. The streaming of primary cosmic rays responsible for the solar diurnal variation is known as the Solar Diurnal Anisotropy (ξ_{SD}). The streaming perpendicular to the ecliptic plane is observed as a sidereal diurnal variation in the count rate of a recording instrument. This streaming is known as the North-South Anisotropy (ξ_{NS}). Since the anisotropies are produced from solar modulation it is possible to derive solar parameters such as mean-free paths of particles and gradients in the number densities from observations of the anisotropies. For example, see the analyses by Yasue (1980) and Bieber and Chen (1991a).

The majority of observations employed for these types of analyses have been obtained from northern hemisphere detectors, usually neutron monitors. Southern hemisphere observations and similar analyses at the same and higher primary energies may help to provide new insight into cosmic ray modulation. By determining the Solar Diurnal and North-South Anisotropies and deriving modulation parameters, predictions of modulation models can be tested. Thus, knowledge of the magnetic and solar processes in the heliosphere can be gained.

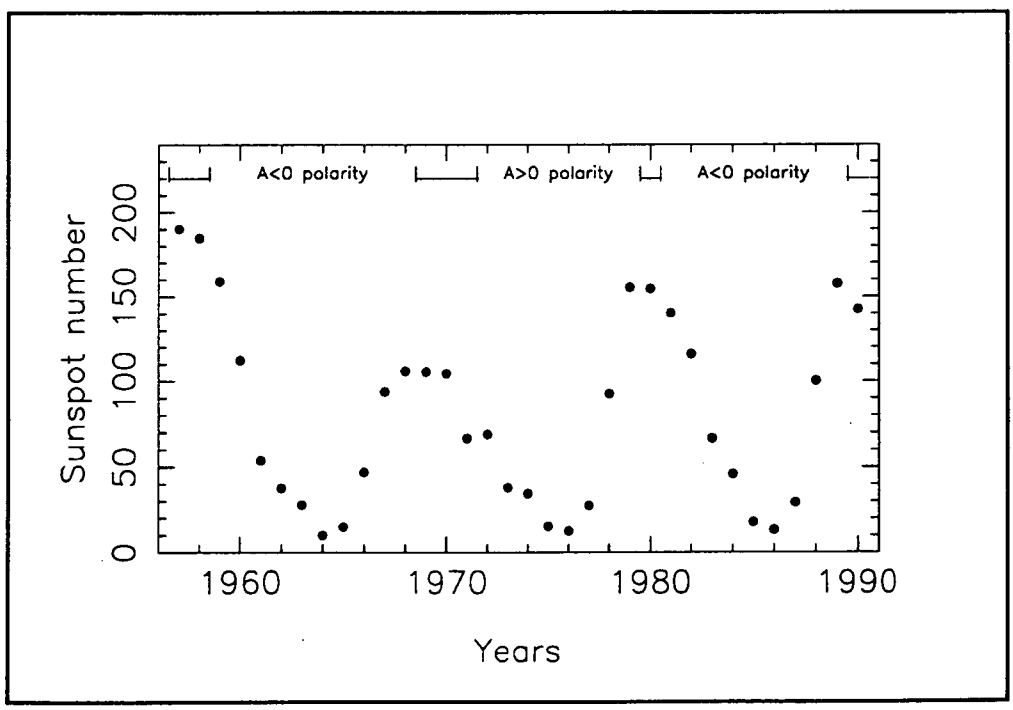

Figure 1.1 Solar activity cycle as represented by the yearly averaged sunspot numbers (Coffey 1993). There is an 11-year cycle for times of minimum sunspot numbers. Solar polarity cycle is determined from the polarity of the Sun's magnetic dipole. $A<0$ indicates the Sun's northern hemisphere has southern magnetic polarity. $A>0$ indicates the Sun's northern hemisphere has northern magnetic polarity. The dipole is observed to reverse direction (indicated by the ⊢⊣) about every 11 years which implies a 22-year cycle for complete restoration of the dipole direction.

1.1 Preview of the thesis

The following chapters present results of analysing cosmic ray data from neutron monitors and muon telescopes to determine the sidereal and solar diurnal anisotropies of high-energy particles. The rest of this chapter reviews the literature to provide the necessary background information about such anisotropies. Included in this is a review of the basic theoretical models describing modulation and their relation to modulation parameters.

In Chapter 2 the techniques employed in the analyses are presented. Also given is a brief description of the instruments used to collect the data and their locations.

Chapter 3 is concerned with the determination of the solar diurnal variation and the corresponding anisotropy (ξ_{SD}) of cosmic rays with rigidities in excess of 2 GV. The rigidity spectrum and solar modulation parameters related to the anisotropy are derived. The spectrum is inferred by the use of two novel techniques. Modulation parameters derived from ξ_{SD} are presented and compared to theoretical predictions and previous determinations.

In Chapter 4 similar techniques to those in Chapter 3 are used to examine the sidereal diurnal variation and the North-South anisotropy at high rigidities. An attempt to derive the rigidity spectrum of the anisotropy is made. From this anisotropy, one of the key modulation parameters - the radial number density gradient (G_r) is determined for various rigidities of primary cosmic rays. A comparison is made of the values of these gradients with previous observations and current theoretical predictions. The limitations of this analysis are discussed with special attention paid to the contamination of the results by another anisotropy predicted (Nagashima et al. 1982) but never observed before.

The final chapter concerning data analyses combines the results of Chapters 3 and 4 to derive the mean-free path of cosmic rays of various rigidities up to 200 GV. Some of the mean-free paths are compared to previous determinations while others have never been obtained before. At the end of this chapter the implications of the values of these mean-free paths to solar modulation are discussed, particularly the relative magnitudes of mean-free paths parallel and perpendicular to the IMF.

Finally, the results of Chapters 3 to 5 are summarised and future research problems are discussed. Publications and conference presentations which were produced while undertaking this study are listed in Appendix 9.

1.2 Review of the literature

This review is separated into four sections. Although this thesis is primarily concerned with experiments and analyses of data, the theoretical expressions used to model solar modulation and anisotropic flows of particles are reviewed first. Thus the reader can become familiar with all the relevant nomenclature of cosmic ray modulation and the processes involved. The second section will present the history and status of knowledge about the characteristics of the solar diurnal anisotropy. The third section reviews the sidereal diurnal variation and

North-South anisotropy. Finally, the fourth section presents the results of previous determinations of parameters related to solar modulation.

1.2.1 Theoretical models of solar modulation and their predictions

Modulation theories essentially attempt to model the effect of the Sun's interplanetary magnetic field on the distribution of the galactic cosmic rays in the heliosphere. Cosmic rays are influenced by the Sun by three main processes - convection, diffusion and gradient and curvature drifts in the IMF. The IMF is frozen into the solar wind (this is required to keep the Lorentz force on the plasma ions zero) and dragged radially away from the Sun at roughly 400 km sec^{-1} through the heliosphere. As cosmic rays enter the heliosphere they gyrate around the field lines of force and travel towards the Sun. The IMF is not a completely regular field and contains dynamic irregularities. The gyro-orbits of particles are affected by these irregularities and particles are scattered until a new orbit is found along a regular portion of an IMF line. The net effect of this is parallel and perpendicular scattering of the particles and the motion of the bulk distribution of the cosmic rays can be described by diffusion parallel and perpendicular to the IMF. The same scattering mechanism is partly responsible for the convection of particles outwards from the Sun by the solar wind. Convection is also produced in the cosmic rays' reference frame by an electric field drift (**ExB**) in the velocity of particles due to the electric field set up in the solar wind plasma and the IMF carried out by the plasma.

The IMF has an Archimedean spiral configuration in the heliosphere caused by the solar wind dragging the Sun's magnetic field radially outward and the solar rotation axis not being aligned with the magnetic axis (for a summary of this process see the review on the IMF by Wilcox 1968 and references therein). The curvature of the field lines and the gradient in field intensity leads to drift velocities of the cosmic ray particles in the interplanetary medium. All these mechanisms combine to produce the solar modulation of galactic cosmic rays. The theoretical basis of modulation was formalised by Forman and Gleeson (1975) and has essentially remained unchanged. The theory presented here is a summary of that formalism plus a brief description of the treatment of the distribution function of cosmic rays from which the theory is derived (Isenberg and Jokipii 1979; Baker 1993).

If $F(\mathbf{x}, \mathbf{p}, t)$ is a distribution function of particles such that $p^2F(\mathbf{x}, \mathbf{p}, t)\, d^3x\, dp\, d\Omega$ is the number of particles in a volume d^3x with momentum $\mathbf{p}$ to $\mathbf{p} + d\mathbf{p}$ centred in the solid angle $d\Omega$ then it can be shown (Isenberg and Jokipii 1979) that

$$\frac{\partial U}{\partial t} + \nabla \cdot \mathbf{S} = 0 \qquad (1.1)$$

where

$$U(\mathbf{x}, p, t) = p^2 \int_{4\pi} F(\mathbf{x}, \mathbf{p}, t)\, d\Omega$$

and $\mathbf{S}$ is the streaming vector:

$$S(x,\ p,\ t) = CUV - \kappa\left(\frac{\partial U}{\partial r}\right)_{\|} - \frac{\kappa}{1+(\omega\tau)^2}\left(\frac{\partial U}{\partial r}\right)_{\perp} - \frac{\omega\tau\kappa}{1+(\omega\tau)^2}\left[\frac{\partial U}{\partial r} x \hat{\mathbf{B}}\right] \qquad (1.2)$$

and

ω = Gyro-frequency of the particle's orbit;
τ = mean time between scattering;
κ = (isotropic) diffusion coefficient;
C = Compton-Getting coefficient (Compton and Getting 1935, Forman 1970);
V = solar wind velocity and
U = number density of particles.

The first term of equation (1.2) describes the outward convection of the particles by the solar wind, the second term describes parallel diffusion, the third describes perpendicular diffusion and the fourth involves the gradient and curvature drifts. Writing equation (1.2) in terms of a diffusion tensor

$$S = CUV - \underline{\underline{\kappa}} \cdot (\nabla U), \quad \underline{\underline{\kappa}} = \begin{pmatrix} \kappa_{\perp} & \kappa_T & 0 \\ -\kappa_T & \kappa_{\perp} & 0 \\ 0 & 0 & \kappa_{\|} \end{pmatrix} \qquad (1.3)$$

where $\kappa_{\perp}$, $\kappa_{\|}$, are respectively the perpendicular and parallel diffusion coefficients and the off-diagonal elements are related to gradient and curvature drifts, then

$$\frac{\partial U}{\partial t} = -\nabla \cdot \left(CUV - \underline{\underline{\kappa}} \cdot \nabla U\right). \qquad (1.4)$$

Equation (1.4) is a standard time dependent diffusion equation. It is commonly called the transport equation because if we note that

$$\begin{aligned} \left(\frac{\partial U}{\partial t}\right)^D &= \nabla \cdot \left(\underline{\underline{\kappa}} \cdot \nabla U\right) \\ &= \nabla \cdot \left(\underline{\underline{\kappa}}^S \cdot \nabla U\right) + \left(\nabla \cdot \underline{\underline{\kappa}}^A\right)(\nabla U) \\ &= \nabla \cdot \left(\underline{\underline{\kappa}}^S \cdot \nabla U\right) + V_D \cdot \nabla U \end{aligned} \qquad (1.5)$$

where $\left(\frac{\partial U}{\partial t}\right)^D$ refers to only the non-convective terms in equation (1.4) and $\underline{\underline{\kappa}}^S$ and $\underline{\underline{\kappa}}^A$ refer to $\underline{\underline{\kappa}}$ being split into symmetric and anti symmetric tensors, we find that $\nabla \cdot \underline{\underline{\kappa}}^A$ is the drift velocity (V_D) of a charged particle in a magnetic field which has a gradient and curvature. Equation (1.4) is an equation explicitly representing the transport of cosmic rays in the heliosphere by convection, diffusion and drifts as mentioned earlier.

Predictions of modulation models

From 1977 to 1983 a series of papers by Jokipii and co-workers presented the results of numerically solving the transport equation (equation 1.4) for U(x,p,t) including drift processes in the calculations (Jokipii et al. 1977, Isenberg and Jokipii 1978, Jokipii and Kopriva 1979, Jokipii and Thomas 1981, Jokipii and Davila 1981, Kota and Jokipii 1983; hereafter called Papers *I*, *II*, *III*, *IV*, *V* and *VI*). These papers all highlighted the importance of including drifts in the calculations.

Papers *I* and *II* showed that because the IMF is characterised by two distinct polarity configurations over 22 years (termed A>0 and A<0, see Figure 1.1) the drifts would have opposite effects on modulation in these two states. Conventional diffusion mechanisms on the other hand, are not dependent on the IMF polarity. The implications of drifts to the transport of poistively charged particles in the heliosphere are that during A>0 IMF polarity states particles will travel into the inner heliosphere from the poles and exit via routes along the heliospheric equator. During A<0 IMF polarity states the particles will predominantly travel into the heliosphere along the equator and out via high helio-latitudes.

Paper *III* predicted that these drift effects (coupled to the diffusion of particles) would lead to a larger radial gradient of particles during A<0 epochs than in A>0 epochs. It was also suggested that because of the differences of cosmic ray trajectories during these two IMF configurations (as explained above), the density of particles would be a minimum at the solar equator during A>0 states. Alternatively, during A<0 IMF polarity epochs the drifts of the particles were predicted to produce a local maximum in the density at the equator and a minimum at some higher heliolatitude. This should be observable as a bi-directional (symmetric) latitudinal gradient which reverses direction after every IMF polarity reversal.

It was suggested that the inclination of the neutral sheet was an important factor to solar modulation (Kota 1979) and paper *IV* included this in the numerical calculations. Previously the neutral sheet had only been included as a flat sheet lying on the solar equatorial plane. Results of this model indicated that the neutral sheet was more important to modulation during A<0 epochs than for A>0 epochs. This was explained by the fact that during A<0 epochs particles will travel along the neutral sheet (rather than the solar equator when the neutral sheet is flat). Thus the particles will be affected by the neutral sheet during this IMF configuration more than in the A>0 state when their travelling routes in the heliosphere are from predominantly high latitudes. At high latitudes the neutral sheet is seldom present and is therefore only a small influence on particle transport during A>0 IMF configurations.

Paper *V* was an extension to paper *III*. By using a wavy neutral sheet in the calculations and more realistic diffusion coefficients it was shown that the latitude gradient (magnitude and sign) was sensitive to the values of these coefficients. Paper *VI* was even more realistic (being a full 3-dimensional model) and indicated that the minimum in density at the solar equator during A>0 states predicted by previous models could be displaced by a small distance. Density at the solar equator would never be a minimum, leading to short term observations indicating a negative latitude gradient near the solar equatorial plane for both IMF polarity states. It would seem that considering Figure 1a of Paper *VI* (reproduced here as Figure 1.2) a long term average density sample (taken over 10 or so solar rotations) close to the solar equator would yield a minimum in density for this polarity state and hence a

predicted positive latitude gradient. This gradient is consistent with that predicted by Jokipii (1989).

Potgeiter and Moraal (1985) have independently made the same predictions as Jokipii and others with a self-consistent model which uses just one set of diffusion coefficients. Their model predicts a radial gradient of cosmic rays which is smaller during periods of A>0 IMF polarity and a bi-directional latitudinal gradient which changes direction after IMF polarity reversals.

Jokipii and Kota (1989) suggested that the IMF at the heliospheric poles may be less radial than previously thought. They have incorporated an IMF into their model which has more transverse field lines at the poles than before. This model predicts an almost invariant radial gradient at times of solar minimum during different IMF polarity states. This newer model also predicts that the latitudinal gradient should reverse when the IMF polarity reverses (Jokipii 1989). These predictions are supported by the model of Moraal (1990) which includes a more transverse polar magnetic field.

Baker (1993) numerically modelled the modulation of 1-10 GV particles. The modelling of 10 GV particles is about an order of magnitude larger in rigidity than most researchers attempt. His results predicted an almost negligible dependence of the radial gradient at 1 A.U. on rigidity.

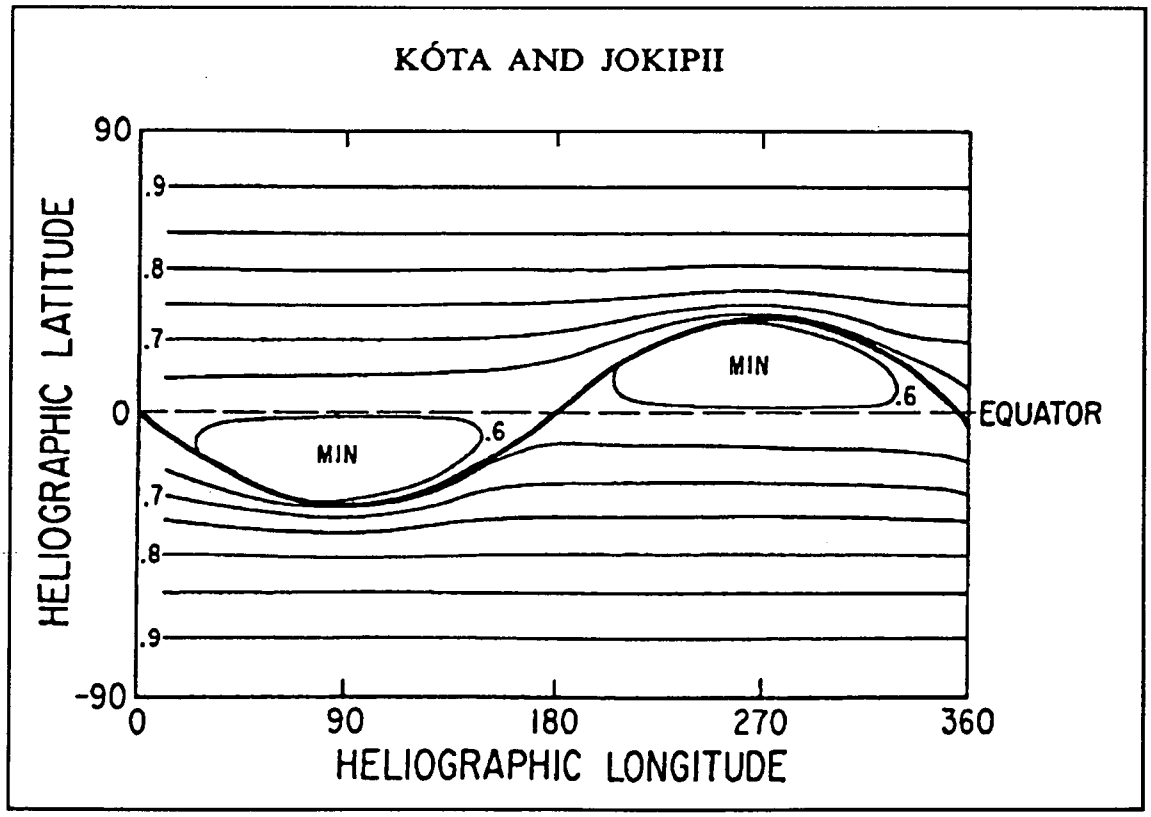

Figure 1.2 Predicted latitudinal distribution of galactic cosmic rays during the A>0 interplanetary magnetic field polarity configuration. Note the predicted local minima in density displaced from the solar equatorial plane. Taken from Kota and Jokipii (1983).

The theory can be extended to attempt to model the streaming (anisotropies of cosmic rays) caused by solar modulation processes. Some of these models and predictions are presented here as an introduction to the anisotropies which will be examined in the rest of this thesis.

By noting that $\xi = \frac{3S}{\upsilon U}$ (Gleeson 1969) and defining $\hat{x}$ and $\hat{z}$ in the ecliptic plane with $\hat{z}$ along the direction of the IMF away from the Sun, it can be shown (Bieber and Chen 1991a) that by transforming the gradient vector into a spherical coordinate system centred on the Sun the components of ξ in the coordinate system are

$$\begin{aligned} \xi_x &= \xi_c \sin\chi - \lambda_\perp G_r \sin\chi + \rho G_\theta \mathrm{sgn}(B) \\ \xi_y &= \mathrm{sgn}(B)\rho G_r \sin\chi + \lambda_\perp G_\theta \\ \xi_z &= \xi_c \cos\chi - \lambda_{||} G_r \cos\chi \end{aligned} \qquad (1.6)$$

where

ξ_c = Compton-Getting anisotropy (3CV/v);
χ = angle of the IMF with the Earth-Sun line;
$\hat{\theta}$ = unit vector in the direction of increasing solar co-latitude;
ρ = gyro-radii of the particles;
G_r = radial gradient of cosmic ray density;
G_θ = latitudinal gradient of cosmic ray density;
V = solar wind speed;
v = speed of the cosmic ray particles;
(ξ_x, ξ_z) = anisotropy responsible for the solar diurnal variation;

To define sgn(B) we must realise that the solar wind moving out from the Sun at 400 km sec^{-1} will cause the two hemispheres of the heliosphere to be separated by a thin magnetically neutral sheet. In one hemisphere the IMF will have a northern polarity and be directed *away* from the Sun. In the other hemisphere the IMF will have a southern polarity and be directed *toward* the Sun. The Sun rotates once every 27 days and the neutral sheet corotates with it, passing the Earth at about 400 km sec^{-1}. Since the neutral sheet is wavy and not flat, during a 27 day period the Earth will be alternatively above and below the neutral sheet as the undulations in the sheet overtake the Earth. IMF = A refers to a position in the heliosphere where the IMF is directed away from the Sun. This is called an *Away IMF sector.* Conversely, IMF = T refers to the opposite side of the neutral sheet - a *Towards IMF sector.*

Then :

$$\mathrm{sgn}(B) = \begin{cases} +1, & \mathrm{IMF} = \mathrm{A} \\ -1, & \mathrm{IMF} = \mathrm{T} \end{cases}$$

It is through this term in equation (1.6) that drifts affect anisotropies.

Early modellers recognised that by neglecting drift terms in equation (1.6) and other effects such as perpendicular diffusion, vector addition of the remaining streaming components would lead to an overall streaming of particles in a direction parallel to the Earth's orbit around the Sun. The particles would seem to corotate with the Sun. This corotating streaming (or anisotropic flow) of particles could be observed as a diurnal variation in the count rate of a cosmic ray detector as the detector's viewing cone rotated through 360 degrees of space in one day. The anisotropy is the Solar Diurnal Anisotropy. The anisotropy, manifested as a diurnal variation, would have the time of maximum count rate (phase) at 1800 local solar time (streaming along the tangent to the Earth's orbit). This effect has long been known to exist in data from cosmic ray recording instruments (see the next section of this chapter).

Parker (1964) proposed that corotation was a combination of the random walk (scattering by magnetic irregularities) of particles in the IMF and an electric field drift velocity. Forman and Gleeson (1975 and references therein) built on this model and produced the present theory (equation 1.2). They showed that pure corotation will arise if there is no net radial streaming (and drifts are considered negligible). Their model implied that the magnitude of the solar diurnal anisotropy is 0.6% of the average isotropic background flux of cosmic rays. If perpendicular diffusion is not neglected the amplitude of the anisotropy will be less than 0.6% and will be a function of the relative importance of perpendicular and parallel diffusion (see Appendix 1).

Levy (1976) included the curvature and gradient drifts in a model which showed that these drifts could be responsible for changing the direction of the anisotropy in alternate solar cycles. This could explain the 22-year cycle observed in the anisotropy (see the next section). A similar result was obtained by the model of Erdös and Kota (1979). Their model predicted that the direction of streaming during $A<0$ IMF polarity states should be along the direction of the Earth's orbit. Drifts included in this model were considered responsible for the model indicating that the streaming should change direction during the next IMF polarity state and this streaming would be observed as a diurnal variation with a phase around 1500 in local solar time. This model predicted that the anisotropy's amplitude and phase would be insensitive to rigidity but the amplitude would be sensitive to the neutral sheet warp.

Section 1.2.1 has illustrated some of the predictions of models of solar modulation. The two most important predictions of modulation models which incorporate standard solar magnetic fields are

- G_r should be smaller during solar minima when the IMF polarity is $A>0$; and
- there should exist a bi-directional latitudinal gradient which reverses direction with polarity reversals of the Sun's magnetic field.

1.2.2 Characteristics of the solar diurnal anisotropy

If one examines the average hourly count rate of a cosmic ray detecting instrument from a series of complete solar days an approximately sinusoidal variation with a period of 24 hours is observed. Harmonic (Fourier) analysis of the data will yield the time of maximum (phase) and amplitude of the variation, with the amplitude usually being expressed in terms of a percentage deviate from the mean hourly count rate. This sinusoidal variation is the solar diurnal variation introduced in the previous sections. When first discovered (Lindholm 1929,

as cited by Bennett et al. 1932), it was thought that the diurnal variation was related to the daily variation of some unknown atmospheric effect. Daily variations in cosmic ray intensity (after the data have been corrected for fluctuations in atmospheric pressure and temperature) are caused by spatial anisotropies outside the influence of the Earth's atmosphere and geomagnetic field (see, for example Figure 1.3).

On an individual daily basis the statistical uncertainties associated with the results of the harmonic analysis are usually quite large. By collecting data over many days and averaging the results of each day's harmonically analysed data the average solar diurnal variation for that period is found. Long term averages (from data spans of months or years) are more precise (the uncertainties being derived from the scatter of the individual days), yielding information about the average behaviour of cosmic rays in the vicinity of the Earth.

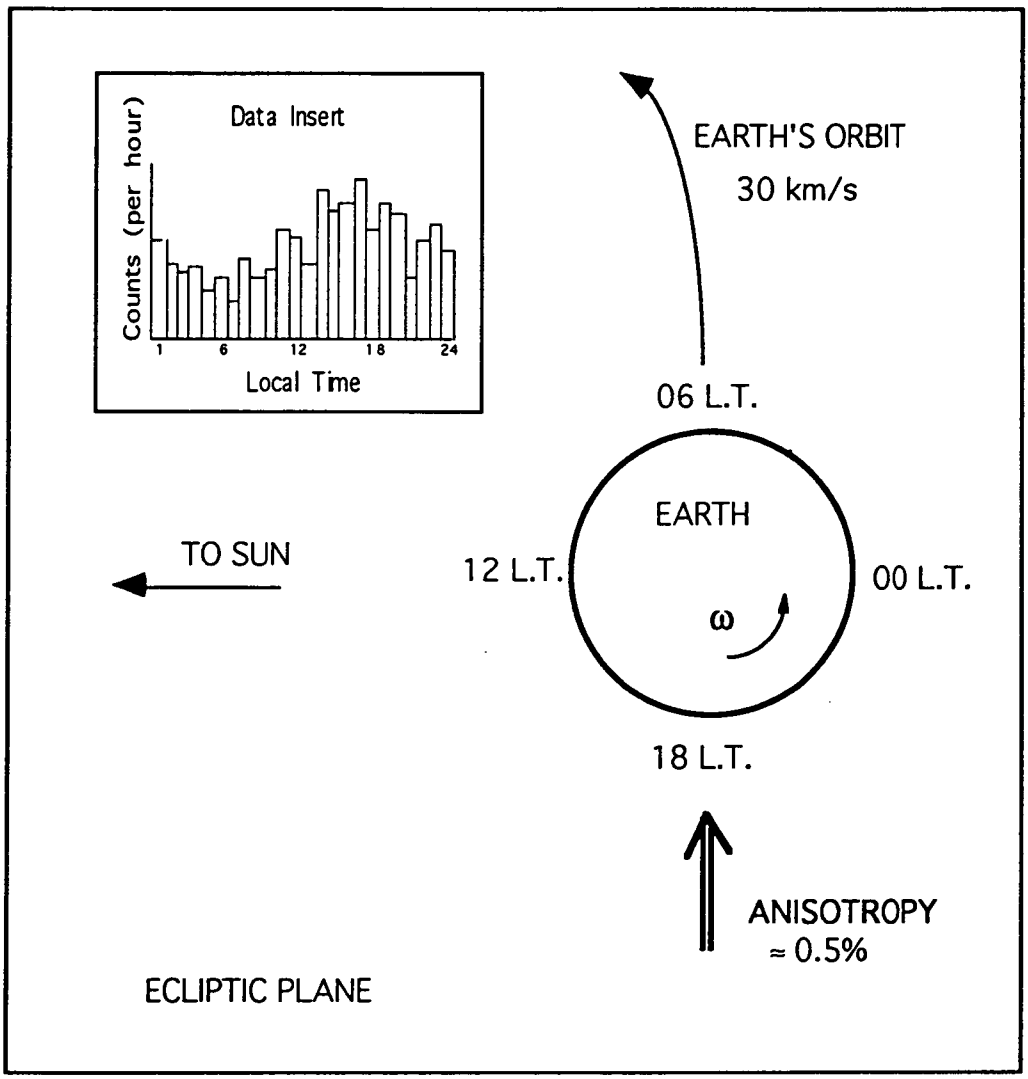

Figure 1.3 Solar diurnal anisotropy in the local time coordinate system. The Earth's rotation causes the asymptotic cone of view of an instrument to sweep through the anisotropy once a day. This gives rise to a diurnal variation in count rate data (insert) with a time of maximum around 1800 local time.

Following the discovery that the solar diurnal variation in cosmic ray data was related to a spatial anisotropy in the primary cosmic ray distribution (Elliott and Dolbear 1951) this anisotropy was, and still is, a greatly studied phenomenon. By the mid 1960's, ionisation chambers had been in operation for over 30 years, collecting data in 2- and 1-hour intervals. Thus began a concentrated effort to understand the solar diurnal variation and the processes responsible for producing the associated anisotropy in galactic cosmic rays.

An *asymptotic direction of approach* is the direction that a cosmic ray particle is travelling (in free space) before it is deflected by the Earth's magnetic field. Rao et al. (1963) defined the *asymptotic cone of acceptance* as "the solid angle containing the asymptotic directions of approach that significantly contribute to the counting rate of a detector." It had been realised that the acceptance cone of a recording instrument depends on its physical dimensions, position on the Earth and the geomagnetic field. The asymptotic cone of a telescope is seldom directly overhead and this causes the recorded phase of the diurnal variation to vary from station to station. By taking account of the asymptotic cones of acceptance of individual instruments, Rao et al. (1963) concluded from two years of neutron monitor data that the solar diurnal anisotropy (ξ_{SD}) had an invariant amplitude and phase in free space and was caused by an anisotropic streaming of particles coming from somewhere close to 90 degrees East of the Earth-Sun line.

It was assumed that the spectrum of ξ_{SD} could be represented as a power law of rigidity ($|\xi| = \eta P^{\gamma}$, where η is an amplitude constant and P is rigidity). It had been realised for some time that there should be some upper limit to the rigidities of particles participating in the solar diurnal variation. The rigidity where the anisotropy vanishes has become known as the Upper Limiting Rigidity (P_u) of ξ_{SD}. In reality P_u is the rigidity where the anisotropy ceases to be significant. Rao et al. (1963) showed that the anisotropy was independent of rigidity ($\gamma = 0$) and P_u was 200 GV.

Following the analysis of Rao et al. (1963) many studies have attempted to verify their conclusions. Jacklyn and Humble (1965) found that P_u was not constant and that this may have caused the amplitude to have an apparent variation. Duggal et al. (1967) presented results indicating that the amplitude of the solar diurnal variation was not invariant. They showed that the amplitude decreased during epochs when the count rate of neutron monitors was at a maximum. In the same year, Forbush (1967) showed there existed a 20 year cycle in the solar diurnal variation recorded by ionisation chambers from 1937 to 1965. He concluded that the solar diurnal variation was due to two components, one related to geomagnetic activity and the other containing a 20 year variation, hinted at being related to the IMF. At the same time Peacock and Thambyahpillai (1967) and Peacock et al. (1968) concluded that P_u of the solar diurnal variation was also non-invariant. They estimated that P_u reduced from 130 GV during the epoch 1960-1964 to about 70 GV in 1965. It was thought that the variation in the spectrum of ξ_{SD} may explain the apparent variance of its amplitude. Jacklyn et al. (1969) disproved this notion when they concluded that P_u did indeed decrease from 1958 to 1965 (in reasonable agreement with Peacock et al.) but that the corresponding amplitude of the anisotropy (after taking P_u into account) also had a small variation in the sense described by Duggal et al. (1967). They also showed that the spectrum must have a slightly negative exponent ($\gamma = -0.2$) for the anisotropy to be consistent with the current models. At the same time other investigations of the spectrum of the solar diurnal variation also concluded that P_u was a non-invariant (Ahluwalia and Erickson 1969; Humble 1971) but could not agree on the spectral index. Humble's results indicated that γ was

probably positive while Ahluwalia and Erickson concluded that zero was the best estimate of γ.

While the debate on the correct rigidity spectrum continued the amplitude and phase of the solar diurnal variation were still being investigated in light of the conflicting reports by Rao et al. (1963), Duggal et al. (1967) and Forbush (1967). Duggal et al. (1969) examined the two components suggested by Forbush, concluding that they both had the same rigidity spectrum. Duggal and Pomerantz (1975) conclusively verified there is a 22-year variation in the solar diurnal anisotropy related to the IMF in good agreement with Forbush (1967). They also showed that the variation in the anisotropy of 30 GV particles was larger than in that of 10 GV particles. The variation could not be explained solely in terms of a varying rigidity spectrum. Ahluwalia (1988a,1988b) disputed the existence of the two independent components proposed by Forbush (1967) and Duggal et al. (1969), but conceded that two independent components are present in the anisotropy during the IMF polarity configuration A>0. One of these is aligned with the E-W direction (i.e. at 1800 local solar time) termed the E-W Anisotropy and the other is aligned in the direction radially outward from the Sun, called the Radial Anisotropy. He concluded that the radial anisotropy vanishes during A<0 IMF configurations. The radial anisotropy appearing in alternative sunspot cycles explained the apparent 22-year wave in the phase of the solar diurnal variation. Swinson et al. (1990) analysed about 20 years of underground muon data and correlated the radial component of the solar diurnal variation with the square of the IMF magnitude. This showed that the radial anisotropy was related to the convection of particles away from the Sun by inhomogeneities in the IMF carried out radially from the Sun by the solar wind. The correlation was greater during the A>0 polarity state, interpreted as indicating that the radial anisotropy is more prevalent during this epoch, in agreement with Ahluwalia (1988a,b).

Currently it is believed that the ξ_{SD} is a superposition of two anisotropies (E-W and radial anisotropies) at 90 degrees to each other (Ahluwalia 1988a, 1988b; Swinson et al. 1990) contrary to previous conclusions. It is perhaps surprising that Bieber and Chen (1991a) have shown that the solar diurnal variation varies with a period of 22 years around an axis aligned with the IMF; and this axis is very close to the direction of one of the components proposed by Forbush (1967).

The works of Ahluwalia (1988a, 1988b) were consequences of an earlier study. Ahluwalia and Riker (1987) had investigated the solar diurnal anisotropy and its rigidity spectrum from 1965 to 1979, which had continued to be derived inconsistently with previous determinations. Here they concluded that P_u varied in a cyclic manner (in agreement with the above mentioned studies) with low values of P_u at solar minimum and high values of P_u at solar maximum. They showed that the spectral index of the anisotropy's rigidity spectrum could be anywhere between -0.5 and 1.0, with zero or a negative value being the most likely. Alania et al. (1983) had previously analysed data from the world wide network of neutron monitors from 1965 to 1982. They determined the average spectral index for this period to be -0.5, in marked contrast to most studies except for perhaps Jacklyn et al. (1969) and more recently with Ahluwalia and Riker (1987). By 1993, Ahluwalia (1991) and Ahluwalia and Sabbah (1993) had showed that the P_u failed to decrease after solar maximum in 1979 and unexpectedly increased to 180 GV in 1983. This led to a correlation between P_u and the magnitude of the IMF being discovered. The correlation is not only simple but seems intuitively correct, explaining (in part) why relatively large values of P_u and amplitudes of the solar diurnal variation were present during the period 1982-1984. The correlation found by

Nagashima et al. (1987) between the amplitude of the solar diurnal variation (only at rigidities greater than 60 GV!) and the Sun's magnetic dipole moment has also been proposed as partly explaining the large amplitudes in the solar diurnal variation after 1979.

Obviously, much knowledge about the solar diurnal anisotropy has been gained in the past 30 years. The amplitude and phase of the anisotropy are known to have cyclic variations but the exact causes of these variations are not agreed on. The spectral index γ and P_u are not completely agreed on although it is generally accepted P_u is always less than 200 GV and declines to values less than 100 GV at times of solar minimum.

1.2.3 Characteristics of the sidereal (North-South) anisotropy

Ionisation chamber data collected for an entire year at half hourly intervals and arranged in sidereal time were examined by Compton and Getting (1935) for an average sidereal diurnal variation. The variation was observed to have a phase at about 2000 local sidereal time. This indicated that the anisotropy producing the variation must have had a fixed direction relative to the stars, unlike the solar diurnal anisotropy which has its direction fixed with respect to the Earth-Sun line. Compton and Getting attributed the sidereal diurnal variation in the data to the motion of our solar system through the galaxy and our own galaxy rotating, producing a relative motion of the Earth through extragalactic cosmic rays towards a declination of 47 degrees and right ascension 20 hours and 40 minutes, sidereal time. Elliot and Dolbear (1951) subsequently found a sidereal diurnal variation in data collected in the southern hemisphere with a phase around 12 hours earlier. Not only did their results indicate that the sidereal diurnal variation was dependent on the hemisphere of observation, but they also indicated that cosmic rays were not produced extragalactically.

Jacklyn (1966) studied the sidereal diurnal variation in underground muon data collected during the 1960s. The two telescopes which were used in the analysis were at the same location (Hobart) but had their asymptotic cones of view directed in the opposite heliospheric hemispheres. The sidereal diurnal variations in the data had a phase around 0600 local sidereal time in the northern heliospheric hemisphere (in good agreement with other observations cited by Jacklyn) and 1800 sidereal time in the southern hemisphere. The discrepancy could not be related to temperature effects and was attributed to a bi-directional streaming of cosmic rays along the galactic magnetic field, prior to entry into the heliosphere. Further discussion of any true galactic anisotropies appearing at these rigidities will be deferred until Chapter 4.

Swinson (1969) proposed a different explanation for the phase differences in the sidereal diurnal variation observed from opposite hemispheres. He proposed that the anisotropy responsible for the sidereal diurnal variation was IMF sector polarity dependent and was directed perpendicular to the ecliptic plane. The streaming of particles perpendicular to the ecliptic would have a component in the geo-equatorial plane which would be observed as a diurnal variation in data in sidereal time. The mechanics behind the anisotropy are presented in Figure 1.4 : the particles gyrate around a field line in the vicinity of the Earth and may be detected by Earth based instruments. The direction of flow can be represented as $\mathbf{B}\mathbf{x}\mathbf{G}_r$. Due to the radial gradient in the number density of cosmic-rays, the flow of particles approaching from outside the Earth's orbit differs from the flow due to particles coming from inside the Earth's orbit. The two flows are in opposite directions and an Earth based instrument will

record the excess streaming from the direction corresponding to the flow of particles which originated in the region of higher density. If the field line reverses direction (the Earth in a different IMF sector) the excess streaming at Earth will reverse direction. Consequently, at times, a northern hemisphere telescope will detect a larger intensity of particles than a southern hemisphere telescope and vice-versa. This is called the North-South Anisotropy (ξ_{NS}). The effect was conclusively demonstrated by analysing underground muon data (Swinson 1971). In reality the streaming of particles perpendicular to the ecliptic plane is a net anisotropic flow caused mainly by curvature and gradient drifts in the IMF. These results suggested that the amplitude of ξ_{NS} was constant during the period 1965-68 and had an upper limiting rigidity of about 75 GV.

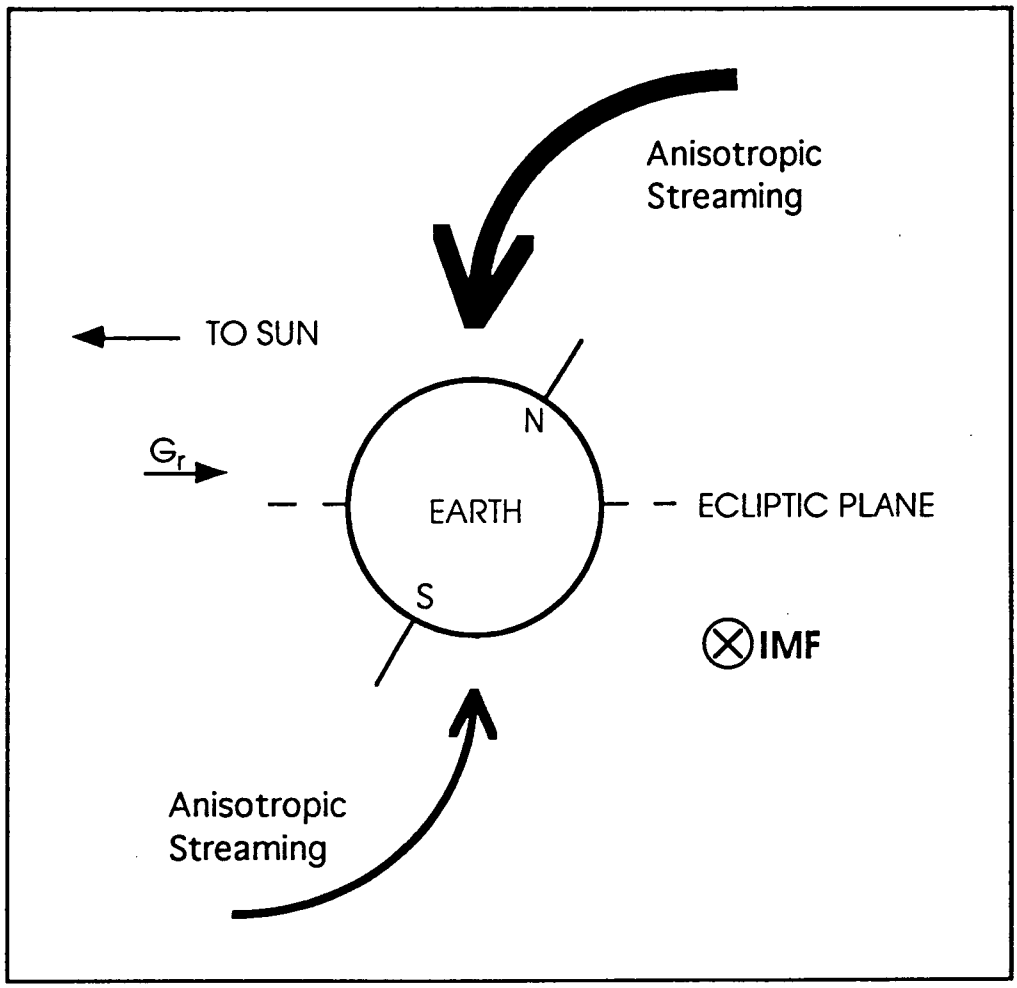

Figure 1.4 The N-S anisotropy in a Towards interplanetary magnetic field (IMF) sector. The excess streaming will be from the northern hemisphere (see text).

By 1979, ξ_{NS} was so generally accepted that the IMF sector polarity near the Earth could be inferred from the anisotropy's observation (Mori and Nagashima 1979). This method of inferring the IMF sector was shown to be in about 75% agreement with spacecraft measurements of the sector type .

Yasue (1980) derived the spectrum of ξ_{NS} for the combined years 1968 to 1972. He found that the anisotropy was weakly proportional to the rigidity of the particles ($P^{0.3}$) and that P_u was between 150 and 300 GV. He was the first to show conclusively that the anisotropy was

from the direction perpendicular to the ecliptic plane. He did this by examining all three dimensions of the anisotropy relative to the Earth's equator (i.e. due to the ecliptic plane being tilted 23.5 degrees to the Earth's rotation axis). He examined both of the components of ξ_{NS} observable at Earth - a component in the geo-equatorial plane (sidereal diurnal intensity variation) and a component along the Earth's rotation axis (North-South asymmetry in particle intensity). ξ_{NS} can be derived from the measurement of either of these variations in intensity. His results were consistent with a time invariant ξ_{NS}.

It is well known that if a solar anisotropy (1 cycle/solar day) is modulated by some seasonal or other process with a period of 1 year (1/365 cycles per solar day) then there will be an apparent variation in the data with 366 cycles a year. This would be present in the data arranged in sidereal time and contaminate a real sidereal diurnal variation. Nagashima et al. (1985) demonstrated that the bi-directional solar anisotropy is seasonally modulated by the yearly variation of the direction of the IMF at the Earth. This leads to a spurious sidereal diurnal variation in cosmic ray data. The appropriate corrections for removing this spurious signal from cosmic ray data were presented, but of course Yasue's analysis (1980) did not incorporate these corrections.

Bieber and Pomerantz (1986) examined the North-South asymmetry component of ξ_{NS} from 1961 to 1983 using data from polar based neutron monitors. They concluded that there was a variation in the magnitude of the anisotropy with a ten year period. No dependence of the anisotropy on the solar magnetic polarity was observed.

Swinson (1988) found little variation in the sidereal diurnal variation recorded by underground muon telescopes from 1965 to 1985. He concluded that ξ_{NS} depends only weakly on the cycles in solar activity and magnetic polarity.

The lack of agreement on the variance (or invariance) of the ξ_{NS} was increased by an observation which showed that 27-day waves in the amplitude of the ξ_{NS} were modulated with a period of 11 years (Swinson and Yasue 1991).

Baker et al. (1993a) and Baker (1993) used neutron monitor and muon telescope data to examine the North-South asymmetry from 1982 to 1985. They showed, as expected, that for non-polar instruments the North-South asymmetry was relatively hard to detect, but nonetheless the results indicated that at high rigidities a variation in ξ_{NS} does exist.

The ξ_{NS} is present in fluxes of particles with rigidities up to at least 150 GV. Although its general characteristics are known, its rigidity spectrum has not been studied in detail. At low rigidities ξ_{NS} seems to have some variation but at P>100 GV it is not obvious from the literature if this variation is definitely present; hence there is much to be learnt from a study of its temporal behaviour.

1.2.4 Observations of modulation parameters

Observations of modulation parameters such as G_r, G_θ, $\kappa_{||}$ and $\kappa_\perp$ are important model constraints. Measurements of these parameters provide knowledge of the magnetic conditions and processes in interplanetary space. They are also the only way of testing predictions made by theoreticians. Essentially, interplanetary space is a large laboratory with

which a scientist can test the predictions of theories by direct and indirect observations of modulation parameters.

Radial density gradient

There are two ways of measuring the radial gradient (G_r) of the number density of galactic cosmic rays in interplanetary space. One method is a direct measurement of the gradient by sampling and comparing the density of particles at different spatial positions with spacecraft. The other is by inferring G_r from data collected at Earth by cosmic ray telescopes. Direct observations in space are restricted to measuring particles with relatively low rigidities (less than 5 GV and usually less than 1 GV). On the other hand, gradients inferred from Earth based observations are usually made from monitors which have median rigidities greater than 10 GV and in the case of underground muon telescopes the median rigidity of response is usually greater than 100 GV. Little comparison between the results of the two methods is possible other than a qualitative one. Results presented in this thesis are inferred from Earth based measurements so only a brief review of the results of spacecraft measurements is given here.

Most studies of the radial density gradient are made by comparing the spatial difference in density of particles recorded by the Voyager and Pioneer spaceprobes and Earth orbiting satellites such as IMP8. By comparing the counting rates of comparable detectors aboard any two of these spacecraft the magnitude of G_r is usually calculated from the relation :

$$G_r = \frac{\ln(C_1/C_2)}{r_1 - r_2} \tag{1.7}$$

where C_i are the count rates of the instruments and r_i are the positions of the spacecraft. A time delay for the solar wind propagation from r_2 to r_1 is usually included to ensure that any temporal variability of the radial gradient is removed from the analysis.

Spacecraft observations have consistently reported a positive radial gradient (i.e. greater density of particles further away from the Sun). See, for example the review on radial density gradients by Venkatesan and Badruddin (1990) and references therein. Essentially, most gradients are reported to be about 1 to 4% AU^{-1}, at various distances from the Earth out to 40 AU. These values of G_r are integral measurements, with particles having $E>60$ MeV/nucleon (rigidity, $P>0.4$ GV). A key prediction of drift theories (other than those which incorporate a non-standard IMF in the polar regions of the heliosphere) is that the magnitude of G_r is sensitive to the polarity state of the Sun's IMF (see Section 1.2.1). This is not observed, with most studies reporting lower gradients at times of solar minimum than at solar maximum but little or no dependence of G_r on the solar polarity (Venkatesan and Badruddin 1990, Webber and Lockwood 1991, McDonald et al. 1992).

Inferences of G_r from data collected by Earth based cosmic ray instruments are made by measuring the North-South anisotropy. (See equation 1.6 and also Chapter 4 for the relation between the North-South Anisotropy and G_r). Swinson (1969, 1971) inferred that G_r of particles with rigidities greater than 100 GV was positive from 1965 to 1970. This is consistent with spacecraft observations of G_r.

Kudo and Wada (1977) examined the North-South anisotropy of particles with rigidities ranging from 10 GV to 200 GV. They found that G_r decreases with rigidity and is lower at solar mimimum than at solar maximum. This is consistent with spacecraft observations.

Duggal and Pomerantz (1977) inferred G_r from examining the North-South anisotropy derived from 12 years of neutron monitor data (approximately 10 GV particles). They estimated that the average G_r was about 2% AU^{-1} at these rigidities from 1964 to 1975. Extending their analysis to the period 1961 to 1983, Bieber and Pomerantz (1986) showed that the average G_r of 10 GV particles was 1.6% AU^{-1} and G_r varied periodically, having lower values at solar minima. They found no dependence of G_r on the polarity of the IMF in agreement with spacecraft observations and verified at higher rigidities (Yasue 1980, Swinson 1988), although Yasue found no significant variation in G_r from 1968 to 1972.

Qualitatively, the results from spacecraft observations of G_r seem to be consistent with those inferred terrestrially, although the temporal behaviour of G_r is uncertain.

Latitudinal density gradient

In section 1.2.1 it was noted that an important prediction of modulation models which incorporate drift velocities is the existence of a bi-directional latitudinal gradient (symmetric with respect to the neutral sheet). Since about 1970, three techniques have been used to attempt to confirm its existence (or lack thereof). The simplest method (in theory) is that which uses spacecraft separated by some latitudinal distance and compares the counting rates of instruments aboard them. Unfortunately, until recently most space probes have been confined close to the ecliptic plane, with the relatively new data obtained by the Ulysses mission just starting to emerge in the literature. This spaceprobe will eventually pass over both geographic poles of the Sun, making a complete orbit out of the ecliptic plane by around 1998.

Previous reports of latitudinal gradients (G_θ) from spaceprobes have been conflicting. McKibben et al. (1979) used observations from Pioneer 11 to show there existed a bi-directional latitudinal gradient directed away (positive) from the solar equatorial plane. The data were collected during the $A>0$ polarity state (1970's) by monitors aboard Pioneer 11 which responded to particles with $E>260$ MeV. This observation was in good agreement with theoretical predictions. Conversely, negative symmetric latitudinal gradients were reported to exist during the same period (Newkirk et al. 1986), while McKibben (1989) reanalysed the data of McKibben et al. (1979) and concluded that the positive G_θ present in the heliosphere during 1975-78 was probably uni-directional, contrary to their previous result. During 1981-1990 the IMF polarity was negative ($A<0$) and theories predict that the bi-directional latitudinal gradient should be directed towards the solar equatorial plane. This has been confirmed (Christon et al. 1986, Cummings et al. 1987, Webber and Lockwood 1992).

Terrestrial measurements of G_θ are made by either measuring particle intensity along the Earth's orbit or using the contribution of the latitudinal gradient to the solar diurnal variation. Results presented in this thesis are derived from the latter technique, but a short summary of the results derived from the former method is worthwhile to fully depict the state of knowledge about latitudinal gradients.

The Earth orbits the Sun in a year, during which it ascends to 7.25 degrees north of the solar equator and descends to 7.25 degrees south of the equator. By measuring the intensity of cosmic rays during a year, one can examine any latitudinal variation in the density of cosmic rays across the solar equatorial plane. Any latitudinal variation in density will be observed as a variation in cosmic ray instruments' count rates. Of course, a gradient inferred from any cosmic ray data obtained on the Earth is for primary particles with at least 2 GV of rigidity. A uni-directional G_θ will manifest as an annual variation while a bi-directional G_θ will manifest as a semi-annual variation in the data. This method (as reviewed by Venkatesan and Badruddin 1990) has demonstrated that a southward (unidirectional) G_θ existed during 1960-75. Other studies reviewed by Venkatesan and Badruddin have shown a symmetric G_θ was present in unison with the uni-directional G_θ from 1962 to 1973. The symmetric gradient supposedly reversed direction after the solar polarity reversal from 1969-1971. The same technique has also shown that both the uni- and bi-directional G_θ were present from 1953 to 1979 and both these gradients reversed at solar polarity reversals (Antonucci et al. 1985). Obviously, these results have caused a great amount of uncertainty regarding the form of latitudinal gradients.

The final technique of inferring G_θ makes use of the gradient and drift velocities of cosmic rays. The direction of streaming due to drifts can be represented as **BxG** (see equation 1.2). If G_θ exists, drift fluxes (**BxG**) in the two hemispheres (separated by the neutral sheet) related to the G_θ will on average be in the ecliptic plane. This will lead to the solar diurnal anisotropy having an IMF sector polarity dependence. This mechanism was first proposed by Swinson (1970) who showed that during 1967 and 1968 data from an underground muon telescope analysed for the solar diurnal variation indicated a south pointing (uni-directional) G_θ existed with a magnitude less than G_r. This was verified by Hashim and Bercovitch (1972) by examining the solar diurnal variation in neutron monitor data. The gradient was shown to have a dependence on rigidity of $P^{-0.6}$.

Swinson (1976) extended his analysis to encompass the period 1965-73 (which includes the solar polarity reversal during 1969-71). The results indicated that a south pointing (uni-directional) gradient existed across the ecliptic plane for the entire period. The results also indicated that the magnitude of this gradient decreased at times of solar minimum. This conclusion was contradicted by the results of analysing neutron monitor and underground muon telescope data for the solar diurnal variation (Swinson and Kananen 1982). This study indicated that a uni-directional gradient was present during this period which reversed at the solar polarity reversal (1969-1971). Swinson et al. (1986) used four underground muon telescopes to extend this analysis to the epoch 1965-1983. Again the results were interpreted differently from before. The results were interpreted as indicating that prior to 1971, a south pointing uni-directional (asymmetric) gradient existed at the same time as a smaller bi-directional (symmetric) gradient which was directed towards the heliographic equatorial plane. The asymmetric gradient was proposed to be caused by excess solar activity in the northern hemisphere of the Sun. After the IMF polarity reversed they proposed that the asymmetric gradient vanished and the symmetrical gradient reversed direction. Swinson et al. (1991) refuted this explanation and devised a simpler model which assumed that only a symmetric gradient existed, always directed towards the neutral sheet. It was proposed that the neutral sheet can be displaced to heliolatitudes other than the solar equatorial plane due to asymmetric solar activity. This would transform a non-reversing symmetric G_θ (with respect to the neutral sheet) to an asymmetric G_θ relative to the Earth. The direction of the apparent unidirectional gradient would be dependent on the hemisphere of the Sun containing excess

activity. This model was not supported by neutron monitor data analysed from 1953 to 1988 (Chen et al. 1991). However, Bieber and Chen (1991a) did conclude that the solar diurnal variation results from analysing neutron monitor and ionisation chamber data supported the view that an IMF polarity dependent symmetric G_θ existed from 1930 to 1988. Chen et al. (1991) showed that the symmetric gradient was present in unison with an asymmetric gradient which had no IMF polarity dependence or observable trends. Ahluwalia (1993) has concluded that the symmetric gradient exists in particles with rigidities up to 300 GV.

The existence of a latitudinal variation of cosmic rays is not disputed, however its form (uni- or bi-directional) is. Knowledge of the existence and form of this gradient is a key ingredient to a better understanding of solar modulation.

Diffusion coefficients and mean-free paths

Diffusion coefficients (κ) of cosmic rays are related to mean-free paths (λ) by

$$\lambda = \frac{3\kappa}{\upsilon} \tag{1.8}$$

where υ is the speed of the particles (usually taken to be the speed of light).

There are two types of *diffusion* in the heliosphere - parallel (||) and perpendicular ($\perp$) to the IMF lines. These are caused by the random walk of particles in the heliosphere. The particles are scattered from their gyro-orbits by irregularities in the IMF and the bulk distribution essentially diffuses along and across field lines (see section 1.2.1 for a more comprehensive explanation). As particle rigidities increase eventually the gyro-orbits are so large that particles will not be effected by the irregularities and regular particle motion will prevail (Erdös and Kota 1979). Regular motion is just the usual gyration of particles in the IMF combined with the curvature and gradient drifts of their trajectories.

The diffusion processes are characterised by parallel and perpendicular diffusion coefficients. These can be related to corresponding parallel and perpendicular mean-free paths, interpreted physically as the average length a particle will travel before being scattered by an irregularity in the IMF and prevented from travelling any further through the heliosphere in that particular direction. For example a small perpendicular mean-free path ($\lambda_\perp$) implies that the perpendicular velocity of a particle's gyration is often interrupted by irregularities in the IMF. This does not prevent parallel motion continuing and hence parallel diffusion dominates. Conversely, a large $\lambda_{||}$ would imply that particles seldom have their parallel component of velocity *scattered*, hence limiting the relative amount of perpendicular diffusion. The theoretical expressions relating to anisotropies incorporate these mean-free paths. By analysing cosmic ray data for the relevant anisotropies, information about the corresponding mean-free path can be obtained.

Not only are the magnitudes of mean-free paths important, but also the relative importance ($\alpha = \kappa_\perp/\kappa_{||} = \lambda_\perp/\lambda_{||}$) of the two mean-free paths is needed for a better understanding of solar modulation processes. Palmer(1982) reviewed many of the studies of $\lambda_\perp$ and $\lambda_{||}$ and estimated *consensus* values. He estimated that $\lambda_{||}$ ranges from 0.08 to 0.3 AU for particles

between 0.001 and 4 GV and that $\lambda_\perp$ is approximately 0.0067 AU at these rigidities. This would imply that perpendicular diffusion is only 2% to 8.3% as important as diffusion parallel to the IMF. These values of α can be compared to other determinations. Ip et al. (1978) estimated $\alpha = 0.26 \pm 0.08$ for particles with E>480 MeV (P>0.3 GV). Recently, Ahluwalia and Sabbah (1993) determined that α must be below 0.09.

By using the solar diurnal variation in neutron monitor and ionisation chamber data, the coupled parameter $\lambda_{||}G_r$ can be determined (see equation 1.6 and Chapter 3). This quantity has been shown to be dependent on rigidity and vary with an 11- and 22-year cycle and is lower at times of solar minima during A>0 IMF polarity states than during A<0 (Bieber and Chen 1991a). It has been shown that this occurs because $\lambda_{||}$ is solar polarity dependent (Bieber and Chen 1991b, Chen and Bieber 1993). These researchers claim that their observations are meaningless in terms of drift theory if $\alpha > 0.16$, not inconsistent with Ahluwalia and Sabbah's conclusion. On the other hand Ahluwalia and Sabbah (1993) and Ahluwalia (1993) claim that $\lambda_{||}G_r$ is rigidity independent. They do find however that $\lambda_{||}G_r$ is IMF polarity dependent but make no suggestions as to whether this is caused by a variation in $\lambda_{||}$ or G_r or both.

Summary

Due to economics and geography most cosmic ray research has been performed from locations in the northern hemisphere. Consequently, many studies of cosmic ray modulation have used data from instruments which have only been directed north of and in the ecliptic plane. The count rates of cosmic ray instruments drop off very quickly as the primary rigidity of response of the instruments increase. This causes the statistical reliability of the data to decrease at higher rigidities so most investigators are loathe to work with instruments like underground muon telescopes. For these reasons analyses of cosmic ray data collected by the University of Tasmania and Australian Antarctic Division can only help to improve our knowledge of the solar modulation of cosmic rays. The data are not only recorded by neutron monitors but an extensive collection of underground muon telescopes responding to primary cosmic rays with rigidities in excess of 150 GV.

The distribution of cosmic rays in the heliosphere is affected by the Sun's interplanetary magnetic field by three different processes. These are convection, diffusion and curvature and gradient drifts. Numerical models suggest that solar modulation of galactic cosmic rays will produce a radial and latitudinal density gradient of the distribution which are both dependent on the polarity of the Sun's IMF configuration. The radial gradient is predicted to always be positive, but smaller during the A >0 polarity state than during the A <0 polarity state. The latitudinal gradient is predicted by the models to be bi-directional and negative (local maximum in density at the neutral sheet) during the A <0 polarity state of the IMF. After a solar magnetic polarity reversal the bi-directional gradient is predicted to reverse direction and have a minimum in the number density at the neutral sheet. It has been noted that newer models now incorporate a solar magnetic field which is less radial at polar heliolatitudes than previously used (Jokipii and Kota 1989, Moraal 1990). These models predict that the radial gradient is not as IMF polarity dependent as previous models. Cosmic

Table 1.1 Predictions and observations of solar modulation parameters

Quantity	Model Predictions	Observations	P (GV)	Notes
G_r	IMF polarity dependence	Not confirmed.	≤10	e.g. Potgieter and Moraal (1985) and others.
	No IMF polarity dependence		≤10	Jokipii and Kota (1989) and Moraal (1990).
		Confirmed :		
		1–4% AU^{-1}	spacecraft	Venkatesan and Badruddin (1990).
		1–3% AU^{-1}	10	Bieber and Pomerantz (1986) – 10-year variation.
		3.0±1.1% AU^{-1}	10	Yasue (1980) –
		1.8±0.7% AU^{-1}	20	negligible temporal variation.
		0.7±0.3% AU^{-1}	80	
		0.5±0.2% AU^{-1}	150	
		.9% AU^{-1}	20	Kudo and Wada (1977) –
		.4% AU^{-1}	80	definite cyclic variation of about 11
		.3% AU^{-1}	150	years.
		.2% AU^{-1}	230	
G_θ	Bi-directional and reverses direction at IMF polarity reversal.		≤10	e.g. Jokipii (1989) and others.
		Confirmed :		
			spacecraft	e.g McKibben et al. (1979) and others.
			10	Antonucci et al. (1985).
		2% AU^{-1}	17	Bieber and Chen (1991a) –
		0.5% AU^{-1}	67	assumed $\alpha = 0.01$
			130	Swinson et al. (1986).
		0.03% AU^{-1}	300	Ahluwalia and Sabbah (1993).
		Disputed :	spacecraft	e.g. McKibbin (1989) and others.
			130	Swinson et al. (1991).
$\lambda_{\parallel}$	–	0.08–0.3 AU	≤4	Palmer (1982).
		>0.5 AU	17	Chen and Bieber (1993) – polarity dependent.
		0.2 AU	10	Yasue (1980).
		1.0 AU	100	
$\alpha=\lambda_\perp/\lambda_{\parallel}$	–	0.02–0.083	≤4	Palmer (1982).
		0.26±0.08	spacecraft	Ip et al. (1978).
		≤0.16	17	Chen and Bieber (1993).
		0.09	≤300	Ahluwalia (1993).

ray studies can search for the existence of these gradients and estimate their magnitudes. The predictions of these models are summarised in Table 1.1 with the observations which have either supported or refuted their accuracy.

Modulation causes anisotropic streaming of cosmic rays in the heliosphere. The largest non-transient anisotropies are the Solar Diurnal Anisotropy and the North-South Anisotropy. These anisotropies cause a diurnal variation in the count rates of instruments in solar (solar diurnal anisotropy) and sidereal (North-South anisotropy) time. These anisotropies have been the focus of many studies over the years. Although much has been revealed about the anisotropies there still remains some uncertainty about their rigidity spectra and temporal variations.

Many inconsistant derivations of the spectrum of the solar diurnal anisotropy have been reported. The spectral index γ has been shown to be anywhere from -0.5 to 1.0. Researchers do agree that P_u is non-invariant and less than 200 GV. It is even agreed that P_u reduces to about 50 GV at times of solar minima and is larger at solar maxima. Just how large however, and the mechanisms responsible for the variation in P_u, is not entirely clear.

Most investigators will agree that the magnitude of the solar diurnal anisotropy is not constant in free-space and has an 11-year cycle. It is also noted that the phase of the anisotropy is rigidity dependent and has a 22-year cycle. One group believe this is due to a contribution to the anisotropy from a component which is directed at 135 degrees east of the Earth-Sun line (Forbush 1967, Duggal et al. 1967, Duggal and Pomerantz 1975; Bieber and Chen 1991a). Another group claim that the responsible agent for this variation is an anisotropy outward from the Sun which is more prominent during the A>0 polarity state (Ahluwalia 1988a, 1988b; Swinson et al. 1990).

Chapter 3 is an analysis concerning the solar diurnal anisotropy. In Chapter 3 the results of analysing cosmic ray data from neutron monitor and underground muon telescopes to obtain the yearly averaged solar diurnal variations are presented. The yearly averaged solar diurnal variations in the data are used to derive the rigidity spectrum of the solar diurnal anisotropy. Two methods for this are explained. The average rigidity spectrum is obtained for the period 1957 to 1990 and the spectra for each year are also derived. These spectra are compared to past determinations, as are the corresponding amplitude and phase of the solar diurnal anisotropy in free space. The temporal behaviour of P_u is examined for correlations with the IMF and other solar quantities in an attempt to explain its variation. It was hoped that this study would dispel some of the contradictions in the literature about the solar diurnal anisotropy.

It has been noted that modulation theories make predictions about radial and latitudinal density gradients. The solar diurnal anisotropy can give information about the latitudinal gradient. This gradient is very controversial due to some investigations inferring a bi-directional gradient which behaves in accordance with theoretical predictions (Antonucci et al. 1985, Swinson et al. 1986, Bieber and Chen 1991a) while others dispute these claims. Included in Chapter 3 is the inference of the latitudinal gradient of cosmic rays with rigidities up to about 200 GV from the solar diurnal anisotropy. The results of this study are compared to theoretical predictions and previous determinations summarised in Table 1.1. Recently, two studies of the solar diurnal anisotropy have investigated the temporal behaviour

of the modulation parameter $\lambda_{||}G_r$ with conflicting conclusions about its rigidity dependence (Bieber and Chen 1991a, Ahluwalia and Sabbah 1993) . Chapter 3 includes a determination of this parameter over a range of rigidities in an attempt to resolve this discrepancy.

Only a small number of studies have tried to derive the spectrum of the North-South anisotropy. These have shown that the anisotropy is present in fluxes up to at least 200 GV. The temporal behaviour of the anisotropy is important since the radial gradient can be inferred from the anisotropy's magnitude. Results of studies about the temporal behaviour of the anisotropy and hence the radial gradient have been inconsistant. Some studies have shown the anisotropy (and the radial density gradient) to be essentially constant (Yasue 1980, Swinson 1988) while others have shown the anisotropy (and gradient) to have significant variations over a large number of years (Kudo and Wada 1977, Bieber and Pomerantz 1986, Baker et al. 1993a). Regardless though, no study has shown G_r to be polarity dependent. The rigidity spectrum of the North-South anisotropy is thought to be positive and the upper limiting rigidity about twice as large as that of the solar diurnal variation (Yasue 1980). No other studies of the spectrum have been done except by Swinson (1971) who concluded that the upper limiting rigidity was about 75 GV, much lower than the results of Yasue. Chapter 4 presents the results of an investigation into the rigidity spectrum of the North-South anisotropy and the temporal behaviour of this anisotropy from 1957 to 1990. Neutron monitor and underground muon telescope data are used to obtain yearly averaged sidereal diurnal variations from 1957 to 1990 and the corresponding North-South anisotropy.

We have seen in the literature that the temporal behaviour of G_r is somewhat ambiguous. In Chapter 4 the North-South anisotropy is used to infer G_r. The polarity dependence of G_r is investigated as are any year to year variations. The values of the radial gradient inferred from these results are compared with past determinations summarised in Table 1.1.

Knowledge of modulation parameters such as $\kappa_{||}$, $\kappa_{\perp}$, $\lambda_{||}$ and $\lambda_{\perp}$ is needed for more accurate numerical models and better understanding of modulation processes. Chapter 5 culminates this thesis by combining the results from Chapters 3 and 4 to study $\lambda_{||}$ from 1957 to 1990 at various rigidities from about 10 to 200 GV. Past determinations of the mean-free paths have yielded reasonably consistent results (see Table 1.1) but recent studies conclude that these mean-free paths may be magnetic polarity dependent (Bieber and Chen 1991b, Chen and Bieber 1993). In Chapter 5 this dependence of $\lambda_{||}$ (or lack of it) on the IMF polarity is investigated by using the anisotropies (solar diurnal and North-South) obtained from neutron monitor data. The analysis is also extended to underground muon telescopes to search for any dependence of $\lambda_{||}$ on IMF polarity in the rigidity range 100–200 GV. In this chapter an estimate of the relative importance of perpendicular and parallel diffusion from about 10 GV up to 200 GV for three consecutive solar cycles is also made and compared to current estimates.

CHAPTER 2

DATA AND METHODS OF ANALYSES

This chapter is concerned with presenting all the methods and techniques employed in this thesis to process and analyse cosmic ray data for investigating cosmic ray anisotropies in the heliosphere. The section immediately following this introduction tabulates all the cosmic ray observing stations and instruments used in this thesis. Neutron monitor and muon telescopes (surface and underground) are used to cover as broad an energy range of the primary spectrum as possible. Numerous telescopes are used in an attempt to observe as great a region of space around the Earth as possible and collect as much data as possible in order to gain greater statistical accuracy. The southern hemisphere stations are critical in this respect (as noted in Chapter 1) and their continued operation should be of paramount importance to all researchers. The remaining sections of this chapter concern terrestrial effects on the cosmic ray distribution (both primary and secondary components) and techniques to infer the spatial anisotropies from diurnal variations in data in light of these effects.

Terrestrial effects such as atmospheric pressure and temperature affect the production of the secondary components and hence an instrument's count rate. Variations in atmospheric parameters such as sea level pressure, temperature of the pion production level and height of the muon production level change the number of particles detected at sea level for a constant primary flux. Before any conclusions can be made from data these effects must be taken into account. Section 2.2 presents the coefficients (and their derivation) used to correct these effects in the data.

Once data are corrected for terrestrial influences, the hourly count rate (arranged in solar or sidereal time) for a complete day can be harmonically (Fourier) analysed to calculate the best fit sinusoidal variations present (if any). On a day to day basis the uncertainties associated with the calculated diurnal variations in the data are large. For this reason an average over many days is used to obtain more accurate results. Suitable time periods may be chosen to average out and remove unwanted variations from the results. Sections 2.3 and 2.4 present the techniques used to Fourier analyse the data.

Particle paths can be deflected by the geomagnetic field before the production of secondaries and anisotropic streaming directions are not normally parallel to the direction of view of an instrument. For example, a telescope in Antarctica may ultimately observe secondaries produced by primary particles which were travelling in the heliosphere parallel to the equator. These problems imply that an instrument may only detect a small fraction of a complete anisotropy. Hence the diurnal variation in the data recorded by an instrument may not sufficiently describe the corresponding anisotropy in free-space unless the coupling of the instrument's count rate to the primary flux of cosmic rays is adequately known. *Coupling coefficients* take account of these effects and allow the results of harmonic analyses to be interpreted properly. Section 2.5 explains the theoretical basis for using these coefficients to infer free-space anisotropies from diurnal variations in data.

Even if all the above effects are corrected, the resultant average diurnal variation may not be caused by a single anisotropy. For example, the solar diurnal variation in neutron monitor data is caused by an anisotropic flow of particles from the eastern side of the Earth-Sun line. In muon telescopes this diurnal variation can be caused by a combination of the solar diurnal anisotropy and an apparent anisotropy caused by the motion of the Earth through unmodulated cosmic rays. Effects such as this, present in Fourier analysis results are called spurious modulations and Section 2.6 presents the methods used to remove them.

2.1 Cosmic ray observing stations

Table 2.1 lists the characteristics of the stations, muon telescopes and neutron monitors used in this thesis. The details of the Hobart station have been described by Fenton et al. (1961) and Jacklyn (1970), the Mawson underground instruments by Duldig (1989) and the Mawson surface muon telescope by Parsons (1959). Minor parameters of the other instruments can be found in Fujimoto et al. (1984) and Yasue et al. (1982). The data obtained with the Socorro and Embudo underground muon telescopes were kindly supplied by Professor D. B. Swinson of the University of New Mexico. Data from the neutron monitors at Deep River and Kerguelen were taken from the National Geophysical Data Centre CD-ROM data disc : NGDC-05/1.

2.2 Atmospheric effects

The dynamic nature of the atmosphere affects the secondary components of cosmic rays. Balloon studies of cosmic ray density in the atmosphere have shown that at an altitude of about 18km there exists a maximum called the *Pfotzer-maximum altitude* (Sandstrom 1965). Above this height, atmospheric nuclei are sparsely distributed and the probability of primary particles interacting to produce secondary particles is low. Loss mechanisms of the secondary component of cosmic rays depend on the interaction cross-section of secondaries with atmospheric nuclei, so as the density of the atmosphere increases below 18km the mechanisms which produce secondary decay and capture become more likely. At the Pfotzer-maximum altitude the density of cosmic rays (the sum of primaries and secondaries) is greater than at any other altitude in the atmosphere.

Three processes affect the probability that secondary particles will reach sea-level. If the air pressure increases then more secondaries interact with the atmosphere due to the increased mass of absorbing matter and will not survive to be detected at sea-level. This is the *pressure effect.* If the temperature at the mean pion production level (approximately 120 mb air pressure) increases then the density of the atmosphere decreases and the probability for negatively charged pions to be captured by atmospheric nuclei decreases. This is called the *positive temperature effect* as the number of detected muons will rise (due to the larger number of negative pions that survive to decay into muons) as the temperature increases. If the mean height of muon production (corresponding to approximately 100 – 150 mb air pressure) increases due to thermal expansion of the atmosphere then the muons have a larger distance to travel to ground level. The muons must then travel for a longer time in the atmosphere allowing more muons to decay (to electrons and positrons) and consequently not

Table 2.1 Station and instruments used in this thesis. P_{med} is the median rigidity of response to the galactic flux. (UG = underground)

Station	Mnemonic	Instrument Type	Geographic Latitude	Geographic Longitude	Zenith Angle	Data Availability	P_{med} (GV)
Brisbane	BNM	Neutron Monitor	28°S	153°E	-	1965-1990	28
Darwin	DNM	Neutron Monitor	12°S	131°E	-	1978-1990	50
Deep River	DRNM	Neutron Monitor	46°N	78°W	-	1965-1988	17
Embudo	EMBV	UG Muon	35°N	106°W	0°	1965-1990	135
	EMBN	UG Muon			45°N	1965-1990	140
Hobart	HNM	Neutron Monitor	43°S	147°E	-	1968-1990	17
	HUV	UG Muon			0°	1957-1989	185
	HUI	UG Muon			43°N	1973-1989	195
Kerguelen	KNM	Neutron Monitor	49°S	70°E	-	1965-1988	17
Mawson	MNM	Neutron Monitor	68°S	63°E	-	1957-1990	17
	MSV	Surface Muon			0°	1957-1971	50
	MUN	UG Muon			24°N	1973-1990	165
Mt. Wellington	MTNM	Neutron Monitor	43°S	147°E	-	1971-1990	17
Poatina	POAMU	UG Muon	42°S	138°E	0°	1972-1985	1400
Socorro	SOCV	UG Muon	34°N	107°W	0°	1968-1985	300
	SOCS	UG Muon			45°S	1968-1985	335
	SOCW	UG Muon			45°W	1968-1985	365

be detected. This is called the *negative temperature effect* - i.e. if the temperature increases the intensity of muons decreases.

Correction for these three effects needs to be made when considering cosmic ray data from muon telescopes. Neutron monitor count rates are not affected by the two temperature effects but all cosmic ray observations include variations due to pressure fluctuations. If one has enough atmospheric data then corrections for the atmospheric effects can be obtained using ordinary regression analysis (Fenton et al. 1961).

2.2.1 Correcting for the pressure effect

Baker et al. (1993b) presented the method of correcting for atmospheric effects and Baker (1993) explained the intricacies of this in his Ph.D. thesis. Only a quick review of this procedure is warranted here and the reader is directed to the above publications for a more thorough treatment.

To correct the recorded count rate C(t) of an instrument for fluctuations of the air pressure P(t), we assume that the intensity of secondary cosmic rays is exponentially related to pressure. The count rate can then be related to fluctuations of the pressure from some reference pressure (P_0) by

$$C(t,P) = C_{corr}(t)e^{\alpha_P(P(t)-P_o)} \tag{2.1}$$

The reference pressure is usually taken to be the mean pressure at the location of the instrument. α_P is called the total pressure coefficient and can be determined from a regression analysis of the count rate data with local atmospheric pressure recorded at the same time. Once α_P is determined the corrected count rate C_{corr} (i.e. the count rate that would have been determined if the pressure remained constant) can be found at any time (as long as the barometric pressure is continuously recorded) by

$$C_{corr}(t) = C(t,P)e^{-\alpha_P(P(t)-P_o)} \tag{2.2}$$

The pressure coefficient depends on the energy of the secondary particles (at higher energies pressure variations will affect the count rate less). The greater the atmospheric depth an instrument is viewing through (for example, an inclined telescope) the more effect pressure variations will have on the observed count rate. For these reasons, α_P must be determined for each instrument at an observing site. Most sea-level neutron monitors with geomagnetic cutoff rigidities less than about 3 GV will respond to the same energetic particles and hence can use the same pressure coefficient for correcting data (Hatton 1971). In practice different stations may use slightly different values.

2.2.2 Correcting for the temperature effects

The two temperature effects only influence the muon component of secondary cosmic rays. The same technique is employed to correct the count rate of muon telescopes for changes in the height of the muon production level and the temperature of the pion production level

(Duperier 1949). The pressure effect also needs to be accounted for but the total pressure coefficient can not be used when temperature corrections are made. In this case the partial pressure coefficient must be determined as must the partial temperature and height coefficients from the assumption

$$C(t,P,H,T) = C_{corr}(t)e^{[\alpha_P(P(t)-P_o)+\alpha_H(H(t)-H_o)+\alpha_T(T(t)-T_o)]} \tag{2.3}$$

The coefficients can again be calculated from a regression analysis of the count rate variation with atmospheric pressure, temperature of the muon production level and height of the pion production level. Baker et al. (1993b), when determining the temperature coefficients for surface muon telescopes at Mawson, Antarctica, used the height of the 125 mbar level as the mean height of pion production. This altitude of pressure has a variation between about 13 km and 14.5 km during a year. The mean temperature of the atmosphere between the 80 and 200 mbar levels was used as the temperature of the muon production level. This temperature varies between -40° C and -80° C during a year above Mawson.

Since the coefficients are small

$$C_{corr}(t) = \frac{C(t,P,H,T)}{1+[\alpha_P(P(t)-P_o)+\alpha_H(H(t)-H_o)+\alpha_T(T(t)-T_o)]} \tag{2.4}$$

None of the muon telescopes employed in the following investigations of cosmic ray anisotropies were corrected for temperature effects. Only total pressure coefficients were used to correct the data for atmospheric effects because :

- the net affect of the positive and negative temperature effects on Hobart underground muon telescopes' count rates are almost negligible (Fenton et al. 1961);
- the correcting coefficients at Embudo and Socorro are not known; and
- at Mawson, correcting for temperature effects is impossible for a complete day's data because height and temperature data are collected only twice a day by radiosondes on weather-balloons. However, the daily variations of the temperature of the atmosphere at this height over Mawson are relatively small and therefore temperature effects will be small when considered over the course of only a day. On the other hand, the seasonal variation of the temperature near Mawson is quite large compared to lower latitudes and any study requiring the direct comparison of Mawson-data collected at markedly different times of the year will need to be corrected for temperature effects. The MUN telescope (Table 2.1) was designed at a depth underground which is similar to that of the HUV undergound telescope to minimise the effects of the atmosphere. Being slightly shallower than HUV, the temperature effects do not cancel each other to the same extent as at HUV.

It should be noted that the difficulty of continuously obtaining radiosonde data applies to all the stations. This means that even if the coefficients for the Embudo and Socorro instruments were known, the same problem encountered when attempting to correct the Mawson data would be present.

2.3 Fourier analysis of cosmic ray data

To derive the diurnal variation in count rate data collected by a cosmic ray detecting instrument it is assumed that the count rate C(t) can be described as a series expansion F(t).

$$C(t) \approx F(t) = \sum_{m=1}^{\infty} A_m \cos\frac{2\pi m}{24}(t - t_m)$$

i.e.

$$= \sum_{m=1}^{\infty}\left[a_m \cos\frac{2\pi m}{24}t + b_m \sin\frac{2\pi m}{24}t \right] \tag{2.5}$$

where

$$A_m = \sqrt{(a_m)^2 + (b_m)^2}$$

$$t_m = \frac{24}{2\pi m}\arctan\left(\frac{b_m}{a_m}\right) \tag{2.6}$$

From a set of N observations of an instrument's count rate ($U_0, U_1, U_2, \ldots U_{N-1}$) collected over equal sampling times, the best fit F(t) to the data will be found from

$$a_m = \frac{2}{N}\sum_{k=0}^{N-1} U_k \cos\left(\frac{2\pi mk}{N}\right)$$

$$b_m = \frac{2}{N}\sum_{k=0}^{N-1} U_k \sin\left(\frac{2\pi mk}{N}\right) \tag{2.7}$$

In deriving the Fourier components (a_m, b_m) of the daily variation in the data, it is usual to derive the amplitude as a percentage deviation from the mean count rate of the time interval over the day. This is done by defining each ordinate U_k as

$$U_k = \frac{C_k - \overline{C}}{\overline{C}} \times 100\% \tag{2.8}$$

where C_k is the total number of counts recorded by an instrument during a pre-determined time interval and $\overline{C}$ is the *average* count rate for the time interval determined from the complete day's data. Usually the time interval is one hour (N=24). The solar diurnal variation is found when m=1 and the solar semi-diurnal variation when m=2.

The above expressions are only correct for instantaneous measurements of U_k. In the expression (2.7) if N=24, data accumulated during hour 1 (midnight to 0100) is U_0. Therefore, the ordinate U_k can only be considered accurate at the time half way between hour k+1 to k. In effect, the ordinate U_k can be thought of as an average value of the data at k hours plus 30 minutes. For N ordinates the calculated phase t_m needs to be corrected by 12/N hours because the fitting procedure begins at midnight but should begin at 0000 + 12/N hours.

i.e. $$t_m = \frac{24}{2\pi m}\arctan\left(\frac{b_m}{a_m}\right) + \frac{12}{N} \quad \text{(hours)} \tag{2.9}$$

This also produces a small correction to the amplitude (Parsons 1959) :

$$A_m = \frac{\omega}{\sin\omega}\sqrt{(a_m)^2 + (b_m)^2}\ , \text{ where } \omega = \frac{m\pi}{N} \tag{2.10}$$

The above illustrates the theory of Fourier analysing data for a periodic variation. This thesis is only concerned with diurnal variations which have a period of 24 hours (m=1). In deriving the yearly averaged results of Fourier analysed cosmic ray data some other factors must also be considered. The procedure used to derive the yearly averaged solar, sidereal and anti-sidereal diurnal variations in this thesis is outlined below.

Each day is classed according to the sector polarity of the IMF for that day. IMF polarity determinations from 1957 to 1990 were made from a variety of sources : direct spacecraft measurement of the IMF (Couzens and King 1986), IMF inferred directions from polar magnetograms (Svalgaard 1976), the Stanford Mean Solar Magnetic Field (Solar Geophysical Data Prompt Reports) moved forward in time by 5 days and polar rain data (Gussenhoven 1990). The IMF database was compiled over the years by Dr. J. E. Humble and his colleagues up to the end of 1985 and extended for this thesis up to the end of 1990 from polar rain data which were supplied by M. S. Gussenhoven (1993).

All hourly data are pressure corrected as described in Section 2.2.1. Individual days of data arranged in solar time were rotated around the mean of the day to remove secular trends (long-term modulation effects and any efficiency changes in the counters) and then harmonically (Fourier) analysed. To remove any secular trends from day_J a straight line is fitted between the average value of U_0 of day_J and U_{23} of day_{J-1} and the average value of U_{23} of day_J and U_0 of day_{J+1}. This allows the magnitude of the line at the hour boundary between U_{11} and U_{12} (i.e. the midpoint of day_J) to be taken as the mean point for the rotation of the data for day_J. Secular trends are removed in this manner for every day of the year except the first and final days of each year which are omitted from the analysis.

Days with an hourly residual value (after harmonic analysis) greater than 4-sigma (5-sigma for IQSY neutron monitors) were rejected. This technique removed Forbush decreases, ground level enhancements and other transient phenomena.

Each year of results were then segregated into three groups - days corresponding to times when the Earth was in a Towards IMF sector, an Away IMF sector and a group comprised of the complete set of Fourier results for the year regardless of the IMF sector at the Earth. The individual yearly averaged vectors of these three groups were obtained by simply averaging the vector components (a_m, b_m). The uncertainties in the resulting average components were calculated from the scatter of the values for individual days.

A similar analysis was repeated in sidereal and anti-sidereal time. Anti-sidereal time has no physical meaning, but the results obtained were used to remove an unwanted spurious

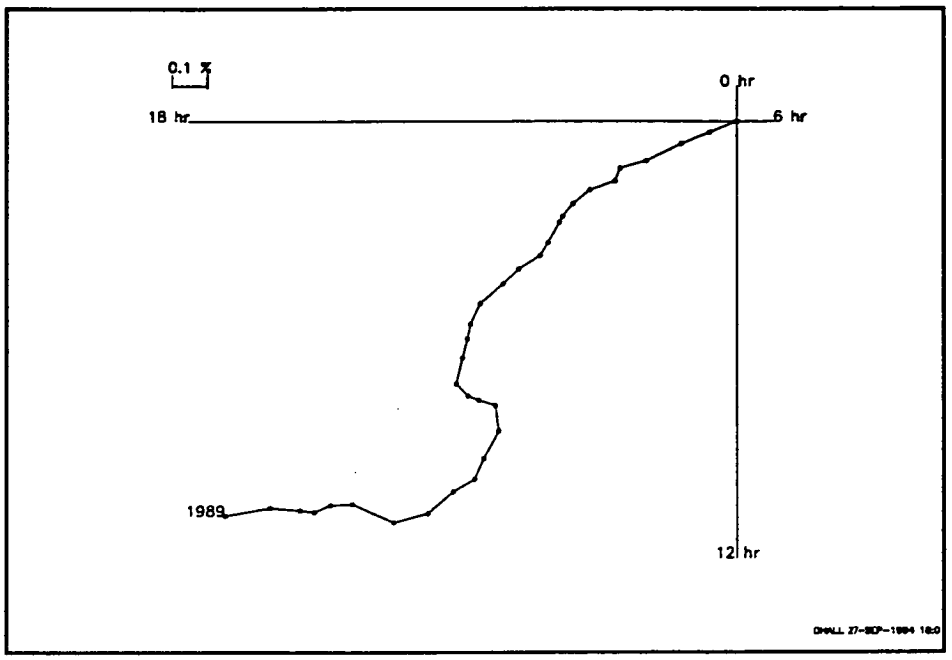

Figure 2.1a Vector sum diagram of the yearly averaged solar diurnal variation in Hobart underground muon telescope (HUV) data from 1957 to 1989. The median rigidity of HUV is 185 GV.

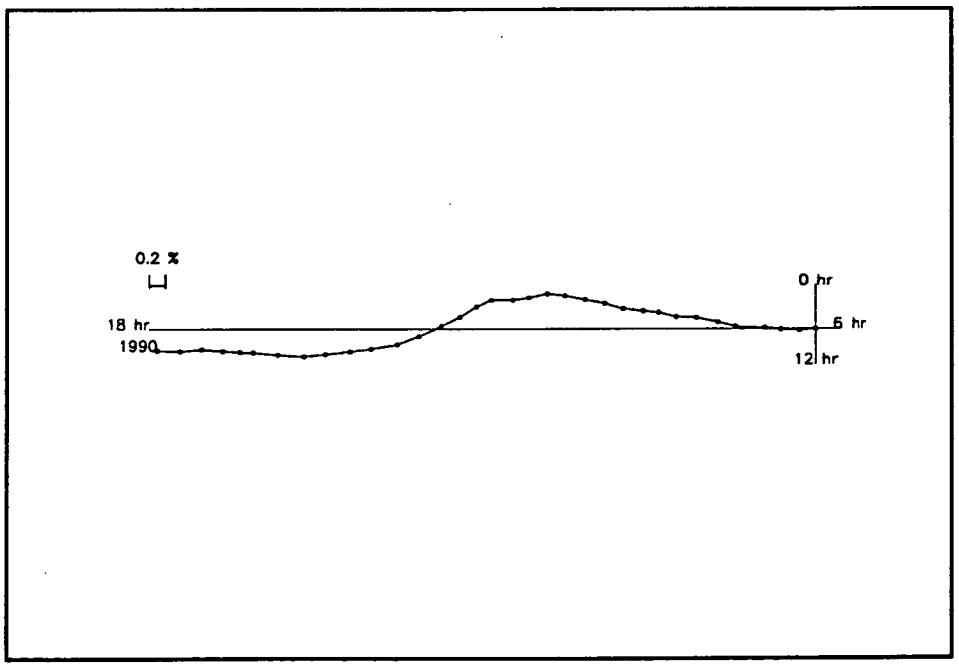

Figure 2.1b Vector sum diagram of the yearly averaged solar diurnal variation in Mawson neutron monitor (MNM) data from 1957 to 1990. The median rigidity is 17GV.

modulation present in the sidereal time data. This spurious signal is due to the annual modulation of the solar semidiurnal anisotropy (Nagashima et al. 1985) which produces a sidereal and an anti-sidereal variation and is explained in more detail in Section 2.6.

The results of harmonically analysed data for the m=1 harmonic can be represented as a vector with length A_1 and angle $(2\pi t_1/24)$ relative to 0 degrees. A plot of these vectors is called an harmonic dial. The usual practice is to present an harmonic dial with angle zero degrees (midnight) upwards and time moving forwards in the clockwise direction. To represent the results from analysis of many years' data a vector sum diagram can be made by adding successive vectors at the end of a preceding year's vector on an harmonic dial. In this way any variations of the amplitude and/or the phase from year to year can easily be seen.

The vector sums, plotted on harmonic dials, have been presented in Figure 2.1 for neutron monitor and underground muon data analysed in solar time from 1957 to the last solar maximum. Note the variation in the phase has a period of about 22 years. It is also obvious that the variation in the phase is larger in the muon telescope results. The amplitudes also have a variation, being smaller around years of solar minimum.

2.4 Missing data

For various reasons such as power failures, laboratory fires and electronic faults, the continuous operation of a cosmic ray instrument for an entire year is almost impossible and principal investigators of cosmic ray projects should be commended for the quality of data available today. Nonetheless, some years' data do have significant numbers of days missing from them, occasionally more than a month. Yearly averaged results which are obtained from data with many months missing are probably not free of seasonal effects. It was decided that years which had more than one whole month of data missing should have the yearly averaged results corrected by using the data from the corresponding months in the years directly preceding and following that erroneous year. Years which were missing more than five months of data would be rejected from the studies entirely. An example of the correcting procedure applied to the results of analysing the Mawson underground muon telescope MUN in solar time is outlined below. This instrument was inoperative for three months during 1978 following a fire in the laboratory.

The average components (a,b) for February to April of 1977 and 1979 were obtained from the relation

$$X_{\text{Feb-April}} = \frac{\text{Days}_{\text{Feb}} X_{\text{Feb}} + \text{Days}_{\text{March}} X_{\text{March}} + \text{Days}_{\text{April}} X_{\text{April}}}{\text{Days}_{\text{Feb}} + \text{Days}_{\text{March}} + \text{Days}_{\text{April}}} \qquad (2.11)$$

where X is either component a or b.

e.g. the correction procedure applied to MUN Fourier analysis results for 1978 :

Notes 1st harmonic	Days	a (% x 1000)	b (% x 1000)
Incorrect 1978 (Jan + May to Dec)	244	-71	-30
1977			
Feb	28	70	-53
March	31	-27	-24
April	30	-5	-14
Feb to April	89	11	-30
1979			
Feb	25	20	-159
March	31	-1	-142
April	30	-51	-75
Feb to April	86	-12	-124
Corrected 1978	419	-41	-37

To correct the 1978 (a, b) components :

$$X_{corrected} = \frac{Days_{1977}X_{1977} + Days_{1978}X_{1978} + Days_{1979}X_{1979}}{Days_{1977} + Days_{1978} + Days_{1979}}$$

e.g.
$$a_{corrected} = \frac{(89 \times 11) + (244 \times -71) + (86 \times -12)}{89 + 244 + 86}$$

Of course the number of terms in (2.11) depend on the number of months missing from the particular year. This procedure was applied to solar, sidereal and anti-sidereal time results. Surprisingly, only 6 instrument-years were completely rejected and 9 instrument-years needed to be corrected by the above method, a very small amount considering that over 300 instrument-years of data were used (Table 2.2).

Table 2.2 Data corrected for missing months and completely rejected

Telescope data corrected	Year	Months	Telescope data rejected
BNM	-	-	1974 1975 1976
HNM	1973 1978	Oct., Nov., Dec. Jan., Feb., Mar.	1974 1975
HUI	1973	Jan., Feb., Mar., Apr., May	-
HUV	1957	Jan., Feb., Mar., Apr.	-
MNM	1957 1972	Jan., Feb., Mar. Oct., Nov., Dec.	1973
MSV	1957	Jan., Feb., Mar., Apr.	-
MUN	1973 1978	Jan., Feb., Mar. Feb., Mar., Apr.	-

2.5 Coupling coefficients

Once a primary particle enters the Earth's magnetosphere its direction of motion will be altered as it gyrates around the Earth's magnetic field lines. Secondary particles travel such short distances that they are not noticeably affected by the geomagnetic field, but particles detected at one location on Earth with a certain arrival direction are likely to be due to primaries that entered the magnetosphere from another direction. The original direction of travel is termed the particle's *asymptotic direction of approach*, and the alteration of a particle from its asymptotic direction by the geomagnetic field is called *geomagnetic deflection.*

The magnetic deflection of primaries can cause the local time of maximum of the variation (indicative of the streaming direction of particles; see Figure 1.3) to be quite different from the actual direction of streaming of primaries in free-space. Magnetic deflection will also spread out the anisotropic distribution in the magnetosphere causing the apparent magnitude of the anisotropy to be smaller than its true value. Also, particles need greater magnetic rigidity to reach equatorial regions since they must travel across magnetic lines of force to gain access. At any given latitude, part of the spectrum of particles below a *cut-off* rigidity (P_c) is consequently cut-off from detection. There is also a smaller cut-off rigidity affect on the longitude of particle detection because the geomagnetic field is offset from and inclined relative to the rotation axis. In effect, this means that the asymptotic cone of acceptance (see Chapter 1) of a cosmic ray telescope may not be located in the direction which the instrument

is pointing. It is this displacement of the asymptotic cone of acceptance of an instrument which allows some instruments in Antarctica (used in the example of geomagnetic deflection in the introduction to this chapter) to respond ultimately to primary particles with equatorial asymptotic directions. Therefore we must make use of the asymptotic cone of acceptance of an instrument to investigate cosmic ray anisotropies.

The asymptotic cone of acceptance is a function of particle energy, geographic longitude and latitude, detector response to secondaries and the varying geomagnetic field. Detectors of different types or having different local viewing directions will have different asymptotic cones of acceptance even if they are at the same location. The muon and neutron components of secondary cosmic rays are produced by different mechanisms; different numbers of secondaries are produced depending on the energy of the primary particle. Hence, the response of instruments to the primary flux depends on the component of secondary cosmic rays being detected and the instruments' asymptotic cones of view (Rao et al. 1963). Thus, two detectors that observe the same anisotropy's diurnal variation may see different times of maximum and different amplitudes. Coupling coefficients will remove these differences by taking into account the above processes and are used to relate the variation seen at Earth by different telescopes to the actual anisotropy in free space (Nagashima 1971, Yasue et al. 1982, Fujimoto et al. 1984).

The notion of coupling an instrument's count rate to the primary intensity in free-space has been used for many years (Rao et al. 1963, Humble 1971). Nagashima (1971) formulated a theory for relating an observed diurnal variation to an anisotropy. Not only does this formalism take account of the processes described above but also that a single anisotropy can be responsible for multiple variations in the intensity of secondary particles. For example, a bi-directional anisotropy will be observed as only a semi-diurnal variation in the data recorded by an instrument which has its cone of view scanning the celestial equator. The same anisotropy will appear as a diurnal variation and smaller semi-diurnal variation in data recorded by an instrument with its cone of view scanning mid-latitudes. Nagashima's formalism accounts for this by using spherical harmonic expansions of anisotropies. This formalism is used throughout this thesis, so a summary of the theory is required. A more detailed treatment can be found in Nagashima (1971).

2.5.1 Nagashima's formalism

In his theory, Nagashima assumes that an anisotropy is symmetric about some axis. If this is not true, the anisotropy can be decomposed into a series of axis symmetric anisotropies and the theory applied to each term in the series separately. For now we assume a single axis symmetric anisotropy.

Consider the intensity $I(P,\chi,\Lambda)$ of primary particles directed from a point J in space toward O, related to the symmetry axis **OR** of an anisotropy as shown in Figure 2.2. $I(P,\chi,\Lambda)$ has an anisotropic component $\delta I(P,\chi,\Lambda)$ and an isotropic component $I(P)$.

i.e. $$I(P,\chi,\Lambda) = I(P) + \delta I(P,\chi,\Lambda) \qquad (2.12)$$

The anisotropy relative to the average intensity is

$$\frac{\delta I(P,\chi,\Lambda)}{I(P)} = \frac{I(P,\chi,\Lambda) - I(P)}{I(P)} \tag{2.13}$$

We assume that rigidity is separable from the spatial coordinates (and naturally the Λ dependence vanishes due to the symmetry) :

$$\frac{\delta I}{I} = F(\chi)G(P) \tag{2.14}$$

$F(\chi)$ is called the *space distribution* of the anisotropy. $G(P)$ is the *rigidity spectrum* of the anisotropy. The space distribution can be written as a series expansion of ordinary Legendre Polynomials, each with an amplitude η_n.

i.e. $$F(\chi) = \sum_{n=0}^{\infty} F_n(\chi) = \sum_{n=0}^{\infty} \eta_n P_n(\cos\chi) \tag{2.15}$$

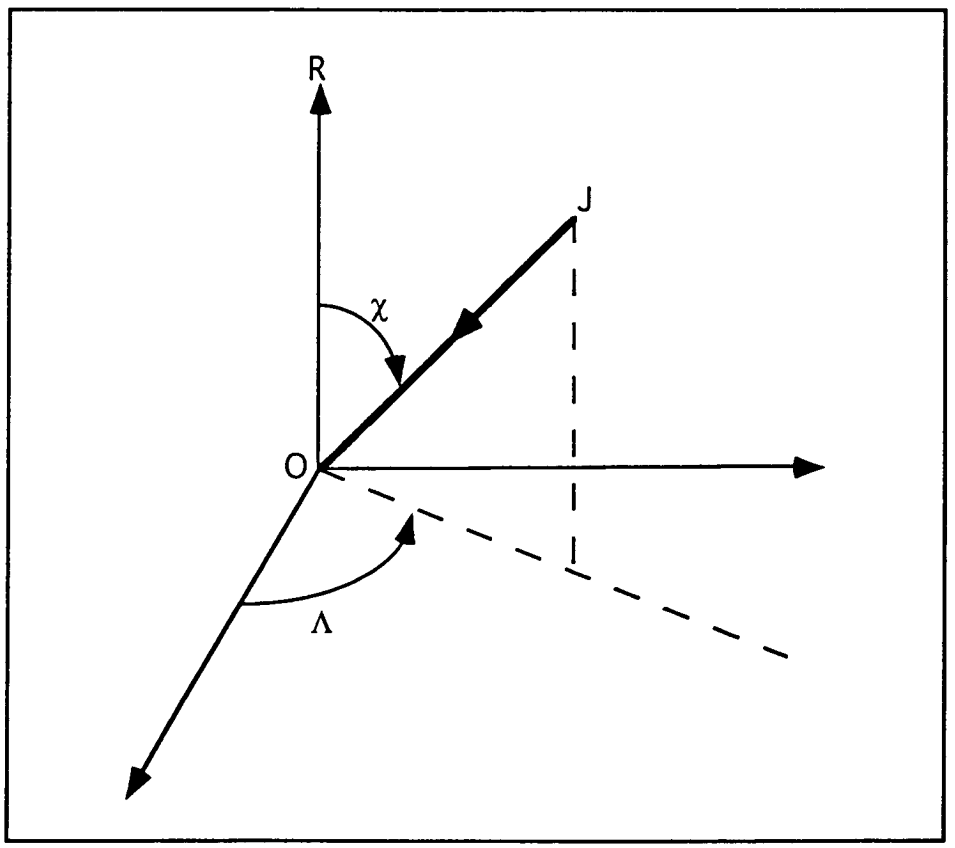

Figure 2.2 Intensity of cosmic rays along the direction **JO** relative to the axis of symmetry **OR**

Each $F_n(\chi)$ is called the nth space-distribution of $F(\chi)$. Essentially, $F(\chi)$ is the total anisotropic distribution, made up of many anisotropies with the same reference axis **OR**. Whether or not every $F_n(\chi)$ in the anisotropy exists is another question entirely, and is not addressed in this thesis. In fact it is assumed that most $F_n(\chi)$ do not exist.

If the direction of the reference axis, the rigidity spectrum G(P) and each η_n in (2.15) are known then we know everything about the anisotropic distribution of primary cosmic rays.

Each space distribution $F_n(\chi)$ is relative to **OR**. The reference system to which every Earth based instrument is related is the celestial sphere (equatorial coordinate system). Each space distribution $F_n(\chi)$, relative to **OR**, can be related to the equatorial system by summing the n+1 projections of $F_n(\chi)$ in the equatorial system.

i.e.
$$F_n(\chi) = \sum_{m=0}^{n} \eta_n f_n^m(\theta_R, \alpha_R, \theta_J, \alpha_J) \tag{2.16}$$

where (θ_R, α_R) are the co-declination and right-ascension of the reference axis, (θ_J, α_J) are the co-declination and right-ascension of the particles directed along **JO**,

$$f_n^m(\theta_R, \alpha_R, \theta_J, \alpha_J) = P_n^m(\cos\theta_R) P_n^m(\cos\theta_J) \cos m(\alpha_J - \alpha_R) \tag{2.17}$$

where

$$P_n^m(x) = \begin{cases} P_{n,m}(x), & m = 0 \\ \sqrt{\dfrac{(n-m)!}{(n+m)!}}\, P_{n,m}(x), & m \neq 0 \end{cases}$$

$P_n^m(x)$ are called the semi-normalized spherical functions, related to associated Legendre polynomials $P_{n,m}(x)$.

Then
$$\begin{aligned} F(\chi) &= \sum_{n=0}^{\infty} \eta_n P_n(\cos\chi) \\ &= \sum_{n=0}^{\infty} \sum_{m=0}^{n} \eta_n f_n^m(\theta_R, \alpha_R, \theta_J, \alpha_J) \end{aligned} \tag{2.18}$$

Consider our previous example, a bi-directional (and no other) anisotropy with the symmetry axis along (θ_R, α_R). This anisotropy will have :

$$\begin{aligned} F(\chi) &= \eta_2 P_2(\cos\chi) \\ &= \sum_{m=0}^{2} \eta_2 f_2^m(\theta_R, \alpha_R, \theta_J, \alpha_J) \\ &= \eta_2 f_2^0 + \eta_2 f_2^1 + \eta_2 f_2^2 \end{aligned} \tag{2.19}$$

f_2^2 is the anisotropy's component responsible for the semi-diurnal variation and f_2^1 is responsible for only a diurnal variation. $P_n^m(\cos\theta_J)$ is called the *latitude factor* and describes the dependence of the observed diurnal variation on the latitude of the asymptotic cone of acceptance.

Nagashima defines the *Space Harmonic Component* $S_n^m(t)$ as

$$\begin{aligned} S_n^m(t) &= \eta_n P_n^m(\cos\theta_R)\cos m(\alpha_J - \alpha_R) \\ &= \eta_n P_n^m(\cos\theta_R)\cos\frac{2\pi m}{24}(t_J - t_R) \\ &= x_n^m \cos\frac{2\pi m}{24}t_J + y_n^m \sin\frac{2\pi m}{24}t_J \end{aligned} \tag{2.20}$$

where

$$\begin{aligned} \eta_n P_n^m(\cos\theta_R) &= \sqrt{\left(x_n^m\right)^2 + \left(y_n^m\right)^2} \\ t_R &= \frac{24}{2\pi m}\arctan\left(\frac{y_n^m}{x_n^m}\right) \\ \alpha &= \frac{2\pi}{24}t \end{aligned} \tag{2.21}$$

The space harmonic component $S_n^m(t)$ is the time variation that an instrument would see in free-space during a day due to the m'th projection of $F_n(\chi)$ in the equatorial coordinate system. It is also called the *free-space time variation.*

Strictly speaking, the above formalism is only correct for anisotropies fixed with respect to the stars. A solar anisotropy will be fixed with respect to the Sun and during a year θ_R and α_R will vary as the Earth orbits the Sun. Nagashima has, however, transformed θ_R and α_R into ecliptic coordinates and shown that yearly averages of solar anisotropies with reference axes close to the ecliptic plane will satisfy the theory and we can consider the $P_n^m(\cos\theta_R)$ term to be $P_n^m(0)$ (Nagashima and Ueno 1971).

We want to measure $S_n^m(t)$ from Earth. Each $S_n^m(t)$ will produce a diurnal variation $D_n^m(t)$ in an instrument's count rate at Earth.

$$\begin{aligned} D_n^m(t) &= A_n^m \cos\frac{2\pi m}{24}(t - t_n^m) \\ &= a_n^m \cos\frac{2\pi m}{24}t + b_n^m \sin\frac{2\pi m}{24}t \end{aligned} \tag{2.22}$$

The observed daily variation of the count rate will be

$$D(t) = \sum_{n=0}^{\infty}\sum_{m=0}^{n} D_n^m(t) \tag{2.23}$$

We can use $D_n^m(t)$ to infer $S_n^m(t)$. Assuming we can isolate $D_n^m(t)$, Fourier analysis allows us to determine a_n^m and b_n^m and hence A_n^m and t_n^m. We need the transformations δA_n^m and δt_n^m which allow us to infer the *amplitude* and *phase* $(\eta_n P_n^m(\cos\theta_R), t_R)$ of the space

harmonic component from the amplitude and phase (A_n^m, ζ_n^m) of the observed diurnal variation. If G(P) and θ_R are known then the anisotropy of cosmic rays can be determined.

The transformations are the coupling coefficients mentioned previously and depend on the asymptotic cone of acceptance and hence the latitude and longitude of the detector, the geometry of the detector and the response of the detector to the primary flux. Thus they depend on the rigidity spectrum of the free-space anisotropy and the response function of the instrument. Coupling coefficients (in their simplest form) actually relate (a_n^m, b_n^m) to (x_n^m, y_n^m) by

$$\begin{aligned} a_n^m &= c_n^m x_n^m + s_n^m y_n^m \\ b_n^m &= -s_n^m x_n^m + c_n^m y_n^m \\ \text{then} \quad A_n^m &= (\delta A_n^m)\eta_n P_n^m(\cos\theta_R) \\ t_n^m &= t_R - \delta t_n^m \\ \text{where} \quad \delta A_n^m &= \sqrt{\left(c_n^m\right)^2 + \left(s_n^m\right)^2} \\ \delta t_n^m &= \frac{24}{2\pi}\arctan\left(\frac{s_n^m}{c_n^m}\right) \end{aligned} \tag{2.24}$$

The relations in (2.24) are essential for deriving free-space anisotropies from ground based observations of the corresponding daily variations.

The rigidity spectrum G(P) used to calculate coupling coefficients is usually based on the form

$$G(P) = \begin{cases} \left(\frac{P}{10}\right)^{\gamma}, & P \le P_u \\ 0, & P > P_u \end{cases} \tag{2.25}$$

This shows how the coupling coefficients are explicitly dependent on the spectral index γ, and the upper limiting rigidity P_u of an anisotropy.

δA_n^m couples the observed amplitude of a diurnal variation (A_n^m) to the amplitude of the responsible space distribution's (F_n) projection $(\eta_n P_n^m(\cos\theta_R))$ into the equatorial coordinate system. δt_n^m is the amount of deflection (in time) that the phase (t_R) of a space distribution undergoes due to the geomagnetic field.

Using coupling coefficients

If G(P) and θ_R of the anisotropy is known or assumed then a single observation of $D_n^m(t)$ will give

$$\eta_n = \frac{A_n^m}{(\delta A_n^m) P_n^m(\cos\theta_R)} \qquad (2.26)$$

$$\text{and} \quad t_R = t_n^m + \delta t_n^m$$

This technique is employed in Chapters 3 and 4 to infer the free-space amplitude and phase of the solar and sidereal diurnal anisotropies and derive modulation parameters from them. The rigidity spectra and knowledge of the reference axes of the anisotropies are assumed in these sections.

If G(P) is not known, the formalism can be used to simultaneously derive the free-space harmonic component and the rigidity spectrum. By observing many $a_{n,i}^m$, $b_{n,i}^m$ from i=1,...,k instruments and using the relations in (2.24) we can define χ^2 as (Nagashima 1971):

$$\begin{aligned}\chi^2 &= \sum_{i=1}^{k}\left[\left(a_{n,i}^m - a_n^m\right)^2 + \left(b_{n,i}^m - b_n^m\right)^2\right] \\ &= \sum_{i=1}^{k}\left[\left(a_{n,i}^m - \left(c_{n,i}^m x_n^m + s_{n,i}^m y_n^m\right)\right)^2 + \left(b_{n,i}^m - \left(-s_{n,i}^m x_n^m + c_{n,i}^m y_n^m\right)\right)^2\right]\end{aligned} \qquad (2.27)$$

For an assumed G(P) the best fit x_n^m, y_n^m to the anisotropy can be found and χ^2 evaluated. Choosing another spectrum (i.e. changing γ and P_u) the best fit x_n^m, y_n^m can again be determined and the corresponding value of χ^2 evaluated and compared to the previous value of χ^2. The lowest χ^2 in the entire space of γ and P_u will indicate the most likely rigidity spectrum of the anisotropy and also the values of the corresponding components of $S_n^m(t)$. This technique is also employed in Chapters 3 and 4 to derive the rigidity spectra of the solar diurnal anisotropy and the North-South anisotropy. In those analyses, the space of (γ, P_u) considered to contain the true spectra of these anisotropies consists of $\gamma \in$ [-1.5, 1.0] and $P_u \in$ [30, 1000 GV].

2.5.2 Calculation of coupling coefficients

The coupling coefficients c_n^m and s_n^m for muon telescopes can be calculated from (Baker 1988) :

$$\begin{aligned} c_n^m &= \frac{1}{I}\int_{P_c}^{\infty}\int_{\Omega} Y A G(P) P_n^m(\cos\theta)\cos\left[m(\psi_{or} - \psi_{st})\right] d\omega\, dP \\ s_n^m &= \frac{1}{I}\int_{P_c}^{\infty}\int_{\Omega} Y A G(P) P_n^m(\cos\theta)\sin\left[m(\psi_{or} - \psi_{st})\right] d\omega\, dP \end{aligned} \qquad (2.28)$$

where $I = \int_{P_c}^{\infty}\int_{\Omega} Y A \, d\omega\, dP$ and

Y = Y(P, d, x, θ, ψ) is the response function, in units of particles $s^{-1}m^{-2}str^{-1}$, which gives the number of muons produced by primary particles of rigidity P, arriving at a telescope

looking through an atmospheric depth of d and a rock depth of x along the direction defined by (θ, ψ);

A = $A(\theta, \psi)$ is the geometric factor which gives the relative overlap of the two outer trays constituting the muon telescope in the direction (θ, ψ), in m^2str^1;

$\theta_{or} = \theta_{or}(P, \lambda_{st}, \psi_{st}, \theta, \psi)$ is the geographic co-latitude defining the asymptotic direction of approach of primary particles with rigidity P which produce muons arriving with a local direction defined by (θ, ψ) at the telescope site with geographic latitude and longitude of $(\lambda_{st}, \psi_{st})$;

$\psi_{or} = \psi_{or}(P, \lambda_{st}, \psi_{st}, \theta, \psi)$ is the corresponding geographic longitude;

Ω is the solid angle subtended by the muon telescope trays; and

$d\omega$ is the element of solid angle (= $\sin\theta\, d\theta\, d\psi$).

A similar expression is used for the calculation of neutron monitor coupling coefficients except the response functions are significantly different and do not depend on rock depth x.

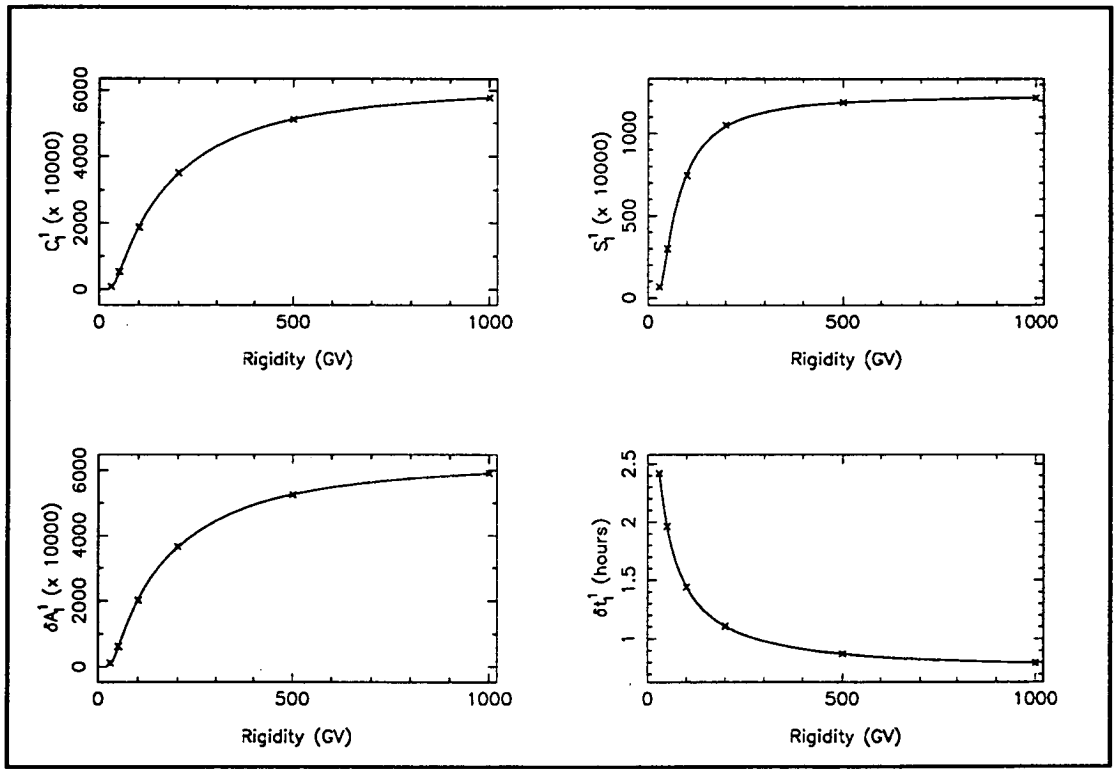

Figure 2.3 Coupling coefficients evaluated for the Hobart vertical underground muon telescope. The points indicate the coefficients calculated from the differential coupling coefficients and the solid lines are the interpolation functions used to calculate coupling coefficients for non-standard combinations of the spectral parameters (γ, P_u). In this case $\gamma = 0$.

c_n^m and s_n^m have been tabulated for standard combinations of (γ, P_u) for all the cosmic ray neutron monitors and underground muon telescopes used in these analyses except for MSV and MUN (Yasue et al. 1982, Fujimoto et al. 1984). The method used to calculate the coupling coefficients of these two instruments will be presented in the following section.

Differential coupling coefficients have also been tabulated by Yasue et al. (1982) and Fujimoto et al. (1984). These coefficients (dc_n^m, ds_n^m) express the coupling (as explained above) of the secondary flux to the primary flux *between* rigidity bands for an assumed rigidity spectrum with $\gamma = 0$. From these coefficients one can derive the integral coupling coefficients (c_n^m, s_n^m) for any γ (in 2.25) in the tabulated discrete steps of P_u.

In the analyses presented in Chapters 3 and 4, coupling coefficients were needed for combinations of (γ, P_u) other than those previously reported. The differential coupling coefficients were used to evaluate c_n^m and s_n^m at P_u = (30, 50, 100, 200, 500 and 1000 GV) for all the instruments in Table 2.1 (except MSV and MUN) at any value of γ. The corresponding coupling coefficients δA_1^l and δt_1^l were calculated, enabling interpolation of coupling coefficients for other values of P_u. The interpolation function used was usually a third order polynomial. From the above procedures any values of c_1^l, s_1^l, δA_1^l and δt_1^l could be obtained for γ between -1.5 and 1.0 and for P_u between 30 and 1000 GV (see Figure 2.3). Most values of the coefficients calculated by this method were less than 2% different from those tabulated and all were within 5%. Nagashima suggests that his calculations have at least 5% uncertainty so these interpolations should be acceptable.

Coupling coefficients of the Mawson surface and underground muon telescopes

Baker (1988) and Baker et al. (1990) developed computer software to calculate coupling coefficients using Nagashima's (1971) theory. This software was employed to calculate the coupling coefficients of the MSV and MUN telescopes at Mawson, tabulated in Table 2.1. Coupling coefficients were calculated for the required γ values and the standard values of P_u. Interpolation was carried out as described above.

A subtle correction was used for MUN before the interpolating procedure. MUN is a multi-section telescope which comprised Geiger counters in its earlier years and proportional counters more recently. The sections were of equal size from 1973 to 1982 and the effective surface areas of each of the six counter trays of the sections were 0.5 m^2. Hence the coupling coefficients of each section are the same as the overall telescope formed when the data are combined. From 1982 to the beginning of 1984 four of the Geiger sections were replaced by a telescope made from proportional counters with two sections, each with an area of 2.3 m^2. The coupling coefficients of the Geiger tube and proportional counter sections were different so the combined telescope's coupling coefficients needed to be an average of the coupling coefficients of two different sections, each term of the average being weighted by the corresponding section's surface area. The efficiencies of Geiger and proportional counters are slightly different due to quantum effects in the recombination of the ions produced in the process of detecting a particle passing through the tube. The average count rates of the two systems could also have been used in the averaging proceedure to determine the coupling coefficients of the combined telescope but it was felt that the surface area effects would be more dominant. The same process was used for the coupling coefficients for MUN data recorded from 1984 to the present. At the beginning of this period the other Geiger sections were replaced by two sections comprised of proportional counters with equal surface areas of 1.8 m^2. During 1984, the coincidence system of MUN was completely changed from a triple coincidence system to a double coincidence system. This method of detection employs a double resolving time in the electronic coincidence circuit to remove

accidental (chance) coincidence counts from the data and is described fully by Jacklyn and Duldig (1987).

Neutron monitor coupling coefficients at solar maximum and minimum

From solar maximum to minimum, the primary proton rigidity spectrum changes significantly in the energy range to which neutron monitors respond. Hence the coupling coefficients change during this time. The neutron monitor coupling coefficients data-base compiled by Fujimoto et al. (1984) contains two sets of coefficients - one for solar maximum conditions and the other for solar minimum conditions. Both sets have been used in the above procedure to calculate coupling coefficients depending on the solar activity at the time the cosmic ray data were recorded. Years when the yearly averaged sunspot number was greater than 50 have been defined as solar maximum conditions throughout this thesis. See Figure 1.1 for the yearly sunspot numbers from 1957 to 1990. Table 2.3 lists these years and those of solar minimum.

Table 2.3 Years corresponding to times of solar maximum and minimum.

Solar maximum years	Solar minimum years
1957 - 1961	1962 - 1966
1967 - 1972	1973 - 1977
1978 - 1983	1984 - 1987
1988 - 1990	

2.6 Spurious modulations

It was noted at the beginning of this chapter that certain procedures can be used to remove unwanted variations from Fourier analysis results. Since the daily variation of the data is caused by the superposition of many space harmonic components we would like to remove all variations other than the variation under investigation. For example, removing days of Forbush decreases and GLE's from the data will remove most $D_n^0(t)$ variations from the results and yearly averages will remove any seasonal variations from solar time results. Unfortunately, when all the above methods are used to study the yearly averaged solar and sidereal diurnal variations, the results of the Fourier analyses may still be contaminated by spurious diurnal variations related to other anisotropies which have the same forms of space distributions. This section is concerned with removing these contaminations from the yearly averaged results before attempting to infer the free-space anisotropies.

2.6.1 Spurious sidereal diurnal variation

The a_2 and b_2 components which result from Fourier analysing data in solar time (see equations 2.5 to 2.7) are significant and are due to the *solar semi-diurnal anisotropy*. This bi-directional anisotropy is a depletion of particles along the direction of the IMF. The co-declination of the reference axis of this anisotropy undergoes an annual variation as the Earth orbits the Sun. This is akin to modulating a signal with 365 cycles per year by a signal with 1 cycle per year. This will produce a signal with 365 ± 1 cycles per year. Consequently, part of the yearly averaged sidereal diurnal variation (366 cycles per year) is due to the annual modulation of the solar semi-diurnal variation. There will also be a diurnal variation in the data arranged in anti-sidereal time (364 cycles per year) due solely to the annual modulation of the solar semi-diurnal anisotropy. It has been shown that the yearly averaged sidereal diurnal variation caused by the solar semi-diurnal anisotropy occurs 4.53 hours earlier than the yearly averaged anti-sidereal diurnal variation and is 0.947 times smaller (Nagashima et al. 1985). Hence, the anti-sidereal variation can be used to remove the contribution of the solar semi-diurnal variation from the sidereal diurnal variation results.

The procedure to remove the unwanted semi-diurnal variation contamination from the results of the sidereal diurnal variation analysis is outlined below :

1. Fourier analyse data in sidereal and anti-sidereal time and obtain the yearly averaged first harmonic results.
2. Rotate the anti-sidereal vector anti-clockwise by 4.53 hours.
3. Multiply the amplitude of the anti-sidereal vector by 0.947.
4. Subtract the rotated and shortened vector from the yearly averaged sidereal diurnal variation vector.

The resultant vector will be the yearly averaged sidereal diurnal variation free from the influence of the annual modulation of the solar semi-diurnal variation. This procedure has been applied to all the sidereal diurnal variation results used in this thesis.

2.6.2 Spurious solar diurnal variation

Obtaining the amplitude and phase of the solar diurnal variation in neutron monitor data is a relatively simple task and involves only harmonically analysing the hourly data. Most of the response of underground muon telescopes is ultimately from primary particles with rigidities greater than 100 GV. Since the upper limit to the rigidity of particles that will participate in the diurnal anisotropy (P_u) is of this order (see Chapter 1) then an additional correction to results obtained from muon data is required. The additional correction is to remove a contamination of the data by particles with greater rigidity than P_u but which are still detected by the telescope. This contamination manifests itself as a spurious diurnal variation (Ahluwalia and Erickson 1969) termed the Orbital Diurnal Variation and is a Compton-Getting anisotropy (ξ_{CG}, Compton and Getting 1935).

Compton and Getting first quantitatively described an observer moving (with respect to a stationary frame of reference) in an isotropic flux of cosmic-ray particles. The result is an observed anisotropy related to the velocity of the observer. Forman (1970) was able to dispel

any confusion about the Compton-Getting effect, producing the expression for the resulting free space anisotropy :

$$\xi_{CG}(\chi) = \eta_{CG} P_1(\cos\chi) \tag{2.29}$$

which has amplitude :

$$\eta_{CG} = (2+\alpha(T)\gamma)\frac{v}{c} \tag{2.30}$$

where

v = speed of the observer;
c = speed of the particles (i.e. speed of light);
γ = spectral index of the differential energy spectrum of galactic cosmic rays.
$\alpha(T) = \frac{T+2E_o}{T+E_o}$, where E_o is the rest mass energy and T is the kinetic energy of the particles.

Since we assume that the solar diurnal variation ceases to exist for all rigidities $P > P_u$, then as the Earth orbits the Sun with a relative velocity of 30 km sec^{-1}, primary particles with $P > P_u$ will produce a diurnal variation with a period of 24 hours and time of maximum around 0600 local time. In the case of the orbital diurnal anisotropy (ξ_{ODV}) we assume $c = 3x10^8$ m sec^{-1}, $\gamma = 2.5$, $\alpha = 1$ and the anisotropy is described by the space harmonic component :

$$\begin{aligned}
\xi_{ODV}(\chi) &= S^1_{ODV}(t) \\
&= \eta_{ODV} P^1_1(\cos\theta_R)\cos\frac{2\pi}{24}(t_J - t_{R,ODV}) \\
&= \eta_{ODV}\cos\frac{2\pi}{24}(t_J - t_{R,ODV}) \qquad (2.31)\\
\text{where } \eta_{ODV} &= \eta_{CG} \\
&= 0.045\% \\
\text{and } t_{R,ODV} &= 0600
\end{aligned}$$

The ξ_{ODV} can be directly observed with underground muon telescopes if the upper cutoff rigidity to the solar diurnal variation is sufficiently low so that only primary particles of $P > P_u$ produce a response from the telescope. ξ_{ODV} has been observed using this method in good agreement with theory (Peacock et al. 1968, Mori et al. 1991).

Since the ξ_{ODV} is the same type of anisotropy as the solar diurnal anisotropy (i.e. they both are unidirectional and in the ecliptic plane) then the manifestation of these two anisotropies as two waves in the count rate of an instrument will only be seen as one wave with a period of 24 hours. This will be detected by muon telescopes as the *total observed* diurnal variation ($D^1_1(t)$). If the ξ_{ODV} was not modulated by the geomagnetic field as described in

Section 2.5, then it would be a simple matter to remove the ξ_{ODV} contamination from the total observed diurnal variation in muon telescope data.

i.e. $$D^1_{SDV}(t) = D^1_I(t) - D^1_{ODV}(t) \tag{2.32}$$

where $D^1_{ODV}(t)$ is the diurnal variation caused by the orbital diurnal anisotropy and $D^1_{SDV}(t)$ is the *true* diurnal variation caused by the solar diurnal anisotropy.

To remove $D^1_{ODV}(t)$ from the data recorded by a particular telescope we must know the relation between it and ξ_{ODV}. This is accomplished by using coupling coefficients which are appropriate to the ξ_{ODV} and the relations in (2.24) :

$$\begin{aligned} A_{ODV} &= (\delta A_{ODV})\eta_{ODV} \\ t_{ODV} &= t_{R,ODV} - \delta t_{ODV} \end{aligned} \tag{2.33}$$

With regards to the coupling coefficients which correspond to the ξ_{ODV}, the integral in equation (2.28) needs to be evaluated from P_u (*not* P_c) to infinity since we assume that all particles which do not participate in the solar diurnal variation will be present in the ξ_{ODV}. Infinite rigidity is approximated by 1000 GV and then we can use pre-determined coupling coefficients calculated using the methods described in Section 2.5.2 and

$$\begin{aligned} c^1_{I,ODV} &= \left[c^1_I\right]^{1000}_{P_c} - \left[c^1_I\right]^{P_u}_{P_c} \\ s^1_{I,ODV} &= \left[s^1_I\right]^{1000}_{P_c} - \left[s^1_I\right]^{P_u}_{P_c} \end{aligned} \tag{2.34}$$

where the $\left[\ \right]^{P_2}_{P_1}$ indicates that the integral (see equation 2.28) has been evaluated from P_1 to P_2. The orbital diurnal variation is a purely kinematic effect related to the Earth's motion through space and does exist in data at all rigidities. We must remove its affect on data by the above method for particles with rigidities greater than P_u before any quantitative analyses can be performed. In the following chapter the orbital diurnal variation's effect in the results of analysing the free-space anisotropy will be discussed.

The true solar diurnal variation in muon data then has amplitude A_{SDV} and phase t_{SDV} which are obtained purely from the algebraic addition of two cosine waves with equal periods :

$$\begin{aligned} A_{SDV} &= \sqrt{(A_1)^2 + (\eta_{ODV}\delta A_{ODV})^2 - 2A_1\eta_{ODV}\delta A_{ODV}\cos\frac{2\pi}{24}\left[t_1 - (t_{R,ODV} - \delta t_{ODV})\right]} \\ t_{SDV} &= \frac{24}{2\pi}\arctan\left[\frac{A_1\sin\frac{2\pi}{24}t_1 - (\eta_{ODV}\delta A_{ODV})\sin\frac{2\pi}{24}(t_{R,ODV} - \delta t_{ODV})}{A_1\cos\frac{2\pi}{24}t_1 - (\eta_{ODV}\delta A_{ODV})\cos\frac{2\pi}{24}(t_{R,ODV} - \delta t_{ODV})}\right] \end{aligned} \tag{2.35}$$

Obviously, if $\eta_{ODV}\delta A_{ODV} << A_1$ in (2.35), then the relation reduces to

$$A_{SDV} = A_1$$
$$t_{SDV} = t_1 \qquad (2.36)$$

which is just the simple case for neutron monitor results.

In the past, investigations which varied coupling coefficients corrected for ξ_{ODV} only once for an arbitrary value of P_u (e.g. Humble 1971). For all the analyses in this thesis the corrections for ξ_{ODV} for all muon telescope results are made simultaneously with the assumed value of P_u. This is very important for the χ^2 analyses in Chapter 3 since P_u is continuously being changed.

As a test, the technique proposed above should enable one to observe the ξ_{ODV} in data which does not have any contribution from the solar diurnal anisotropy. The Socorro south and west pointing underground muon telescopes are estimated to have median rigidities of response of about 335GV and 365GV respectively. These rigidities are at least six times as high as the average P_u to the solar diurnal anisotropy from 1975 to 1977 (Ahluwalia and Riker 1987). The contribution of the solar diurnal anisotropy to the results of harmonically analysed data collected from 1975 to 1977 from these two telescopes should be negligible. Assuming this is true, the averaged free-space diurnal anisotropy inferred from the data and the relations in (2.35) should be ξ_{ODV}.

i.e.
$$\eta_{ODV} = \frac{A_1}{\delta A_{ODV}}$$
$$t_{RODV} = t_1 + \delta t_{ODV}$$

Figure 2.4 depicts the results of such an analysis. The coupling coefficients were calculated by assuming a flat spectrum to the ξ_{ODV} and approximating infinite rigidity by 1000 GV.

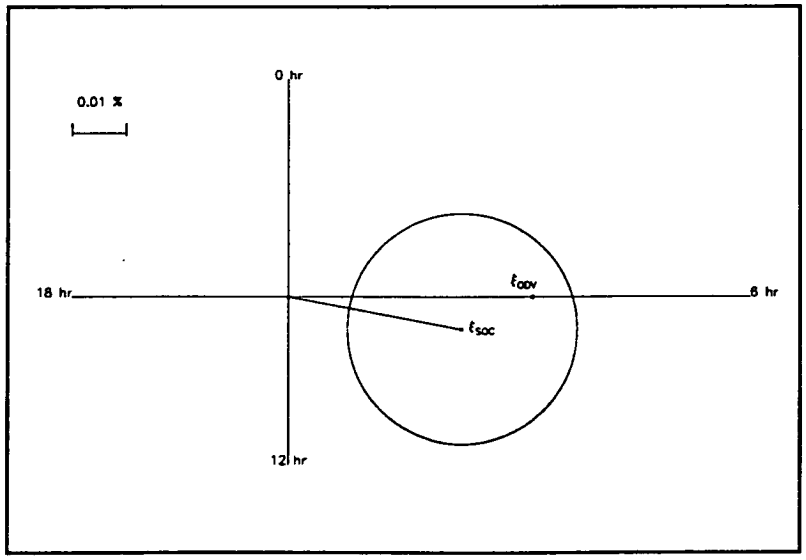

Figure 2.4 Average free-space (solar time) diurnal anisotropy (ξ_{SOC}) inferred from data collected by Socorro west and south pointing underground muon telescopes from 1975 to 1977. The 1-sigma uncertainty level is indicated by the circle centred on the head of the vector. The theoretical Orbital Diurnal Anisotropy (ξ_{ODV}) is also indicated.

The results are not particularly statistically sound (the average hourly count rate being about 8000 counts per hour, compared to the Hobart 9-counter IQSY neutron monitor which records about 300000 counts per hour) but within errors the average free-space solar diurnal variation can be interpreted as the ξ_{ODV} in free-space. It should be noted that any true solar diurnal anisotropy (phase about 12 hours later than the orbital diurnal anisotropy) present in the data will reduce the response of these telescopes to the orbital diurnal anisotropy. This is also consistent with the observed result.

Summary

This chapter presented all the methods and techniques used in this thesis for analysing cosmic ray data and investigating anisotropies in the heliosphere.

Section 2.1 introduced the instruments used to obtain the results presented in the following chapters. The median rigidities, which the instruments used in this thesis respond to, range from about 17 GV in the case of neutron monitors to about 300 GV for the Socorro underground muon telescopes. The Poatina underground muon telescope has a median rigidity of about 1400 GV. Data from this instrument are used to explain the contamination of some of the results presented in Chapter 4.

Section 2.2 was concerned with illustrating the effects on cosmic rays of the terrestrial environment in which the data collecting instruments are located. The variation of atmospheric pressure will influence the count rates of both neutron monitors and muon telescopes and data must have this effect removed before any analyses can begin. This has been done for all data in this thesis. Temperature effects only influence the muon component of secondary cosmic rays and to a much lesser extent than the pressure. None of the muon data in this thesis were formally corrected for temperature effects but most data are not believed to be significantly influenced by these effects.

Much information about the free-space distribution of cosmic rays can be obtained by Fourier analysing a complete day's data for the solar and sidereal diurnal variations. Sections 2.3 and 2.4 presented the methods used in this thesis for obtaining the yearly averages of these variations.

The geomagnetic field also affects the data recorded by an instrument and coupling coefficients must be used to infer the distribution of particles in free-space from diurnal variation results. The final sections of this chapter were concerned with explaining how coupling coefficients can be used with diurnal variation results to infer the responsible cosmic ray anisotropies in free-space. By using the methods outlined in Section 2.5, coupling coefficients and diurnal variation results have been used in the following chapters, to infer the complete descriptions of the solar diurnal and the North-South anisotropies introduced in Chapter 1. These investigations are presented in Chapters 3 and 4. Not only are the space distributions calculated, but the coupling coefficients are used to derive the rigidity spectra of the anisotropies and these results are then used to infer modulation parameters.

CHAPTER 3

SOLAR DIURNAL VARIATION

In Chapter 1 the characteristics of the solar diurnal anisotropy (ξ_{SD}) and recent determinations of solar modulation parameters were reviewed. The most important results discussed were :

- the average rigidity spectrum of ξ_{SD}, G(P) = (γ, P_u) is not agreed on but thought to be (0.0, < 200 GV);
- the temporal variation of P_u is such that at times of solar minimum it has a much lower value than at times of solar maximum (Ahluwalia and Erickson 1969, Humble 1971, Ahluwalia and Sabbah 1993). Ahluwalia (1991) suggested that this variation is probably caused by a change in the magnitude of the interplanetary magnetic field;
- in free-space after the effects of the Earth's geomagnetic field and the spectrum of the anisotropy are taken into account, the anisotropy varies. The amplitude of the anisotropy (η_{SD}) has an 11-year variation and the phase (t_R) has a 22-year variation (Duggal et al. 1967, Jacklyn et al. 1969, Duggal and Pomerantz 1975, Ahluwalia 1988a, 1988b, Bieber and Chen 1991a). The variation of the free-space phase may depend on the rigidity;
- ξ_{SD} can be used to derive some of the parameters related to solar modulation, specifically the product of the parallel mean-free path and the radial density gradient ($\lambda_{||}G_r$) and the symmetric (bi-directional) latitudinal gradient (G_θ^{sym}). By deriving these parameters directly from observations of ξ_{SD} we can test the predictions of modulation theories (Bieber and Chen 1991a, Ahluwalia and Sabbah 1993);
- $\lambda_{||}G_r$ has been shown to have a 22-year variation related to a variation in $\lambda_{||}$ (Bieber and Chen 1991b, Chen and Bieber 1993) but the rigidity dependence of $\lambda_{||}G_r$ is not agreed on (Ahluwalia 1993); and
- modulation models predict that G_θ^{sym} should reverse direction following a solar magnetic polarity reversal. This behavior has been observed by some investigations but not others.

The analyses presented in this chapter were undertaken in an attempt to dispel the confusion about the rigidity spectrum of the anisotropy and investigate the behavior of the anisotropy and modulation parameters. Specifically the aims of this investigation were to :

- gain better knowledge of the average and temporal behavior of the rigidity spectrum of ξ_{SD};
- verify the correlation of P_u and the IMF;
- derive the free-space anisotropy (using the correct rigidity spectrum) and study any temporal variations;
- use the correct rigidity spectrum and free-space anisotropy to derive the modulation parameters $\lambda_{||}G_r$ and G_θ^{sym} for particles with rigidities between 10 and 200 GV and study any rigidity dependence of these parameters; and

- study the temporal behavior of the modulation parameters and compare their behavior to that predicted by modulation theories which include drifts.

Section 3.1 extends the general theory presented in Chapter 1 and relates the solar diurnal anisotropy to the modulation parameters. Section 3.2 explains how the Fourier analysis and coupling coefficients formalism outlined in Chapter 2 can be applied to the solar diurnal variation so that the free-space anisotropy and correct rigidity spectrum can be determined. Two (similar) methods of determining the rigidity spectrum will be described, the second method being much more versatile than the first as it simultaneously determines both spectral parameters, whereas the first of the methods is only useful for determining P_u for an assumed spectral index.

Section 3.3 contains all the results relevant to the determination of the spectral and space-distribution parameters describing the anisotropy. The rigidity spectrum results are presented (Sections 3.3.1 and 3.3.2) and compared to previous analyses. The results are examined for any temporal and rigidity dependencies by examining averages over distinct magnetic polarity states and examining yearly averages. These results are used in Section 3.3.2 to determine the free-space parameters of ξ_{SD}.

Section 3.4 presents the results of calculations of modulation parameters and compares these results to those referred to in Section 1.4. The parameters are calculated using the determined rigidity spectra in Section 3.3.

3.1 Theoretical description of the solar diurnal anisotropy

Forman and Gleeson's (1975) theory of cosmic ray streaming was summarised in Section 1.2 and it was shown that the anisotropy of cosmic rays (ξ) in the heliosphere can be described in three dimensions (equation 1.6). The coordinate system of these equations is $\hat{\mathbf{x}}$ and $\hat{\mathbf{z}}$ in the ecliptic plane with $\hat{\mathbf{z}}$ along the direction of the IMF away from the Sun. As mentioned in Chapter 1 the components of ξ in this coordinate system which are in the ecliptic plane are :

$$\begin{aligned} \xi_x &= \xi_c \sin\chi - \lambda_\perp G_r \sin\chi + \rho G_\theta \mathrm{sgn}(B) \\ \xi_z &= \xi_c \cos\chi - \lambda_{||} G_r \cos\chi \end{aligned} \tag{3.1}$$

These are the components of the anisotropy of cosmic rays responsible for ξ_{SD}. According to Nagashima's formalism outlined in Section 2.5 the space distribution of the solar diurnal anisotropy $F(\chi)$ (in the absence of other components of the space distribution) can be represented as the first order ordinary Legendre polynomial :

$$F(\chi) = \eta_{SD} P_1(\cos\chi) \tag{3.2}$$

where

$$\xi_{SD} = F(\chi)G(P)$$

$$\text{and} \quad G(P) = \begin{cases} \left(\frac{P}{10}\right)^{\gamma}, & P \le P_u \\ 0 \quad , & P > P_u \end{cases} \tag{3.3}$$

The reference axis **OR** (see Figure 2.2) is assumed to be in the azimuthal direction around the Sun in the ecliptic plane. Over a year this axis will have a variation of its co-declination and right-ascension but as has already been noted in Chapter 2, if a solar anisotropy is defined close to the ecliptic plane then the yearly averaged space distribution can be taken to have its reference axis defined by a co-declination of 90 degrees. Therefore, following Nagashima's formalism :

$$\text{i.e.} \qquad F(\chi) = \sum_{m=0}^{1} \eta_{SD} f_1^m(\theta_R, \alpha_R, \theta_J, \alpha_J) \tag{3.4}$$

where (θ_R, α_R) are the co-declination and right-ascension of the reference axis, (θ_J, α_J) are the co-declination and right-ascension of the particles directed along **JO** and

$$f_n^m(\theta_R, \alpha_R, \theta_J, \alpha_J) = P_n^m(\cos\frac{\pi}{2}) P_n^m(\cos\theta_J) \cos m(\alpha_J - \alpha_R) \tag{3.5}$$

$P_n^m(x)$ are the semi-normalized spherical functions, defined in Section 2.5.

The space distribution $F(\chi)$ will produce two space harmonic components (zeroeth and first orders). The zeroeth order space harmonic component is along the rotation axis of the Earth and is constant. The first order space harmonic component ($S_{SD}(t)$) is directed parallel to the equator :

$$\begin{aligned} S_{SD}(t) &= \eta_{SD} P_1^1(0) \cos(\alpha_J - \alpha_R) \\ &= \eta_{SD} \cos\frac{2\pi}{24}(t_J - t_R) \\ &= x_{SD} \cos\frac{2\pi}{24} t_J + y_{SD} \sin\frac{2\pi}{24} t_J \end{aligned} \tag{3.6}$$

where

$$\begin{aligned} \eta_{SD} &= \sqrt{(x_{SD})^2 + (y_{SD})^2} \\ t_R &= \frac{24}{2\pi} \arctan\left(\frac{y_{SD}}{x_{SD}}\right) \\ \alpha &= \frac{2\pi}{24} t \end{aligned} \tag{3.7}$$

The free-space harmonic component $S_{SD}(t)$ will produce the solar diurnal variation D(t) in an instrument's count rate at Earth. Fourier analysis can be used to derive the components of this variation as described in Section 2.3. Using the relations in (2.24) and (2.26) we find :

$$\begin{aligned} D(t) &= A_{SD}\cos\frac{2\pi}{24}(t-t_{SD}) \\ &= a_{SD}\cos\frac{2\pi}{24}t + b_{SD}\sin\frac{2\pi}{24}t \\ a_{SD} &= c_1^1 x_{SD} + s_1^1 y_{SD} \\ b_{SD} &= -s_1^1 x_{SD} + c_1^1 y_{SD} \\ A_{SD} &= (\delta A_1^1)\eta_{SD} \\ t_{SD} &= t_R - \delta t_1^1 \\ \text{where}\quad \delta A_1^1 &= \sqrt{(c_1^1)^2 + (s_1^1)^2} \\ \delta t_1^1 &= \frac{24}{2\pi}\arctan\left(\frac{s_1^1}{c_1^1}\right) \end{aligned} \tag{3.8}$$

So, from an observation of the solar diurnal variation and applying the coupling coefficients to the Fourier derived amplitude (A_{SD}) and the phase (t_{SD}) the free-space harmonic component of the solar diurnal anisotropy can be derived. From these quantities the amplitude constant (η_{SD}) and the reference axis or free-space phase (t_R) can be calculated and we can describe the entire solar diurnal anisotropy.

Once one has derived the solar diurnal anisotropy (G(P), η_{SD}, t_R) it is desirable to relate it to the theoretical components of the anisotropy presented in equation (3.1). By considering Figure 3.1 and noting that

$$\begin{aligned} |\xi_{SD}|^2 &= (\xi_x)^2 + (\xi_z)^2 \\ (\eta_{SD}G(P))^2 &= (\xi_x)^2 + (\xi_z)^2 \end{aligned} \tag{3.9}$$

we find

$$\begin{aligned} \xi_x &= \eta_{SD}G(P)\sin(\chi + t_R) \\ \xi_z &= \eta_{SD}G(P)\cos(\chi + t_R) \end{aligned} \tag{3.10}$$

Note that χ now represents the angle between the Earth-Sun line and the IMF.

The relations in (3.10) are only true in a frame of reference which is fixed with respect to the Sun. The observations which derive (η_{SD}, t_R) are made from the Earth, which is orbiting the Sun at a speed of 30 km sec^{-1}. This motion will result in another anisotropy being present in the free-space results, a Compton-Getting anisotropy. We must correct the observations (in

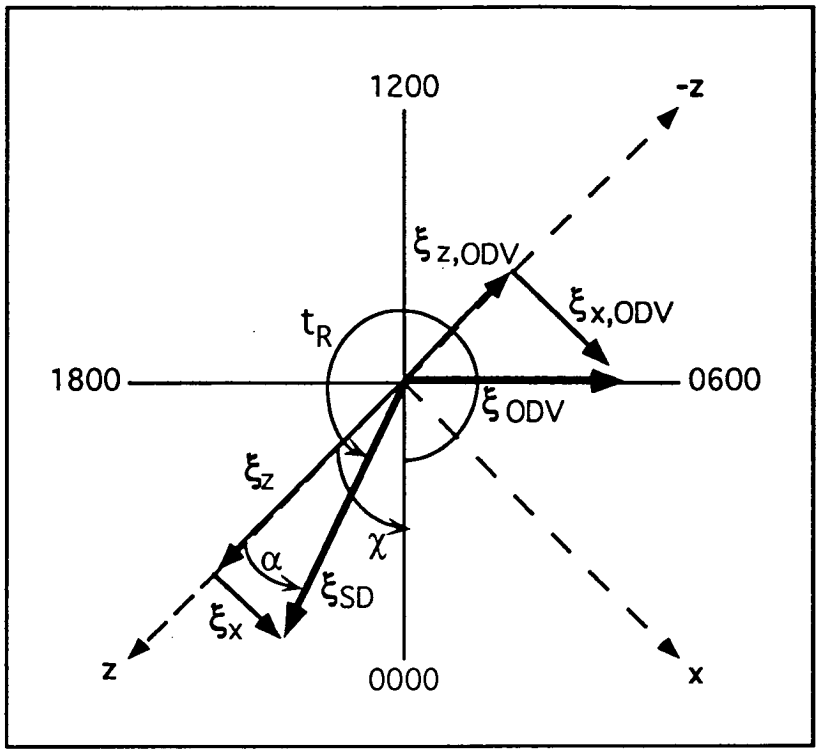

Figure 3.1 The solar diurnal anisotropy (ξ_{SD}) depicted as the vector derived from the data recorded by a cosmic ray instrument. The orbital diurnal anisotropy (ξ_{ODV}) is pictured similarly. The reference axes are parallel and perpendicular to the interplanetary magnetic field line which makes an angle (χ) with the Earth-Sun line. Times are indicated in local solar time.

free-space) for the loss of signal which results from this Compton-Getting anisotropy, which is also depicted in Figure 3.1. It is exactly the same as the correction made to underground muon data because of the Orbital diurnal variation described in Section 2.6, except that all observations suffer from this and we know the free-space amplitude and phase of this Compton-Getting anisotropy. There is no geomagnetic deflection to be concerned with. Hence by removing the components of this Compton-Getting anisotropy from the observations (in actual fact including the response of the solar diurnal anisotropy which has been masked from the observation) :

$$\begin{aligned} \xi_x &= \eta_{SD} G(P) \sin(\chi + t_R) - \eta_{CG} \cos(\chi) \\ \xi_z &= \eta_{SD} G(P) \cos(\chi + t_R) + \eta_{CG} \sin(\chi) \\ \eta_{CG} &= 0.045\% \end{aligned} \tag{3.11}$$

Previously, the Compton Getting Effect was noted to be present in the total daily variation recorded by an underground muon telescope as a diurnal variation with a maximum in the 0600 L.T. direction. This diurnal variation is caused by the Earth moving through unmodulated cosmic rays ($P > P_u$) and will combine with the diurnal variation produced by the solar diurnal anisotropy. Consequently, the response of an instrument to the solar diurnal anisotropy will be altered if it has a significant response to primaries with rigidities greater than P_u. Underground muon telescopes have a significant response to these particles. To

remove the contribution of this spurious diurnal variation from the diurnal variation recorded by an underground instrument one needs to use coupling coefficients appropriate to this orbital anisotropy in equation (2.35) as outlined in Section 2.6.2. There it was shown that this correction needs to be made prior to any analyses of the results in free-space.

If one is still uneasy about the Compton-Getting Effect due to the Earth's motion about the Sun effectively being corrected for twice in the analysis (equations 3.11 and 2.35), consider the following scenario : assume that there exist *no* cosmic ray particles with rigidities greater than P_u. Naturally there will be no orbital diurnal variation present in the observed diurnal variation in muon telescope data and the correction made in (2.35) in Section 2.6 is unnecessary. We can then immediately derive the free space solar diurnal anisotropy using the relations (3.8) to (3.10). We must still transform the vector to a stationary frame of reference via the Compton-Getting Effect in (3.11). If we now assume that there do exist particles with rigidities greater than P_u (as there is in reality) then the Orbital diurnal variation will exist (as described in Section 2.6) and the additional corrections must be made to the observations. Essentially the problem is that the Compton-Getting correction must be made for all rigidities (especially when using muon data), but due to the nature of terrestrial modulation we must make the correction for particles with $P<P_u$ at a different stage to correcting for particles with $P>P_u$. Since neutron monitors mainly respond to primaries with rigidities much less than P_u the Orbital diurnal variation correction is negligible in this case and only the free space vector must be corrected as in (3.11).

The relations in (3.11) are in terms of the viewing directions of the instruments which means that they are actually describing anisotropic streaming in the opposite direction to the true streaming. To correct this the relations are transformed by 180 degrees.

i.e.
$$\begin{aligned} \xi_x &= -\eta_{SD} G(P) \sin(\chi + t_R) + \eta_{CG} \cos\chi \\ \xi_z &= -\eta_{SD} G(P) \cos(\chi + t_R) - \eta_{CG} \sin\chi \end{aligned} \qquad (3.12)$$

The component of anisotropy due to the convection of cosmic rays in the solar wind can be removed by transforming the anisotropy into the reference frame of the solar wind. This is accomplished by removing the convective anisotropy (ξ_c) by taking the solar wind speed to be 400 km sec^{-1} and the Compton-Getting coefficient to be 1.5 (Baker 1992). By removing this effect, the components of ξ_{SD} are related purely to streaming which is parallel (||) and perpendicular ($\perp$) to the IMF. The components of the anisotropy can then be written as

$$\begin{aligned} \xi_\perp &= \xi_x - \xi_c \sin\chi \\ &= -\lambda_\perp G_r \sin\chi + \rho G_\theta \mathrm{sgn}(B) \\ &= -\eta_{SD} G(P) \sin(\chi + t_R) + \eta_{CG} \cos\chi - \eta_c \sin\chi \\ \xi_{||} &= \xi_z - \xi_c \cos\chi \\ &= -\lambda_{||} G_r \cos\chi \\ &= -\eta_{SD} G(P) \cos(\chi + t_R) - \eta_{CG} \sin\chi - \eta_c \cos\chi \end{aligned} \qquad (3.13)$$

To avoid any bias of the yearly averaged results from unequal sampling of the anisotropy in towards and away IMF sectors during the year an average of the results over sector polarities can be calculated. By assuming that $\chi_T \approx \chi_A = \chi$ we have :

$$\left(\frac{\xi_{\parallel,T}+\xi_{\parallel,A}}{2}\right)=\left(\frac{-\lambda_{\parallel,T}G_{r,T}\cos\chi_T-\lambda_{\parallel,A}G_{r,A}\cos\chi_A}{2}\right)$$
$$=-\overline{\lambda_{\parallel}G_r}\cos\chi \qquad (3.14)$$

$\overline{\lambda_{\parallel}G_r}$ denotes the numerical average of $\lambda_{\parallel}G_r$ over towards and away IMF sectors.

Similarly, an average over IMF sectors of the perpendicular anisotropy yields :

$$\left(\frac{\xi_{\perp,T}+\xi_{\perp,A}}{2}\right)=\left(\frac{-\lambda_{\perp,T}G_{r,T}\sin\chi_T-\rho_TG_{\theta,T}-\lambda_{\perp,A}G_{r,A}\sin\chi_A+\rho_AG_{\theta,A}}{2}\right)$$
$$=-\overline{\lambda_{\perp}G_r}\sin\chi-\rho\left(\frac{G_{\theta,T}-G_{\theta,A}}{2}\right) \qquad (3.15)$$

where it has been assumed that $\rho_T\approx\rho_A=\rho$ and $\overline{\lambda_{\perp}G_r}$ is the average of $\lambda_{\perp}G_r$ over towards and away IMF sectors. From these relations (3.14) and (3.15) we can use the solar diurnal variation to derive information about the product of the parallel mean-free path and the radial density gradient and also the bi-directional latitudinal gradient.

3.1.1 The modulation parameter $\overline{\lambda_{\parallel}G_r}$

From the relations in (3.8), (3.13) and (3.14) we obtain :

$$\overline{\lambda_{\parallel}G_r}=\frac{\frac{A_{SD}}{\delta A_1^1}G(P)\cos(\chi+t_{SD}+\delta t_1^1)+\eta_{CG}\sin\chi+\eta_c\cos\chi}{\cos\chi} \qquad (3.16)$$

where A_{SD} and t_{SD} are now the yearly averaged values of the amplitude and phase of the solar diurnal variation also averaged over IMF sector polarities. Sections 2.3 to 2.5 describe how to obtain these quantities in towards and away IMF sectors. The averages of these values are taken and substituted into (3.16) with the appropriate rigidity spectrum of the solar diurnal anisotropy and coupling coefficients. In the following analyses $\eta_c=3CV_{sw}/v$, where V_{sw} is the speed of the solar wind (400 km sec^{-1}), v is the speed of the cosmic ray particles (approximately the speed of light) and C is the Compton-Getting coefficient mentioned briefly when deriving equation (3.13). This results in $\eta_c=0.6\%$. The spiral angle of the IMF at 1 AU is taken to be 45 degrees to the Earth-Sun line. Both the solar wind speed and the spiral angle vary with the 11-year solar cycle but the variations are small. Using in-situ measurements of these two quantities does not improve calculations appreciably (Bieber and Chen 1991a).

The above method is used in this thesis to determine $\overline{\lambda_{\parallel}G_r}$ from the data recorded by instruments responding to primary particles from about 10 GV to 200 GV. The value of $\overline{\lambda_{\parallel}G_r}$ is calculated from 1957 to 1990 to study any temporal variations. The average value of this modulation parameter is also evaluated over epochs around solar minima and for complete solar cycles. These results are presented in Section 3.4.1.

As has already been mentioned, the correct rigidity spectrum is important when including the coupling coefficients in equation (3.16). In Chapter 1, the review of the literature indicated that there is some disagreement on the true rigidity spectrum of the anisotropy, but that the spectrum is close to being flat and that the upper cut-off rigidity is lower than 100 GV at times of solar minimum. Before $\overline{\lambda_{\parallel} G_r}$ can be determined accurately, an investigation into the correct rigidity spectrum of ξ_{SD} will be performed (Sections 3.2.1 and 3.2.2).

3.1.2 The modulation parameter $G_{|z|}$

The latitudinal density gradient (G_θ) has been reviewed in Chapter 1. It is commonly accepted that this gradient is not invariant across the neutral sheet and has been best represented as the sum of two components - an asymmetric latitudinal gradient (G_θ^{assym}) and a symmetric gradient (G_θ^{sym}). Figure 3.2 shows an idealised representation of these two components.

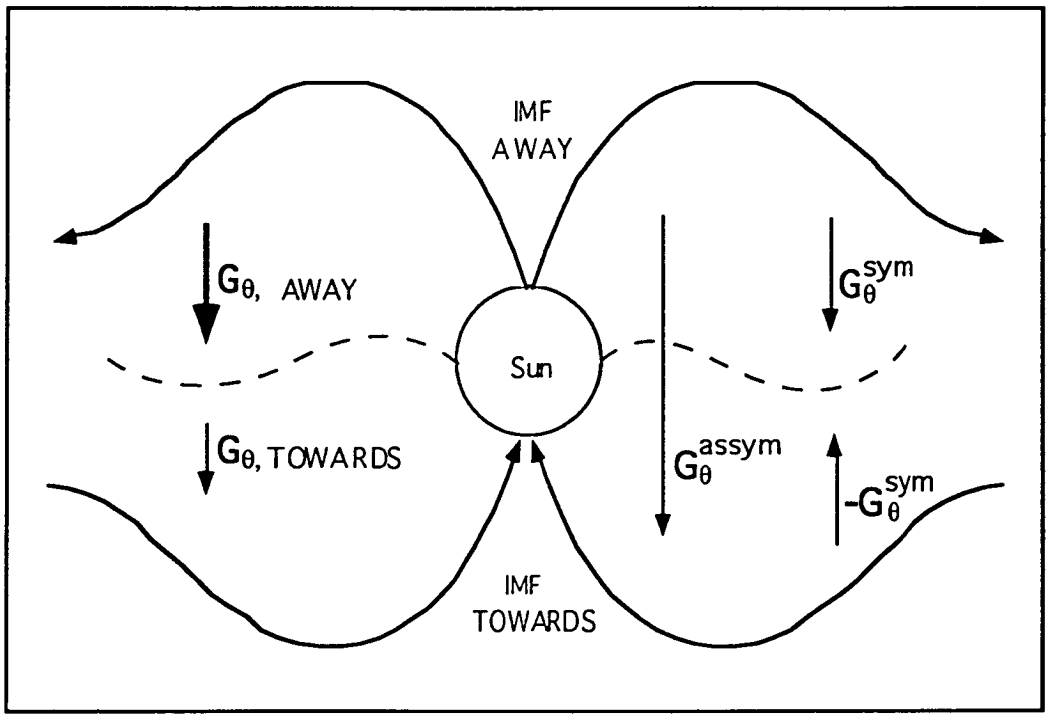

Figure 3.2 The asymmetric (unidirectional) latitudinal gradient G_θ^{assym} and the symmetric (bi-directional) latitudinal gradient G_θ^{sym} combine on opposite sides of the neutral sheet (shown by the dashed line). The combination of these two components of the latitudinal gradient G_θ produce a larger G_θ on one side of the neutral sheet than the other. For this example G_θ is larger (bolder) in the away interplanetary magnetic field (IMF) sector.

IMF gradient and curvature drifts of cosmic rays produce streaming (anisotropy) in the direction parallel to **BxG**. Naturally this streaming will have a component in the direction $\mathbf{B}\times G_\theta$ (see equation 1.2 and the derivation of 1.6), which is a component of the solar diurnal

anisotropy. In the following it will be explained how observations of ξ_{SD} can be used to determine the symmetric latitudinal gradient.

The streaming due to the asymmetric component of G_θ ($B \times G_\theta^{assym}$) will be truly asymmetric with respect to opposite sides of the neutral sheet. The streaming due to the symmetric component will be in the same direction on each side of the neutral sheet. Therefore by averaging the net streaming of particles over IMF sector polarities, the contribution to the streaming from the asymmetric latitudinal gradient will be removed. Figure 3.3 shows an example of this.

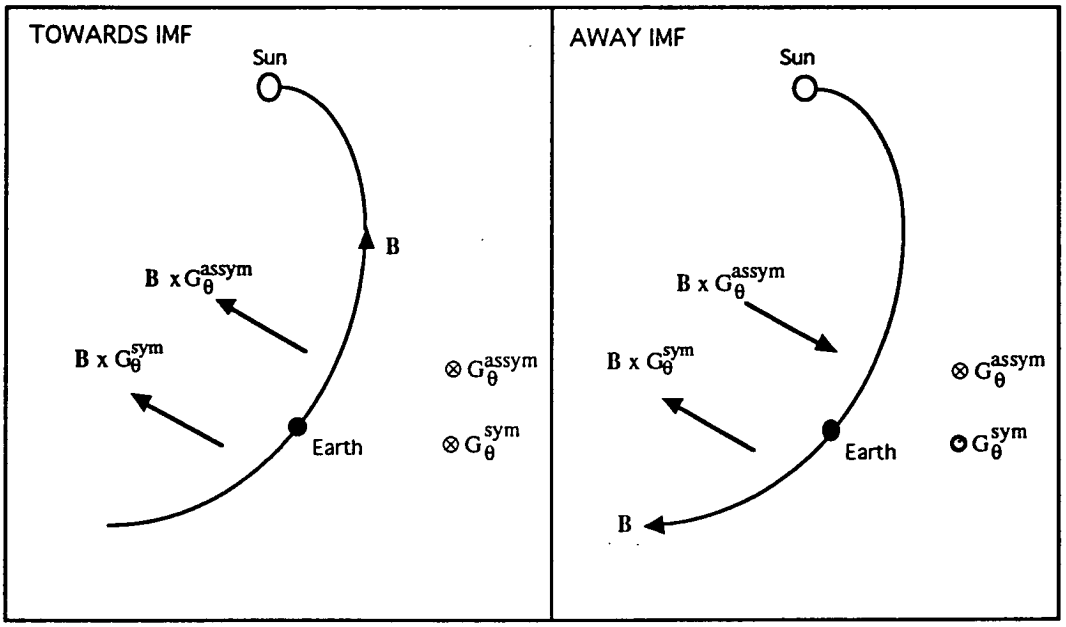

Figure 3.3 The streaming of particles due to the asymmetric latitudinal gradient ($B \times G_\theta^{assym}$) observed at Earth is in opposite directions depending on the IMF sector which the Earth is in. The streaming of particles due to the symmetric latitudinal gradient ($B \times G_\theta^{sym}$) observed at Earth is always in the same direction. By averaging observations over sector polarities the streaming due to $B \times G_\theta^{assym}$ is averaged to zero.

Equation (3.15) refers to an average over sector polarities of the perpendicular anisotropy (or streaming) and contains a difference between the *overall* latitudinal gradient in opposite sector polarities. This is exactly the scenario depicted above because this will average to zero the unidirectional gradient streaming and leave only the streaming caused by the symmetric gradient.

$$\rho\left(\frac{G_{\theta,T}-G_{\theta,A}}{2}\right)=\rho\left(\frac{G_{\theta,T}^{sym}-G_{\theta,A}^{sym}}{2}\right)$$

i.e.
$$=\pm\rho G_{\theta}^{sym} \qquad (3.17)$$
$$=-\overline{\lambda_{\perp}G_r}\sin\chi-\left(\frac{\xi_{\perp,T}+\xi_{\perp,A}}{2}\right)$$

The ± sign arises because when the magnetic polarity state of the heliosphere reverses, the sign of the bi-directional latitudinal gradient in towards and away IMF sectors will reverse. This is because the $\hat{\underline{\theta}}$ direction stays constant when the IMF reverses polarity causing the gradients to change sign even if they don't change physical direction. We would like some sort of standard measure of the bi-directional gradient that takes into account the change in heliospheric polarity state and whose sign is meaningful. Defining a new $\hat{\underline{z}}$ axis which increases in the opposite sense to $\hat{\underline{\theta}}$ and the function :

$$\mathrm{sgn}(I)=\begin{cases}+1, & A>0 \quad \text{IMF polarity states}\\ -1, & A<0 \quad \text{IMF polarity states}\end{cases}$$

then by multiplying both sides of the relations in (3.17) by sgn(I) and substituting the perpendicular relations of (3.13) into (3.17) we find :

$$G_{|z|}\equiv \mathrm{sgn}(I)\left(\frac{G_{\theta,T}-G_{\theta,A}}{2}\right)$$
$$=\frac{\mathrm{sgn}(I)}{\rho}\left(-\overline{\lambda_{\perp}G_r}\sin\chi+\frac{A_{SD}}{\delta A_1^1}G(P)\sin(\chi+t_{SD}+\delta t_1^1)-\eta_{CG}\cos\chi+\eta_c\sin\chi\right) \qquad (3.18)$$

where A_{SD} and t_{SD} are the averaged (over IMF sector polarities) amplitude and phase of the solar diurnal variation recorded by an instrument.

$G_{|z|}$ is a quantity which directly represents the symmetric latitudinal gradient of cosmic rays. It is not only a measure of the magnitude of this gradient but also indicates in which *sense* the bi-directional gradient is *pointing*. Consider the four possible configurations of the bi-directional gradient in the heliosphere throughout the 22-year solar magnetic cycle illustrated in Figure 3.4.

Regardless of the polarity state of the heliosphere, $G_{|z|}$ will indicate in which direction from the neutral sheet the cosmic ray density has a gradient. $G_{|z|}>0$ implies a local minimum in the number density at the neutral sheet. $G_{|z|}<0$ implies a local maximum in the number density at the neutral sheet.

All the quantities in equation (3.18) needed to determine $G_{|z|}$, except $\overline{\lambda_{\perp}G_r}$, are either measurable or known. To be able to calculate $G_{|z|}$ we need to know this parameter. Thus we make use of the parameter α which is the ratio of perpendicular diffusion to parallel diffusion

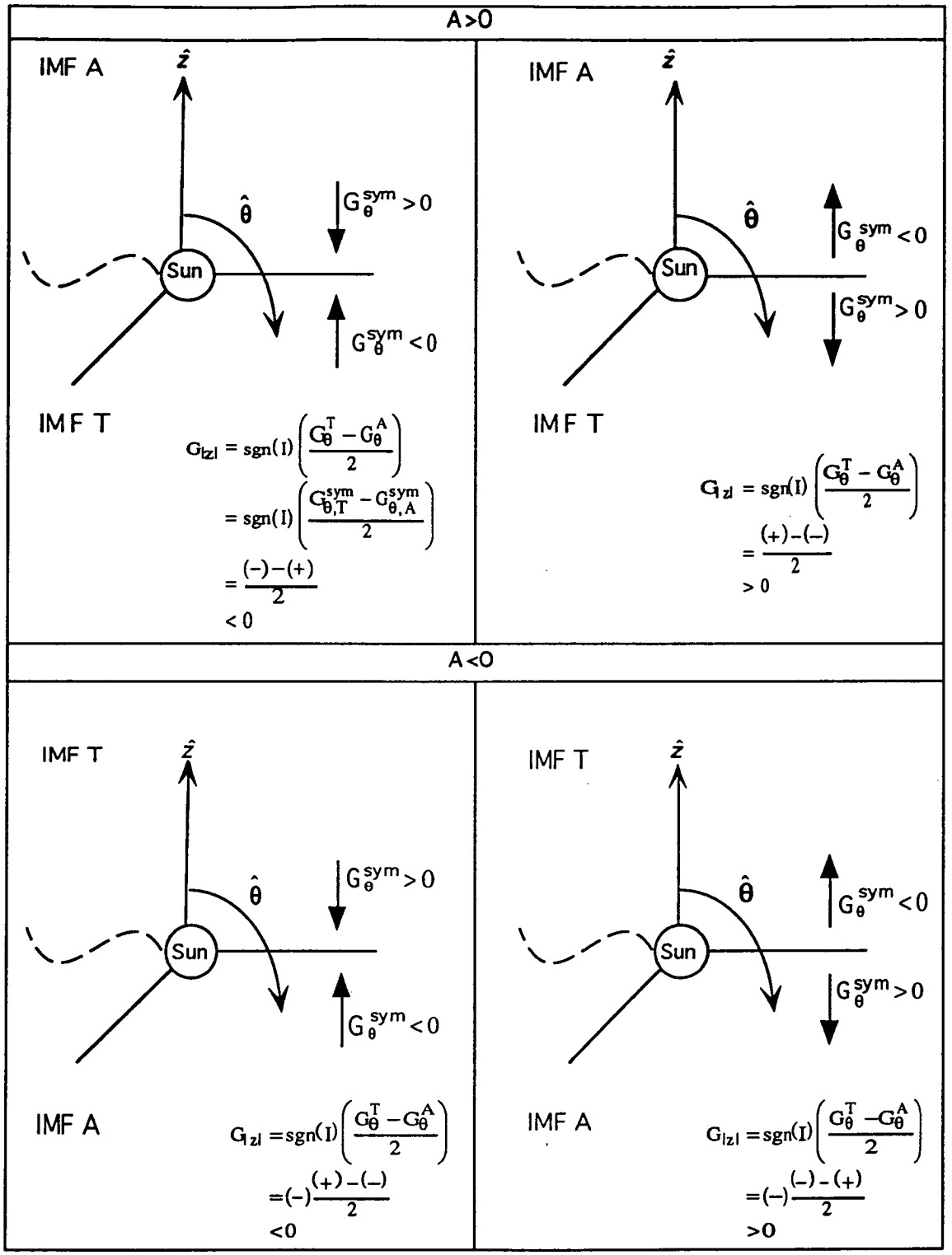

Figure 3.4 The direction of the symmetric latitudinal gradient is represented by the vector G_θ^{sym} which is directed at increasing cosmic ray density. The neutral sheet is represented by the dashed line. In all cases the resulting average gradient $G_{|z|}$ indicates increasing density towards the neutral sheet when $G_{|z|}<0$ and increasing density of cosmic rays away from the neutral sheet when $G_{|z|}>0$.

introduced in Chapter 1, i.e. $\alpha = \kappa_\perp/\kappa_{||} = \lambda_\perp/\lambda_{||}$. By using this parameter and assuming

$$\overline{\lambda G} = \overline{\lambda}\,\overline{G}$$
$$\text{then} \quad \overline{\lambda_\perp G_r} = \alpha \overline{\lambda_{||} G_r} \tag{3.19}$$

We can substitute the value of $\overline{\lambda_{||} G_r}$ obtained by the method outlined in Section 3.1.1 into equation (3.18) :

$$G_{|z|} = -\frac{sgn(I)}{\rho}\left(\alpha\overline{\lambda_{||}G_r}\sin\chi - \frac{A_{SD}}{\delta A_1^1}G(P)\sin(\chi + t_{SD} + \delta t_1^1) + \eta_{CG}\cos\chi - \eta_c \sin\chi\right) \tag{3.20}$$

To derive the yearly average value of $G_{|z|}$ one proceeds in exactly the same manner as described in Section 3.1.1 and also substitutes the resulting value of $\overline{\lambda_{||} G_r}$ into equation (3.20) with a suitable assumption of α. As described in Section 3.1.1 for $\overline{\lambda_{||} G_r}$, $G_{|z|}$ will be determined from the data recorded by instruments responding to primary particles from about 10 GV to 200 GV. The yearly averaged value of $G_{|z|}$ is calculated from 1957 to 1990 to study any temporal variations. By examining the temporal behavior of the symmetric latitudinal gradient one can examine the predictions of drift theories. These results are presented in Section 3.4.2.

In summary, if we know the free space solar diurnal anisotropy then we can calculate the components of the anisotropy in a coordinate system relative to the IMF. We can relate these components to $\overline{\lambda_{||} G_r}$ and the symmetric (bi-directional) latitudinal density gradient of galactic cosmic rays. For an accurate determination of the modulation parameters as described above the correct rigidity spectrum of the anisotropy must be known so that the correct coupling coefficients can be used. Two methods of determining the rigidity spectrum of the solar diurnal anisotropy are presented in the next section.

3.2 Data analyses

The methods outlined in Sections 2.3 and 2.4 were used to obtain the Fourier coefficients relevant to the solar diurnal variation present in the data collected by the instruments used in the following analyses. The yearly averages of the Fourier components were derived for each year of available data and were also averaged over times of the year according to the sector polarity of the IMF at the Earth. These (IMF separated) data will be used later in the determination of the modulation parameters $\overline{\lambda_{||} G_r}$ and $G_{|z|}$. The spurious solar diurnal variation present in the underground muon telescope data (described in Section 2.6.2) was removed when calculating the free-space anisotropy for a particular rigidity spectrum with the appropriate coupling coefficients. Recall that Figures 2.1a and 2.1b contained plots of the harmonic dials of the results from Fourier analysing the MNM and HUV instruments for the solar diurnal variation. Appendix 2 contains the solar time harmonic dials from all the other instruments used in this study.

As mentioned above the correct rigidity spectrum of the anisotropy is important for an accurate determination of the free-space solar diurnal anisotropy and associated modulation parameters. In the following, the methods to determine the rigidity spectrum are presented.

Underground muon telescopes will respond differently to an anisotropy than neutron monitors because they are detecting secondaries produced by primary cosmic rays of different energies. Hence their coupling coefficients are different. Figure 2.3 indicates that the coupling coefficients (and specifically δA_1^1) for underground muon telescopes change significantly over the range of P_u from 30 GV to 500 GV. Consequently, the value of $\overline{\lambda_{||} G_r}$ derived from equation (3.16) using underground muon telescope diurnal variation results depends on the choice of P_u used in the calculation of δA_1^1. Neutron monitor coupling coefficients are much less sensitive to the value of P_u used for the calculation of the relevant coupling coefficient δA_1^1. By comparing the η_{SD} derived from an underground muon telescope (η_{SD}^{μ}) as a function of the assumed P_u to that derived from neutron monitor observations of the diurnal variation (η_{SD}^{n}), there should be a distinct value (or at least range) of P_u where the corresponding values of η_{SD}^{μ} and η_{SD}^{n} are be the same. At other values of P_u the corresponding free-space amplitude constants should be significantly different. The region of equality should indicate the most reasonable and accurate value of P_u to use in a determination of the free-space parameters describing the anisotropy. This is the basis of all previous analyses of the rigidity spectrum of ξ_{SD} (Jacklyn and Humble 1965, Jacklyn et al. 1969, Ahluwalia and Erickson 1969, Humble 1971, Alania et al. 1983, Ahluwalia and Riker 1987) and also the basis of the following methods of determining the spectrum of the solar diurnal anisotropy.

3.2.1 Determining the rigidity spectrum of the ξ_{SD} - method 1

The fourth relation of (3.8) is rewritten here explicitly showing the spectral dependence of the derived amplitude constant of ξ_{SD} due to the coupling coefficients:

$$\eta_{SD}(\gamma, P_u) = \frac{A_{SD}}{\delta A_1^1(\gamma, P_u)} \tag{3.21}$$

By assuming the rigidity spectrum in (3.3) and making a choice of the spectral index γ, the free-space amplitude constant (η_{SD}^{μ}) can be derived from an underground muon telescope observation of the amplitude of the solar diurnal variation. η_{SD}^{μ} can be compared as a function of P_u to the amplitude constant (η_{SD}^{n}) determined from a neutron monitor observation of the amplitude of the solar diurnal variation (A_{SD}^{n}). As described above, the point of intersection (e.g. see Figure 3.5) determines the best estimate of P_u to the anisotropy for that choice of γ. Section 3.3.1 contains the results of this analysis from the comparison of the yearly averaged solar diurnal amplitudes recorded by five underground muon telescopes to five neutron monitors paired to maintain independence over as long a time frame as possible (see Table 3.1).

Table 3.1 Pairs of telescopes used in the analysis.

Pair #	Instrument	Years
1	MNM HUV	1957-1989
2	DRNM EMBV	1965-1988
3	KNM EMBN	1965-1988
4	MTNM MUN	1973-1990
5	HNM HUI	1976-1990

Figures 3.5a and 3.5b show the comparison of free space amplitude constants for the Hobart underground muon telescope HUV and the Mawson neutron monitor MNM for 1970 and 1976 under the assumption of $\gamma = 0$. (Under this assumption the free-space amplitude is the free-space amplitude constant). The points of intersection of $\eta^{\mu}_{SD}(P_u)$ and $\eta^{n}_{SD}(P_u)$ imply the best estimates of P_u for those years.

The uncertainty in the point of intersection is not correctly determined from the overlap of the error-bars of the two amplitude constants (Humble 1971) but involves the analysis of the errors in the two determinations as explained below.

We know that :

$$\eta^{n}_{SD}(P_u) = \frac{A^{n}_{SD}}{\delta A^{1}_{1,n}(P_u)}$$

and

$$\eta^{\mu}_{SD}(P_u) = \frac{A^{\mu}_{SD}}{\delta A^{1}_{1,\mu}(P_u)}$$

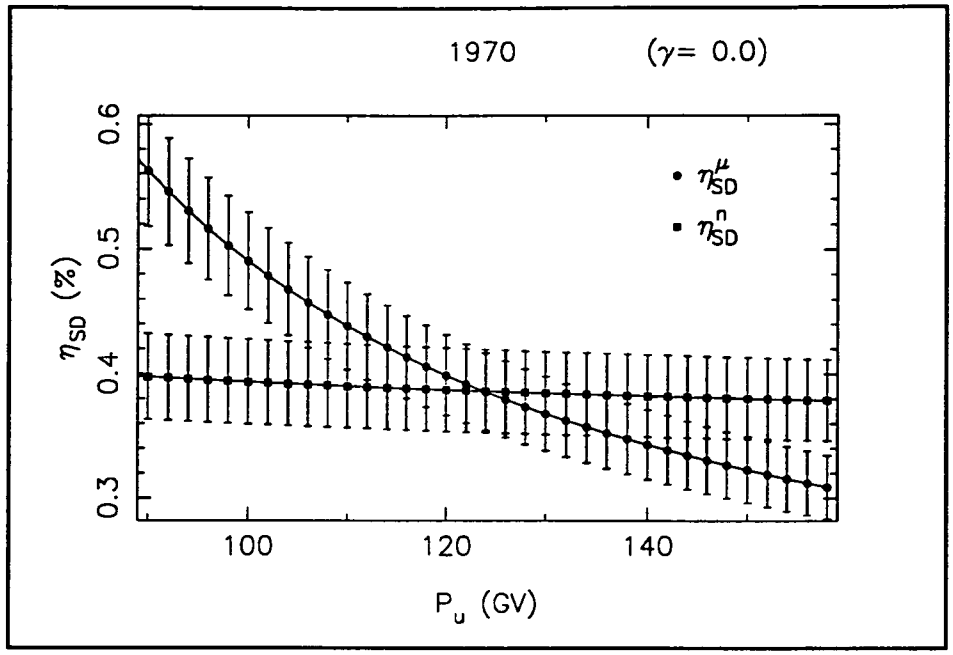

Figure 3.5a The functional dependence on upper limiting rigidity (P_u) of the amplitude constants of the solar diurnal anisotropy determined from the Hobart vertical underground muon telescope (η^{μ}_{SD}) and the Mawson neutron monitor (η^{n}_{SD}) observations of the solar diurnal variation during 1970. The best estimate of the upper rigidity for 1970 is indicated from the point of intersection at 124 GV.

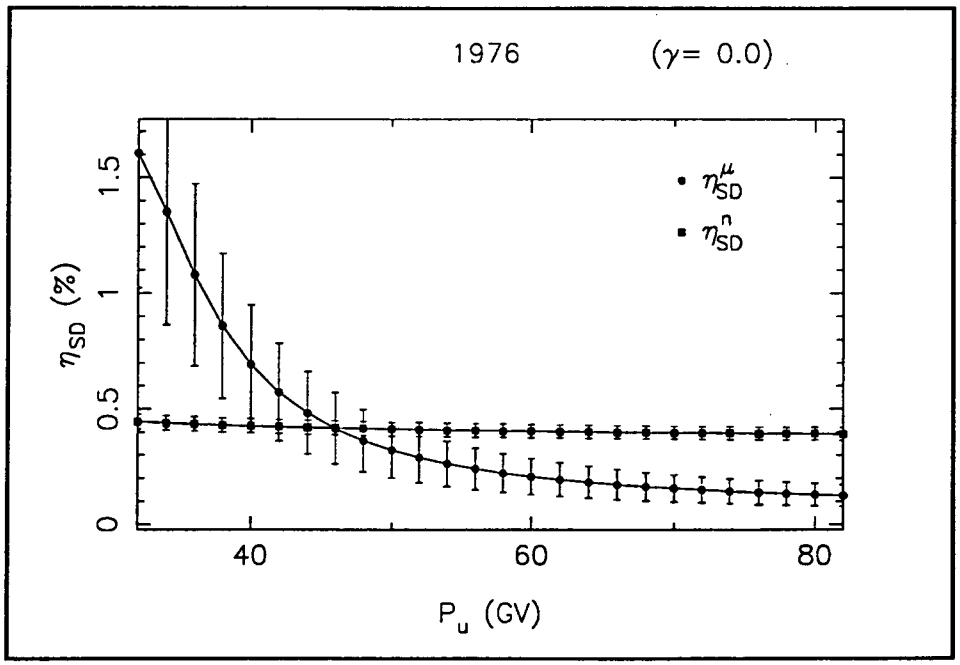

Figure 3.5b Same as Figure 3.5a except for the year 1976. The best estimate of the upper limiting rigidity for 1976 is indicated from the point of intersection at 46 GV.

A^{μ}_{SD} and A^{n}_{SD} are measurements of the true values of $\left(A^{\mu}_{SD}\right)^0$ and $\left(A^{n}_{SD}\right)^0$ and are related to the true values by errors σ_μ and σ_n such that $A^{\mu}_{SD} = \left(A^{\mu}_{SD}\right)^0 \pm \sigma_\mu$ and $A^{n}_{SD} = \left(A^{n}_{SD}\right)^0 \pm \sigma_n$. We are measuring the value of rigidity (P) where the values of the free-space amplitude constants are equal. This value P has an error σ_P related to the true value P^0 by $P = P^0 \pm \sigma_P$.

Therefore $$A^{\mu}_{SD}\delta A^{1}_{1,n}(P) = A^{n}_{SD}\delta A^{1}_{1,\mu}(P)$$

and substituting the above relations :

$$\left[\left(A^{\mu}_{SD}\right)^0 \pm \sigma_\mu\right]\left\{\delta A^{1}_{1,n}(P^0 \pm \sigma_P)\right\} = \left[\left(A^{n}_{SD}\right)^0 \pm \sigma_n\right]\left\{\delta A^{1}_{1,\mu}(P^0 \pm \sigma_P)\right\}$$

A Taylor's series expansion of the rigidity term yields :

$$\left[\left(A^{\mu}_{SD}\right)^0 \pm \sigma_\mu\right]\left\{\delta A^{1}_{1,n}(P^0) \pm \sigma_P \frac{d}{dP}\delta A^{1}_{1,n}(P^0) \pm \ldots.\right\} =$$
$$\left[\left(A^{n}_{SD}\right)^0 \pm \sigma_n\right]\left\{\delta A^{1}_{1,\mu}(P^0) \pm \sigma_P \frac{d}{dP}\delta A^{1}_{1,\mu}(P^0) \pm \ldots.\right\}$$

With a little manipulation, the first order approximation of this expression is

$$\pm\sigma_\mu \delta A^{1}_{1,n}(P^0) \pm \left(A^{\mu}_{SD}\right)^0 \sigma_P \frac{d}{dP}\delta A^{1}_{1,n}(P^0) = \pm\sigma_n \delta A^{1}_{1,\mu}(P^0) \pm \left(A^{n}_{SD}\right)^0 \sigma_P \frac{d}{dP}\delta A^{1}_{1,\mu}(P^0)$$

Solving this expression for σ_P and calculating the variance of σ_P (var(σ_P)) :

$$\mathrm{var}(\sigma_P) = \frac{\left(\sigma_n \delta A^{1}_{1,\mu}(P^0)\right)^2 + \left(\sigma_\mu \delta A^{1}_{1,n}(P^0)\right)^2}{\left(\left(A^{\mu}_{SD}\right)^0 \frac{d}{dP}\delta A^{1}_{1,n}(P^0) - \left(A^{n}_{SD}\right)^0 \frac{d}{dP}\delta A^{1}_{1,\mu}(P^0)\right)^2} \qquad (3.22)$$

The standard error in P^0 is $\sqrt{\mathrm{var}(\sigma_P)}$. When calculating the cross-over rigidity P_u and its error (equation 3.22) it is standard to use the measured values of the diurnal variation amplitudes as estimates of the true values of the amplitudes, the values of the coupling coefficients at the measured cross over P_u as estimates of the values of the coupling coefficients at the true value of P_u and the derivatives of the coupling coefficients at the measured cross-over P_u as estimates of the values of the derivatives at the true cross-over P_u. To calculate the derivative a simple numerical procedure was devised and used as an approximation to the true derivative :

$$\frac{d}{dP}\delta A(P_1) \approx \frac{1}{2}\left\{\frac{\delta A(P_1 + P_2) - \delta A(P_1)}{P_2} + \frac{\delta A(P_1) - \delta A(P_1 - P_2)}{P_2}\right\}$$

This analysis can determine quite accurate values for P_u, for example the uncertainty in the derived value shown in Figure 3.5b is ±6 GV. Naturally, any pair of muon

telescope / neutron monitor observations should arrive at the same point of intersection (or at least have the same region of significant intersection. An average value of P_u (from as many determinations of the same yearly value of P_u as there are independent pairs of instruments for that year) can then be performed.

The temporal variation of P_u will be studied by this method from 1957 to 1990 for various assumed values of the spectral index. The assumed values of γ were -0.2 to 0.3 in steps of 0.1. The results of this analysis are presented in Section 3.3.1.

3.2.2 Determining the rigidity spectrum of the ξ_{SD} - method 2

Method 1 does have one flaw - only the upper limiting rigidity can be determined for an assumed spectral index to the rigidity spectrum, i.e. the entire rigidity spectrum cannot be calculated. Of course one could devise a calculation that examined the individual yearly determinations of P_u from the five pairs of instruments in Table 3.1 for their degree of agreement as a function of γ but this would not be as accurate as a method which compares all instruments' results to each other simultaneously. We need an analysis that simultaneously derives both the spectral index and the upper rigidity while taking into account the results of all the instruments. Such an analysis was described by Nagashima (1971) and introduced in this thesis in Section 2.5.1. The following section describes the analysis to derive the rigidity spectrum of ξ_{SD} based on Nagashima's formalism. In essence this is similar to Method 1 but compares all the amplitudes of the anisotropy recorded by instruments and not just those recorded by pairs of instruments. The comparison is done in two-dimensional space (γ, P_u) to determine both spectral parameters.

The χ^2 function defined in Section 2.5.1 (equation 2.27) essentially examines the agreement between independent observations of the two free-space components of the space harmonic component of an anisotropy as a function of the spectral parameters. A minimum in the χ^2 function determines the best estimate of these parameters and also the best fit values of the free-space components. This form of the χ^2 function is used in the next chapter of this thesis to determine the rigidity spectrum of the North-South anisotropy but is not suitable for ξ_{SD}. To use equation (2.27) exactly one needs assurance that the phase of the free-space harmonic component is rigidity independent. The solar diurnal anisotropy's phase in free-space is rigidity dependent (Bieber and Chen 1991a) and so a more suitable χ^2 function needs to be defined. In the formalism, the amplitude constant is (by definition) rigidity independent (this is the fundamental rule which allows the analysis of Method 1). Since

$$\eta_{SD}(\gamma, P_u) = \frac{A_{SD}}{\delta A_1^1(\gamma, P_u)}$$

the χ^2 function used in this analysis will be defined as

$$\begin{aligned} \chi^2(\gamma, P_u) &= \sum_{i=1}^{k} w_i \left[\left(A_{SD,i} - A_{SD} \right)^2 \right] \\ &= \sum_{i=1}^{k} w_i \left[\left(A_{SD,i} - \eta_{SD} \delta A_{1,i}^1 \right)^2 \right] \end{aligned} \tag{3.23}$$

where w_i are the weights given to the individual terms in the sum and are simply the inverse of the squares of the errors of the amplitudes.

The amplitude of the yearly averaged diurnal variation recorded by each instrument can be compared to a best-fit amplitude constant η_{SD} and each corresponding instrument's coupling coefficient for an assumed (γ, P_u). The square of the differences is then summed to produce a value of χ^2. By changing the assumed (γ, P_u), the corresponding χ^2 for the best fit η_{SD} can be determined and compared to the previous value of χ^2. If it is significantly lower then the corresponding assumed values of the spectral parameters are obviously better estimates of the true values.

To analytically derive the best-fit η_{SD} one notes that any minimum in the χ^2 function (as a function of varying η_{SD}) will mean :

$$\frac{\partial}{\partial \eta_{SD}}(\chi^2) = 0 \tag{3.24}$$

Therefore

$$\sum_{i=1}^{k} -w_i 2(A_{SD,i} - \eta_{SD}\delta A^1_{1,i})\delta A^1_{1,i} = 0$$

which has the solution :

$$\eta_{SD} = \frac{\sum_{i=1}^{k} w_i \delta A^1_{1,i} A_{SD,i}}{\sum_{i=1}^{k} w_i \left(\delta A^1_{1,i}\right)^2} \tag{3.25}$$

This is the best-fit amplitude constant for a choice of spectral parameters (γ, P_u). The values of η_{SD} and χ^2 can be determined for a complete set of γ and P_u and the smallest value of χ^2 will indicate the most reasonable values of the spectral parameters and the amplitude constant. As mentioned in Chapter 2, the space of (γ, P_u) considered to contain the true spectra of these anisotropies consists of $\gamma \in$ [-1.5, 1.0] and $P_u \in$ [30, 1000 GV].

Examining the propagation of errors in this expression one finds that the uncertainty in this value (σ_η) is related to the errors in the solar diurnal amplitudes recorded by the instruments (σ_A) by

$$\sigma_\eta = \frac{\sqrt{\sum_{i=1}^{k} \left(w_i \delta A^1_{1,i} \sigma_{A,i}\right)^2}}{\sum_{i=1}^{k} w_i \left(\delta A^1_{1,i}\right)^2} \tag{3.26}$$

Section 3.3.2 contains the results from such an analysis of the solar diurnal anisotropy. The yearly averaged amplitudes from the 12 cosmic ray instruments listed in Table 3.2 were used

to examine the best fit rigidity spectra for each year from 1957 to 1990. The average rigidity spectrum for the entire period was also determined from the above process by including all the yearly averaged diurnal amplitudes in the sum in (3.25). Averages over other epochs were obtained by selecting the yearly averaged diurnal amplitudes derived for those epochs and including these in the sum in (3.25). The epochs of interest for this thesis are periods of distinct solar polarity. Comparing results from different epochs allows examination of any solar polarity dependence of the rigidity spectrum. These results are also presented in Section 3.3.2.

Table 3.2 Stations and instruments used in the determination of the best-fit rigidity spectrum of the solar diurnal anisotropy. Data from these instruments are also used in the calculations of the modulation parameters.

Station	Mnemonic	Data Availability	P_{med} (GV)
Brisbane*	BRNM	1965-1990	28
Darwin	DNM	1978-1990	50
Deep River	DRNM	1965-1988	17
Embudo	EMBV	1965-1990	135
Hobart+	HNM	1968-1990	17
	HUV	1957-1989	185
	HUI	1973-1989	195
Kerguelen	KNM	1965-1988	17
Mawson#	MNM	1957-1990	17
	MSV	1957-1971	50
	MUN	1973-1990	165
Mt. Wellington	MTNM	1971-1990	17

* Years 1974, 1975 and 1976 missing
\+ Years 1975 and 1976 missing (for HNM only)
\# 1973 missing (for MNM only)

3.3 Rigidity spectrum determinations

3.3.1 Method 1

Each pair of cosmic ray recording instruments in Table 3.1 had their amplitude constants examined as a function of P_u (for an assumed γ) for each year that both instruments were operating. As explained in Section 3.2.1, by comparing the amplitude constants determined from a neutron monitor and underground muon telescope for a given year, a good estimate of P_u for that year can be determined. Appendix 3 shows the results from each pair of instruments for each γ from -0.2 to 0.3. Each set of results is very similar, with P_u having an obvious variation regardless of the choice of γ. The values of P_u determined from the analysis decrease as γ increases. The three minima in the average values of P_u are statistically the same (about 50 GV) over the three solar cycles and all occur around solar minimum. A recurrence tendency rather than a definite period is seen in the maxima. As γ increases the variation remains but is smaller.

Since the analysis gives no information about the most likely value of γ to the rigidity spectrum, one can only make quantitative measurements in the remainder of this section by making a suitable choice of γ. For the reasons explained in Chapter 1 we will use the results pertaining to $\gamma = 0$ during the rest of this section.

In the case of $\gamma = 0$ the average values of the upper limiting rigidity (Figure 3.6) are in excellent agreement with those found by Ahluwalia and Riker (1987) who presented values of P_u from 1965 to 1979 using a different method. The values are not as high as those presented by Ahluwalia (1991) when he used the underground muon telescope at Socorro.

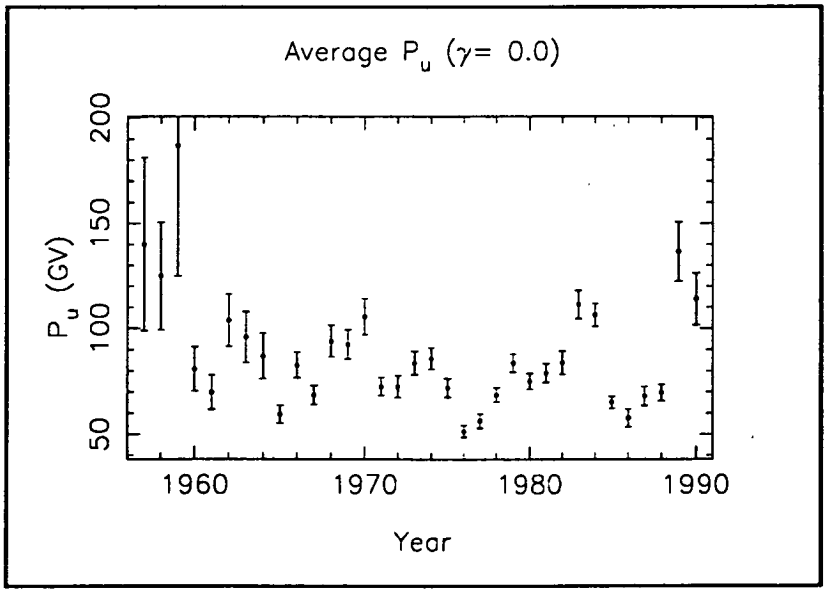

Figure 3.6 Average upper limiting rigidity (P_u) determined from the comparison of the free-space amplitude constant derived from underground muon telescopes and neutron monitor observations of the solar diurnal variation. The associated uncertainties are at the 67% confidence level.

Controlling mechanism of P_u

Ahluwalia (1991) has correlated the large values of P_u from 1983-1985 with the unusually large values of the interplanetary magnetic field for that period. It has been noted that his results for this epoch have slightly higher values than those in Figure 3.6. As noted in Chapter 1, this correlation is not surprising since one would imagine that a particle with high rigidity is more likely to be modulated when the IMF is stronger.

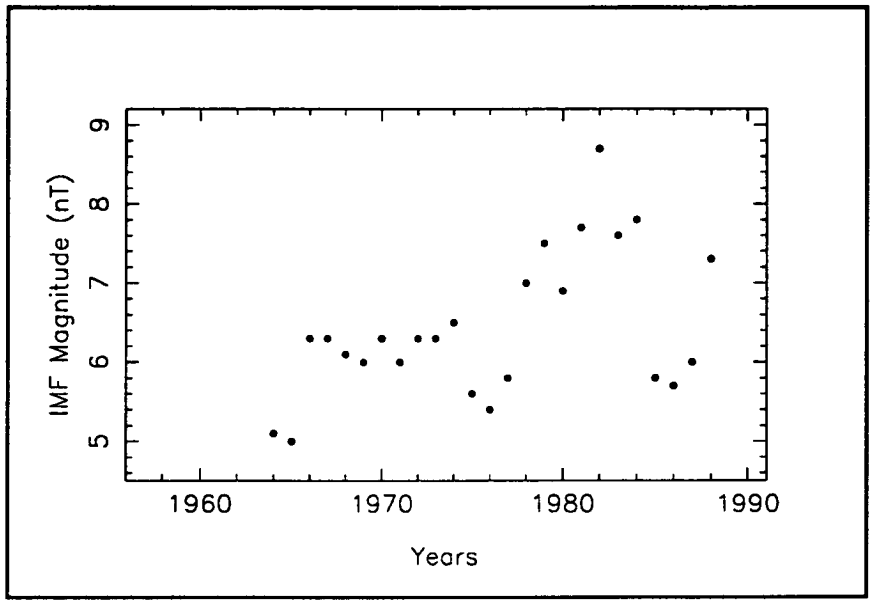

Figure 3.7 Yearly averaged magnitude of the interplanetary magnetic field (IMF) from 1965 to 1988.

Figure 3.7 shows the yearly averaged value of the IMF for the period 1964 to 1988, determined from the hourly measurements of the IMF documented on the OMNI-tape from the National Space Science Data Center (Couzens and King 1986, King 1989). When these are correlated with the values of P_u in Figure 3.6 the correlation coefficient is 0.66. The probability of this occurring by chance is 0.0001. This correlation, shown in Figure 3.8 is exactly the same correlation found by Ahluwalia (1991).

The upper limiting rigidity to the solar diurnal variation does vary over of a solar cycle with the minimum value of P_u, about 50 GV, corresponding to times of solar minimum. The maximum values of P_u are about twice the minimum value and could possibly occur twice throughout a solar cycle, as speculated by Ahluwalia (1991) and Hall et al. (1993).

Unfortunately Method 1 is very limited with respect to the information obtainable about the complete rigidity spectrum of the solar diurnal anisotropy.

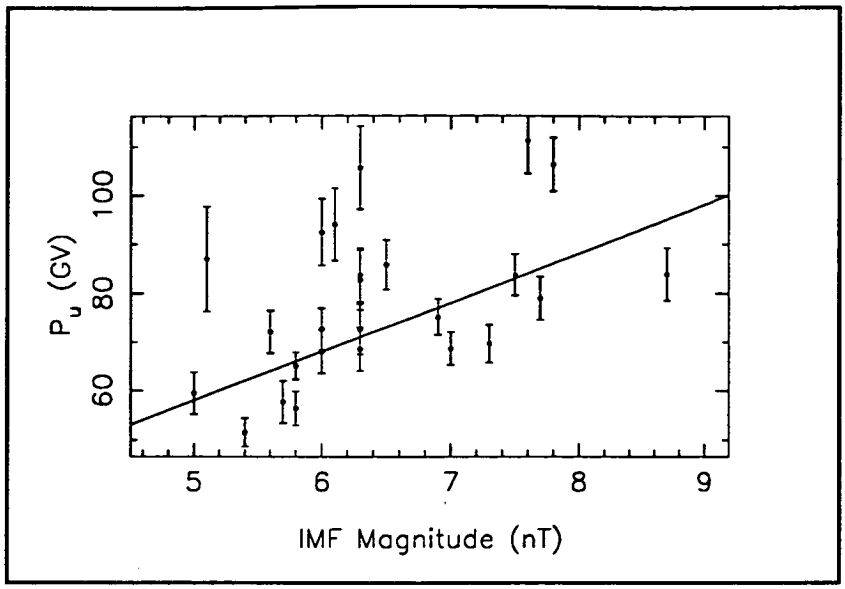

Figure 3.8 Correlation of the magnitude of the interplanetary magnetic field strength (IMF) and the upper limiting rigidity (P_u) to the solar diurnal anisotropy. The correlation coefficient is 0.66. The associated uncertainties are at the 67% confidence level.

3.3.2 Method 2

Average rigidity spectrum

All the yearly averaged harmonic analysis results from the instruments in Table 3.2 were included in the sum in (3.25) to determine the best fit *average* η_{SD} for a specific choice of (γ, P_u) and the corresponding value of χ^2 (equation 3.23). The spectral parameters were changed, the corresponding best-fit η_{SD} calculated and the appropriate value of χ^2 derived and compared to the previous value. The calculations were performed as described in Section 3.2.2 for values of P_u in the range 30GV to 1000GV and for values of γ in the range -1.5 to 1.0 to determine the most likely rigidity spectrum of the anisotropy for the average period 1957 to 1990. The results from this technique are presented in Figure 3.9.

The smallest value of χ^2 corresponds to a most likely rigidity spectrum of (-0.1, 100 GV) which is similar to previous determinations and suppositions reviewed in Chapter 1. A flat rigidity spectrum (0.0, 100 GV) is well within the 1σ region. This leads us to an interesting and important discussion about the spectral parameters and their uncertainties.

As mentioned in Chapter 1, P_u cannot be strictly considered as the value of rigidity where the anisotropy abruptly ceases to exist for more magnetically rigid particles. The formalism certainly treats P_u as having this magical characteristic, but in reality it is erroneous to think that this could occur. P_u must be thought of as a value of rigidity where the anisotropy

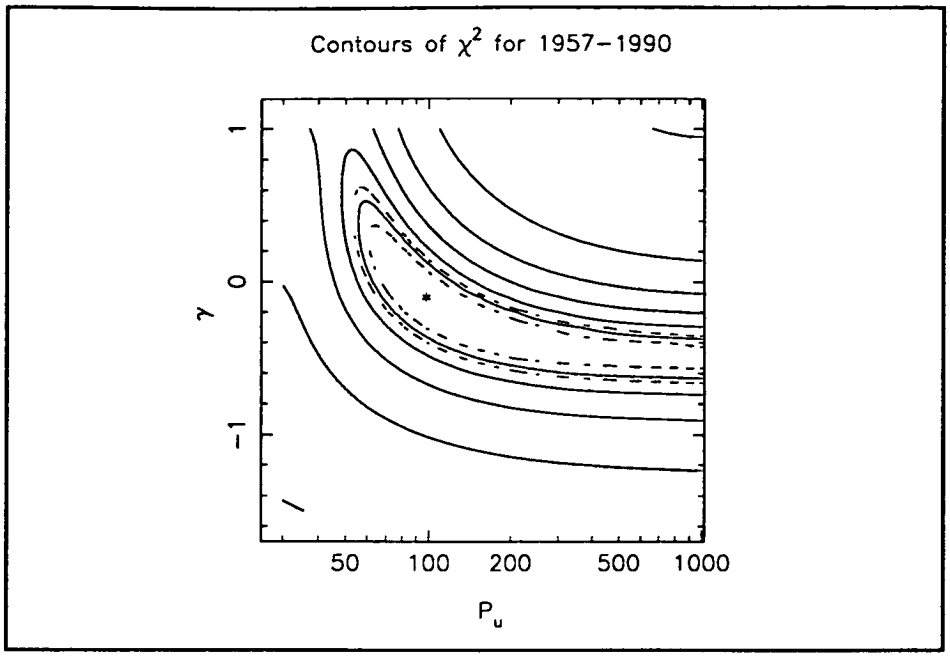

Figure 3.9 Contours of χ^2 as a function of (γ, P_u) for all data from 1957 to 1990. The outer contour has a value of ≈34000 and other contour levels have decreasing values of 19000, 11000, 7000, 5500, and 4500. The minimum value of χ^2 is indicated by the asterisk at (-0.1, 100 GV) and has a value of 3570. The innermost dashed contour region represents the 67% (1σ) confidence interval and the outer dashed contour region represents the 90% confidence interval.

begins to have much less influence than at lower rigidities. With this mind, one can speculate on the dependence that γ has on P_u from a derivation such as the one above. Four of the instruments used in this analysis have median rigidities of response much greater than 100 GV but all of these observe a diurnal variation due to the solar diurnal anisotropy. Clearly then, the anisotropy is present (on average) at rigidities greater than 100 GV but the magnitude of the anisotropy is starting to diminish at rigidities around 150 to 200 GV. This could be why the analysis finds a slightly negative spectrum when we ignore the confidence region. This region of uncertainty is reasonably large (extending up to 1000 GV) but can be reduced by physical arguments. The Socorro underground muon telescope (SOCV) has a threshold rigidity of about 45 GV and a median rigidity of about 300 GV. On average, this instrument observes ξ_{SD}, but at times of solar minimum the diurnal variation in the data is zero. Therefore, on average, P_u must be greater than 45 GV (which is indicated by the confidence intervals being greater than 50 GV). Poatina underground muon telescope (PUM) observes no significant solar diurnal variation. The threshold rigidity of this instrument is about 200 GV and the median rigidity is 1400 GV. One assumes that if P_u was as high as 500 GV then PUM would have a significant solar diurnal variation. Therefore P_u is probably less than 500 GV, significantly reducing the uncertainty region in Figure 3.9. The absolute uncertainties of P_u and γ are then about (-40GV, +400 GV; $\pm$0.4) but these are the worst they could be and are certainly not rectangular around the spectral parameters at the minimum χ^2 value. For example, the rigidity spectrum cannot be (0.3, 100 GV).

If one considers the region of significance (1σ region) around the χ^2 minimum and examines the significant values obtainable along the horizontal (P_u) and vertical (γ) directions (as seems to be the method used by Yasue (1980) when deriving the rigidity spectrum of the North-South anisotropy), then $\gamma = -0.1 \pm 0.2$ and $P_u = 100 \pm 25$ GV. These results and the corresponding best fit amplitude constant η_{SD} are summarised in Table 3.3.

Table 3.3 Values of the best fit average parameters of the solar diurnal anisotropy derived for various periods. The errors are to 1σ and are calculated from an inspection of the contour lines (see text).

Period	γ	P_u (GV)	η_{SD} (%)
1957-1990	-0.1 ± 0.2	$\approx 100 \pm 25$	0.42 ± 0.002
1960-1968, 1981-1989 A<0	-0.3 ± 0.2	$\approx 150^{+150}_{-50}$	0.42 ± 0.003
1972-1979 A>0	$+0.5 \pm 0.3$	$\approx 60 \pm 10$	0.35 ± 0.003

Magnetic polarity dependent rigidity spectra

Figure 3.10 contains contour plots of the results from the same analysis except that the harmonics used in the sum in equation (3.25) were separated into two sets - years when the solar magnetic polarity state was A>0 (1972-1979) and years when A<0 (1960-1968 and 1981-1989). These results are also shown in Table 3.3.

One can conclude that during these two distinct polarity states of the heliosphere the solar diurnal anisotropy has two distinct characteristics. In the A<0 state ξ_{SD} has a similar form to that of the 34 year average result. Its spectrum is close to flat or slightly negative and the amplitude is 0.42%. Note that 18 years of data out of the total 34 years analysed are from the A<0 epochs. Only eight years out of the total 34 are from the A>0 epoch. With this in mind the similarities between the average and A<0 polarity state results could probably be expected. The rigidity spectrum of the anisotropy during the A>0 polarity state is different. During this epoch the anisotropy most likely has a positive spectrum. The P_u which is determined is lower than 100 GV which perhaps shows the dependent nature of the two spectral parameters in the analysis or could be a real effect. Regardless, the analysis indicates that these spectra best describe the anisotropy for these two periods according to the formalism which we use. Note that the average amplitude constant for the A>0 magnetic polarity state is reduced slightly.

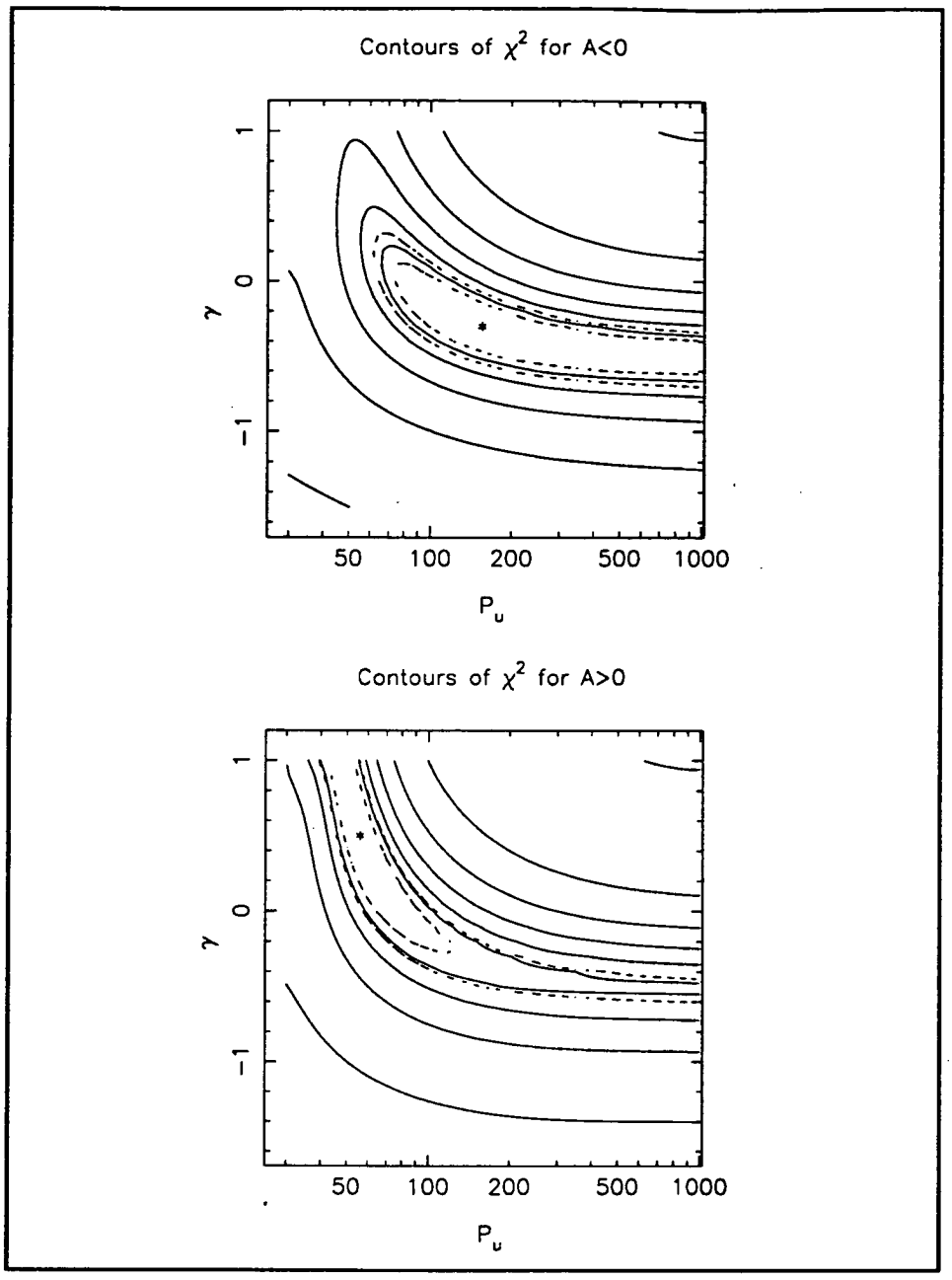

Figure 3.10 Same as Figure 3.9 except that the amplitudes of the diurnal variation were analysed according to the magnetic polarity of the heliosphere. The contours of χ^2 values for the A > 0 polarity state are 10000, 5000, 2900, 1700, 1200, 900 and have a minimum at 575. The contours for the A < 0 polarity state are 18000, 10000, 6000, 4000, 3000, 2700 and have a minimum at 2200. The number of data-years in the A > 0 polarity state analysis was 74 while the number in the A < 0 polarity state analysis was 141.

In light of other researchers' work it is not surprising that ξ_{SD} should have a different rigidity spectrum during the A > 0 polarity state of the heliosphere. We have already seen that the anisotropy has an earlier phase in this polarity state compared to the A < 0 polarity state for all rigidities (Duggal and Pomerantz 1975, Ahluwalia 1988a, Bieber and Chen 1991a). This phase change has been ascribed to the appearance or enhancement of the radial component of

the solar diurnal anisotropy which has a positive rigidity spectrum (Ahluwalia 1988b); the spectral index being about +0.3. This may be reflected in this analysis by the higher spectral index being the better representation of the spectrum in the A>0 magnetic polarity state. There are physical reasons for such an anisotropy being present in alternate magnetic polarity states. We know from the review of the theoretical literature (Section 1.2.1) that drift models predict that cosmic ray particles will drift down from polar latitudes during the A>0 polarity state and travel to the outer regions of the heliosphere along the neutral sheet. Coupled to the convection of particles by the solar wind, the net streaming could produce an anisotropy of particles radially from the Sun (1200 local time direction) that would be much larger than in the A<0 polarity state when the drift streaming and the convection are predicted to be in opposite directions. This simple model would certainly explain the differences between the derived rigidity spectra in Figure 3.10. A consequence of polarity dependent streaming may be that the mean free-paths of particles may also be polarity dependent. This will be tested in Chapter 5.

It should be noted though, that while the two minima in the contour plots are significantly different (to 1σ) there is an overlap of the two significant regions in the plots in Figure 3.10 which has a centre at (-0.1, 90 GV) and extends from +0.1 to -0.2 and 80 to 120 GV. Hence, we certainly cannot discount an invariant solar diurnal anisotropy, but it would seem likely that the average anisotropy does have different rigidity spectra in opposite heliospheric magnetic polarity states.

Yearly averaged ξ_{SD}

The results of the rigidity spectra analyses above indicate that on average the spectrum of ξ_{SD} is well represented by

$$G(P) = \begin{cases} \left(\frac{P}{10}\right)^{-0.1\pm0.2}, & P \le 100 \pm 25 \text{ GV} \\ 0, & P > 100 \pm 25 \text{ GV} \end{cases}$$

$$\text{and} \quad |\xi_{SD}| = \eta_{SD} G(P) \qquad (3.27)$$

$$\text{where} \quad \eta_{SD} = 0.420\% \pm 0.002$$

The analyses also indicate that the anisotropy does change character after solar polarity reversals; the spectrum becoming positive during the A>0 polarity state.

In the remaining sections of this chapter, ξ_{SD} is used to determine $\lambda_{||}G_r$ and the bi-directional latitudinal gradient indicator $G_{|z|}$. When deriving these modulation parameters, using the spectrum in (3.27) would give a reasonably accurate indication of their values, but since it is feasible that the spectrum of the anisotropy has a temporal variation it would be wrong not to investigate this possibility in more detail.

This section uses the yearly averaged data recorded by the instruments in Table 3.2 to calculate the sum in equation (3.25) *one year at a time* to examine the best-fit η_{SD} as a function of the spectral parameters and compare the corresponding values of χ^2. In this way, the rigidity spectrum of ξ_{SD} can be examined for every year.

Figure 3.11 shows the most likely spectral parameters of ξ_{SD} for each year from 1957 to 1990. The errors on each γ value are again about ± 0.2 and each P_u value has a typical uncertainty of -25 GV and +50 GV, derived similarly to the errors discussed in the previous section. Appendix 4 contains the contour plots of the χ^2 values of each year.

Three major deductions can be made from the results in Figure 3.11. First, the analysis has resulted in values of P_u which have larger values around years of solar maxima (1959 and 1970) and 1983, and lower values around years of solar minima (1965, 1975, 1986) although there are other years between 1970 and 1980 that have low values of P_u. One would have to assume that the determinations for 1982, 1987, 1988 and 1989 are not completely reliable. These years are associated with the lowest values of γ out of the entire period from 1957 to 1990, lending support to this. As can be seen from the associated contour plots in Appendix 4 the errors of the spectral parameters to these anomalous years are very large (i.e. about 900 GV for P_u and ± 0.3 for γ). All other years seem reliable, the most likely values of P_u varying between 40 and 180 GV. This certainly agrees with previous determinations of P_u surveyed in Chapter 1.

Aside from the years mentioned above, the other determinations of γ are all within the values one might expect. The reliable values range between -0.4 and +0.5 with one very important observation which may increase the evidence for a polarity dependent rigidity spectrum – all the years defined in the $A<0$ polarity state have most likely γ's which are negative or zero. Years during the $A>0$ polarity state are the only years which have positive spectral indices, although three out of these eight years have negative indices. This is by no means a definite result but does agree with the results in Figure 3.10.

The most important conclusion to be drawn from the results in Figure 3.11 is that η_{SD} is not invariant even when the rigidity spectrum is varied. The analysis indicates that η_{SD} has a variation in phase with the sunspot cycle – lower amplitudes around solar minimum and larger amplitudes around years of solar maximum. Of course this variation could be due to the spectrum having been allowed to vary, but other researchers have shown that for a static rigidity spectrum η_{SD} has exactly the same variation (Humble 1971, Ahluwalia and Riker 1987, Bieber and Chen 1991a and other references in Chapter 1). The same result is achieved when the χ^2 values for each year are examined for a constant γ, i.e. choosing a specific γ to remain constant for the entire period, one can determine which value of P_u has the least χ^2 value between 30 and 1000 GV. The corresponding best-fit η_{SD} can then be examined from year to year. Figure 3.12 contains the results of this process for an arbitrary choice of a flat spectrum. The resulting values of the most likely P_u are almost exactly the same as those determined by Method 1 for the same spectral index. Note that the temporal variation of η_{SD} is still present even if γ remains constant.

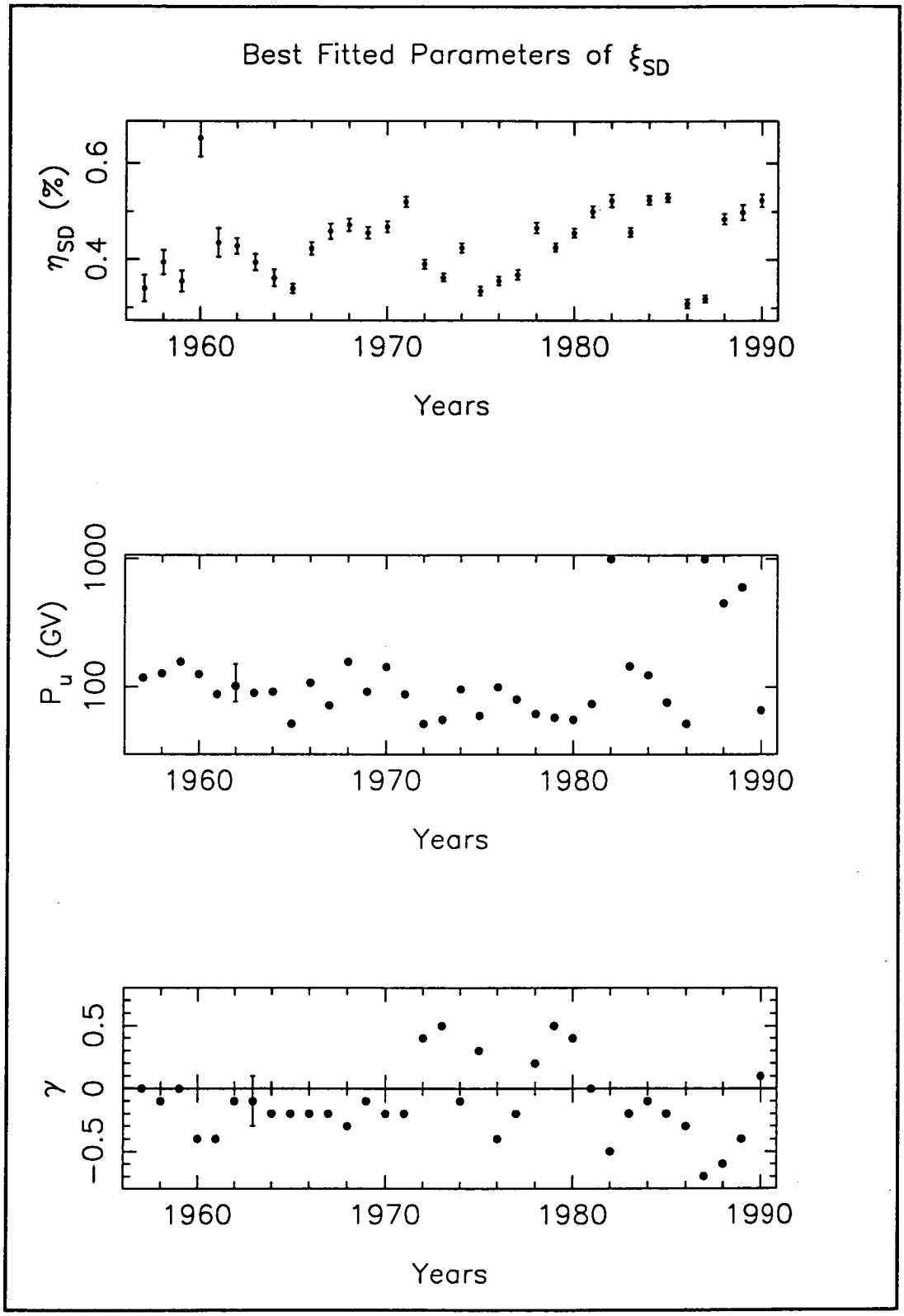

Figure 3.11 Yearly averaged best-fitted parameters of the solar diurnal variation. The values were obtained by using the yearly averaged amplitudes of the diurnal variation recorded by each instrument in Table 3.2. in the sum in equation (3.25). The typical 1σ errors of the derived upper limiting rigidity and spectral index values are shown.

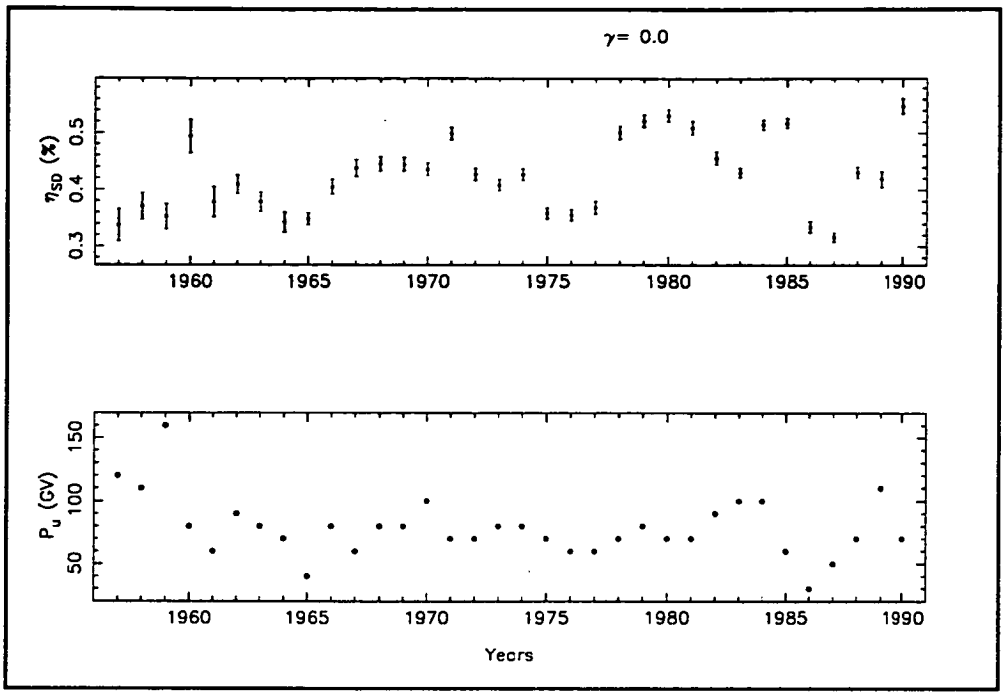

Figure 3.12 Best-fit amplitude constant (η_{SD}) and upper limiting rigidity (P_u) to the solar diurnal anisotropy from 1957 to 1990 derived while assuming a constant spectral index of zero. The associated uncertainties are at the 67% confidence level.

η_{SD} can be calculated from equation (3.25) for every year by assuming a specific combination of (γ, P_u). The values η_{SD}, calculated by assuming that the rigidity spectrum is constantly (0, 100 GV) from 1957 to 1990 are shown in Figure 3.13. We can observe that η_{SD} is still temporally variable.

Regardless of what form the rigidity spectrum of ξ_{SD} takes, it must be concluded that η_{SD} is not constant and has a variation with a period of about 11 years.

The reference axis or free-space phase (t_R) can also be examined as a function of the spectral parameters. Since it is probable that the phase is rigidity dependent, each individual instrument can be examined using the fifth relation in equation (3.8) :

$$t_R(\gamma,P_u) = t_{SD} + \delta t_1^1(\gamma,P_u)$$
$$\text{where} \quad \delta t_1^1 = \frac{24}{2\pi}\arctan\left(\frac{s_1^1(\gamma,P_u)}{c_1^1(\gamma,P_u)}\right) \tag{3.27}$$

Here, equation 3.27 has had the spectral dependence explicitly included.

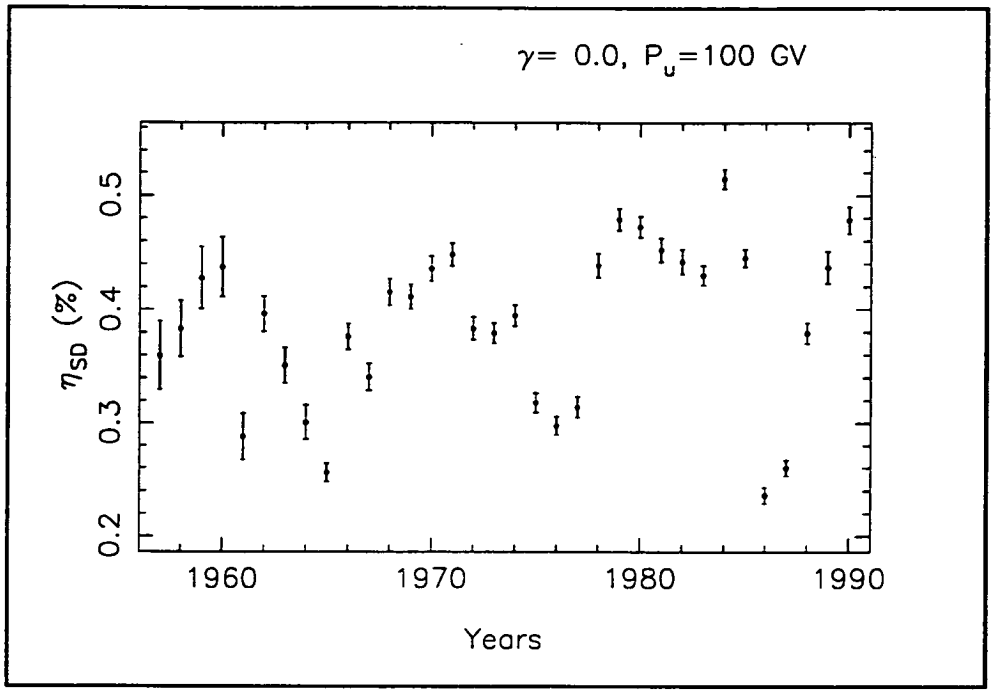

Figure 3.13 Best-fit amplitude constant (η_{SD}) to the solar diurnal anisotropy from 1957 to 1990 derived while assuming a constant spectral index of zero and upper limiting rigidity of 100 GV for each year. The associated uncertainties are at the 67% confidence level.

Figures 3.14 and 3.15 show plots of the phase of the solar diurnal anisotropy from 1957 to 1990 calculated from the solar diurnal variations recorded from two neutron monitors. Note that the results are essentially the same, implying that at about 17 GV the anisotropy has a large 22-year variation in t_R with the earliest time of maximum about 15 hours L.T., occurring around 1976.

Figures 3.16 and 3.17 show the phase for the same period but for observations of median rigidities of 135 and 185 GV, respectively. Here we see that the phase is indeed rigidity dependent with the earliest times occurring for the highest rigidity particles around the year 1976. The other instruments in Table 3.3 agreed with this observation. The phase of ξ_{SD} is virtually unchanged by altering the rigidity spectrum so it can be concluded that this rigidity dependent phase is a real effect and not simply due to a variation in the spectrum.

In the following section the modulation parameters $\lambda_{||}G_r$ and $G_{|z|}$ will be calculated from ξ_{SD} at various rigidities. The rigidity spectrum used to determine the anisotropy will be the yearly averaged results determined here and also the long term average rigidity spectrum (0, 100 GV) determined in the previous section (within errors) and by other researchers.

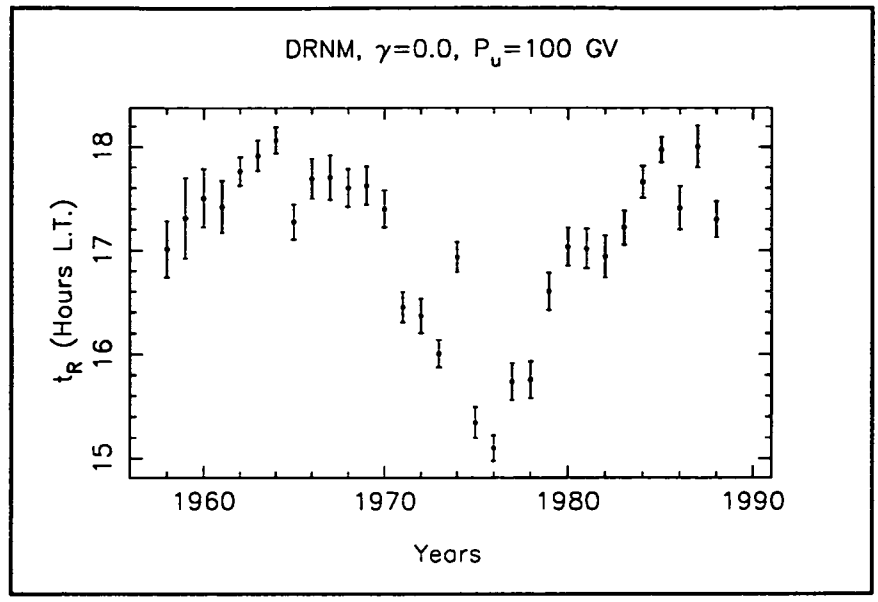

Figure 3.14 The free-space phase (t_R) of the solar diurnal anisotropy from 1958 to 1988 calculated from the yearly average solar diurnal variation recorded at the Deep River neutron monitor. The rigidity spectrum was assumed to be flat with an upper limiting rigidity of 100 GV for each year. The median rigidity of the instrument is 17 GV. Note that the years analysed here are different to those analysed from DRNM in the rest of this thesis. These extra years (1958 to 1964) of data arrived at the Hobart cosmic ray group immediately prior to the submission of this thesis and have only been included here. The associated uncertainties are at the 67% confidence level.

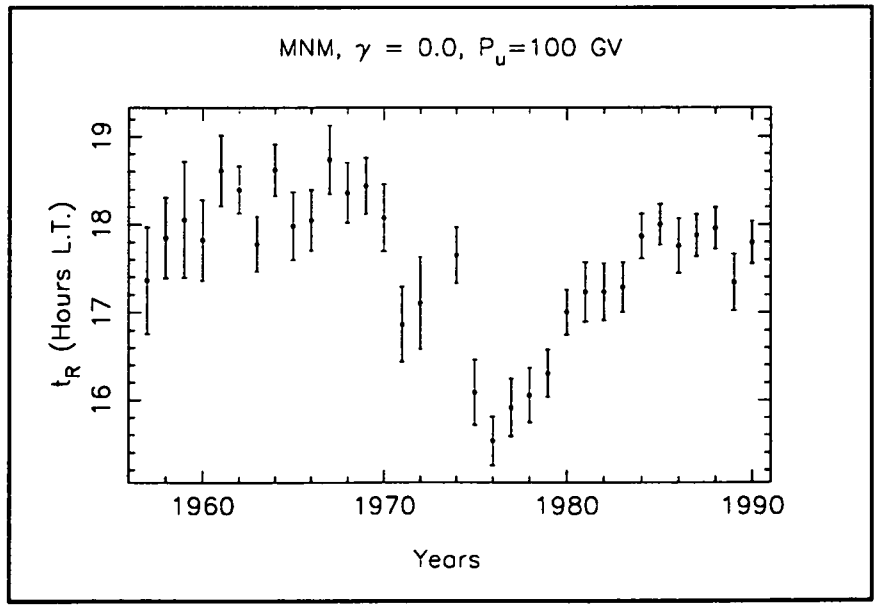

Figure 3.15 Same as Figure 3.14 except the phase is calculated from 1957 to 1990 from the yearly average solar diurnal variation recorded at the Mawson neutron monitor. The median rigidity of the instrument is 17 GV.

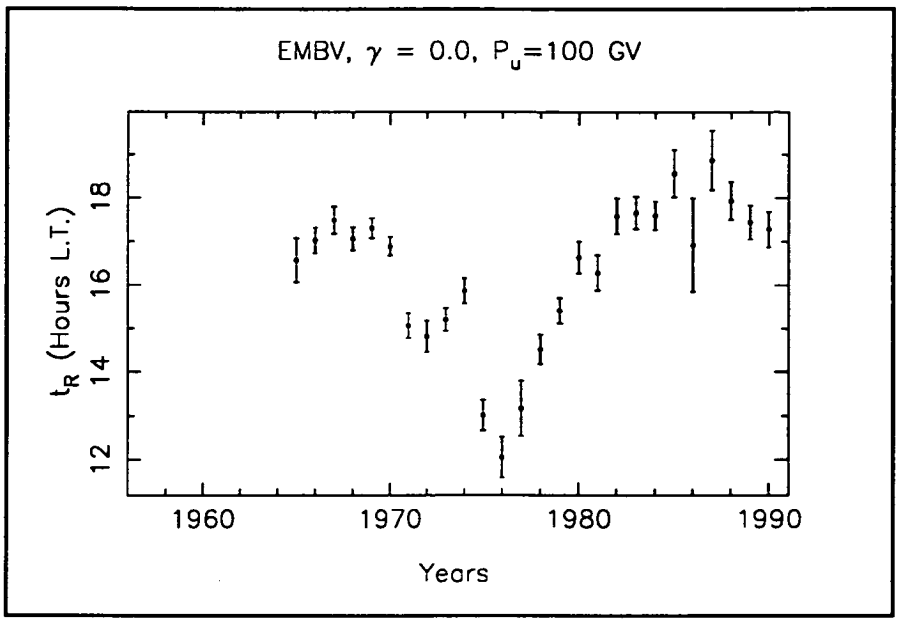

Figure 3.16 Same as Figure 3.14 except the phase is calculated from 1965 to 1990 from the yearly average solar diurnal variation recorded at the Embudo underground muon telescope. The median rigidity of the instrument is 135 GV.

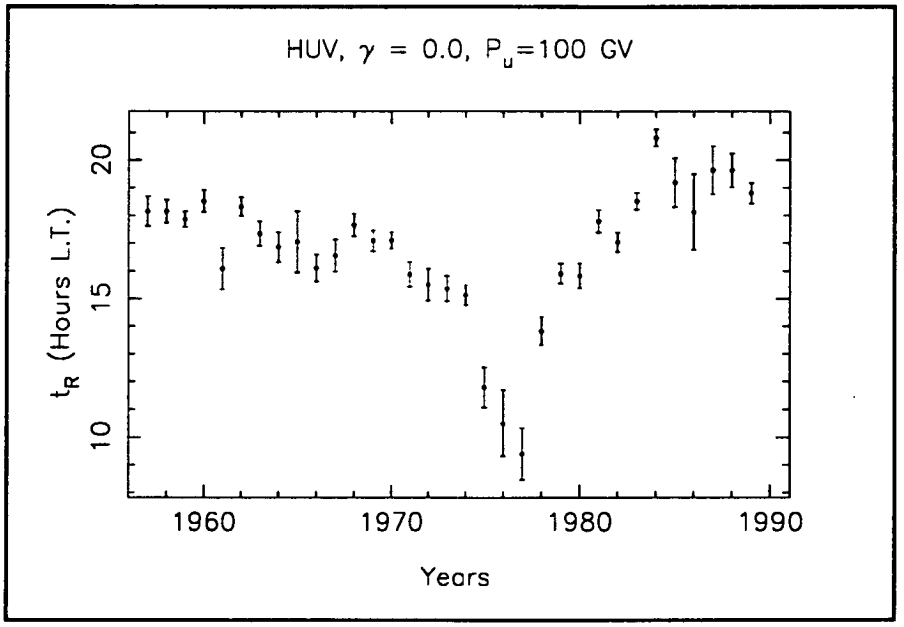

Figure 3.17 Same as Figure 3.14 except the phase is calculated from 1957 to 1989 from the yearly average solar diurnal variation recorded at the Hobart underground muon telescope. The median rigidity of the instrument is 185 GV.

3.4 The modulation parameters $\overline{\lambda_{||}G_r}$ and $G_{|z|}$

Cosmic ray solar modulation models include not only the convection of particles by the solar wind and diffusion of particles in the heliosphere caused by irregularities in the IMF but also IMF gradient and curvature drifts. These have been reviewed in Chapter 1. These models lead to predictions of the density of cosmic ray particles in the heliosphere that have 11- and 22-year periods due to the 11-year solar cycle and the 22-year solar magnetic polarity cycle. A 22-year cycle in the radial gradient of galactic cosmic rays with a smaller gradient for the A>0 polarity state is predicted. The radial gradient is also predicted to be lower at times of solar minimum than at times of solar maximum, implying an 11-year cycle. Another prediction is the existence of a bi-directional latitudinal density gradient that changes direction at every solar polarity reversal. Specifically, the models predict a local maximum in the number density of particles at (and on both sides of) the neutral sheet for years of A>0 and a local minimum in the density during years of A<0 polarity.

By analysing the solar diurnal variation in data from neutron monitors and an ion chamber Bieber and Chen (1991a) conclusively showed that the product of the parallel mean free path and the radial density gradient (averaged over IMF sectors), $\overline{\lambda_{||}G_r}$, of particles with rigidities less than about 70 GV was dependent on the solar polarity. Bieber and Chen (1991a) also showed the bi-directional latitudinal gradient ($G_{|z|}$) to be in excellent agreement with theoretical predictions. This section reports a similar analysis using data obtained from the network of Hobart and Mawson neutron monitors and surface and underground muon telescopes and some other instruments (see Table 3.2). The neutron monitor and surface muon telescope data allow us to obtain results directly comparable with Bieber and Chen (1991a) and the underground muon telescope data (having median rigidities greater than 130 GV) give results at energies twice those previously studied by other researchers except Ahluwalia and Sabbah (1993).

3.4.1 $\overline{\lambda_{||}G_r}$

Figures 3.18, 3.19 and 3.20 show $\overline{\lambda_{||}G_r}$ at various rigidities for the years 1957 to 1990 as calculated from observations of the solar diurnal variation and using equation (3.16). Appendix 5 contains plots of $\overline{\lambda_{||}G_r}$ derived from the other instruments. The rigidity range explored is from about 17 GV to 195 GV. A dominant 22 year cycle and a smaller 11 year cycle are clearly evident with local minima present around times of solar minimum. The rigidity spectrum of ξ_{SD} assumed in the calculations is that which was shown in Section 3.3 to be a good representation of the average rigidity spectrum : $\gamma = 0$ and $P_u = 100$ GV.

Bieber and Chen (1991a) and Ahluwalia and Sabbah (1993) found that $\overline{\lambda_{||}G_r}$ depends on the magnetic polarity state of the heliosphere. The results shown in Figures 3.18 to 3.20 and Appendix 5 indicate that $\overline{\lambda_{||}G_r}$ is suppressed during the solar minimum of the A>0 polarity state, in agreement with the above researchers.

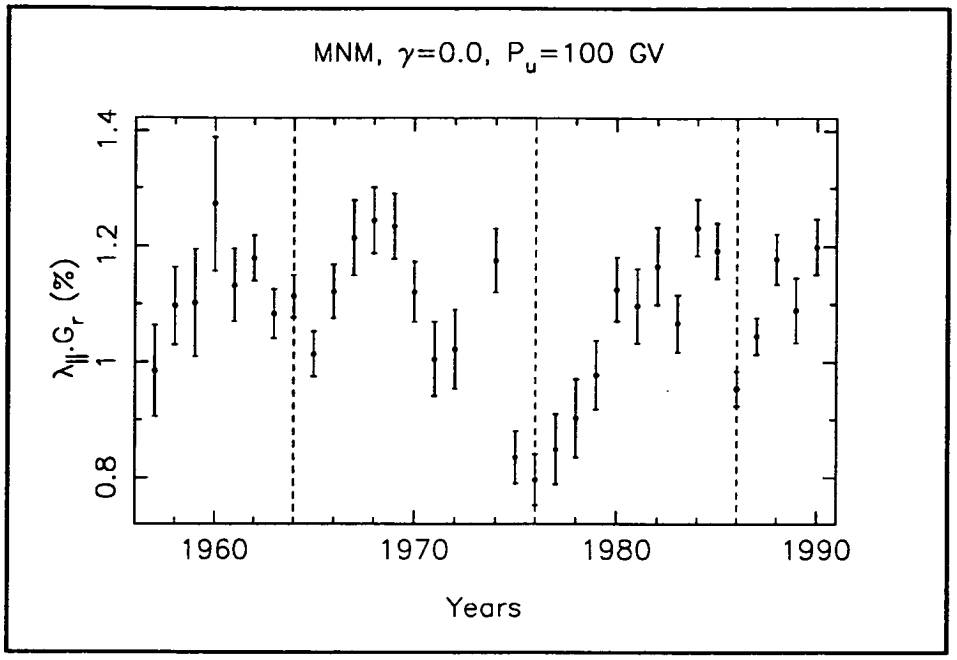

Figure 3.18 $\overline{\lambda_{\|}G_r}$ determined from the solar diurnal variation recorded by the Mawson neutron monitor from 1957 to 1990. The median rigidity of response is about 17 GV. Years corresponding to solar minimum are indicated by the dashed lines at 1964, 1976 and 1986. The associated uncertainties are at the 67% confidence level.

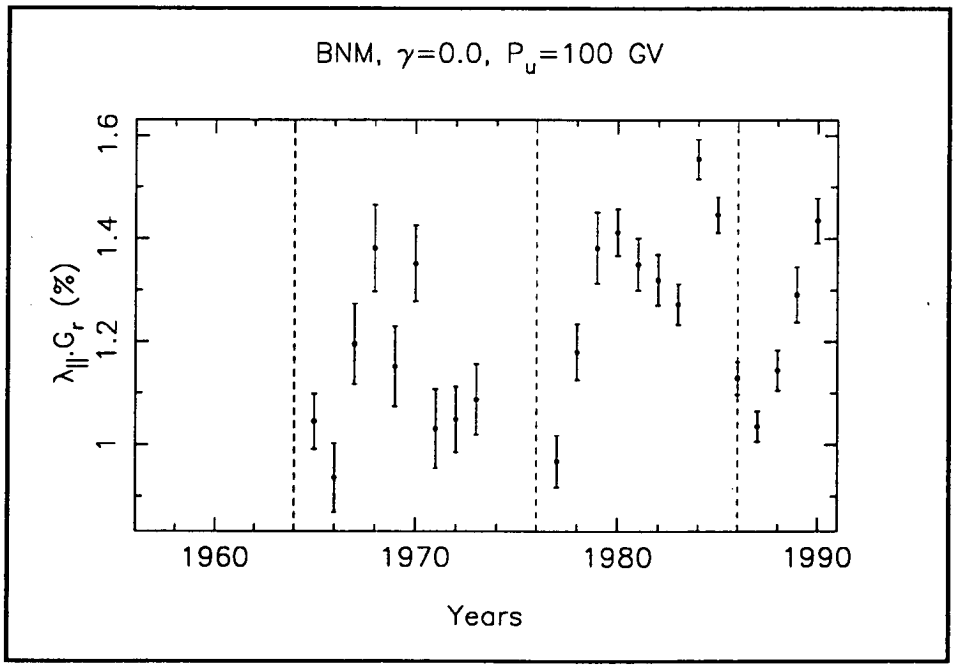

Figure 3.19 $\overline{\lambda_{\|}G_r}$ determined from the solar diurnal variation recorded by the Brisbane neutron monitor from 1965 to 1990. The median rigidity of response is about 28 GV. Note that 1974, 1975 and 1976 are missing.

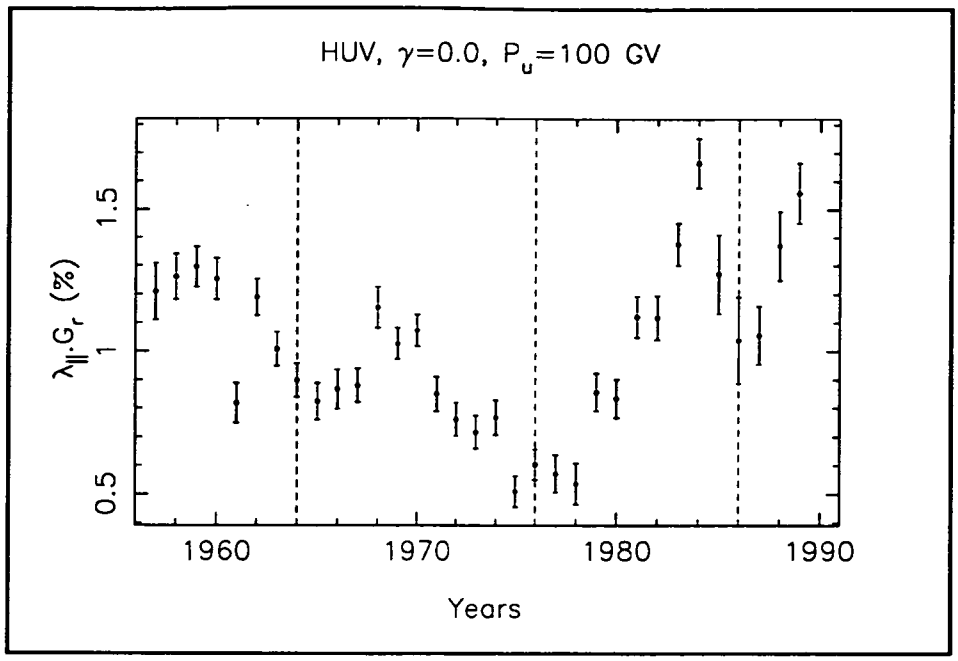

Figure 3.20 $\overline{\lambda_{||}G_r}$ determined from the solar diurnal variation recorded by the Hobart vertical underground muon telescope from 1957 to 1989. The median rigidity of response is about 185 GV.

Bieber and Chen's study also found that the value of $\overline{\lambda_{||}G_r}$ depended inversely on the median rigidity of the cosmic ray particles being detected. They observed this in both polarity states. It is obvious from Figures 3.18 to 3.20 that there is an inverse rigidity dependence of $\overline{\lambda_{||}G_r}$ during the A>0 polarity state. Conversely, Ahluwalia and Sabbah (1993) found no rigidity dependence of this modulation parameter at any time. It should be noted that Ahluwalia and Sabbah's analysis did not include the years 1975 and 1976 in the calculations; years in which Figures 3.18 to 3.20 show $\overline{\lambda_{||}G_r}$ to have the most rigidity dependence.

Table 3.4 contains the average values of $\overline{\lambda_{||}G_r}$ around years of solar minimum but in different magnetic polarity states (i.e. 1963, 64, 65 and 1975, 76, 77 and 1985, 86, 87) and longer averages over years of constant solar magnetic polarity. The results agree with the studies of both Bieber and Chen (1991a) and Ahluwalia and Sabbah (1993). These observations indicate that $\overline{\lambda_{||}G_r}$ does get smaller as the rigidity of the particles in the anisotropic stream increases during years of A>0 polarity, and that between 30 and 130 GV this dependence vanishes and the values of $\overline{\lambda_{||}G_r}$ become constant as a function of rigidity. Calculations from data collected by the Darwin neutron monitor (P_{med} = 50 GV) suggest that $\overline{\lambda_{||}G_r}$ decreases quickly as a function of rigidity up to about 50 GV and then becomes constant. During the A<0 polarity state the results agree with those of Ahluwalia and Sabbah (1993). There is very little polarity dependence of $\overline{\lambda_{||}G_r}$ during these years; only around times of solar minimum could one suggest such a dependence. Note that the high latitude neutron monitor results are all consistent so averages of their values are included in the rest of the analyses.

Table 3.4 Averages of $\overline{\lambda_{\|}G_r}$ over selected epochs. The rigidity spectrum assumed in the calculations was a flat spectrum with an upper limiting rigidity of 100 GV for each year. The associated uncertainties are at the 67% confidence level.

Station	P_{med} (GV)	$\overline{\lambda_{\|}G_r}$ (%) Average A<0#	$\overline{\lambda_{\|}G_r}$ (%) Average A>0#	$\overline{\lambda_{\|}G_r}$ (%) 1963-1965 A<0	$\overline{\lambda_{\|}G_r}$ (%) 1975-1977 A>0	$\overline{\lambda_{\|}G_r}$ (%) 1985-1987 A<0
DRNM	17	1.06± .01	0.85± .01	0.96± .02*	0.76± .01	1.04± .01
HNM	17	1.19± .01	0.93± .02$$	–	0.83± .03	1.16± .02
KNM	17	1.15± .01	0.94± .01	1.04± .03*	0.85± .02	1.11± .02
MNM	17	1.11± .01	0.92± .02**	1.07± .02	0.82± .03	1.03± .02
MTNM	17	1.10± .01	0.88± .01	–	0.79± .02	1.08± .02
NM Average	17	1.12± .01	0.90± .01	1.02± .01	0.81± .01	1.08± .01
BNM	28	1.25± .01	–	1.05± .05*	0.97± .05*	1.19± .02
DNM	50	0.91± .01	–	–	–	0.79± .02
MSV	50	1.04± .01	–	1.00± .02	–	–
EMBV	135	0.98± .01##	0.65± .02	–	0.54± .02	0.96± .05*
MUN	165	1.06± .02	0.67± .02**	–	0.62± .03	0.96± .02
HUV	185	1.06± .02	0.66± .02	0.91± .04	0.56± .03	1.11± .02
HUI	195	1.17± .02	0.62± .03**	–	0.52± .05	1.08± .05

* One year only.

** One year missing

$$ Two years missing

\# Averaged over complete epochs

Averaged over 1966-69 and 1981-85.

These results suggest a peculiar phenomena - during the A>0 polarity state, $\overline{\lambda_{\|}G_r}$ is not only smaller than $\overline{\lambda_{\|}G_r}$ during the A<0 polarity state, but also has an inverse dependence on the rigidity of the particles, whereas in the A<0 polarity state this dependence is insignificant.

Of course, this observation may be due to the static rigidity spectrum being used in the calculations. Table 3.5 shows the results of repeating the calculations but assuming the more dynamic rigidity spectra determined in Section 3.3.2 from analysing all years individually. These calculations have used the spectra from Figure 3.11. When assuming the other rigidity spectra derived in Section 3.3.2 all the results are similar to those in Table 3.4, suggesting the phenomena is a real effect.

Table 3.5 Averages of $\overline{\lambda_{\parallel} G_r}$ over selected epochs. The calculations for each year assumed the individual rigidity spectrum presented in Figure 3.11. For the outliers of Figure 3.11 (i.e. 1982, 1987, 1988, 1989) the spectrum (-0.3, 150 GV) was assumed. The associated uncertainties are at the 67% confidence level.

Station	P_{med} (GV)	$\overline{\lambda_{\parallel} G_r}$ (%) Average A<0#	$\overline{\lambda_{\parallel} G_r}$ (%) Average A>0#	$\overline{\lambda_{\parallel} G_r}$ (%) 1963-1965 A<0	$\overline{\lambda_{\parallel} G_r}$ (%) 1975-1977 A>0	$\overline{\lambda_{\parallel} G_r}$ (%) 1985-1987 A<0
NM Average	17	1.11 ± .01	0.90 ± .01	1.03 ± .01	0.82 ± .01	1.06 ± .01
BNM	28	1.24 ± .01	-	1.12 ± .05*	1.02 ± .05*	1.18 ± .02
DNM	50	0.91 ± .02	-	-	-	0.81 ± .02
MSV	50	1.02 ± .01	-	1.00 ± .02	-	-
EMBV	135	0.92 ± .01##	0.64 ± .02	-	0.58 ± .02	0.98 ± .05*
MUN	165	0.93 ± .01	0.68 ± .02**	-	0.64 ± .03	0.88 ± .02
HUV	185	0.99 ± .01	0.67 ± .03	0.96 ± .04	0.62 ± .03	0.95 ± .05
HUI	195	0.98 ± .02	0.64 ± .04**	-	0.59 ± .04	0.98 ± .04

* One year only.

** One year missing

\# Averaged over complete epochs

Averaged over 1966-69 and 1981-85.

The implications of such a polarity dependent parameter are strange. In the negative magnetic polarity state the gradient and mean-free path of all energetic particles may be the same. The analyses reviewed in Chapter 1 all found that the radial gradient decreases as the rigidity of the cosmic rays increases. This means that in the negative polarity state, the mean-free path of particles parallel to the IMF increases as a function of rigidity at the same rate as the radial gradient decreases as a function of rigidity. In the positive polarity state, either the radial density gradient is smaller than in the negative polarity state, in which case a key prediction of drift theories has been observed, or the mean-free paths of particles are smaller

during this epoch. Bieber and Chen (1991b) and Chen and Bieber (1993) have shown at neutron monitor rigidities that it is the latter of these two possibilities - the parallel mean-free path of particles with rigidities about 17 GV is suppressed during the solar minimum years of the A >0 polarity state. Chapter 5 will investigate this possibility for other rigidities.

These results indicate that drift theory is directly applicable to cosmic-ray rigidities up to at least 100-200 GV. The values of $\overline{\lambda_{\parallel} G_r}$ at these high rigidities also have a solar magnetic cycle dependence but as yet it is not known if the dependence is in either or both the mean-free path and the radial gradient. This will be investigated in Chapter 5. It is interesting that modulation of the cosmic ray distribution does exist near 200 GV, emphasising that ξ_{SD} does not simply vanish when rigidity is greater than P_u.

3.4.2 $G_{|z|}$

Figures 3.21 to 3.26 show $G_{|z|}$ for the years 1957 to 1990, calculated according to the method described in Section 3.1.2 from observations of the solar diurnal variation by the various instruments in Table 3.2. Appendix 5 contains plots of $G_{|z|}$ calculated from the solar diurnal variation recorded by the other instruments in Table 3.2. To directly compare these calculations with those of Bieber and Chen (1991a) the ratio of perpendicular to parallel diffusion (α, introduced in Chapter 1) has been assumed to be 0.01 in equation (3.20). For calculating $G_{|z|}$ from each instrument's yearly averaged solar diurnal variation the median rigidity of response of the corresponding instrument was used in the calculation of gyro-radius. The results shown assume the rigidity spectrum ($\gamma = 0$, $P_u = 100$ GV) for every year and an invariant IMF strength of 5 nT. Times of solar magnetic polarity reversals are shown as the hatched regions in the plots and should be ignored since these periods are times when the heliosphere is magnetically unstable.

The neutron monitor results are in excellent agreement with each other and with those presented by Bieber and Chen (1991a). They suggest that the bi-directional latitudinal gradient does reverse direction after a solar polarity reversal. This reversal of direction is one of the main predictions of drifts models of solar modulation, i.e. during the A <0 epochs, $G_{|z|} < 0$, indicating that G_{θ}^{sym} is directed towards the neutral sheet and there is a maximum in the density of particles at the sheet. Conversely, during the A >0 epoch, $G_{|z|} > 0$, which implies that cosmic rays are drifting in the IMF from polar latitudes towards the heliospheric equator.

The results indicate that even at 50 and 135 GV (Figures 3.24 and 3.25) this modulation is still occurring and that the magnitude of the gradient decreases with rigidity. It also seems that the magnitude of $G_{|z|}$ is dependent on the magnetic polarity of the heliosphere. In most of the results, $|G_{|z|}|$ attains largest values in the A <0 magnetic polarity states. This observation is consistent with Chen and Bieber (1993) for particles detected by neutron monitors.

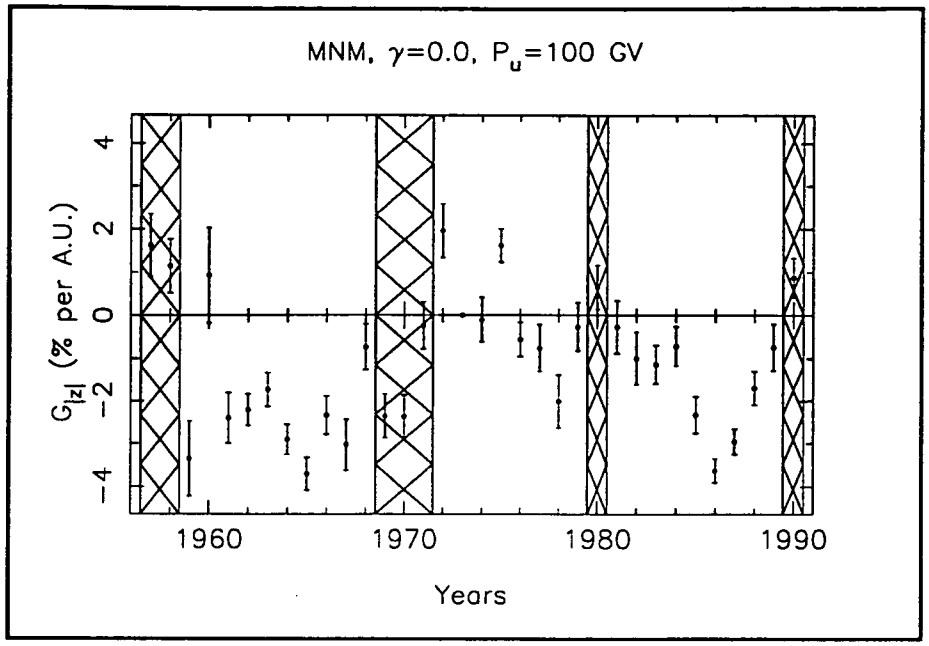

Figure 3.21 The modulation parameter $G_{|z|}$ calculated from the solar diurnal variation recorded by the Mawson neutron monitor from 1957 to 1990. Positive values imply a bi-directional latitudinal gradient which has a minimum in the number density at the neutral sheet. A negative value of $G_{|z|}$ implies a bi-directional latitudinal gradient which has a local maximum in the number density at the neutral sheet and the density reduces away from the sheet. Note that there is no data for 1973. The hatched areas are years when the magnetic polarity state of the heliosphere is not distinctly defined. The associated uncertainties are at the 67% confidence level.

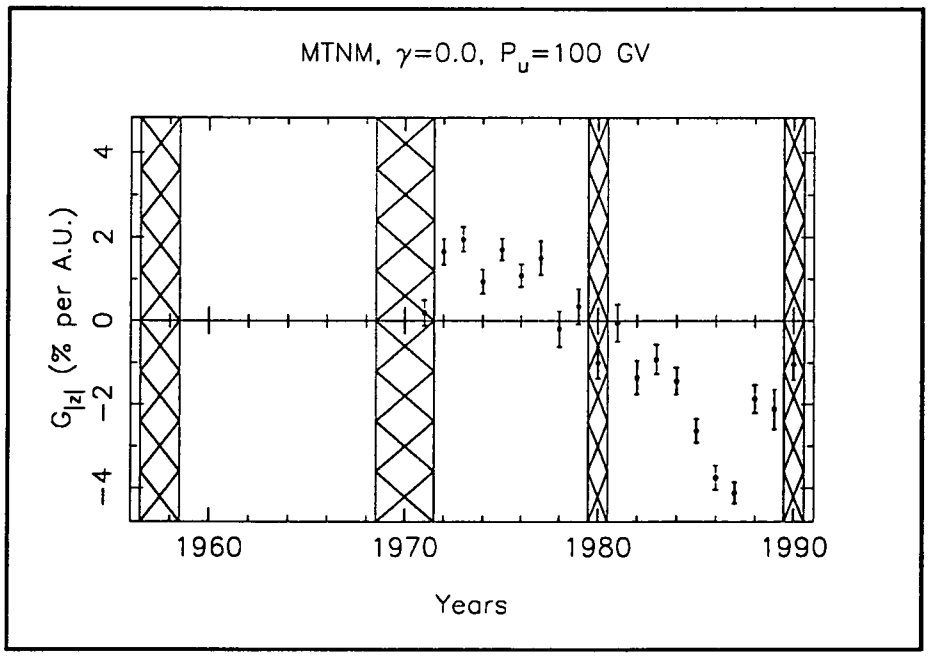

Figure 3.22 Same as Figure 3.21 except $G_{|z|}$ is calculated from the solar diurnal variation recorded by the Mt. Wellington neutron monitor from 1965 to 1988. Note the similarities between the Figures 3.21 and 3.22.

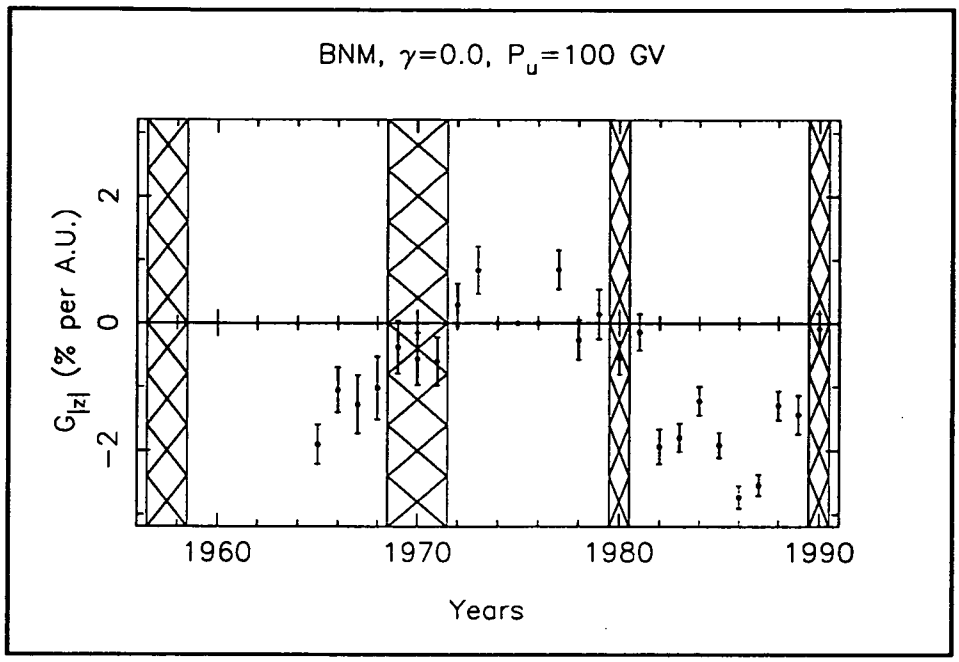

Figure 3.23 Same as Figure 3.21 except $G_{|z|}$ is calculated from the solar diurnal variation recorded by the Brisbane neutron monitor from 1965 to 1990. The median rigidity of response is 28 GV. Note that there are no data for the years 1974, 1975 and 1976.

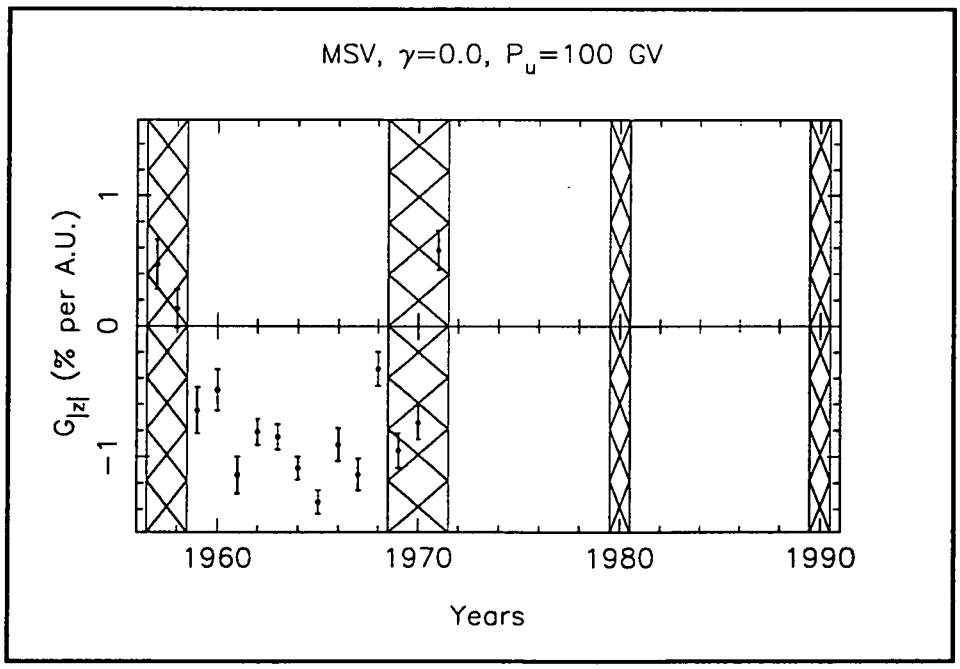

Figure 3.24 Same as Figure 3.21 except $G_{|z|}$ is calculated from the solar diurnal variation recorded by the Mawson surface muon telescope from 1957 to 1971. The median rigidity of response is 50 GV.

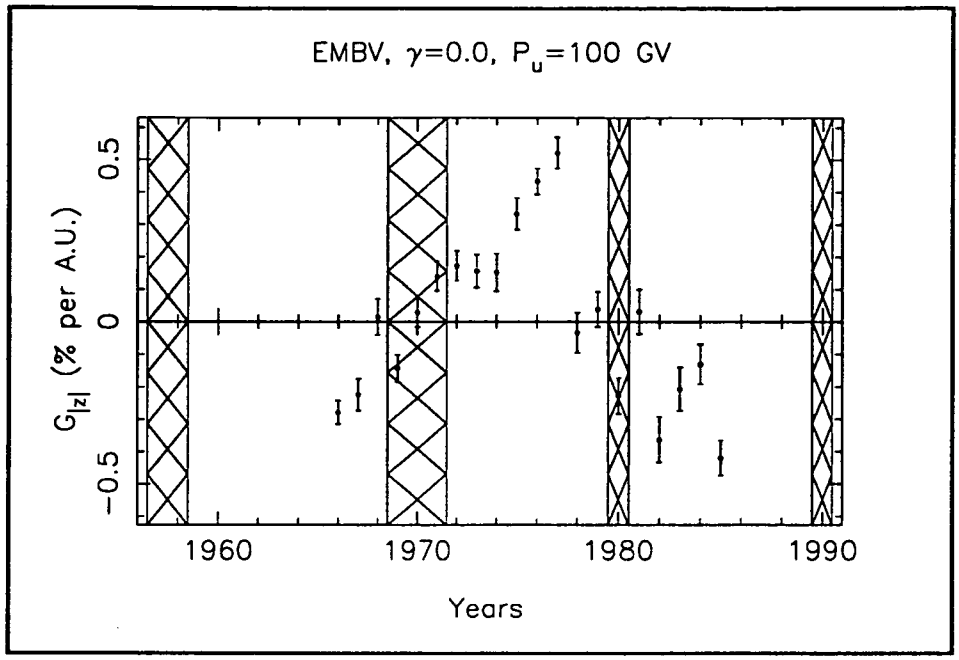

Figure 3.25 Same as Figure 3.21 except $G_{|z|}$ is calculated from the solar diurnal variation recorded by the Embudo underground muon telescope from 1966 to 1985. The median rigidity of response is 135 GV.

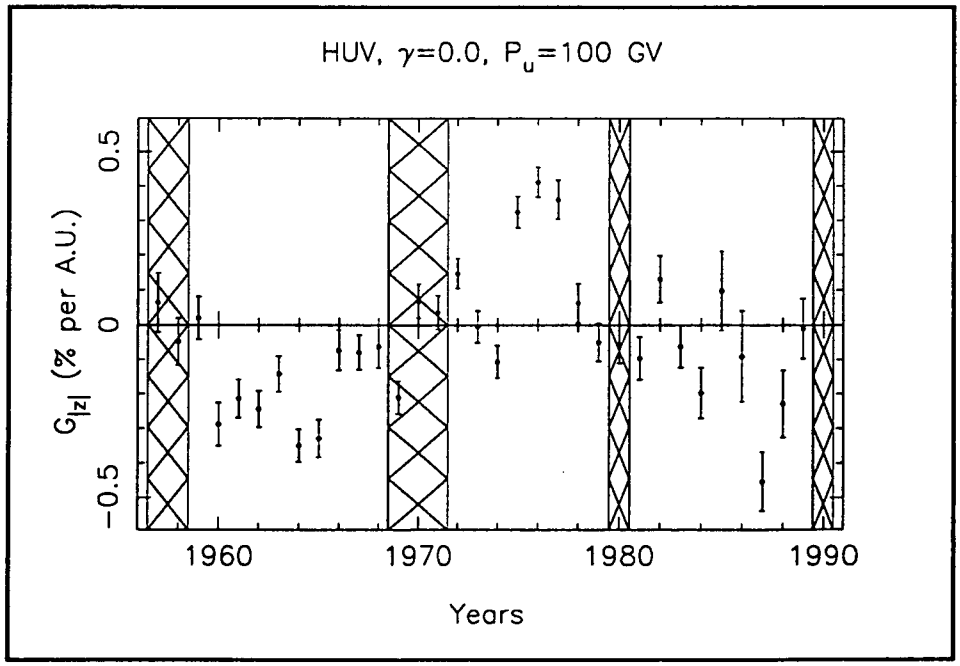

Figure 3.26 Same as Figure 3.21 except $G_{|z|}$ is calculated from the solar diurnal variation recorded by the Hobart vertical underground muon telescope from 1957 to 1989. The median rigidity of response is 185 GV.

The results in Figure 3.26 are from the HUV telescope and were calculated for particles with 185 GV rigidity. Nine of the years have zero as their value of $G_{|z|}$. Six other years are in the hatched regions and should not be considered. This leaves 18 years of results which are significantly non-zero at the 1-σ level. Out of these years, only two years (1974 and 1983) disagree with the lower rigidity results and the predictions of theoretical models. Comparison with the lower rigidity plots indicates strongly that the most significant and largest magnitude results occur around times of solar minimum and reverse sign with regard to solar magnetic polarity. This suggests that modulation is becoming less significant at these high rigidities, but that the expected modulation does occur during periods when the magnetic structure of the heliosphere is well defined - solar minimum conditions. Again the average value of $G_{|z|}$ has decreased to less than 0.5% AU^{-1} suggesting that at much higher rigidities modulation and the bi-directional latitudinal gradient will cease to be significant. One can only speculate that the rigidity where modulation is negligible is greater than 300 GV, in light of Ahluwalia's (1993) claim of a significant observation of G_{θ}^{sym} by the Socorro underground muon telescope of 0.02% AU^{-1}.

So far, only the average rigidity spectrum has been used in the calculation of $G_{|z|}$. Extremely steep rigidity spectra are not entirely suitable for an accurate assessment of $G_{|z|}$ due to the form of equation (3.20). If the spectrum is too positive the values of $|\xi_{SD}|$ will be exceedingly large compared to the other terms, if γ is too negative the other terms of (3.20) will be dominant. The values of P_u derived in Section 3.3.2 can be used in equation (3.20) to calculate $G_{|z|}$ a little more accurately still under the assumption of a flat rigidity spectrum. Figures 3.27, 3.28 and 3.29 show the results of this, obtained from the yearly averaged solar diurnal variation measured at MTNM, MSV and HUV. The neutron monitor and surface muon telescope results are essentially the same as before, which is to be expected since the coupling coefficients change very little for these instruments as a function of upper limiting rigidity. The underground muon telescope results are very different. They imply that G_{θ}^{sym} is virtually non-existent at very high rigidities or if it does exist there is no constant behavior pattern associated with it. This was seen in all the underground muon telescope results.

These results indicate that a bi-directional latitudinal density gradient of galactic cosmic rays, which reverses direction after a solar magnetic field reversal, definitely exists at rigidities less than about 50 GV, but the existence of this gradient cannot be confirmed for particles with rigidity greater than 130 GV when varying the upper limiting rigidity of the solar diurnal anisotropy from year to year. In Chapter 5 the ratio of the perpendicular to parallel diffusion will be varied to examine any dependence of $G_{|z|}$ on this parameter and to include $G_{|z|}$ in determinations of other parameters.

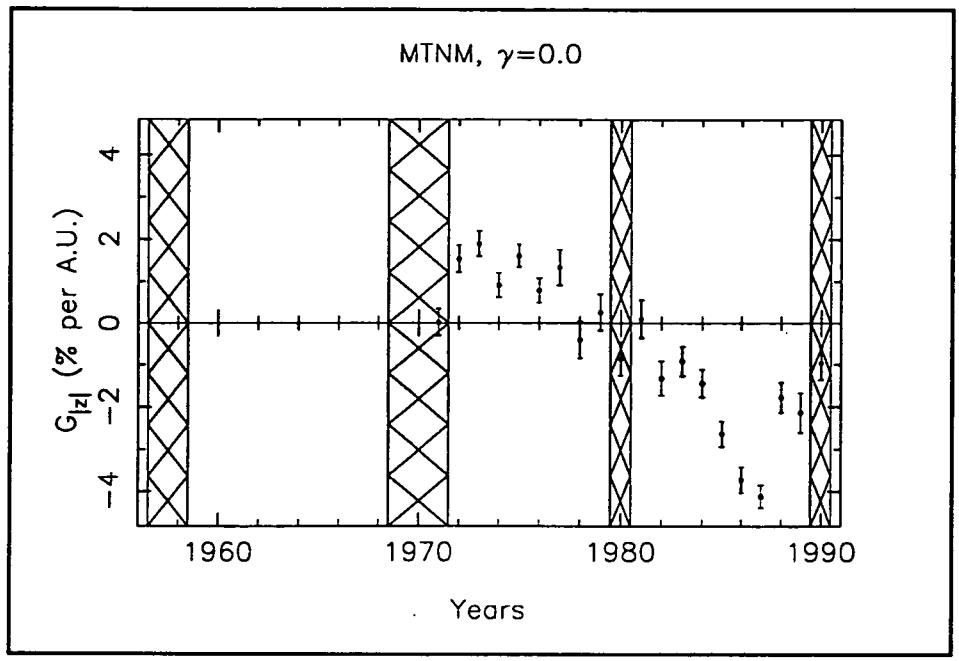

Figure 3.27 $G_{|z|}$ calculated from the yearly averaged solar diurnal variation at the Mt. Wellington neutron monitor from 1965 to 1990. The calculations have been made using a flat rigidity spectrum and the temporally varying values of P_u derived from the analysis in Section 3.3.2 and presented in Figure 3.12. The median rigidity of response is 17 GV. The associated uncertainties are at the 67% confidence level.

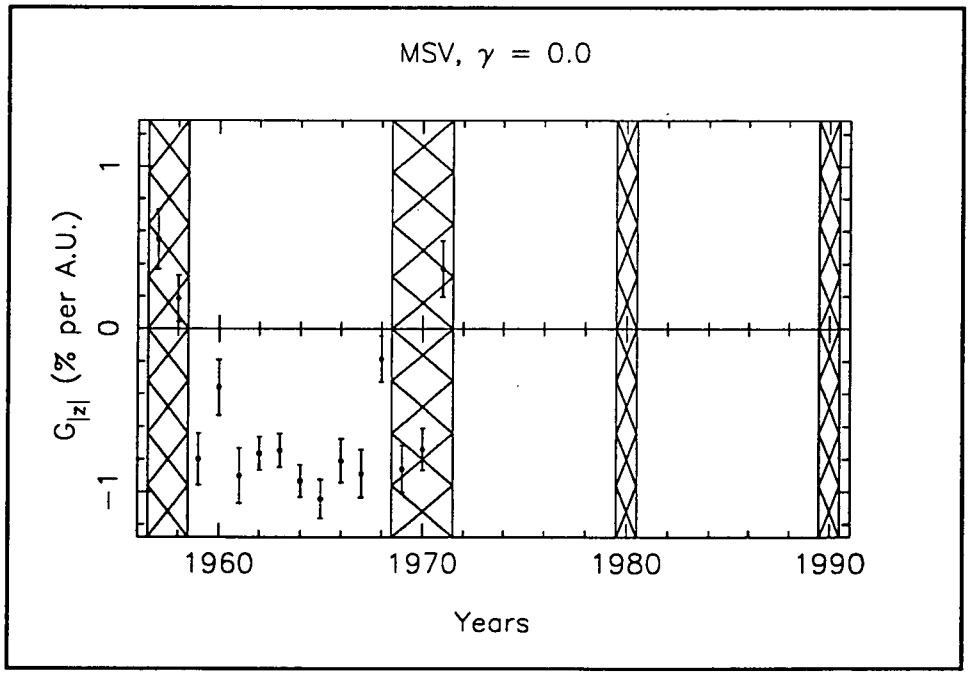

Figure 3.28 Same as Figure 3.27 but $G_{|z|}$ is calculated from the yearly averaged solar diurnal variation at Mawson surface muon telescope from 1957 to 1971. The median rigidity of response is 50 GV.

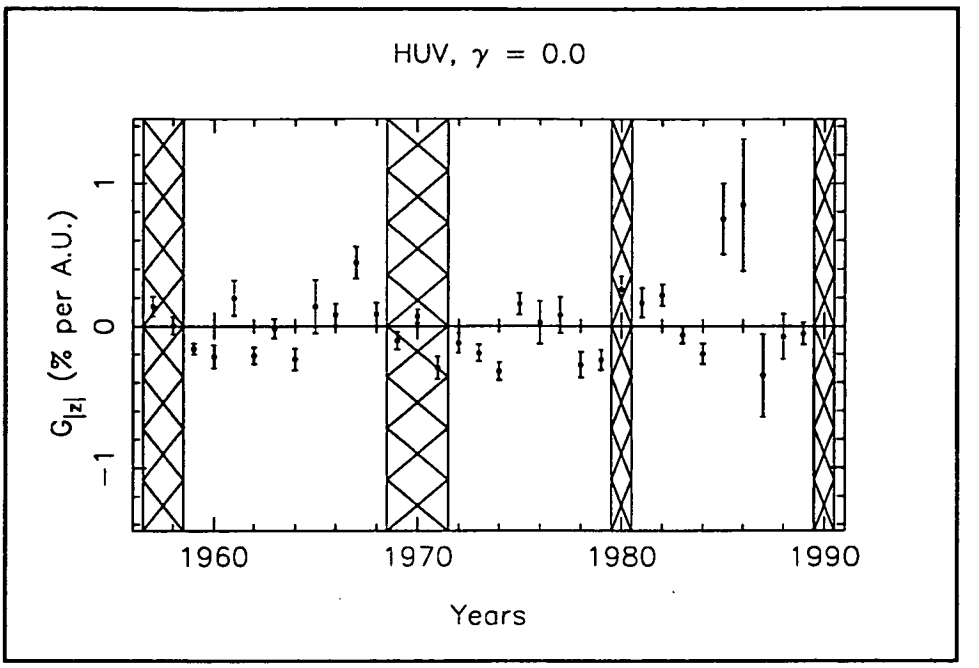

Figure 3.29 Same as Figure 3.27 but $G_{|z|}$ is calculated from the yearly averaged solar diurnal variation at Hobart underground vertical muon telescope from 1957 to 1989. The median rigidity of response is 185 GV.

Summary

By using neutron monitors and surface and underground muon telescopes to observe the solar diurnal variation the product of the parallel mean free path and radial gradient ($\overline{\lambda_{\parallel} G_r}$) of high energy particles and also the bi-directional latitudinal gradient (G_θ^{sym}) has been calculated. The rigidities at which these gradients have been observed range from about 10 GV to 200 GV. These deductions have been made for the years 1957 to 1990. We may conclude that:

- the rigidity spectrum (γ, P_u) of the solar diurnal anisotropy has an average value of (-0.1 ± 0.2, 100 ± 25 GV), in excellent agreement with past and current expectations;
- the rigidity spectrum of ξ_{SD} may be dependent on the magnetic polarity of the heliosphere. This could be because the radial component of the anisotropy becomes dominant during the $A > 0$ polarity state and causes the anisotropy to have a slightly positive spectrum;
- the spectral index is remarkably constant during an epoch of constant solar polarity but the upper limiting rigidity has an 11-year variation roughly in phase with the solar cycle. The maximum values of this rigidity are between 100 and 180 GV and occur during periods of solar maximum while the minimum values of the upper rigidity are about 50 GV and occur around years of solar minimum. These values are in good agreement with previous determinations. This was shown by two methods of analysis;
- the variation of the upper limiting rigidity of ξ_{SD} is well correlated with the magnitude of the interplanetary magnetic field, in agreement with Ahluwalia (1991);

- the amplitude of ξ_{SD} has an 11-year variation which is a real phenomenum that cannot be attributed to any variations in the rigidity spectrum of the anisotropy. The phase of the anisotropy has a 22-year variation of the same nature. This variation gets larger as the rigidity of the particles in the anisotropy increases, causing the higher rigidity anisotropy (in the $A>0$ polarity state) to have a much earlier time of maximum (or reference axis) than the lower rigidity anisotropy. The phase is virtually independent of rigidity at around 18 hours L.T. during the other epoch;
- the modulation parameter $\overline{\lambda_{||}G_r}$ has a 22-year variation and a smaller 11-year variation. The 22-year variation is rigidity dependent. The two variations are in phase and cause the average value of $\overline{\lambda_{||}G_r}$ to be smaller during the $A>0$ polarity state than during the $A<0$ polarity state;
- $\overline{\lambda_{||}G_r}$ is much more rigidity dependent during the $A>0$ polarity state. This causes the values of $\overline{\lambda_{||}G_r}$ to be much lower for higher rigidity particles during this epoch than during the $A<0$ epoch. $\overline{\lambda_{||}G_r}$ reduces by about 30% (relatively) over rigidities from 17 GV to 200 GV during the $A>0$ polarity state, but only reduces by less than 10% during the $A<0$ polarity state;
- the modulation parameter $G_{|z|}$ is an indicator of the bi-directional latitudinal gradient. It indicates that this gradient reverses direction following solar polarity reversals and that the direction is in accordance with current models of solar modulation which include charged particle drift velocities. This latitudinal gradient is present at all rigidities from 17 GV (about 2% AU^{-1}) to 195 GV ($<0.5\%$ AU^{-1}) assuming that the diurnal anisotropy has a constant rigidity spectrum. Its magnitude also seems to attain largest values around times of solar minimum conditions in the heliosphere;
- the reversal of the bi-directional latitudinal density gradient cannot be confirmed at rigidities greater than 50 GV when the rigidity spectrum of the anisotropy is allowed to vary. At lower rigidities the magnitude and direction of the gradient is almost unchanged from that calculated for a static spectrum; and
- the magnitude of $G_{|z|}$ may depend slightly on the magnetic state of the heliosphere, smaller during epochs of $A>0$ magnetic polarity than during epochs of $A<0$ polarity.

CHAPTER 4

SIDEREAL DIURNAL VARIATION – NORTH SOUTH ANISOTROPY

Parts of Chapter 1 reviewed the North-South anisotropy (ξ_{NS}) and the results of inferring the radial density gradient (G_r) of cosmic rays near the Earth from ξ_{NS}. The most important results were :

- ξ_{NS} is indicative of the radial density gradient;
- the rigidity spectrum (γ, P_u) of ξ_{NS} is (0.3 ± 0.1, 200^{+150}_{-50} GV) and the average amplitude constant $\eta_{NS} = 0.077\% \pm 0.02$ (Yasue 1980);
- neutron monitor studies of the temporal variability of ξ_{NS} indicate it has a 10-year variation with the amplitude (η_{NS}) being smaller around times of minimum solar activity (Bieber and Pomerantz 1986);
- underground muon telescope studies indicate little evidence for an 11-year variation in η_{NS} (Swinson 1988); and
- a key prediction of conventional drift theories of the solar modulation of cosmic rays is a heliospheric magnetic polarity dependent G_r. No studies of the temporal behaviour of ξ_{NS} and subsequent inferring of G_r have indicated that this is true.

With these results in mind, the analyses in this chapter were undertaken with the specific aims of :

- verifying Yasue's (1980) results;
- investigating the average amplitude and phase (ϕ_{NS}) of ξ_{NS} averaged over the periods 1957 to 1990 and over epochs of constant heliospheric magnetic polarity;
- investigating the temporal behaviour of η_{NS} and ϕ_{NS} from 1957 to 1990; and
- studying the average values and temporal behaviour of the inferred G_r from ξ_{NS}.

The data used to study ξ_{NS} are summarised in Table 4.1. As noted in the introduction, numerous instruments are used in an attempt to observe as great a region of space around the Earth as possible and collect as much data as possible to gain greater statistical accuracy. By using data collected from instruments responding to primary particles in the rigidity range of about 10 GV to 300 GV practically the entire rigidity range of the anisotropy can be studied. Sections 4.1 and 4.2 describe the analyses of the data for ξ_{NS} and how these results are used to derive the rigidity spectrum and infer G_r. Typical results of the harmonic analyses in sidereal time of various data are presented in Section 4.2.

Section 4.3 contains all the results pertaining to the derivation of the rigidity spectrum and the free-space parameters describing the anisotropy. Section 4.3.1 presents the results of determining the spectra of ξ_{NS} averaged over the period 1957 to 1990 and of studying the temporal variability of the rigidity spectrum - averaged over times with respect to the magnetic polarity state of the heliosphere and year to year variations. In Section 4.3.2 are the results of investigating the average ξ_{NS} during these periods and the temporal behaviour of ξ_{NS} from

1957 to 1990. Data from the Poatina underground muon telescope are used to explain the contamination of the ξ_{NS} results by another anisotropy.

Table 4.1 Stations and instruments used in the analysis of the North-South anisotropy. Results from EMBV and SOCV separated into towards and away IMF sectors were calculated from data supplied by D. B. Swinson extending up to the end of 1985.

Station	Mnemonic	Data Availability	P_{med} (GV)
Deep River	DRNM	1965-1988	17
Embudo	EMBV	1965-1985	135
Hobart	HNM	1968-1990	17
	HUV	1957-1989	185
	HUI	1973-1989	195
Kerguelen	KNM	1965-1988	17
Mawson	MNM	1957-1990	17
	MSV	1957-1971	50
	MUN	1973-1990	165
Mt. Wellington	MTNM	1971-1990	17
Poatina	POAMU	1972-1985	1400
Socorro	SOCV	1968-1985	300

Section 4.4 presents the average G_r inferred from ξ_{NS} under certain assumptions for the above periods. The yearly (averaged) values of G_r from 1957 to 1990 are also presented in this section. The G_r is inferred for particles with rigidities between 10 and 200 GV and is compared to previous determinations. Special assumptions are made during the analyses and these are addressed in Section 4.5 in light of some recent results of Chen and Bieber (1993).

Much of this chapter is an extension of an analysis published by Hall et al. (1994), using data obtained between 1957 and 1985. The analyses of this chapter include data from underground muon telescopes not used in the original analysis and continuing up to the end of 1990. The results and conclusions are generally unchanged from those originally published, although some results are quantitatively different.

4.1 Relationship between theory and observations for ξ_{NS} and G_r

4.1.1 Theory

The theory of solar modulation presented by Forman and Gleeson (1975) uses a coordinate system centered on the Sun. This theory was introduced in Section 1.2.1. By defining $\hat{x}$ and $\hat{z}$ in the ecliptic plane with $\hat{z}$ along the direction of the IMF away from the Sun, $\hat{y}$ out of the plane and directed northwards and using equation (1.6) :

$$\xi_y = \mathrm{sgn}(B)\rho G_r \sin\chi + \lambda_\perp G_\theta \tag{4.1}$$

where

χ = angle of the IMF with the Earth-Sun line;
$\hat{\theta}$ = unit vector in the direction of increasing solar co-latitude;
ρ = gyro-radii of the particles;
G_θ = latitudinal density gradient of cosmic rays;
$\lambda_\perp$ = perpendicular mean-free path; and

$\mathrm{sgn}(B) = \begin{cases} +1, & \mathrm{IMF} = \mathrm{A} \\ -1, & \mathrm{IMF} = \mathrm{T} \end{cases}$ is described in Section 1.2.1.

The non-ecliptic component ξ_y is the North-South anisotropy and depends on the polarity of the IMF, through sgn(B). G_θ is the total latitudinal gradient introduced in Chapter 1 and is the sum of the symmetric gradient (studied in Chapter 3) and an asymmetric latitudinal density gradient (Swinson et al. 1986, Bieber and Chen 1991a, Chen et al. 1991). Note that when considering G_θ on opposite sides of the neutral sheet the total latitudinal gradient is larger in one hemisphere than the other. From Chapter 3 we know that the symmetric latitudinal gradient does exist and is likely to behave in accordance with drift theory predictions. Therefore, the sum of the symmetric and asymmetric latitudinal gradients can be written as

$$G_\theta = -G_{\underline{z}} - \mathrm{sgn}(B)\ \mathrm{sgn}(I)\ G_{|z|} \tag{4.2}$$

where

$G_{|z|}$ = symmetric (bi-directional) latitudinal gradient;
$G_{\underline{z}}$ = asymmetric (unidirectional) latitudinal gradient; and

$$\mathrm{sgn}(I) = \begin{cases} +1, & A > 0 \\ -1, & A < 0 \end{cases} \tag{4.3}$$

This function was introduced in Chapter 3 to derive equations (3.18) and (3.20).

By measuring ξ_y at times when the Earth is in away $\left(\xi_y^A\right)$ and toward $\left(\xi_y^T\right)$ sectors and taking half the difference we can measure the North-South anisotropy averaged over both sides of the neutral sheet :

$$\xi_{NS}^{T\text{-}A} = \frac{1}{2}\left(\xi_y^T - \xi_y^A\right) \tag{4.4}$$

Then

$$\xi_{NS}^{T\text{-}A} = -\rho G_r \sin\chi + \mathrm{sgn}(I)\,\lambda_\perp G_{|z|} \tag{4.5}$$

Note that any contribution from perpendicular diffusion may increase or decrease ξ_{NS}^{T-A} depending on the magnitudes and direction of $\lambda_\perp$ and $G_{|z|}$. It is thought that the perpendicular diffusion term is much smaller than the drift term (Yasue 1980, Bieber and Pomerantz 1986). We will return to this point in Section 4.5 and Chapter 5 in light of recent measurements by Chen and Bieber (1993). Under the above assumption (i.e., $\lambda_\perp G_\theta << \rho G_r \sin\chi$), if we can derive the magnitude and direction of ξ_{NS}^{T-A} for a certain P then

$$G_r(P) \approx -\frac{\xi_{NS}^{T\text{-}A}(P)}{\rho \sin\chi} \tag{4.6}$$

Note that a negative ξ_{NS}^{T-A} would indicate an anisotropic flow from the north of the Earth and a positive (outward) radial gradient.

4.1.2 Relating observations and theory

As noted in Chapters 1 and 2 an asymptotic cone of view not aligned with the rotation axis of the Earth will scan 360 degrees of space in one sidereal day. A spatial anisotropy of particles having a component in the geo-equatorial plane will increase the count rate of a telescope when the telescope's asymptotic cone is directed at the anisotropic component. For a unidirectional anisotropy fixed with respect to the stars the count rate will have a diurnal variation in sidereal time, the phase of the variation indicating the right ascension from which the anisotropic stream is approaching. Nagashima (1971) described how one can relate observed diurnal variations in count rates to the corresponding free-space anisotropy. This was detailed in Section 2.5.1.

We can now apply Nagashima's formalism to the North-South anisotropy. Assuming that ξ_{NS} is symmetric about a reference axis and that no higher order space distributions exist, the free-space distribution of particles due to the anisotropy can be represented as the ordinary Legendre polynomial $P_1(\cos\psi)$ with an amplitude η_{NS} and rigidity spectrum G(P), where ψ is the angle between the direction of viewing and the reference axis (see equations 2.15 to 2.17). Because ξ_{NS} is a unidirectional anisotropy (i.e., n=1) with co-declination θ_R and right ascension δ_R there are two components related to ξ_{NS} in the Earth's equatorial system (equatorial plane component and polar rotation axis component). The component in the equatorial plane can be decomposed into two orthogonal components $\left(\xi_x^{NS}, \xi_y^{NS}\right)$ such that:

$$\begin{aligned}\xi_{NS} &= \eta_{NS} P_1(\cos\psi) G(P) \\ &= \left(\xi_x^{NS} , \xi_y^{NS} , \xi_z^{NS} \right) G(P) \\ &= (\eta_{NS} \sin\theta_R \cos\alpha_R, \eta_{NS} \sin\theta_R \sin\alpha_R, \eta_{NS} \cos\theta_R) G(P)\end{aligned} \tag{4.7}$$

where

$$G(P) = \begin{cases} \left(\frac{P}{10}\right)^{\gamma}, & P \le P_u \\ 0, & P > P_u \end{cases} \tag{4.8}$$

and $(\hat{x},\hat{y},\hat{z})$ are now in the geo-equatorial coordinate system with $\hat{z}$ along the Earth's rotation axis and $\hat{x}$ along 0 hours^{SID}. The North-South asymmetry is the ξ_z^{NS} component and $\left(\xi_x^{NS},\xi_y^{NS}\right)$ are the two components which produce the space-harmonic component $S_{NS}(t)$ (see equations 2.20 and 2.21) and hence the sidereal diurnal variation with free-space amplitude :

$$\eta_{NS} \sin\theta_R = \sqrt{\left(\xi_x^{NS}\right)^2 + \left(\xi_y^{NS}\right)^2} \tag{4.9a}$$

and phase

$$\phi_{NS} = \frac{24}{2\pi} \arctan\left(\frac{\xi_y^{NS}}{\xi_x^{NS}}\right) \text{ hours}^{SID}. \tag{4.9b}$$

One can approximate the reference axis as from the direction of the ecliptic pole ($\theta_R = 23.5^o$ and $\alpha_R = 2\pi\delta_R/24$ radians, δ_R = 18 hours^{SID}, see Yasue 1980). Naturally, δ_R should on average be ϕ_{NS}.

In the absence of all other sidereal diurnal variations the count rate $D^G(t)$ of an instrument due to the space harmonic component of the North-South anisotropy is (see Section 2.3) :

$$D^G(t) = a_{NS} \cos\frac{2\pi t}{24} + b_{NS} \sin\frac{2\pi t}{24} \tag{4.10}$$

As explained in Section 2.5.1 the components (a_n^m, b_n^m) of a time variation recorded by an instrument are related to the anisotropy by the instrument's coupling coefficients (c_n^m, s_n^m) which contain all the information concerning the rigidity spectrum, asymptotic latitude and longitude of the viewing direction, geographical position and geometrical configuration of the instrument. From the relations in (2.24) :

$$\begin{aligned} a_{NS} &= c_1^1 \xi_x^{NS} + s_1^1 \xi_y^{NS} \\ b_{NS} &= -s_1^1 \xi_x^{NS} + c_1^1 \xi_y^{NS} \end{aligned} \tag{4.11}$$

Unlike the solar diurnal anisotropy examined in Chapter 3 the North-South anisotropy is a unidirectional anisotropy such that the free-space phase should be independent of particle rigidity. It is then valid to define the χ^2 function relevant to this analysis of the North-South anisotropy (introduced generally in Section 2.5.1 as equation 2.27) as :

$$\begin{aligned}\chi^2 &= \sum_{i=1}^{N} w_i\left[\left(a_{NS,i}-a_{NS}\right)^2+\left(b_{NS,i}-b_{NS}\right)^2\right] \\ &= \sum_{i=1}^{N} w_i\left[\left(a_{NS,i}-\left(c^1_{1,i}\xi^{NS}_x+s^1_{1,i}\xi^{NS}_y\right)\right)^2+\left(b_{NS,i}-\left(-s^1_{1,i}\xi^{NS}_x+c^1_{1,i}\xi^{NS}_y\right)\right)^2\right]\end{aligned} \tag{4.12}$$

where each term in the sum is weighted by the errors ($\sigma_{a,i}$, $\sigma_{b,i}$) of the Fourier derived components ($a_{NS,i}$, $b_{NS,i}$) by the relation

$$w=\frac{1}{\sqrt{\left(\sigma_a\right)^4+\left(\sigma_b\right)^4}}. \tag{4.13}$$

This weighting function was chosen so as to give slightly greater relative weight to any data with unequal errors ($\sigma_{a,i}$, $\sigma_{b,i}$) than would have been given to the same data had a more standard weighting function been used, e.g. the inverse of the summation of the errors in quadrature. Data of this form have one of their components well determined but poorly represented by standard weighting.

By making N observations of the sidereal diurnal variation and minimising χ^2 as a function of (γ, P_u) (and hence c^1_1, s^1_1), while varying $\left(\xi^{NS}_x,\xi^{NS}_y\right)$ the best fit values of $\left(\xi^{NS}_x,\xi^{NS}_y\right)$ can be found simultaneously with the rigidity spectrum. From the best fit values of $\left(\xi^{NS}_x,\xi^{NS}_y\right)$ one can use (4.9a) and (4.9b) to obtain η_{NS} and ϕ_{NS}.

As in Chapter 3, the best fit values of $\left(\xi^{NS}_x,\xi^{NS}_y\right)$ can be found analytically by looking at the derivatives of χ^2 with respect to the variables $\left(\xi^{NS}_x,\xi^{NS}_y\right)$. The derivation of the analytic solutions is shown in Appendix 6 and only the solutions are presented here :

$$\begin{aligned}\xi^{NS}_x &= \sum_{i=1}^{N}\frac{w_i\left(c^1_{1,i}a_{NS,i}-s^1_{1,i}b_{NS,i}\right)}{\Delta} \\ \xi^{NS}_y &= \sum_{i=1}^{N}\frac{w_i\left(s^1_{1,i}a_{NS,i}+c^1_{1,i}b_{NS,i}\right)}{\Delta} \\ \Delta &= \sum_{j=1}^{N} w_j d_j^{\,2} \\ d_j^{\,2} &= \left(c^1_{1,j}\right)^2+\left(s^1_{1,j}\right)^2\end{aligned} \tag{4.14}$$

The errors of the derived components of the North-South anisotropy are calculated by using standard propagation of errors :

$$\sigma_x^{NS} = \frac{1}{\Delta}\sqrt{\sum_{i=1}^{N} w_i^2\left[\left(c_{1,i}^1\sigma_{a,i}\right)^2 + \left(s_{1,i}^1\sigma_{b,i}\right)^2\right]}$$
$$\sigma_y^{NS} = \frac{1}{\Delta}\sqrt{\sum_{i=1}^{N} w_i^2\left[\left(s_{1,i}^1\sigma_{a,i}\right)^2 + \left(c_{1,i}^1\sigma_{b,i}\right)^2\right]} \qquad (4.15)$$

4.2 Data analysis

The data listed in Table 4.1 were Fourier (harmonically) analysed in sidereal and anti-sidereal time according to the methods described in Sections 2.3 and 2.4. The yearly averaged sidereal and anti-sidereal diurnal variation recorded by each instrument were separated according to the polarity of the IMF sector near the Earth when each measurement was made. The anti-sidereal results were then used to remove the unwanted spurious sidereal diurnal variation present in the sidereal time first harmonic results due to the annual modulation of the solar semi-diurnal anisotropy (Nagashima et al. 1985) as explained in Section 2.6. The vector difference was used to produce the *towards minus away* diurnal variation vector ($D_{NS}^{T\text{-}A}(t)$) caused by the North-South anisotropy. This vector (obtained over large sampling times) should be free from atmospheric effects and any other diurnal variations caused by anisotropies *which are modulated symmetrically with respect to toward and away sectors*, including true galactic anisotropies. $D_{NS}^{T\text{-}A}(t)$ is related to $\xi_{NS}^{T\text{-}A}$ of equation (4.4) by equations (4.7) to (4.15).

Figures 4.1 to 4.6 show the $D_{NS}^{T\text{-}A}(t)$ vectors (not including the factor of 0.5 of equation (4.4) and not corrected for geomagnetic bending) derived from Deep River neutron monitor (DRNM), Hobart underground vertical muon telescope (HUV), Mount Wellington neutron monitor (MTNM), Mawson surface muon telescope (MSV), Mawson underground north pointing muon telescope (MUN) and Socorro underground muon telescope (SUV). These are the *raw* sidereal diurnal variation harmonics used in the following analyses. Naturally they need to have their amplitudes halved before any computations can be performed. These figures should illustrate to the reader the observed sidereal diurnal variation over the entire rigidity range being investigated here. The reader should also note that an error in pressure correcting the data caused Duldig (1991) to report that the (Nagashima) corrected sidereal diurnal variation vectors for MUN were "unrealistic". The error has since been eliminated; now the MUN vectors lie almost constantly along 20 hours sidereal time.

All the neutron monitors have median rigidities about 17 GV and show the trends exhibited by DRNM and MTNM. There are substantial phase changes around 1965, 1969, 1978 and 1985. The neutron monitors all record large amplitudes around 1978 and 1979, *unlike* the muon telescope observations at the same period. Large amplitudes are also recorded in the neutron monitor results in 1984 and 1990. From a comparison of all the observations it seems apparent that the vectors (uncorrected for geomagnetic bending) have a cyclic behaviour with a period about 20 years.

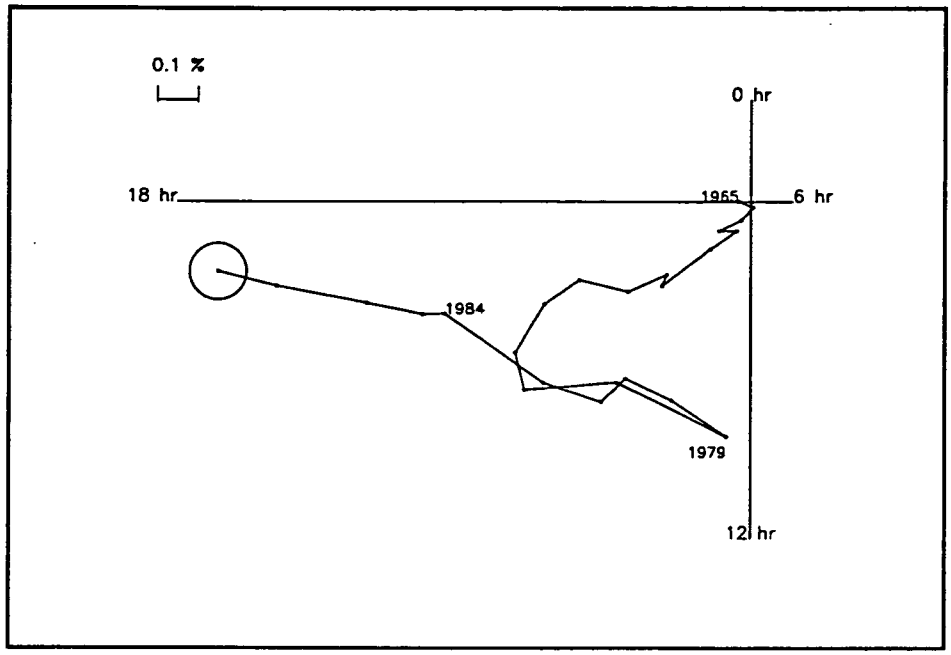

Figure 4.1 Yearly averaged toward - away sidereal diurnal variation (Nagashima corrected) observed by Deep River neutron monitor for 1965 to 1988. Error circles are derived from the combined uncertainties in the sidereal and anti-sidereal diurnal variation and are to 67% confidence. Year labels refer to the head of the corresponding vector. The median rigidity of response is about 17 GV. Significant phase changes are observed after 1965, 1976, 1979 and 1984. 1979 and 1984 are years of relatively large amplitudes.

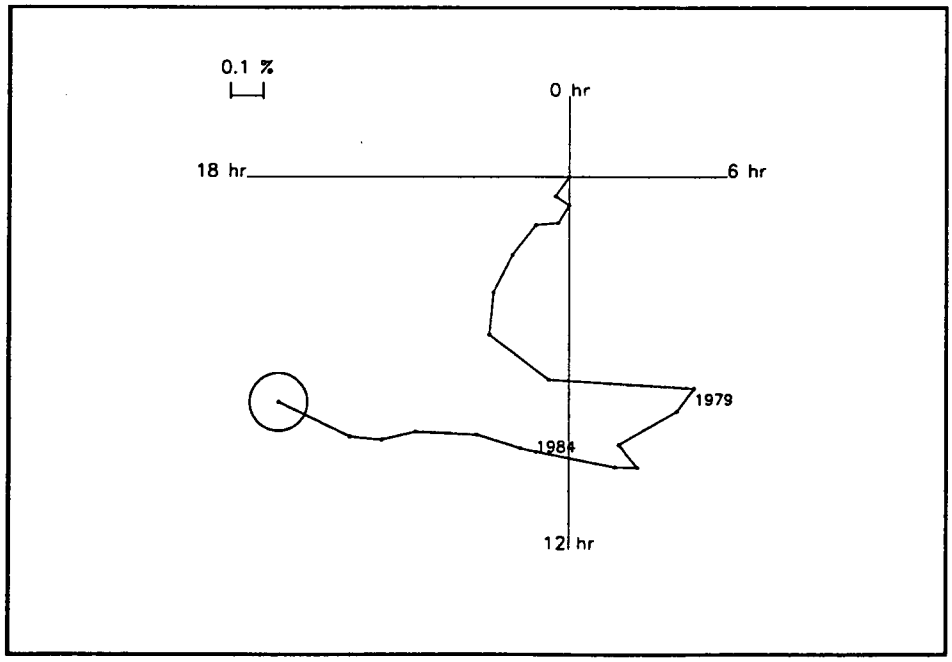

Figure 4.2 Same as Figure 4.1 but for the Mt. Wellington neutron monitor from 1971 to 1990. 1990 also has a relatively large amplitude. The median rigidity of response is about 17 GV.

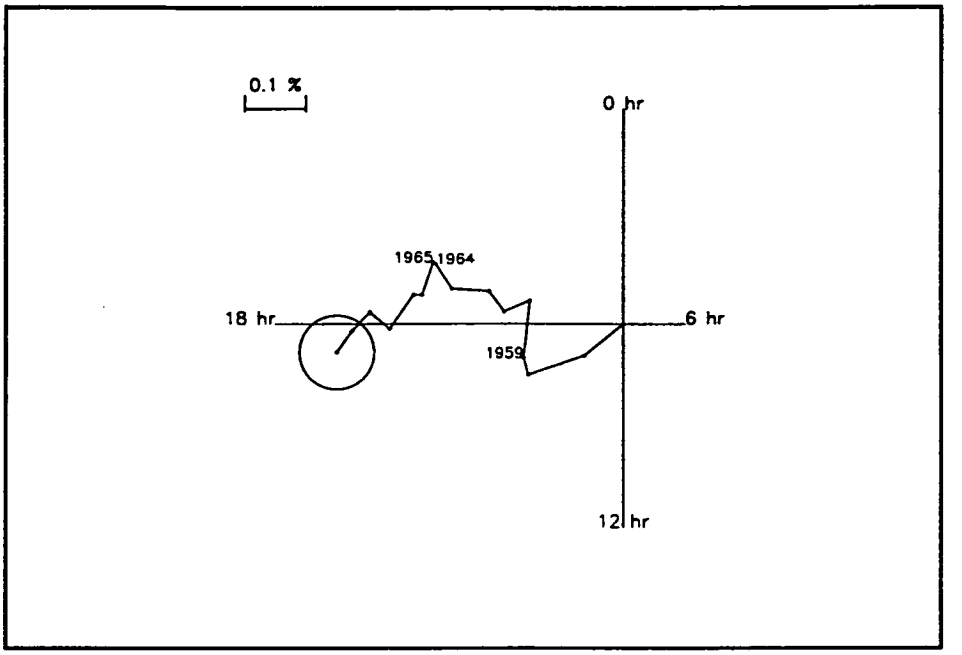

Figure 4.3 Same as Figure 4.1 but for the Mawson surface muon telescope from 1957 to 1971. Significant phase changes around 1959 and 1965 are observable. The median rigidity of response is about 50 GV.

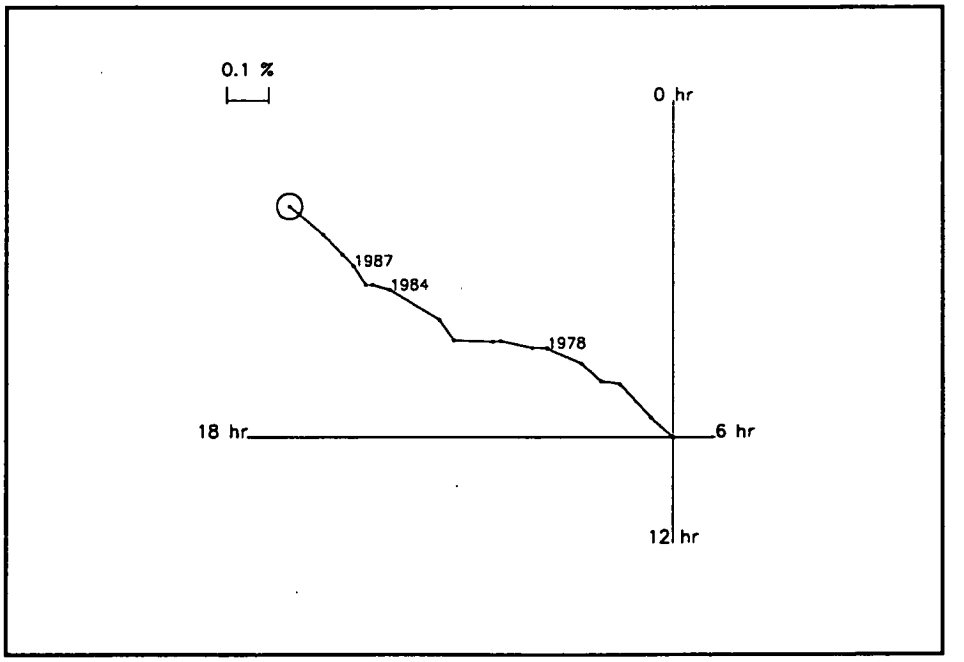

Figure 4.4 Same as Figure 4.1 but for the Mawson underground (inclined) muon telescope from 1971 to 1990. Unlike the neutron monitor results the years 1978 to 1979 have relatively small amplitudes (the 1978 vector is actually hidden by the head of the 1977 vector). Phase changes are noticeable after 1978, 1982 and 1986. 1984 and 1990 have relatively large amplitudes, similar to the neutron monitor results. The median rigidity of response is about 165 GV.

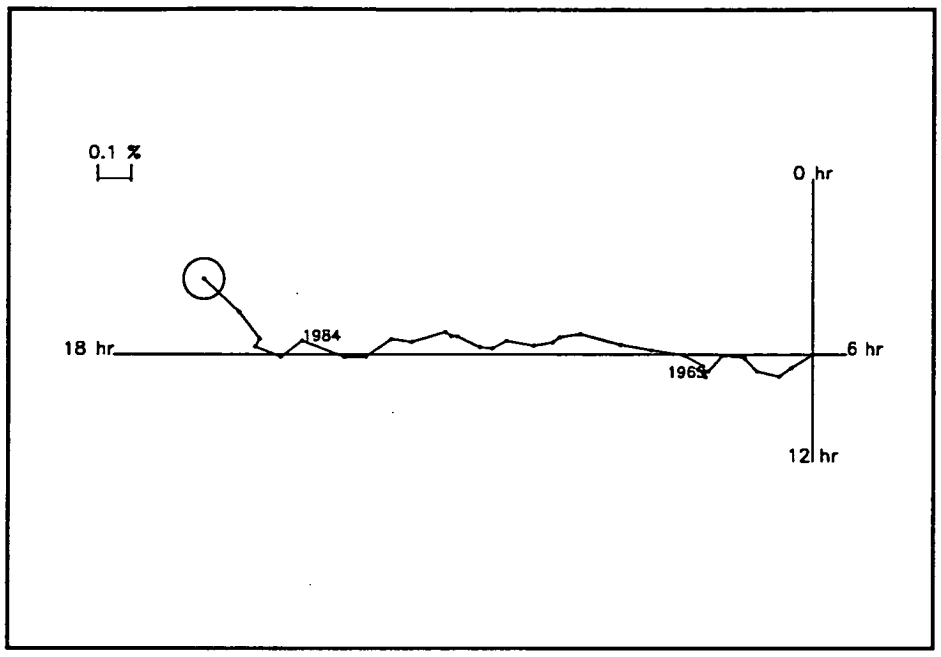

Figure 4.5 Same as Figure 4.1 but for the Hobart underground (vertical) muon telescope from 1957 to 1989. Again the large amplitude of the diurnal variation during 1978-1979 recorded by neutron monitors is not observed in these results although a phase change is observable around this period. Phase changes are also observed around 1965 and 1985, similar to all other results. 1984 and 1989 have large relative amplitudes. The median rigidity of response is about 185 GV.

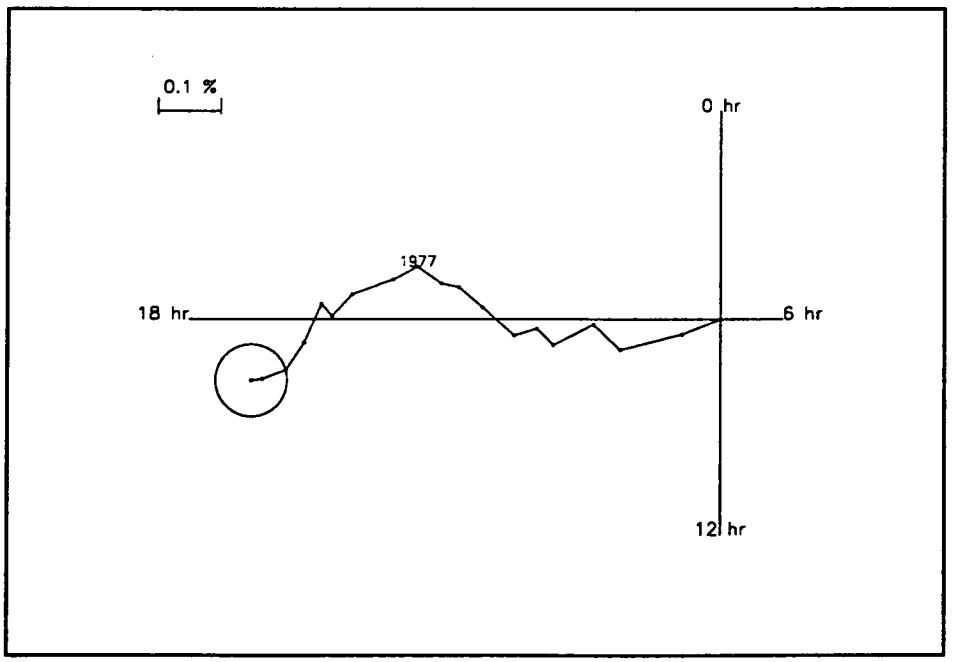

Figure 4.6 Same as Figure 4.1 but for the Socorro underground (vertical) muon telescope from 1968 to 1985. Note the similarities with all the other muon telescope results. Phase changes exist after 1970 and 1977. The median rigidity of response is about 300 GV.

MSV has a phase typically 16 hours (local sidereal time) for the periods 1957–1958, 1965–1971, and about 6 hours later for the other years, with abrupt changes around years 1959, 1965, and 1969. The slightly higher median rigidity of the telescope suggests that the North-South anisotropy seems to have a high degree of consistency for particles below 50 GV.

The HUV vectors lie along 18 hours. Note that the lengths of the vectors for 1978 and 1979 are smaller than usual; a similar trend is seen by MUN. The results from HUV and MUN suggest that after the period 1977 to 1979 the phase becomes a little earlier than during the previous period and that there are also phase changes around 1965 and after 1984. The median rigidities of the MUN and HUV underground muon telescopes are 165 and 185 GV respectively. This behaviour is also observed in the results of the SUV muon telescope which has a median rigidity of response of about 300 GV.

Analysis of data recorded by the instruments in Table 4.1 leads to some interesting observations of the long term behaviour of the ξ_{NS}. For instance, most of the results indicate that the reference axis of the anisotropy has a significant variation with a period of about one solar magnetic cycle. The similarity of the neutron monitor and muon telescope results indicates that the rigidity spectrum of the anisotropy could be similar to that of the solar diurnal anisotropy (i.e. close to being flat) but there are also some differences. The years 1978 and 1979 have markedly different diurnal variations in the neutron monitor and muon telescope data. The diurnal variations in the neutron monitor data for these years have very early times of maximum and large amplitudes while the diurnal variations in the muon telescope data are quite small and do not show the large change in the observed phase. This suggests that the rigidity spectrum is not flat and more likely to have a negative spectral index or very low upper limiting rigidity. On the other hand, the results of 1984 are much more consistent over the entire rigidity range suggesting that whatever caused the increase in the amplitude of the diurnal variation for that year is not an unusual rigidity spectrum but some other effect. The sidereal diurnal variations presented in Figures 4.1 to 4.6 also hint that the amplitudes are relatively smaller around times of solar minima than at other times through the solar cycle. The following analyses endeavor to explore these possibilities.

Following the success, reported in Chapter 3, of determining the rigidity spectrum of the solar diurnal anisotropy a similar determination was attempted of the rigidity spectrum of the North-South anisotropy. Using all the available data from every year (see Table 4.1) and the appropriate coupling coefficients the value χ^2 in equation (4.12) was calculated for the best fit $\left(\xi_x^{NS}, \xi_y^{NS}\right)$ as a function of (γ, P_u). The minimum χ^2 value indicates the best fit rigidity spectrum. In this way, using 244 instrument-years of data the best fit average rigidity spectrum and free space components $\left(\xi_x^{NS}, \xi_y^{NS}\right)$ for the period 1957–1990 have been derived. This analysis has been repeated with diurnal variation results segregated into groups corresponding to different solar magnetic polarity states. This has been done to investigate any magnetic polarity dependence of ξ_{NS}.

For each individual year, the same χ^2 analysis was performed to obtain the best fit $\left(\xi_x^{NS}, \xi_y^{NS}\right)$ and corresponding (γ, P_u) as a function of year. The limitations of this analysis for the period 1957–1965 are fairly obvious, but there is at least one instrument in every year with P_{med} about 17, 50, and 185 GV (i.e. the data are from particles encompassing almost the

entire range of rigidities that are used in the later years, but the analysis is not as statistically accurate). In this way the temporal variation of (γ, P_u) and ξ_{NS} can be examined.

The results of the above analyses can be used to examine the ξ_{NS} while assuming a rigidity spectrum by simply ignoring the value the χ^2 obtained when deriving the components $\left(\xi_x^{NS}, \xi_y^{NS}\right)$ for a specific combination of (γ, P_u) from equations (4.14) and (4.15). This has also been performed to directly compare previous determinations of ξ_{NS} (summarised in Section 1.3) to the results of this thesis.

4.3 Results of the North-South anisotropy analyses

4.3.1 Rigidity spectrum of ξ_{NS}

The rigidity spectrum was investigated over four distinct periods. The spectrum averaged over the entire period was investigated as was any temporal variation of the rigidity spectrum averaged over constant years of magnetic polarity. Any year to year variations of the rigidity spectrum were also studied.

Average Rigidity spectrum

All available data from 1957 to 1990 were used via (4.12) to obtain the best fit average parameters $\left(\gamma, P_u, \xi_x^{NS}, \xi_y^{NS}\right)$ for the entire period. The results relevant to the rigidity spectrum are shown in Table 4.2 and Figure 4.7. The derived rigidity spectrum (0.1, 500 GV) is in reasonable agreement with Yasue's (1980) spectrum of (0.3, 200 GV) and also with the spectrum obtained by Ueno et al. (1984) of (0.5, 300 GV).

Table 4.2 Values of the best fit average rigidity spectra of the North-South anisotropy during derived for various periods.

Period	γ	P_u (GV)
1957-1990	0.1	≈500
1960-1968, 1981-1989 A<0	-0.2	≈800
1972-1979 A>0	0.1	≈750

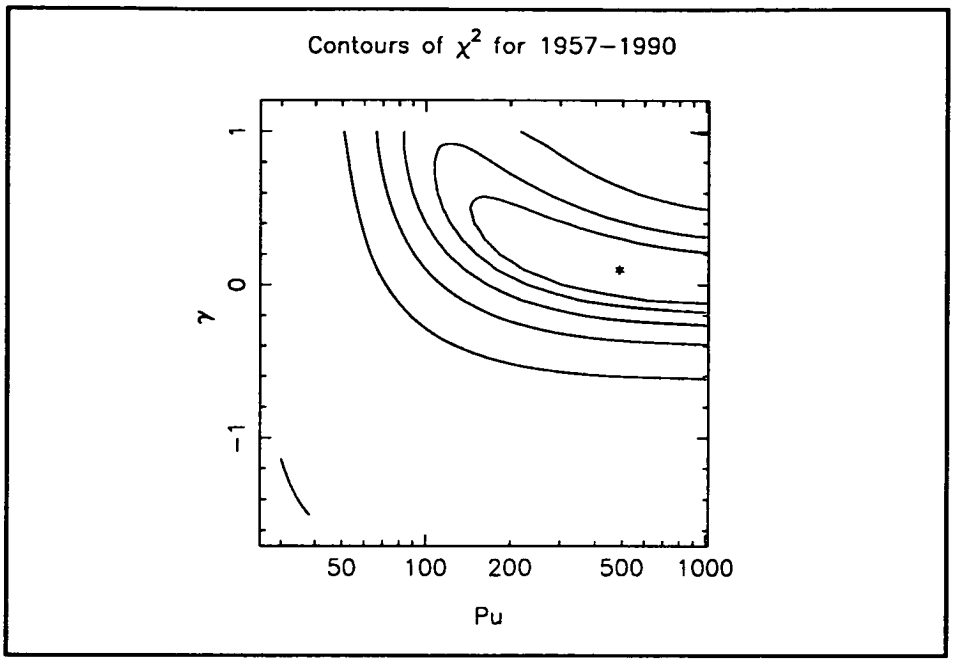

Figure 4.7 Contours of χ^2 as a function of (γ, P_u) for all data from 1957 to 1990. The outer contour has a value of 1685, and other contour levels have decreasing values of 1432, 1303, 1239, 1207, and 1191. The minimum value of χ^2 is indicated by the asterisk at (0.1, 500 GV) and has a value of 1175. All the contours are within the 67% confidence region.

In the previous analysis (Hall et al. 1994) the rigidity spectrum was derived to be (0.5, 450 GV). At the time the sensitivity of the χ^2 analysis of the data for the rigidity spectrum was not known. It is now known that although the derived rigidity spectrum is quite reasonable, the statistical accuracy of the spectrum is very poor; the minimum in the χ^2 contours being quite shallow, subsequently causing the entire space of (γ, P_u) to be within the statistical 67% confidence region. This sort of accuracy is not tolerable so one must concede that the most reliable estimate of the rigidity spectrum is that of Yasue (1980).

Temporal variations of the rigidity spectrum

Solar magnetic polarity dependence. To search for any dependence of the anisotropy on the heliospheric magnetic polarity the analysis was repeated with the sidereal diurnal variation data split into two groups: group$^{(+)}$ (1972–1979) when $A > 0$ and group$^{(-)}$ (1960–1968, 1981–1989) when $A < 0$.

In searching for the best fit rigidity spectrum, statistics and hence sensitivity were again a problem. The results are also shown in Table 4.2. The derived spectra are similar to each other and also with the average spectrum derived earlier although it must be stressed that none of these spectra can be regarded with much confidence as the sensitivity of the χ^2 analysis again is such that the entire spaces of (γ, P_u) for both analyses are statistically within the 67% confidence regions of the correct spectral parameters. It is interesting however, that

all three analyses of the sidereal diurnal variation results derive very similar spectra of the North-South anisotropy.

Year to year variations. The value of χ^2 as calculated by (4.12) was minimized for each individual year of data to search for temporal variations in the rigidity spectrum of the anisotropy. The individual determinations of the rigidity spectra are presented in Table 4.3.

Table 4.3 Values of the best fit rigidity spectrum of the North-South anisotropy for each year from 1957 to 1990.

Year	γ	P_u (GV)	Year	γ	P_u (GV)	Year	γ	P_u (GV)
1957	-0.1	700	1969	1.0	740	1981	-0.4	836
1958	1.0	76	1970	1.0	318	1982	0.3	446
1959	1.0	1000	1971	0.0	1000	1983	0.6	80
1960	-0.1	104	1972	1.0	394	1984	0.3	120
1961	-0.2	30	1973	0.3	180	1985	1.0	88
1962	0.0	702	1974	0.4	216	1986	1.0	38
1963	0.4	138	1975	-0.2	750	1987	0.0	94
1964	-0.1	122	1976	-0.4	1000	1988	-0.4	806
1965	1.0	1000	1977	-0.1	1000	1989	1.0	86
1966	0.6	32	1978	0.0	30	1990	1.0	66
1967	0.6	950	1979	-0.5	30			
1968	1.0	206	1980	0.9	126			

The results are not conclusive, with γ being found to vary in the range -0.5 to +1.0 and with no obvious year to year pattern in P_u. None the less, the results are encouraging with each contour plot (one for each year's data) being similar to that of Figure 4.7.

With the spectrum being indeterminate for each individual year the average rigidity spectrum derived by Yasue (1980) has been used for the rest of the analyses of this chapter except where noted.

4.3.2 Derived components of ξ_{NS}

Average ξ_{NS}

Yasue's spectrum was used in equations (4.14) and (4.15) to estimate the amplitude of ξ_{NS} (i.e. η_{NS}) as 0.087%, and the phase (ϕ_{NS}) of the anisotropy for the entire period was 19.2± 0.2 hours^{SID}. This value of η_{NS} is in excellent agreement with Yasue (1980) but slightly higher than Bieber and Pomerantz's (1986) which was 0.053%. Nagashima et al. (1983a) considered the difference between the ecliptic and solar equatorial planes. The solar magnetic field is defined in the solar equatorial plane and the radial gradient is defined in the ecliptic plane. The predicted yearly averaged direction of the North-South anisotropy (BxG_r) was shown to be 18.57 hours^{SID}, similar to the derived averaged value of ϕ_{NS}. Note that the average ϕ_{NS} derived here contains twice as many years in the derivation of negative heliospheric polarity than of positive heliospheric polarity. If there are any differences in the phase of ϕ_{NS} related to the polarity of the heliosphere (as suggested by the results shown in Figures 4.1 to 4.6) then the average will be slightly biased towards the results of the negative polarity state. This will be tested in the following sub-section. Other spectra were also used to examine the average η_{NS} and ϕ_{NS} and these results are listed in Table 4.4.

Table 4.4 Values of the Best Fit Free-Space Parameters of the North-South Anisotropy averaged over the period 1957 to 1990 for various rigidity spectra. Uncertainties are to 67% confidence.

γ	P_u (GV)	η_{NS} (%)	ϕ_{NS} (hours^{SID})
-0.5	100	0.169 ± 0.010	19.9 ± 0.2
	200	0.175 ± 0.010	19.8 ± 0.2
	500	0.176 ± 0.010	19.7 ± 0.2
0.0	100	0.161 ± 0.010	19.6 ± 0.2
	200	0.138 ± 0.010	19.3 ± 0.2
	500	0.114 ± 0.010	19.1 ± 0.2
0.5	100	0.101 ± 0.010	19.4 ± 0.2
	200	0.059 ± 0.003	19.1 ± 0.2
	500	0.034 ± 0.002	18.9 ± 0.2
0.1	500	0.094 ± 0.004	19.1 ± 0.2
0.3	200	0.087 ± 0.004	19.2 ± 0.2

The phase of the North-South anisotropy is obviously fairly insensitive to the assumed rigidity spectrum. The amplitude on the other hand, is sensitive to the assumed spectrum with higher values being estimated as the rigidity spectrum gets more steeply negative.

Temporal variation of ξ_{NS}

Heliospheric polarity variation. Using an assumed rigidity spectrum the best fit free-space parameters can be examined with the data separated into the two magnetic polarity states. This has been done for various rigidity spectra (see Table 4.5).

Table 4.5 Values of the best fit free-space parameters of the North-South anisotropy separated into groups according to the magnetic polarity of the heliosphere. Uncertainties are to 67% confidence.

		ξ^{+}_{NS}, A>0		ξ^{-}_{NS}, A<0	
γ	P_u (GV)	η_{NS} (%)	ϕ_{NS} (hours^{SID})	η_{NS} (%)	ϕ_{NS} (hours^{SID})
-0.5	100	0.145 ± 0.020	16.4 ± 0.5	0.222 ± 0.010	21.1 ± 0.2
	200	0.150 ± 0.020	16.7 ± 0.4	0.220 ± 0.010	20.9 ± 0.2
	500	0.151 ± 0.010	16.8 ± 0.4	0.217 ± 0.010	20.8 ± 0.2
0.0	100	0.135 ± 0.010	16.9 ± 0.4	0.194 ± 0.010	20.6 ± 0.2
	200	0.115 ± 0.010	17.4 ± 0.4	0.159 ± 0.010	20.2 ± 0.2
	500	0.094 ± 0.010	17.5 ± 0.4	0.129 ± 0.010	20.0 ± 0.2
0.5	100	0.083 ± 0.010	17.5 ± 0.4	0.114 ± 0.010	20.2 ± 0.2
	200	0.048 ± 0.010	17.9 ± 0.4	0.065 ± 0.004	19.7 ± 0.2
	500	0.038 ± 0.003	18.0 ± 0.4	0.037 ± 0.002	19.4 ± 0.2
0.3	200	0.072 ± 0.010	17.7 ± 0.4	0.098 ± 0.010	19.9 ± 0.2

First consider the negative spectra. In these cases we see that the amplitude of ξ_{NS} is essentially dependent on magnetic polarity. These results imply that η_{NS} (and hence the radial gradient) is significantly larger when the polarity of the heliosphere is negative, in agreement with conventional drift theory predictions (e.g. Jokipii and Kopriva 1979; Potgeiter and Moraal 1985).

The positive spectra result in estimations of η_{NS} which are far less dependent on the magnetic polarity of the heliosphere. This implies that the radial gradient is less dependent on the magnetic polarity state, supporting the prediction of Jokipii (1989) when using a model polar heliospheric magnetic field which is largely different to the usual Archimedean spiral (Jokipii and Kota 1989). It would seem unlikely that the rigidity spectrum of the anisotropy remains constant over an entire solar magnetic cycle, since solar activity and also the size of magnetic sectors vary.

The flat spectra ($\gamma = 0$) result in η_{NS} having some polarity dependence but not as great as the negative spectra.

As noted in Chapter 1, Bieber and Pomerantz (1986) found no dependence of η_{NS} on the magnetic polarity state of the heliosphere when assuming a flat rigidity spectrum from 1963 to 1988. The results obtained here, when assuming a positive static rigidity spectrum, are

reasonably consistent within errors with those of Bieber and Pomerantz. Swinson (1988) found very little dependence of the amplitude of the sidereal diurnal variation recorded at Embudo UG Muon Telescope on the polarity state of the heliosphere. This would also seem to be consistent with an η_{NS} which is independent of the magnetic polarity state unless there was a significant change in the spectrum of the anisotropy after magnetic polarity reversals. That is to say, due to the nature of coupling coefficients a large free-space anisotropy with a small P_u could be observed by an UG muon telescope to have the same amplitude of diurnal variation as a small free-space anisotropy with a large P_u. The evidence presented in this thesis (corresponding to Yasue's rigidity spectrum or at least a spectrum with a positive spectral index) would imply very little dependence of η_{NS} on the polarity of the heliosphere.

On the other hand, ϕ_{NS} is extremely sensitive to heliospheric polarity regardless of the assumed spectrum. It is obvious that for the negative polarity state ϕ_{NS} is definitely later than 19 hours^{SID} and usually close to 20 hours^{SID}. When the heliosphere is in the positive polarity state ϕ_{NS} is generally less than 18 hours^{SID}. By assuming Yasue's (1980) rigidity spectrum and taking an average of the two phases in Table 4.5 the long term average is 18.8 hours^{SID}, much closer to that predicted by Nagashima et al. (1983a) and supporting the view that the long term average is being biased towards the results of the negative polarity state. This certainly helps to explain why the average ϕ_{NS} in the previous section was about 0.6 hours^{SID} later than that predicted by Nagashima et al. (1982).

Any departure of the phase of ξ_{NS} from the north ecliptic pole implies that another anisotropy is present and being detected in the analysis along with ξ_{NS}. This will be explored in the following section when the year to year variations of ξ_{NS} will be considered.

Year to year variations. Figures 4.8 to 4.16 show the best fit η_{NS} and ϕ_{NS} of ξ_{NS} from 1957 to 1990 determined from 9(a) and 9(b) while assuming a constant rigidity spectrum for the entire period in the relations in (4.14) and (4.15). The Figures show the results of this analysis for various spectra, similar to those in Tables 4.4 and 4.5. Note that there are definite variations in both η_{NS} and ϕ_{NS}.

The magnitude of the derived amplitude is sensitive to the assumed rigidity spectrum. As the spectral index or the upper rigidity increases η_{NS} decreases. This is intuitively correct but an interesting result is that for the year 1979, a year in which quite remarkable diurnal variation results appear in Figures 4.1 to 4.6. The η_{NS} decreases in an orderly manner as the spectral parameters increase but the value for 1979 decreases much more drastically relative to the other years. Consider Figure 4.8. The η_{NS} for 1979 is the largest out of all the measurements. In Figure 4.14 the spectrum is positive and the η_{NS} for 1979 is one of the smallest out of the 34 years of results. Bieber and Pomerantz's (1986) analysis of the North-South anisotropy was insensitive to the spectrum assumed and showed that η_{NS} for 1979 was close to a maximum value. It has been shown (Figures 4.1 and 4.2) that neutron monitor data have large amplitudes of the sidereal diurnal variation around 1978 and 1979 while muon telescope data do not. The above results plus the derived spectrum for 1979 (although not statistically reliable) presented in Table 4.3 argues strongly in favour for 1979 being a

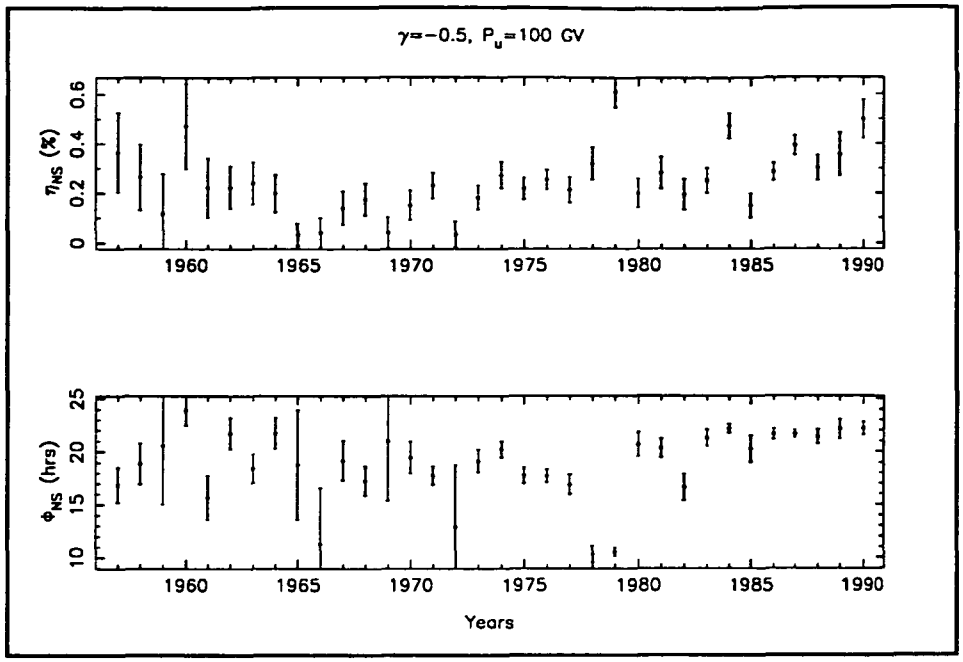

Figure 4.8 The amplitude constant η_{NS} and phase ϕ_{NS} of the North-South anisotropy assuming the constant rigidity spectrum G(P) = (-0.5, 100GV) from 1957 to 1990. The associated uncertainties are at the 67% confidence level.

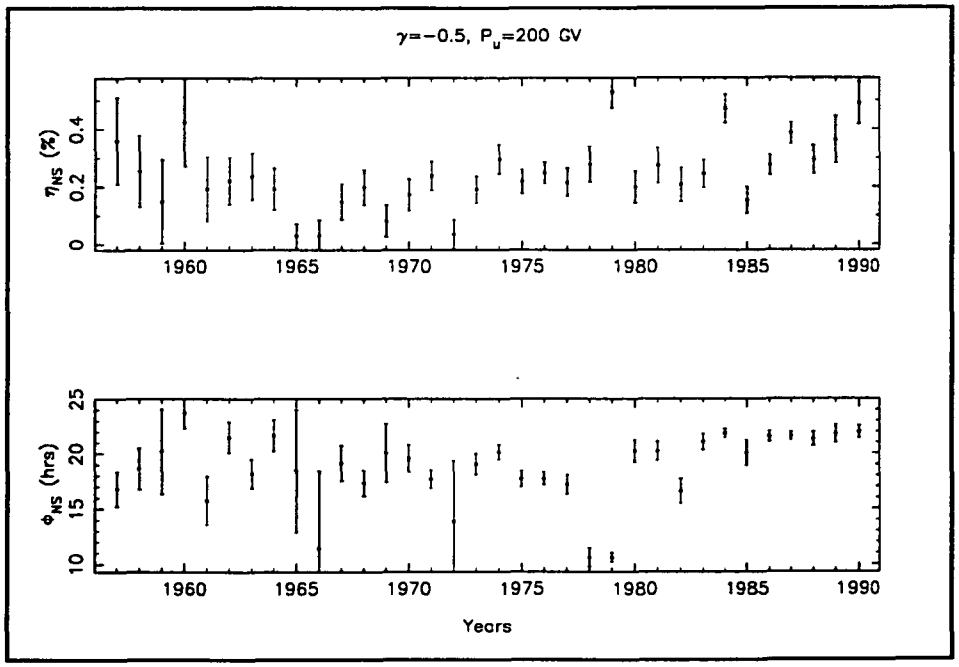

Figure 4.9 Same as for Figure 4.8 but assuming the constant rigidity spectrum G(P) = (-0.5, 200GV).

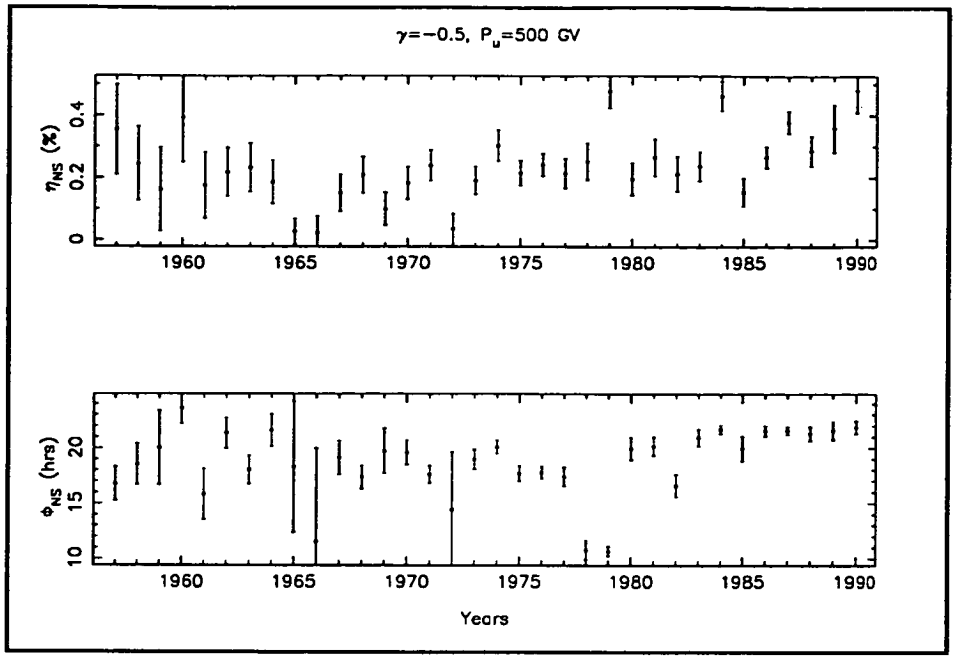

Figure 4.10 Same as for Figure 4.8 but assuming the constant rigidity spectrum G(P) = (-0.5, 500GV).

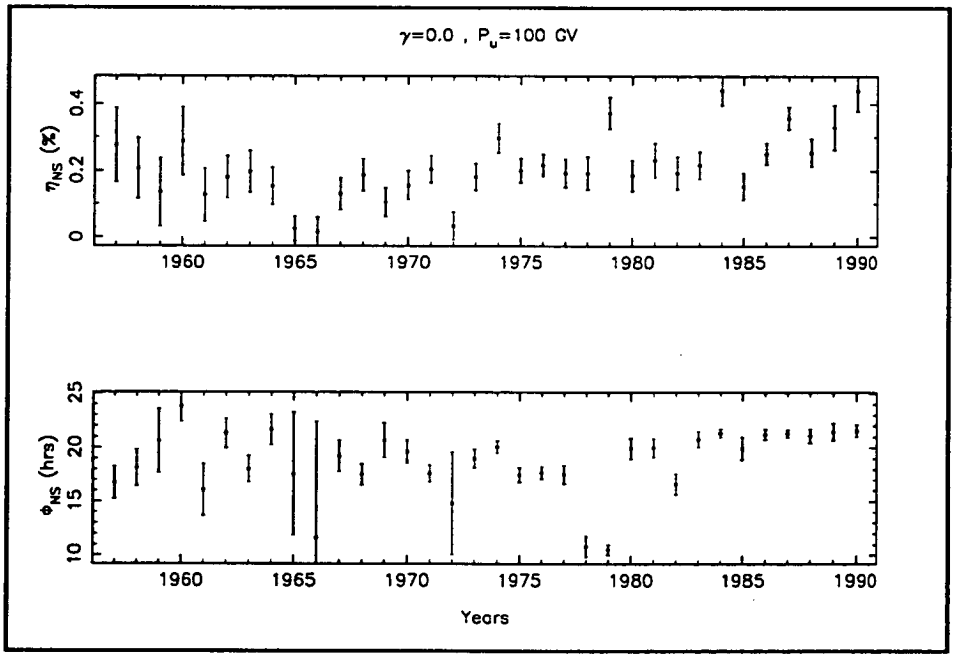

Figure 4.11 Same as for Figure 4.8 but assuming the constant rigidity spectrum G(P) = (0.0, 100GV).

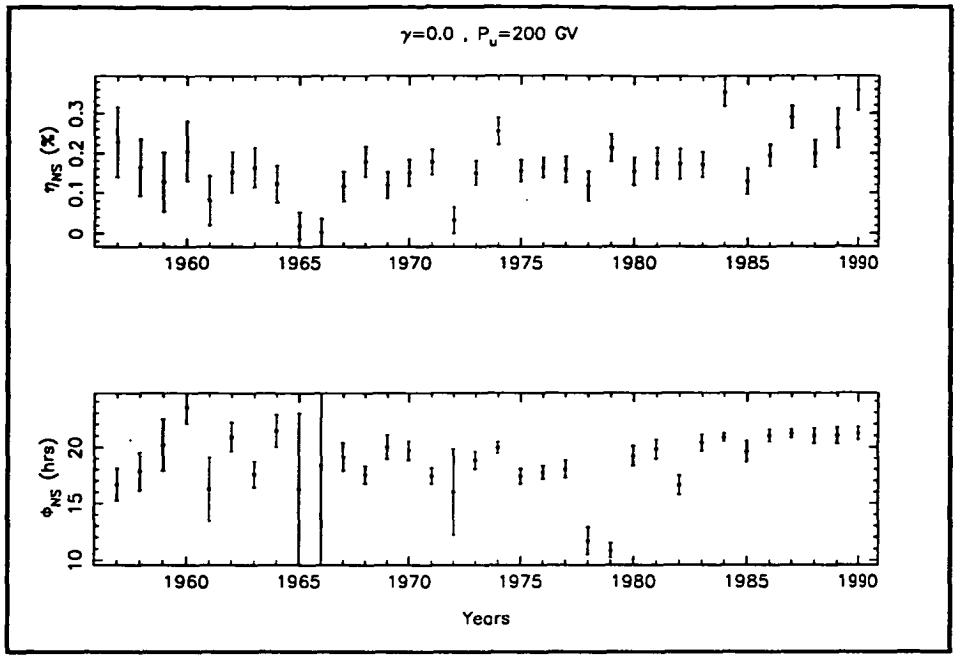

Figure 4.12 Same as for Figure 4.8 but assuming the constant rigidity spectrum G(P) = (0.0, 200GV).

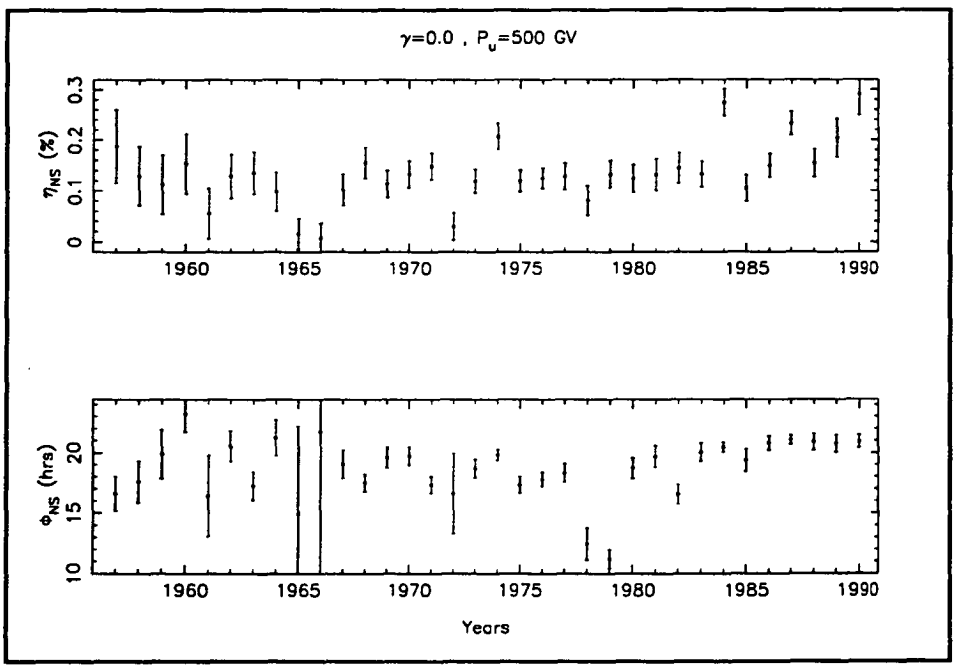

Figure 4.13 Same as for Figure 4.8 but assuming the constant rigidity spectrum G(P) = (0.0, 500GV).

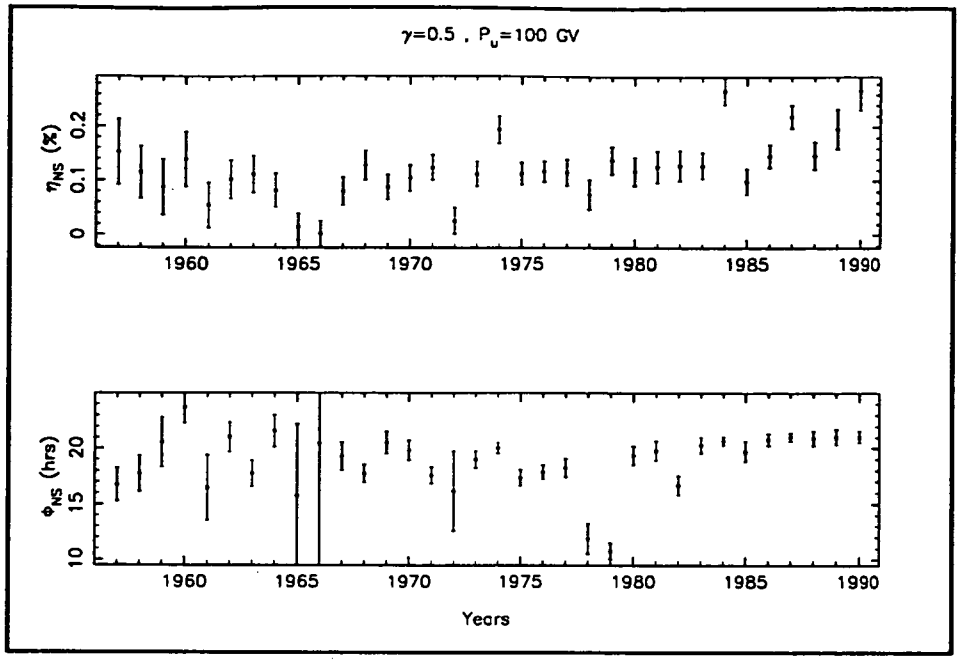

Figure 4.14 Same as for Figure 4.8 but assuming the constant rigidity spectrum G(P) = (0.5, 100GV).

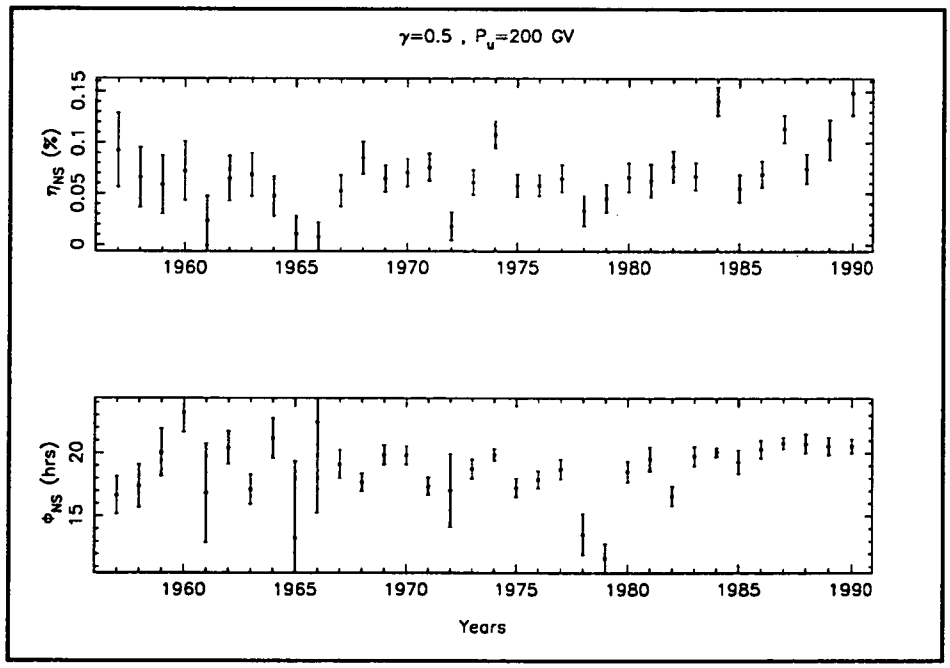

Figure 4.15 Same as for Figure 4.8 but assuming the constant rigidity spectrum G(P) = (0.5, 200GV).

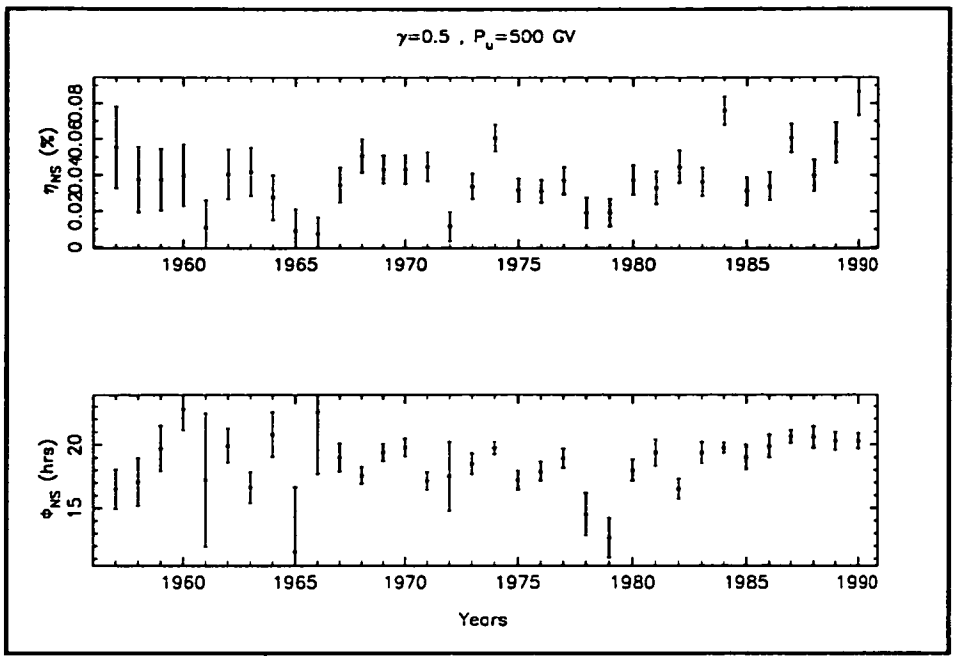

Figure 4.16 Same as for Figure 4.8 but assuming the constant rigidity spectrum G(P) = (0.5, 500GV).

year when ξ_{NS} had a negative spectrum. This was suggested in Section 4.2 to explain the obvious differences in the sidereal diurnal variation results of neutron monitors and underground muon telescopes.

The phase is very insensitive to the assumed spectrum. This is a similar conclusion to that made when studying the heliospheric polarity dependence of ξ_{NS}. It is now obvious that the heliospheric polarity dependence of ϕ_{NS} is due to a wave in the results with a period of about one solar magnetic cycle.

The amplitude η_{NS}. The results shown in Figure 4.17 were derived under the assumption of Yasue's (1980) rigidity spectrum and fitted to a wave with arbitrary amplitude and phase and an 11-year period; that is, $\eta_{NS} = c_\eta + A_\eta \cos\omega(t - \phi_\eta)$. A statistical F-test was performed to test the significance of the wave fitted to the amplitudes. This test compared the variance of the amplitudes from the fitted wave to the variance of the amplitudes from the mean η_{NS}. The F-test indicated that there is only 34% probability that the wave is a better model to the amplitude variation than the mean. Attempts to fit waves of other periods yielded similar results with the most probable wave being one with a 15 year period (84% probability).

A 10-year wave in the amplitude of ξ_{NS} was reported by Bieber and Pomerantz (1986). Swinson (1988) observed the amplitudes of the sidereal variation vectors (uncorrected for geomagnetic effects) to have a small variation over a 20-year epoch. Swinson's analysis was similar to the analysis of this thesis and is qualitatively in agreement with the results

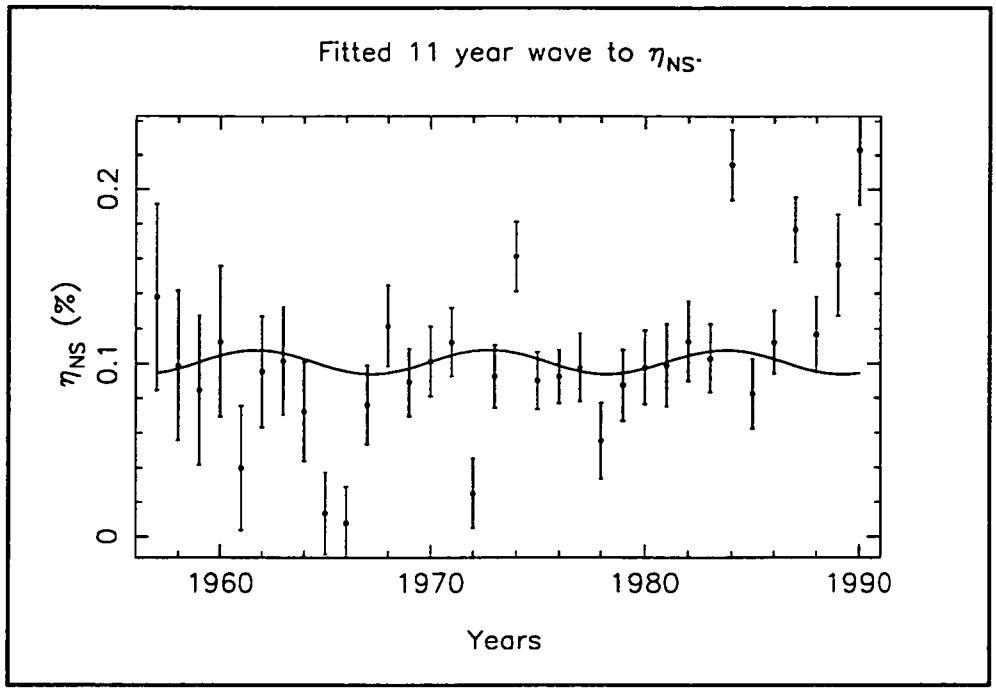

Figure 4.17 Fitted 11-year wave to η_{NS} assuming a static rigidity spectrum G(P) = (0.3, 200 GV). Uncertainties are to 67% confidence.

presented here. He did not derive the free-space anisotropy so direct comparison is impossible. These results are directly comparable to those of Bieber and Pomerantz however, and are in reasonable agreement with their values although there is no definite cyclic variation in the results presented here. This can perhaps be explained by the fact that Bieber and Pomerantz's analysis was only performed on neutron monitor data, although aside from the years 1978 and 1979 the anisotropy seems to be fairly consistent at all rigidities (as inferred from the diurnal variation results in Figures 4.1 to 4.6) so higher rigidity data included in the analysis should only improve the results. A more probable explanation is that the analysis here is contaminated by another anisotropy, suggested previously, which is damping out some of the variation in the results. This contamination will be explained by examining the phase of the anisotropy more closely.

The phase ϕ_{NS}. Year-to-year changes in the phase of ξ_{NS} have only been examined prior to this thesis by Swinson (1988). He used data from underground muon telescopes at Embudo, Bolivia, and Socorro for the period 1965 to 1985 and concluded that (Swinson 1988) "there is good consistency (of ϕ_{NS}) from year to year over the entire period". This is undoubtably true, but close inspection of Figure 2 in his paper shows that even those results had anomalous phases in the sidereal diurnal variation around 1972, 1980, and 1982, although any clear trend is unobservable.

In Figure 4.18 the ϕ_{NS}, although close to 18 hours^{SID} (except for 1960, 1974, 1978 and 1979), does display some remarkable features. There is a hint of a wave with a period about two sunspot cycles (one solar magnetic cycle) with a peak to peak amplitude of about 3

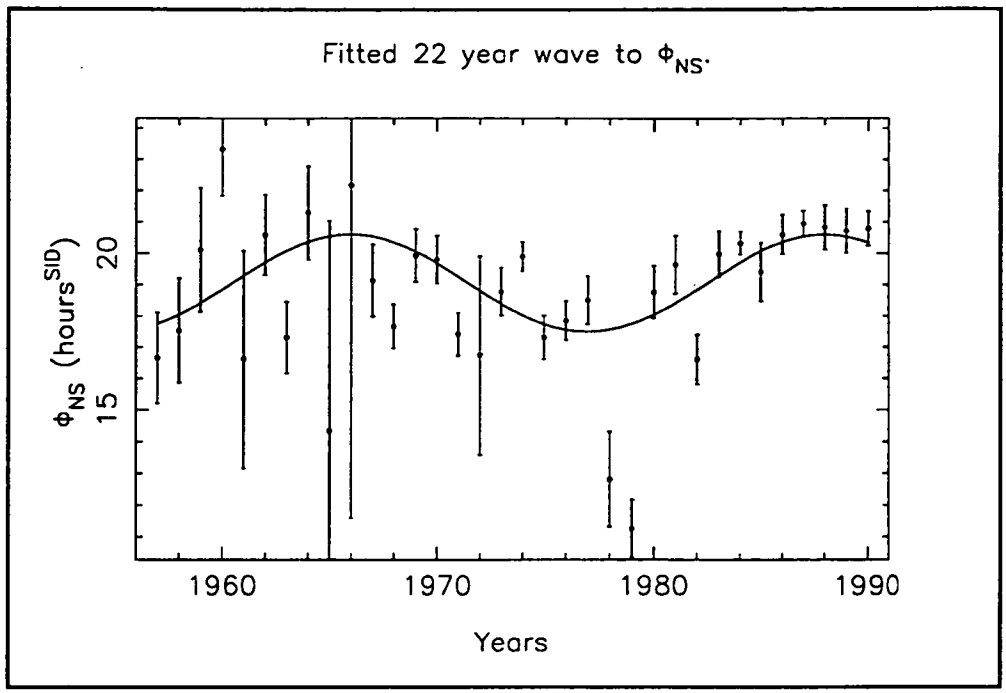

Figure 4.18 Fitted 22-year wave to ϕ_{NS} assuming a static rigidity spectrum G(P) = (0.3, 200 GV). Uncertainties are to 67% confidence.

hours. The phases were fitted to a 22-year wave; that is, $\phi_{NS} = c_\phi + A_\phi \cos\omega(t - \phi_\phi)$. Again an F test was performed to compare the variance from the fitted 22-year wave to the variance from the mean ϕ_{NS}. The test indicated a 99.99% probability that a 22-year wave is a better representation of the data than the mean. The wave has an amplitude of 1.6 hours and peaks during the years 1966 and 1988.

The physical basis of such a wave in the phase of ξ_{NS} is very interesting. The toward–away (IMF) analysis should remove all effects common to both sides of the neutral sheet. This includes any real galactic anisotropy. Nagashima et al. (1982) (hereafter referred to as NMY) proposed that heliospheric modulation of a galactic anisotropy is possible and that toward/away asymmetric modulation of a galactic anisotropy is observable. Some evidence exists that this is the contamination of the analysis.

For the wave in ϕ_{NS} to depend on heliospheric polarity the contamination needs to have the same dependence. A possibility is for the contamination to be describable by a vector whose phase on the harmonic dial lies along the 0-12 hour^{SID} direction and whose amplitude varies with the solar cycle. The amplitude would have to be zero at solar maximum and maximum at solar minimum. Furthermore, the phase must reverse following each solar maximum. Another possibility is for the contaminating anisotropy to have a phase which rotates on the harmonic dial 24 sidereal hours during a solar magnetic cycle. To search for evidence of either of these possibilities the sidereal diurnal variation recorded by the Poatina UG muon telescope (PUM) in Tasmania (300 mwe, P_{med} = 1400 GV, λ_{eff} = 35° S) from 1972 to 1985 has been examined. At this median rigidity it is hard to imagine that any variation in the count rate is induced by solar anisotropies.

Figure 4.19 shows the annual sidereal diurnal variations (ξ_{GAL}) observed by PUM from 1972 to 1985. This is assumed to be caused solely by a galactic anisotropy. Most of the vectors show a diurnal variation of about 0.06 to 0.1 % with a time of maximum around 3 to 5 hours^{SID}. This is in agreement with other observations of a true galactic anisotropy at these high rigidities (Cutler et al. 1981; Ueno et al. 1984; Yasue et al. 1984; Cutler and Groom 1991). The absence of any antisidereal diurnal variation implies that there is no contribution from the solar semidiurnal variation. NMY predict that there should be a noticeable change in the phase of the galactic anisotropy between the heliomagnetic polarity states A>0 (1972–1979) and A<0 (1960–1968, 1981–1985). Bercovitch's (1984) analysis of the sidereal diurnal variation recorded by the Ottawa horizontal muon array (OHMA) failed to observe such a phase change, suggesting that the model heliosphere used by NMY was inadequate.

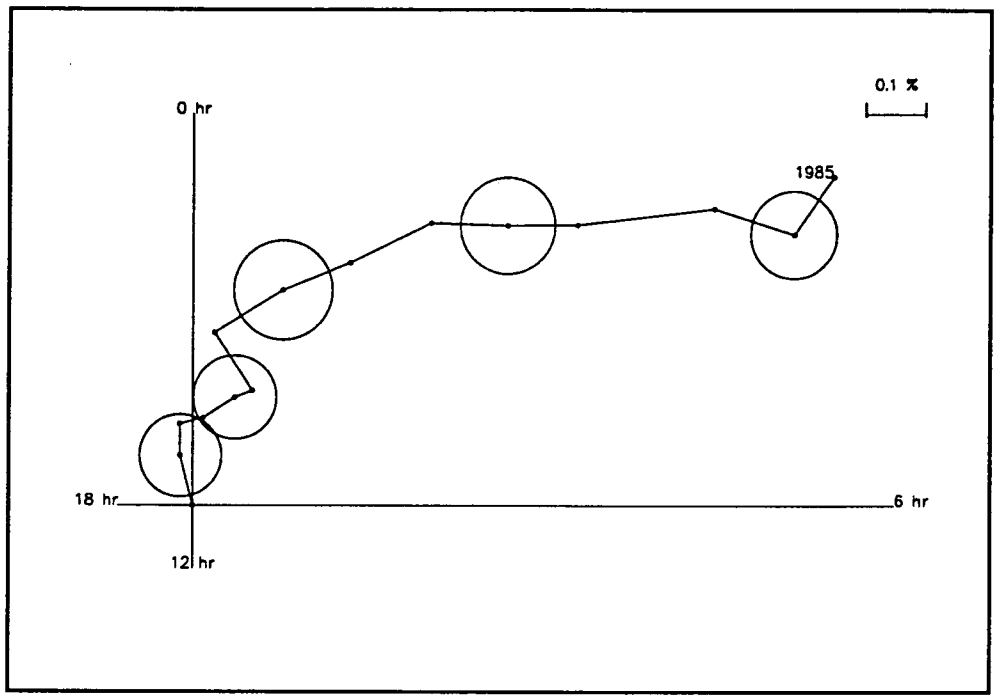

Figure 4.19 Yearly averaged sidereal diurnal variation observed at Poatina underground muon telescope. The associated uncertainties are at the 67% confidence level.

Figure 4.20 shows the average galactic anisotropy for 1972–1979 (ξ^{+}_{GAL}) and for 1981–1985 (ξ^{-}_{GAL}), derived from PUM observations. The phase difference is indeed noticeable and agrees with NMY's prediction for a telescope with an effective latitude of viewing (λ_{eff}) between 30° and 45°. The ratio of the amplitudes of $\xi^{-}_{GAL}/\xi^{+}_{GAL}$ is 2.22, compared to NMY's prediction of about 1.7 when $\lambda_{eff} = 30°$ and 2.4 when $\lambda_{eff} = 45°$ for a galactic anisotropy at 1000 GV. With these results in mind, NMY's predictions and the statistical accuracy of the PUM data seem to be reliable.

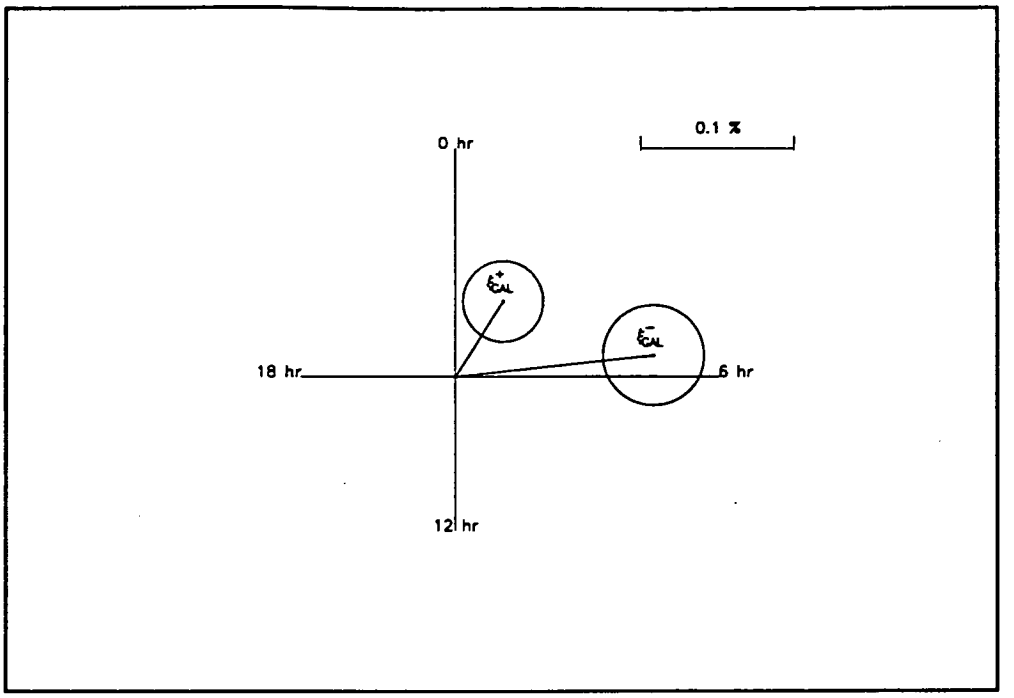

Figure 4.20 Average sidereal diurnal variation observed at PUM for the epochs 1972–1979 (ξ^{+}_{GAL}), when the polarity state of the heliosphere was A>0 and 1981–1985 (ξ^{-}_{GAL}), when A<0. Uncertainties are to 67% confidence.

Figure 4.21 shows the difference between the galactic anisotropy in towards IMF sectors and away IMF sectors (ξ^{T-A}_{GAL}) as inferred from the yearly averaged sidereal diurnal variation vectors recorded by PUM separated into these two groups of IMF sector polarity and averaged accordingly. Most vectors are smaller than their associated errors but nonetheless may reflect 14 years of a 22-year rotation in the phase of the vector on the harmonic dial. Note that the data are certainly not directed along the 0–12 hours^{SID} direction, discounting the earlier explanation of the ϕ_{NS} wave.

NMY predict that there may be heliospheric asymmetric modulation of the galactic anisotropy and that the difference in this modulation (ξ^{T-A}_{GAL}) can be observed and will depend on the warp of the neutral current sheet. The 14-year average ξ^{T-A}_{GAL} vector at PUM is almost zero. This could imply that ξ^{T-A}_{GAL} is always zero (in which case the wave in ϕ_{NS} cannot be explained) except that the vector for 1978 is significant (at the 2-σ level) and non-zero. It could also mean that the rotation of the vectors around the harmonic dial from year to year results in a small long-term average, lending support to the statistically inaccurate data to the hypothesis of asymmetric modulation. The direction of the ξ^{T-A}_{GAL} vectors over the 14-year period are consistent with the contamination needed to add to the static ξ_{NS} (about 18 hours) to produce the observed wave in ϕ_{NS}. Mori et al. (1989) have analysed the sidereal diurnal variation data from the Matsushiro UG muon telescope(MAUM, 220 mwe) and examined the average ξ^{T-A}_{GAL} vector observed there from 1984 to 1989. MAUM has a median rigidity of 660 GV, and its average observed ξ^{T-A}_{GAL} vector has a phase about 21 hours^{SID} and amplitude

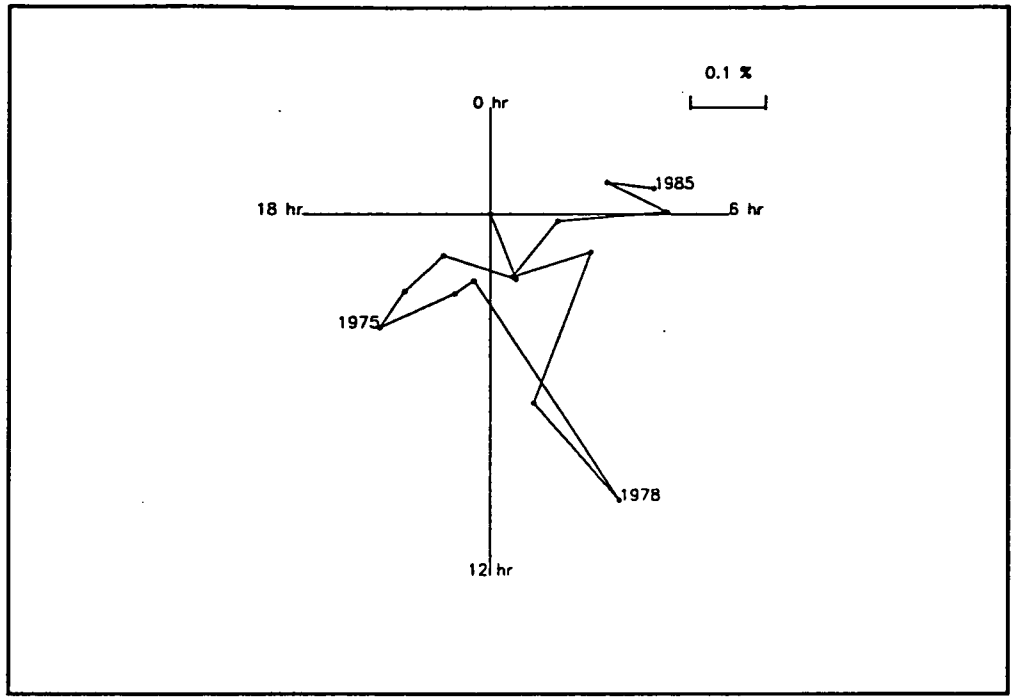

Figure 4.21 Yearly averaged toward-away (T-A) sidereal diurnal variation observed at PUM from 1972 to 1985.

0.01%. This vector could certainly complement the data in Figure 4.21 and be a result of the ξ_{GAL}^{T-A} vectors continuing to rotate anti clockwise around the harmonic dial after 1985.

The data from which ξ_{NS} has been obtained were recorded by instruments responding to primary rigidities from about 10 to 300 GV. Nagashima et al. (1983b) have proposed that the galactic anisotropy has a rigidity dependent source direction. The wave in ϕ_{NS} has been explained by the asymmetric modulation of a galactic anisotropy. Data from PUM, with P_{med} about 1400 GV supports this. The galactic anisotropy producing the wave in ϕ_{NS} is almost certainly not the same anisotropy being detected by PUM, but NMY also predict heliospheric modulation of a galactic anisotropy of low rigidity particles. The predictions about modulation of a galactic unidirectional anisotropy are in terms of three components: two in the equatorial plane and a third component parallel to the Earth's rotation axis. In the high rigidity region the component parallel to the rotation axis does not produce any diurnal variation but it may produce a variation in the low rigidity region. The discrepancy between the phase of the galactic anisotropy recorded by high- and low-rigidity instruments cannot be accounted for by this mechanism (Nagashima et al. 1983a). Note that recently, Nagashima et al. (1994) have explained this discrepancy by invoking a model based on a loss cone of high rigidity particles at the opposite side of the heliosphere to the direction of the galactic rotation and a source cone of low rigidity particles at the heliosphere's magneto-tail. To be able to explain the wave in ϕ_{NS} in terms of a galactic anisotropy one must assume that the asymmetric modulation of the galactic anisotropy in toward and away sectors at rigidities greater than 1000 GV (as observed by PUM) is also valid at rigidities less than 500 GV. The results shown in Figure 4.22 may support this. The $\xi_{GAL}^{+,T-A}$ and $\xi_{GAL}^{-,T-A}$ vectors from PUM are in the directions needed for the difference between ξ_{NS} in Table 4.4 and those derived for

opposite magnetic polarity states (ξ^{+}_{NS} and ξ^{-}_{NS} in Table 4.5); that is, disregarding any biasing of the results from the A <0 magnetic polarity state, ξ_{NS} determined over the 34-year period is assumed to be the average non-contaminated anisotropy. The difference between this vector and those obtained for two separate solar polarity states is ξ^{T-A}_{GAL} during those two epochs.

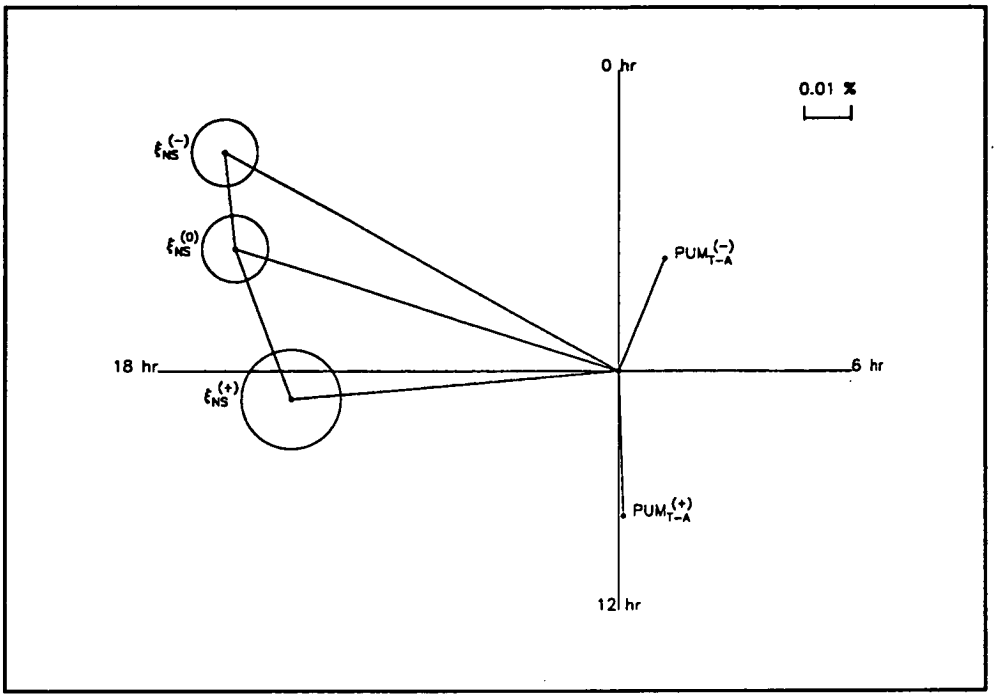

Figure 4.22 Heliospheric magnetic polarity independent and dependent North-South anisotropy and heliospheric polarity dependent average T-A sidereal diurnal variation observed at PUM.

Admittedly the statistically unsound results presented in Figure 4.21 are not very convincing in explaining the wave in ϕ_{NS} in terms of asymmetric heliospheric modulation of a galactic anisotropy. However, considering all the evidence above, it is likely that the 22-year wave in ϕ_{NS} can be interpreted as asymmetric heliospheric modulation of the galactic anisotropy. The evidence is summarised as follows:

- The yearly averaged towards-away (IMF) sidereal diurnal variation vectors derived from Fourier analysing the cosmic ray hourly count rates of each instrument have a temporal variation to their phases;
- the annual ξ^{T-A}_{GAL} vectors recorded at PUM seem to rotate anti clockwise during the 14-year epoch from 1972 to 1985;
- the average (statistically significant) ξ^{T-A}_{GAL} recorded at MAUM for 1984 to 1989 has a phase consistent with the data needed to imply a 22 year period in the phase of ξ^{T-A}_{GAL}; and

- the average $\xi_{GAL}^{+,T-A}$ and $\xi_{GAL}^{-,T-A}$ recorded at PUM during 1972–1979 and 1981–1985 respectively, have phases on the harmonic dial which are required of the contamination.

The outlying ϕ_{NS} in Figures 4.8 to 4.16 (i.e. at 1978 and 1979) are even more peculiar. No explanation is offered except to note that the data from PUM show that the toward-away vector for 1978 (statistically significant to 95%) is in the direction of about 8 hours^{SID} and has an amplitude twice as large as any other vector recorded at PUM for the period 1972–1985. If this contamination (in free space and in the same rigidity region) is about the same magnitude as the ξ_{NS} then it could couple to ξ_{NS} to produce an observed ξ_{NS} vector with phase around 12 hours^{SID}.

4.4 Results of inferring the radial gradient of cosmic rays from ξ_{NS}

There is little doubt that the towards-away analysis of the sidereal diurnal variation to derive the North-South anisotropy is contaminated by the asymmetric modulation of a galactic anisotropy. Since the analysis is contaminated, the radial density gradient (G_r) can only be inferred from ξ_{NS} by assuming that the contamination is small. The results in Figure 4.22 justify this assumption, all vectors representing ξ_{NS} having similar magnitudes.

Table 4.6 presents the average values of G_r for 10 GV and 100 GV cosmic rays inferred from the ξ_{NS} results of Section 4.3 for various rigidity spectra. To infer G_r one makes use of equation (4.6) and with a little manipulation :

$$G_r = \frac{4.5B}{\sin\chi}\eta_{NS}\left(\frac{P}{10}\right)^{\gamma-1} = 31.82\eta_{NS}\left(\frac{P}{10}\right)^{\gamma-1} \qquad (4.16)$$

The following results have assumed that the IMF strength (B) is a constant at 5 nT and that the angle at the Earth of the IMF with the Earth-Sun line (χ) is constantly 45°.

The conclusions drawn from these values are exactly the same as those made in relation to any heliospheric polarity dependence of η_{NS} in Section 4.3.2, i.e. since it is much more likely that the spectrum of ξ_{NS} is positive, it would seem the radial density gradient is only slightly smaller during epochs of $A>0$ heliospheric polarity than when $A<0$. This is in agreement with recent theoretical models (Jokipii and Kota 1989).

Table 4.7 presents the average value of G_r (assuming Yasue's rigidity spectrum) for various energetic particles and a comparison of these values to previous determinations of the radial density gradient. Values calculated in this thesis are in good agreement with all previous values, especially those presented by Yasue (1980). This is not surprising considering the same rigidity spectrum was used, although the analysis could have yielded a result which was extremely different to that of Yasue. It is pleasing that the same results could be derived independently especially when one considers that there is a small amount of contamination to these results which has been ignored.

Table 4.6 Values of the radial density gradient (G_r) of 10 GV and 100 GV particles calculated from equation 4.16 and the results presented in Tables 4.4 and 4.5. Uncertainties are to 67% confidence.

		G_r (% AU^{-1}) Average		G_r (% AU^{-1}) A>0		G_r (% AU^{-1}) A<0	
γ	P_u (GV)	10 GV	100 GV	10 GV	100 GV	10 GV	100 GV
-0.5	100	5.38 ± 0.32	0.17 ± 0.01	4.61 ± 0.64	0.15 ± 0.02	7.06 ± 0.32	0.22 ± 0.01
	200	5.57 ± 0.32	0.18 ± 0.01	4.77 ± 0.64	0.15 ± 0.02	7.00 ± 0.32	0.22 ± 0.01
	500	5.60 ± 0.32	0.18 ± 0.01	4.80 ± 0.64	0.15 ± 0.02	6.90 ± 0.32	0.22 ± 0.01
0.0	100	5.12 ± 0.32	0.51 ± 0.03	4.30 ± 0.32	0.43 ± 0.03	6.17 ± 0.32	0.62 ± 0.03
	200	4.39 ± 0.32	0.44 ± 0.03	3.66 ± 0.32	0.37 ± 0.03	5.06 ± 0.32	0.51 ± 0.03
	500	3.63 ± 0.32	0.36 ± 0.03	2.99 ± 0.32	0.30 ± 0.03	4.10 ± 0.32	0.41 ± 0.03
0.5	100	3.21 ± 0.32	1.02 ± 0.10	2.64 ± 0.32	0.84 ± 0.10	3.63 ± 0.32	1.15 ± 0.10
	200	1.88 ± 0.10	0.59 ± 0.03	1.53 ± 0.32	0.48 ± 0.10	2.07 ± 0.13	0.65 ± 0.04
	500	1.08 ± 0.06	0.34 ± 0.02	0.89 ± 0.32	0.28 ± 0.03	1.18 ± 0.06	0.37 ± 0.02
0.3	200	2.77 ± 0.13	0.55 ± 0.03	2.29 ± 0.32	0.46 ± 0.06	3.12 ± 0.19	0.62 ± 0.04

Table 4.7 Values of the average radial density gradient (G_r) calculated from equation (4.16) and the results of Table 4.4 assuming Yasue's (1980) rigidity spectrum. Previous determinations are included. Uncertainties are to 67% confidence.

P (GV)	G_r (% AU^{-1})	Yasue (1980)	Kudo and Wada (1977)	Bieber and Pomerantz (1986)
10	2.77± 0.13	3.00 ± 1.10	-	2.0
20	1.70± 0.08	1.85 ± 0.68	0.9	-
50	0.90± 0.04	0.97 ± 0.36	-	-
80	0.65± 0.03	0.70 ± 0.26	0.4	-
100	0.55± 0.03	0.60 ± 0.22	-	-
150	0.42± 0.02	0.45 ± 0.17	0.3	-
200	0.34± 0.02	0.37 ± 0.14	-	-
230	0.31± 0.01	-	0.2	-

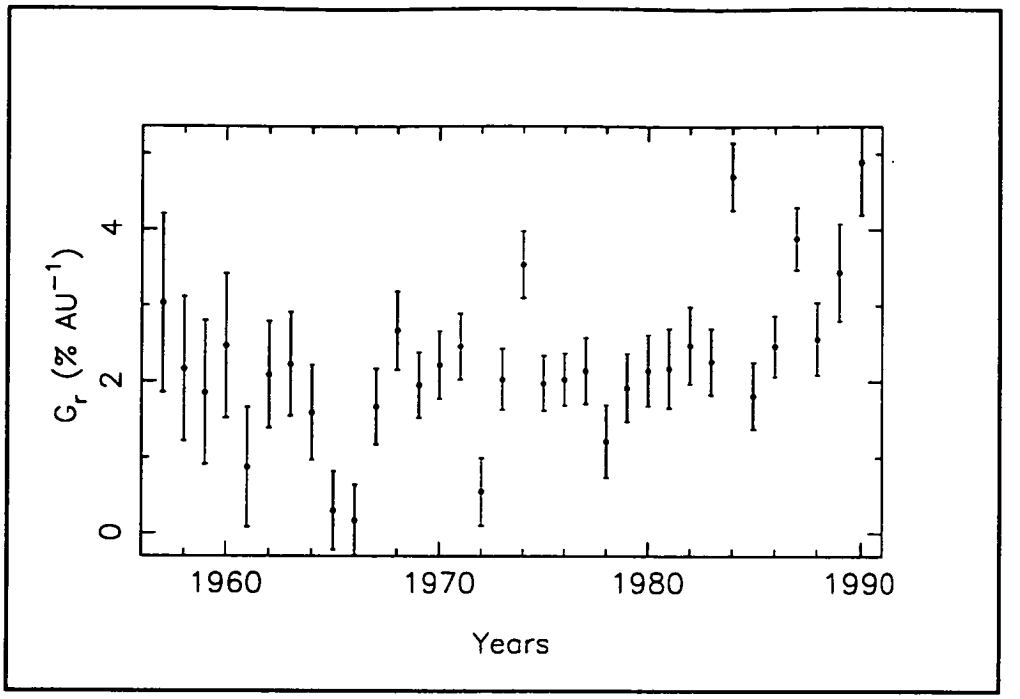

Figure 4.23 Radial gradient of 17 GV particles from 1957 to 1990 assuming the static rigidity spectrum G(P) = (0.3, 200 GV). Uncertainties are to 67% confidence.

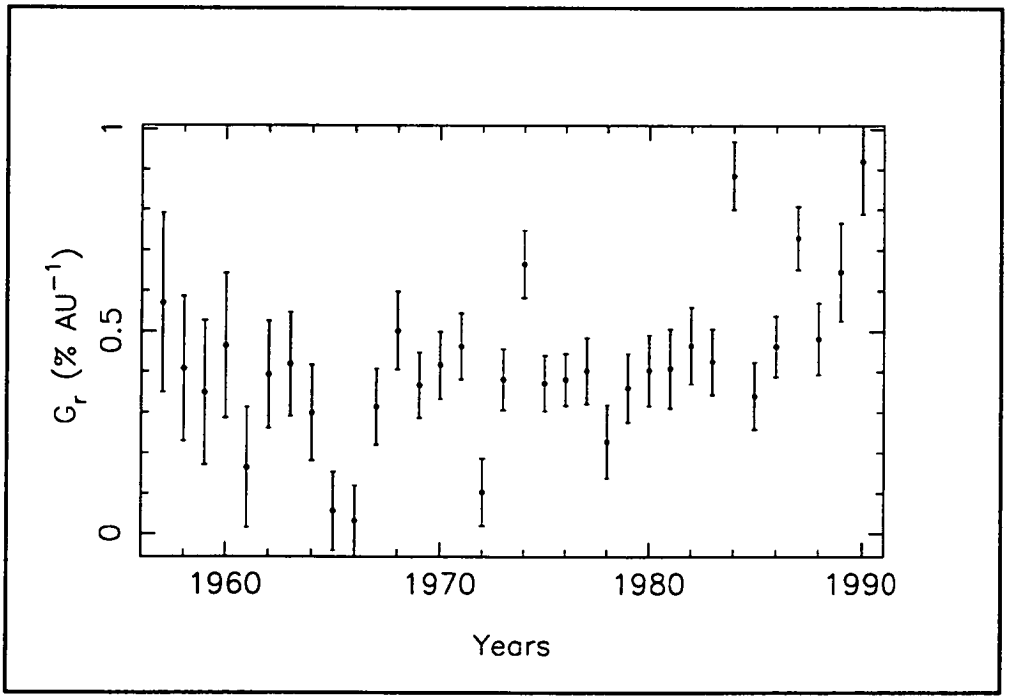

Figure 4.24 Radial gradient of 185 GV particles from 1957 to 1990 assuming the static rigidity spectrum G(P) = (0.3, 200 GV). Uncertainties are to 67% confidence.

The radial gradients of 17 and 185 GV particles inferred from ξ_{NS} for the period 1957–1990 are shown in Figures 4.23 and 4.24 for Yasue's rigidity spectrum. All results are consistent with other observations (Bieber and Pomerantz 1986, Duggal and Pomerantz 1977, Yasue 1980). Note that since the rigidity spectrum is assumed to be constant for the entire time then the same variations in η_{NS}, shown in Figure 4.17 are reflected in the gradient results. The maxima in G_r occur around times of solar maximum and the minima around years of least solar activity. In accordance with the results presented in Section 4.3 little heliospheric polarity dependence is observed. For 185 GV particles we see that except for 1984 and 1990 all years show that G_r is less than about 0.8% AU^{-1}, and the mean is typically about 0.4% AU^{-1}.

4.5 Contribution of perpendicular diffusion

1984 had the highest value of η_{NS} of all the results but is close to the time of solar minimum during that solar cycle. Until now we have assumed that the contribution to ξ_{NS} from cross-field diffusion is negligible (equation 4.5). We know from Chapter 3 that the bidirectional latitudinal gradient ($G_{|z|}$) is in the direction predicted by drift theory (Jokipii 1989). In this case the observed η_{NS} will be suppressed by an amount $\lambda_\perp G_{|z|}$. (If $G_{|z|}$ was opposite to the predicted direction the observed η_{NS} would be enhanced by the same amount.) Bieber and Pomerantz (1986) cite that if $\kappa_\perp = 10^{21}$ cm^2 s^{-1} for 10 GV particles then cross-field diffusion can only contribute 0.01% anisotropy if $G_{|z|}$ is about 2% AU^{-1}. This is only 12% of the mean anisotropy measured from 1957 to 1990 using Yasue's (1980) rigidity spectrum. Yasue (1980) determined the radial diffusion coefficient (κ_{rr}) to be $3.2\times10^{22}\times(P/10)^{0.7}$ cm^2 s^{-1} but claims this may be too low when P > 10 GV. Using Yasue's result and noting that:

$$\kappa_{rr} = \kappa_{\parallel}\cos^2\chi + \kappa_\perp \sin^2\chi \tag{4.16}$$

where χ is the angle between the Earth-Sun line and the IMF, then:

$$\lambda_\perp = \frac{6\kappa_{rr}}{c\left(\frac{1}{\alpha}+1\right)} \tag{4.17}$$

$\alpha = \frac{\kappa_\perp}{\kappa_\parallel}$ and

c = the speed of light.

In Chapter 3, $G_{|z|}$ was determined for particles with rigidities between 17 and 195 GV, assuming that $\alpha = 0.01$. The determinations of $G_{|z|}$ for 17 GV particles were in good agreement with those of Bieber and Chen (1991a). Note that Bieber and Chen's analysis and the results in Chapter 3 show an uncharacteristic zero value around 1983–1984 (see Section 3.4.2 and Appendix 5). The usual value of $G_{|z|}$ when $\alpha = 0.01$ is about 2% AU^{-1} at neutron monitor rigidities. As α increases, $G_{|z|}$ decreases (Bieber and Chen 1991b) and if $\alpha = 0.1$ as suggested by Ahluwalia and Sabbah (1993), Bieber and Chen find that $G_{|z|}$ is usually between 1 and 0.5% AU^{-1} for neutron monitors. For $\alpha = 0.1$ the contribution to the

observed ξ_{NS} from perpendicular diffusion could more likely be about 0.04% for neutron monitors. This is about 45% of the mean anisotropy. If this suppression (manifesting as $G_{|z|}$) is naturally occurring, and for unknown reasons in 1984 the suppression is switched off, then we could see a value of η_{NS} around 0.13% plus the solar cycle contribution to ξ_{NS}. This may explain the unusually high value of η_{NS} (about 0.2%) in 1984 and would mean that the perpendicular diffusion term in (4.5) is more important than assumed. This will be further investigated in Chapter 5. More reliable values of α need to be determined. If, in 1984, we are observing ξ_{NS} free from perpendicular effects then this may mean that the radial gradient is larger than the other data suggest (1957–1983, 1985–1990) by as much as 45% of the inferred value. Note that Bieber and Chen's data and some of those in Chapter 3 suggest that 1983 is also a year when $G_{|z|}$ mysteriously vanishes but the results shown in Figures 4.23 and 4.24 are free from a relatively large increase in η_{NS} for this year.

Summary

By analyzing the sidereal diurnal variation recorded by instruments responding to primary cosmic ray particles with rigidities between about 10 and 300 GV one may conclude that:

- The average rigidity spectrum of ξ_{NS} over the period 1957 to 1990 was determined to be ($\gamma = 0.1$, $P_u \approx 500$ GV). This result is statistically unreliable, but is in close agreement with values found by other investigators (Yasue 1980, Ueno et al. 1984);
- if the rigidity spectrum is assumed to be static and positive then the average amplitude (and hence the radial density gradient) is only slightly affected by the magnetic polarity state of the heliosphere. If the rigidity spectrum is negative, then the average amplitude of ξ_{NS} in the negative magnetic polarity state is larger than in the positive polarity state. The phase is definitely different during opposite heliospheric magnetic polarity states. During the negative polarity state when the Sun's magnetic field is away from the Sun in the southern heliospheric hemisphere the phase of ξ_{NS} is about 20 hours^{SID} while in the positive polarity state the phase is closer to 17 hours^{SID};
- assuming a static rigidity spectrum, the amplitude of ξ_{NS} varies slightly with smaller values around times of solar minima than around times of solar maxima;
- regardless of whether the rigidity spectrum is constant over different magnetic polarity states of the heliosphere, there may be some contamination to ξ_{NS} from another anisotropy which causes the phase of ξ_{NS} to vary with a 22-year period. This anisotropy is probably due to the asymmetric modulation (with respect to the neutral sheet) of a galactic anisotropy as predicted by Nagashima et al. (1982) and has a 22-year (solar magnetic) cycle;
- modulation of a galactic anisotropy in different heliospheric magnetic polarity states is observable. The ratio of the amplitude of the resulting sidereal diurnal variation observed by the Poatina underground muon telescope ($P_{med} = 1400$ GV) during the negative polarity state to that observed in the positive polarity state is 2.22. This is in excellent agreement with the predictions of Nagashima et al. (1982) for a telescope with an effective viewing latitude between 30 and 45 degrees;

- perpendicular diffusion is perhaps more important than previously assumed and could be responsible for underestimating ξ_{NS} and the radial density gradient by as much as 40% of the true value; and
- the values of the radial density gradient of high rigidity galactic cosmic ray particles (between 10 and 300 GV) which have been presented here for the period 1957 to 1990 are in good agreement with investigations by Duggal and Pomerantz (1977), Kudo and Wada (1977), Yasue (1980), and Bieber and Pomerantz (1986). During this period there was a variation in the radial gradient of 185 GV particles between about 0.2 and 1.0% AU^{-1} while the radial gradient of 17 GV particles varies between about 1 and 3% AU^{-1}.

CHAPTER 5

PARALLEL MEAN-FREE PATH

Two major results of Chapter 3 were the yearly determinations of the modulation parameters $\overline{\lambda_{||}G_r}$ and the latitudinal gradient indicator $G_{|z|}$ from 1957 to 1990. These quantities were calculated for cosmic rays with various rigidities from 17 GV to 195 GV; $G_{|z|}$ was calculated while assuming that the ratio of perpendicular to parallel diffusion was 0.01. In Chapter 4 the modulation parameter G_r was calculated for particles with the same rigidities as mentioned above from 1957 to 1990. This parameter was calculated for negligible perpendicular diffusion. Using these results, we are in the position to calculate $\lambda_{||}$ for particles of various rigidities.

Chapter 1 reviewed studies of $\lambda_{||}$ and $\lambda_{\perp}$ determinations and the ratio (α) of these two parameters. Important results of these studies were :

- $\alpha < 0.16$ for particles with rigidities of about 17 GV (Bieber and Chen 1991b, Chen and Bieber 1993);
- $\alpha = 0.09$ for particles with rigidities less than 300 GV (Ahluwalia and Sabbah 1993);
- space probe investigations indicate that $\lambda_{||}$ is less than 0.3 AU for particles with rigidities lower than 4 GV (Palmer 1982);
- at about 17 GV, $\lambda_{||}$ is usually less than 1 AU but it is possibly a factor of two or more higher around times of solar minimum during negative heliospheric magnetic polarity states (Chen and Bieber 1993). This suggests a magnetic polarity dependence of $\lambda_{||}$; and
- $\lambda_{||}$ has been determined to be about 1 AU for 100 GV particles (Yasue 1980).

These results have prompted this study, the main aims of which were to :

- determine $\lambda_{||}$ from 1957 to 1990 and examine any magnetic polarity dependence;
- attempt to determine any limits on α; and
- examine the importance of perpendicular diffusion in the North-South anisotropy.

Section 5.1 describes calculations of $\lambda_{||}$ from the results of the previous two chapters and the results of determining $\lambda_{||}$ are presented in Section 5.2. Section 5.2.1 contains the derivation of $\lambda_{||}$ from the simple quotient of the quantities $\overline{\lambda_{||}G_r}$ and G_r determined previously. Here any polarity dependence of $\lambda_{||}$ is examined by looking at the temporal variation from 1957 to 1990 and averages over years which have distinct magnetic polarity states. Section 5.2.2 contains the results of including perpendicular diffusion in the calculations. This had previously been assumed to be negligible. Here the effect of perpendicular diffusion on the determination of the radial density gradient is also examined.

5.1 Calculating $\lambda_{||}$

Sections 3.4.1 and 3.4.2 contain calculations of $\overline{\lambda_{||}G_r}$ and $G_{|z|}$ at rigidities between 17 GV and 195 GV from 1957 to 1990. These results were obtained from the yearly averaged solar diurnal anisotropy. Section 4.4 contains calculations of G_r from the North-South anisotropy. Obviously it is possible to use the derived quantities to isolate $\lambda_{||}$ from $\overline{\lambda_{||}G_r}$.

In determining G_r it was assumed that $\lambda_{\perp}G_{|z|}$ is negligible compared to the value of $\rho G_r \sin\chi$ (see equation 4.5). As discussed at the end of Chapter 4 this may not always be true. A more accurate method (although perhaps no more significant) of determining G_r (and hence $\lambda_{||}$) would be to include the corresponding values of $G_{|z|}$ in the calculations. These calculations will be performed in Section 5.2.2 and the results will be compared to previous determinations of the modulation parameters, to examine if perpendicular diffusion is important and makes any significant difference.

5.1.1 Approximate method of calculating $\lambda_{||}$

The instruments listed in Table 3.1 have been used to obtain values of $\overline{\lambda_{||}G_r}$ in Chapter 3. Data from many of those instruments were used to calculate G_r in Chapter 4 (see Table 4.1).

In section 5.2.1 these observations will be used to determine $\lambda_{||}$ from

$$\lambda_{||} = \frac{\left(\overline{\lambda_{||}G_r}\right)}{G_r} \tag{5.1}$$

$\lambda_{||}$ is actually an average of the parallel mean-free path on both sides of the neutral sheet. The two quantities in (5.1) are not independent and the relative error of the radial gradient will be more important than $\overline{\lambda_{||}G_r}$ when calculating the error of $\lambda_{||}$. We can examine the inverse of $\lambda_{||}$ for its uncertainty and find that the error in $\lambda_{||}$ is skewed about the value of $\lambda_{||}$. We can calculate the minimum (+) and maximum (-) values of $\lambda_{||}$ ($\lambda_{||}^{\min\max}$), within the 1σ error limits :

$$\lambda_{||}^{\min\max} = \frac{1}{\frac{G_r}{\left(\overline{\lambda_{||}G_r}\right)} \pm \sigma_{\frac{1}{\lambda_{||}}}} \tag{5.2}$$

where

$$\sigma_{\frac{1}{\lambda_{||}}} = \frac{1}{\overline{\lambda_{||}G_r}}\sqrt{\sigma_{G_r}^2 + \left(\frac{G_r}{\left(\overline{\lambda_{||}G_r}\right)}\right)^2 \sigma_{\lambda_{||}G_r}^2} \tag{5.3}$$

$\lambda_{||}$ was determined from equations (5.1) to (5.3) for each year that the instruments listed in Table 3.1 were operating. In determining any yearly average value of $\lambda_{||}$ from the neutron

monitors with median rigidities of 17 GV, all the values of $\overline{\lambda_{\parallel}G_r}$ for a particular year were averaged to produce only one (average) $\overline{\lambda_{\parallel}G_r}$ value (at 17 GV) for each year.

Values of $\lambda_{\parallel}$ were determined from 1957 to 1990 for particles with rigidities of 17, 28, 50, 135, 165, 185, and 195 GV from the results in Sections 3.3.1 and 4.4. These are presented in Section 5.2.1. Average values of $\lambda_{\parallel}$ are then determined for periods of distinct magnetic polarity. When determining averages of $\lambda_{\parallel}$ it is useful to work in the inverse $\lambda_{\parallel}$ space ($\lambda_{\parallel}^{-1}$) where the errors are symmetric around $\lambda_{\parallel}^{-1}$. The results can then be transformed back to $\lambda_{\parallel}$ space. These results are also given in Section 5.2.1 and are used to examine any magnetic polarity dependence of $\lambda_{\parallel}$.

5.1.2 More accurate method of calculating $\lambda_{\parallel}$

Equations (3.14), (3.15) and (4.5) can be rewritten as :

$$\begin{aligned} \xi_y^{T-A} &\equiv \xi_{NS} \\ &= -\rho G_r \sin\chi + \mathrm{sgn}(I)(\alpha\lambda_{\parallel})G_{|z|} \\ \overline{\xi_{\parallel}} &= -\overline{\lambda_{\parallel}G_r}\cos\chi \\ \overline{\xi_{\perp}} &= -\alpha\overline{\lambda_{\parallel}G_r}\sin\chi - \rho\,\mathrm{sgn}(I)G_{|z|} \end{aligned} \tag{5.4}$$

where all quantities have been defined previously and the mean-bars imply an average over towards and away IMF sectors. We have assumed implicitly that :

$$\lambda_{\perp}^{A} \approx \lambda_{\perp}^{T} \equiv \lambda_{\perp}$$
$$\lambda_{\parallel}^{A} \approx \lambda_{\parallel}^{T} \equiv \lambda_{\parallel}$$
$$\rho^{A} \approx \rho^{T} \equiv \rho$$
$$\text{and} \quad \alpha = \frac{\lambda_{\perp}}{\lambda_{\parallel}}$$

By assuming that $\lambda_{\perp} = \dfrac{\alpha\overline{\lambda_{\parallel}G_r}}{G_r}$ and substituting this into the first relation in (5.4) we get

$$\xi_{NS} = -\rho G_r \sin\chi + \mathrm{sgn}(I)\left[\frac{\alpha(\overline{\lambda_{\parallel}G_r})}{G_r}\right]G_{|z|} \tag{5.5}$$

This can be rearranged to give a quadratic equation which can be solved for the magnitude of the radial gradient :

$$G_r = \frac{-\xi_{NS} \pm \sqrt{(\xi_{NS})^2 + 4\rho\sin\chi\,\mathrm{sgn}(I)\alpha(\overline{\lambda_{\parallel}G_r})G_{|z|}}}{2\rho\sin\chi} \tag{5.6}$$

Compared to the relation used by Chen and Bieber (1993), equation (5.6) is exactly the same when one notes that the definition of the North-South anisotropy used in Chapter 4 is such that the anisotropy is negative for streaming from the northern heliospheric hemisphere. This is always true when the towards minus away (IMF) calculation is performed.

Note that all the quantities in (5.6) can be measured or inferred from the solar diurnal anisotropy and the North-South anisotropy so the value of the radial density is only a function of the ratio between perpendicular and parallel diffusion. In Section 5.2.2 all the results in Chapters 3 and 4 are used to evaluate G_r from (5.6) for an assumed value of α. G_r is then back-substituted into the parallel relation of equation (5.1) along with the previously derived value of $\overline{\lambda_{||}G_r}$ to obtain $\lambda_{||}$. In this section the functional dependence of the modulation parameters on α is also examined.

5.2 Results

5.2.1 Approximate results

Figure 5.1 contains average values of $\overline{\lambda_{||}G_r}$ determined in Chapter 3 from 1957 to 1990. The data come from the five neutron monitors listed in Table 3.1 and having median rigidities of 17 GV. Also shown in Figure 5.1 is the G_r of 17 GV particles calculated in Chapter 4. These two quantities are then used to derive $\lambda_{||}$ from equations (5.1) to (5.3). Solid lines are 3-point averages. Although the values have relatively large errors there is a hint that $\lambda_{||}$ is suppressed during the 1970's in agreement with the observations of Bieber and Chen(1991b) and Chen and Bieber (1993).

Figures 5.2 and 5.3 contain the results of calculating $\lambda_{||}$ for particles with rigidities greater than 100 GV. The results are obtained from the determinations of $\overline{\lambda_{||}G_r}$ and G_r from the EMBV and HUV underground muon telescopes (P_{med} = 135 GV and 185 GV, respectively). These higher rigidity calculations also indicate that $\lambda_{||}$ is reduced during the A >0 polarity state.

Determinations of $\lambda_{||}$ from the other instruments listed in Table 3.1 are presented in Appendix 7. They all indicate that $\lambda_{||}$ could have a higher value around times of solar minimum during the A <0 polarity state. Three notable exceptions to this hypothesis are 1984, 1987 and 1990, which always have relatively low values of $\lambda_{||}$ due to the extreme values of G_r calculated for these years.

Table 5.1 contains average values of $\lambda_{||}$ in order of increasing median rigidity of the instruments from which the value was obtained. The averages are over the entire period of data accumulation and epochs of distinct magnetic polarity. In calculating the average values of $\lambda_{||}$ we have worked in the $\lambda_{||}^{-1}$ space and weighted points according to the (symmetric) errors. The final column of Table 5.1 has been assigned to the period 1981 to 1989 (A <0) but excluding 1984 and 1987 since these years have relatively low values and small errors.

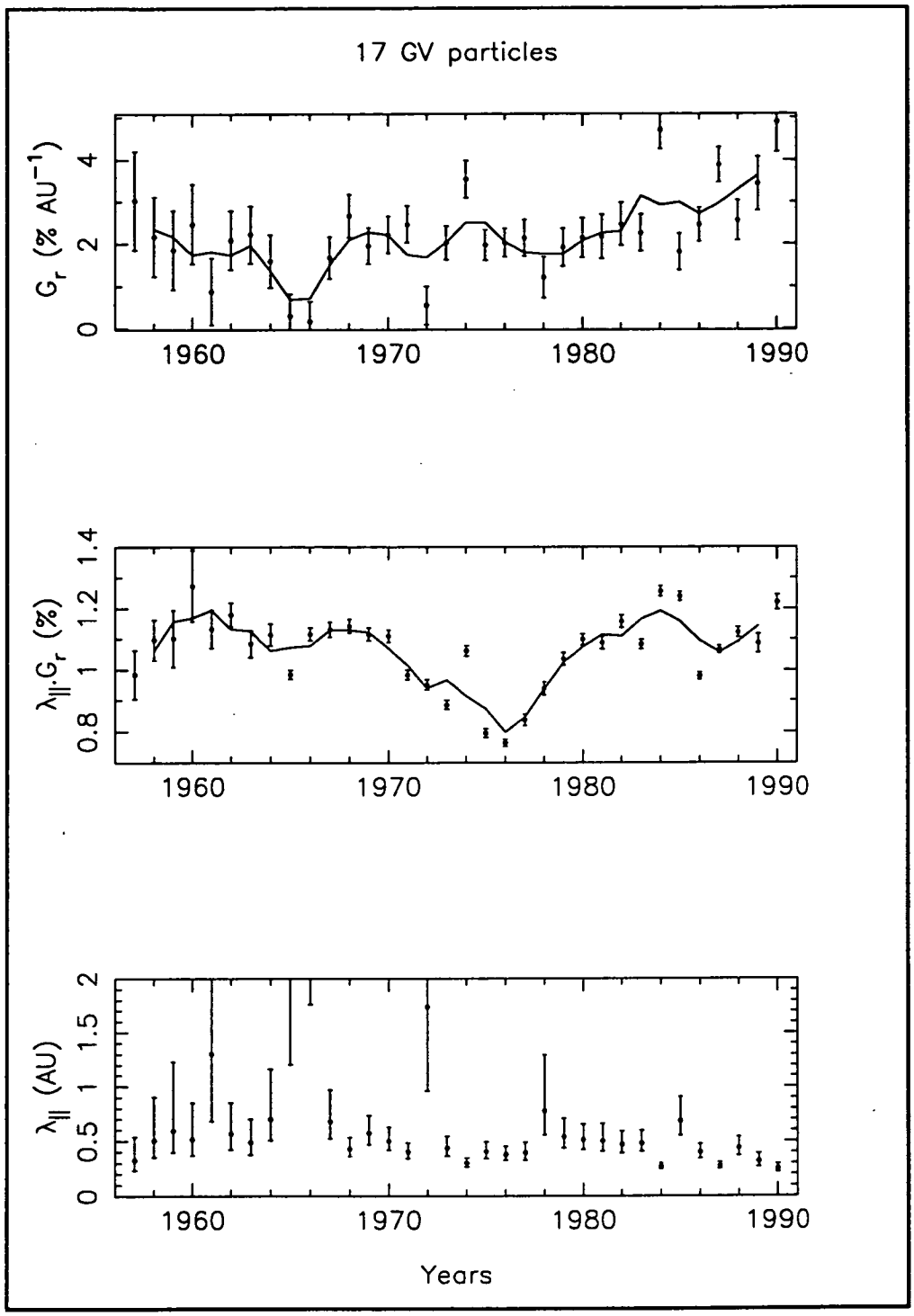

Figure 5.1 The radial gradient (G_r) of 17 GV particles determined from the North-South anisotropy in Chapter 4 from 1957 to 1990 is shown in the upper panel. The average product of the parallel mean-free path and the radial gradient ($\lambda_{||}G_r$) determined from the solar diurnal anisotropy in Chapter 3 recorded by five neutron monitors is shown in the center panel. The solid lines are 3-point moving averages. The bottom panel is the determination of the parallel mean-free path ($\lambda_{||}$) of 17 GV cosmic rays determined from equation (5.1) and the results in the two upper panels. Note that the values of $\lambda_{||}$ for 1965 and 1966 are off the scale at 3 and 5 AU respectively, with errors an order of magnitude larger.

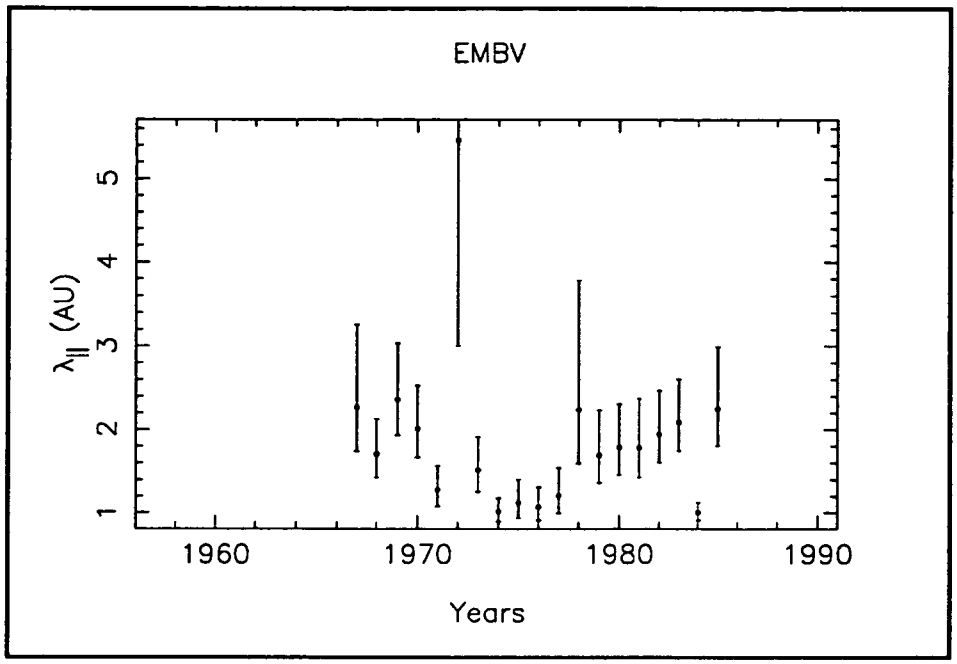

Figure 5.2 Parallel mean-free path ($\lambda_{||}$) of 135 GV particles determined from the Embudo underground muon telescope.

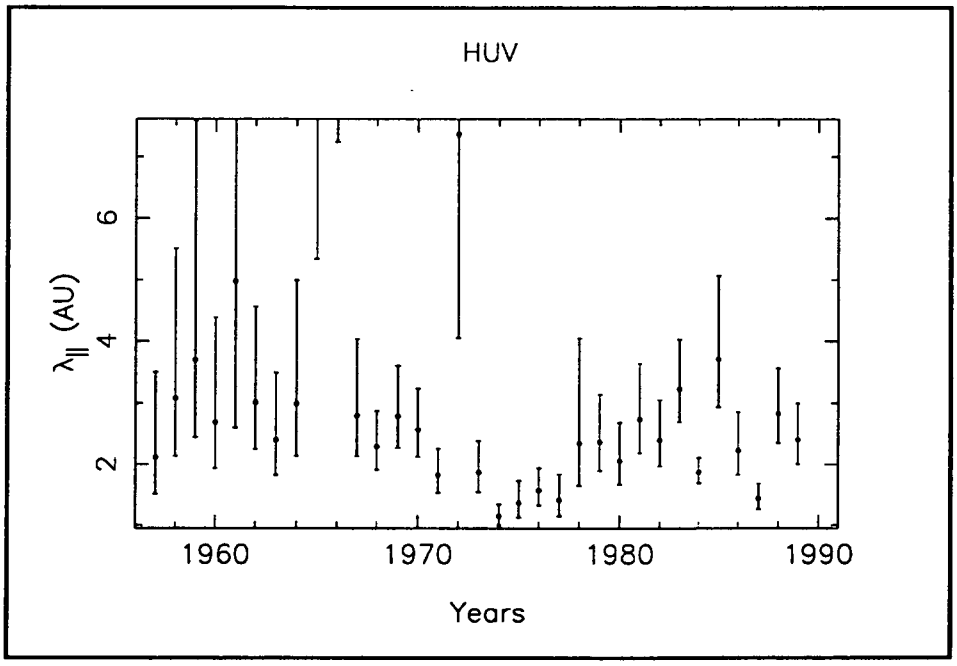

Figure 5.3 Same as Figure 5.2 except $\lambda_{||}$ is determined from the Hobart underground muon telescope from 1957 to 1989. The median rigidity is 185 GV.

These average results suggest not only that $\lambda_{||}$ has a linear relationship with rigidity but that there is also a very strong implication of a polarity dependence. This is a definite result if the column of averages which exclude 1984 and 1987 is considered, but even considering just the complete average values this is a likely phenomenum.

Table 5.1 Average values of the parallel mean-free path $\lambda_{||}$.

Instrument	P_{med} (GV)	$\overline{\lambda_{||}}$ (AU) Average	$\overline{\lambda_{||}}$ (AU) 1959-68	$\overline{\lambda_{||}}$ (AU) 1972-79	$\overline{\lambda_{||}}$ (AU) 1981-89	$\overline{\lambda_{||}}$ (AU) 1981-89#
Neutrons	17	$0.52^{+0.09}_{-0.06}$	$0.77^{+0.12}_{-0.09}$	$0.46^{+0.04}_{-0.03}$	$0.39^{+0.02}_{-0.02}$	$0.47^{+0.04}_{-0.03}$
BNM	28	$0.77^{+0.04}_{-0.03}$	$1.05^{+0.15}_{-0.12}$	-	$0.64^{+0.04}_{-0.03}$	$0.77^{+0.06}_{-0.06}$
DNM, MSV	50	-	$1.54^{+0.24}_{-0.18}$	-	$0.72^{+0.04}_{-0.04}$	$0.86^{+0.07}_{-0.06}$
EMBV	135	$1.75^{+0.09}_{-0.08}$	$2.71^{+0.65}_{-0.44}$	$1.45^{+0.13}_{-0.11}$	$1.67^{+0.15}_{-0.13}$	$2.03^{+0.26}_{-0.20}$
MUN	165	$1.76^{+0.08}_{-0.07}$	-	$1.58^{+0.14}_{-0.12}$	$1.88^{+0.11}_{-0.10}$	$2.22^{+0.19}_{-0.16}$
HUV	185	$2.48^{+0.11}_{-0.10}$	$3.48^{+0.53}_{-0.41}$	$1.90^{+0.18}_{-0.15}$	$2.44^{+0.16}_{-0.14}$	$2.82^{+0.26}_{-0.22}$
HUI	195	$2.13^{+0.11}_{-0.10}$	-	$1.67^{+0.17}_{-0.14}$	$2.27^{+0.15}_{-0.13}$	$2.61^{+0.23}_{-0.20}$

1984 and 1987 excluded

The average results over distinct polarity states in Table 5.1 have been presented graphically in Figure 5.4. The solid line is the line of best fit to the points. It is fairly obvious that the relationship between $\lambda_{||}$ and rigidity is different for the $A>0$ and the $A<0$ epochs. The slopes of the best fitted lines are 0.015 ± 0.001 AU $(GV)^{-1}$, 0.008 ± 0.001 AU $(GV)^{-1}$, and 0.011 ± 0.001 AU $(GV)^{-1}$ for the epochs 1959–68, 1972–79 and 1981–89 respectively. For the 1981 to 1989 epoch which excludes 1984 and 1987 from the averages, the line of best fit has the slope 0.012 ± 0.001. The trends of all the $A<0$ polarity state plots are consistent and are different to that of the $A>0$ polarity state plot.

Table 5.1 also suggests that the magnetic polarity dependence of $\lambda_{||}$ becomes stronger at higher rigidities since the average values of $\lambda_{||}$ during the period 1981 to 1989 are significantly larger than during the 1972 to 1979 period for the two highest rigidity instruments HUV and HUI.

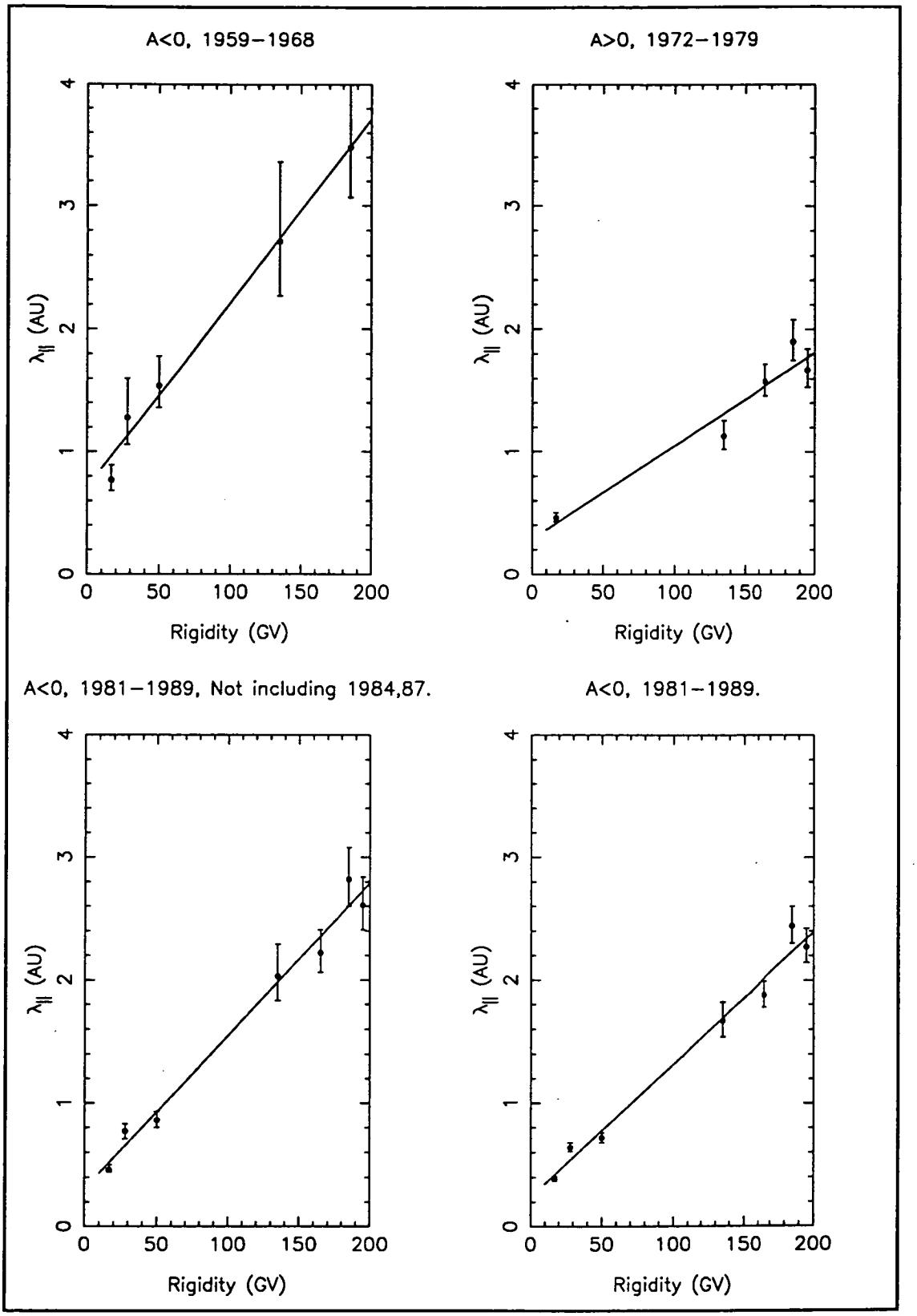

Figure 5.4 Average values of the parallel mean-free path as a function of rigidity. The lines of best-fit have similar slopes for the values calculated for the $A<0$ magnetic polarity states, while the slope of the line for the $A>0$ polarity state is about half the previous values.

These results strongly suggest that $\lambda_{||}$ has a polarity dependence, with lower values being present during years of $A>0$ magnetic polarity. This result is in agreement with neutron monitor studies by Bieber and Chen (1991b) and Chen and Bieber (1993), but observed here at rigidities an order of magnitude higher than before.

5.2.2 Effects of perpendicular diffusion

Equations (5.5) and (5.6) show the complete relation between the North-South anisotropy (ξ_{NS}) and G_r. G_r is reduced (or increased) by the amount $\lambda_{\perp}G_{|z|}$, the values of which can be obtained by using observations of the solar diurnal anisotropy and assuming a value of α. Figures 5.5 and 5.6 show the results of calculating the magnitude of G_r (G_r) and $\lambda_{||}$ for 17 GV and 185 GV particles when including all the calculations made in Sections 3.4.1, 3.4.2 and 4.3.2. Here it has been assumed that the rigidity spectrum of ξ_{NS} is (0.3, 200 GV) and that of ξ_{SD} is (0, 100 GV). It has been assumed that $\alpha = 0.01$. As in the later part of Chapter 3 all five high latitude neutron monitor calculations of the modulation parameters $G_{|z|}$ and $\overline{\lambda_{||}G_r}$ have been averaged to produce one value of each modulation parameter.

The yearly averaged values of G_r for 17 GV and 185 GV particles (from the data recorded by the HUV telescope) are essentially unchanged from the results presented in Chapter 4 (Figures 4.23 and 4.24). The values of G_r around years of solar minimum are affected slightly more than other years, probably because $G_{|z|}$ attains its largest values while ξ_{NS} has its lowest values at these times. The effect of $\lambda_{\perp}G_{|z|}$ in calculating G_r is relatively the largest during these periods. This is consistent with an observation by Chen and Bieber (1993). The values of $\lambda_{||}$ are also affected most by perpendicular diffusion around years of solar minimum.

Figure 5.7 contains the results of calculating G_r and $\lambda_{||}$ for 17 GV particles when $\alpha = 0.11$. Again no significant change is observed in G_r for most years but the influence of perpendicular diffusion on $\lambda_{||}$ during years around solar minimum is quite dramatic. The effect of including α is to significantly change the values of $\lambda_{||}$ around the years of solar minimum, especially the previously off-scale and low significance values for 1965 and 1966. The same effect is noticeable in Figure 5.8 for 185 GV particles. Some years (1960, 1971 and 1978 for the 17 GV plot and 1959, 1966 and 1985 for the 185 GV plot) have unphysical (imaginary) values and indicate that for these years perpendicular diffusion cannot be this high. From most of the instruments' results in Chapters 3 and 4, the yearly averaged values of G_r from 1957 to 1990 calculated for α greater than 0.11 were unacceptable, since in most cases many more years began resulting in unphysical values of G_r. In the following, certain years will be examined for the dependence of their corresponding values of G_r and $\lambda_{||}$ on α.

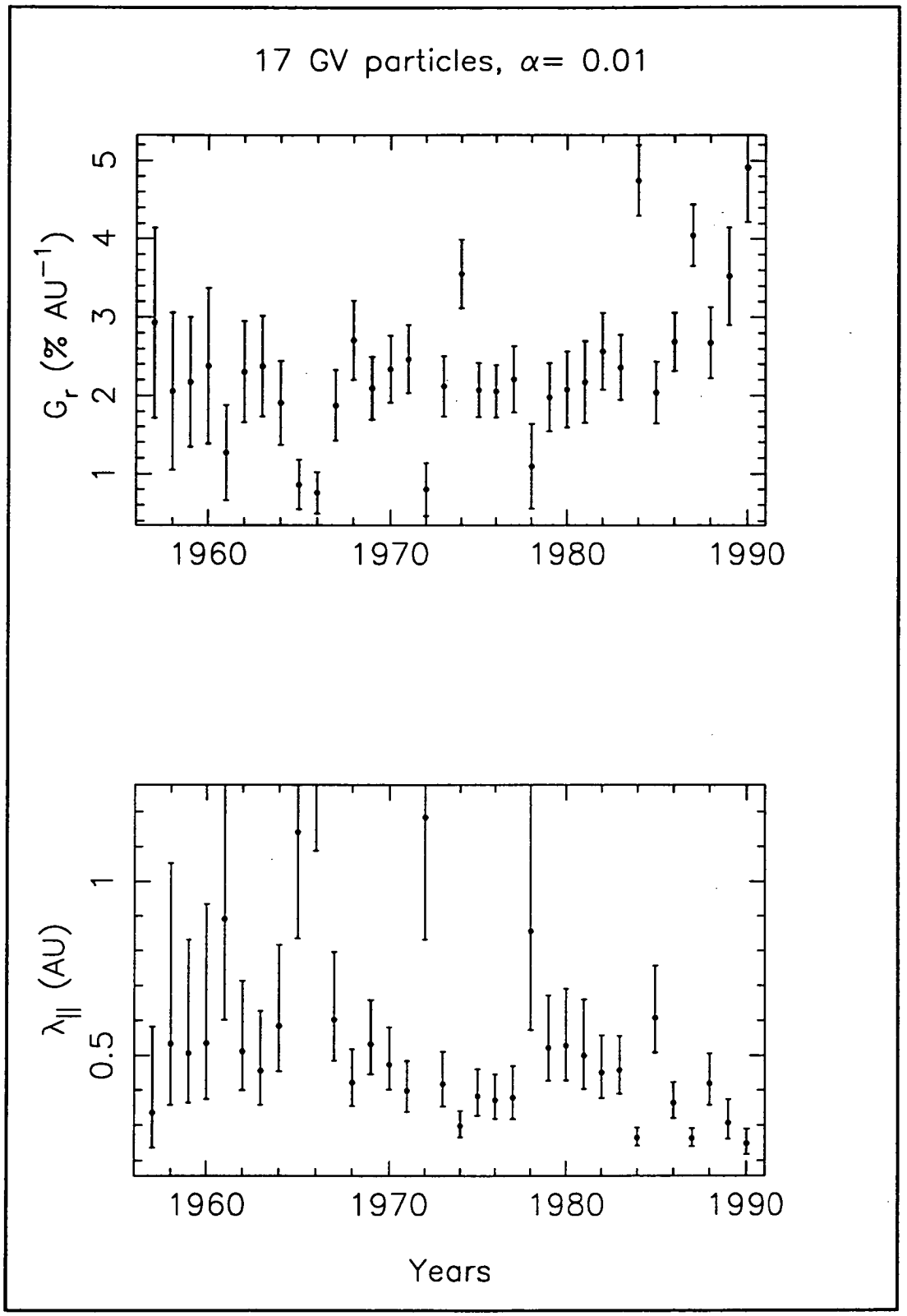

Figure 5.5 Average magnitude of the radial density gradient (G_r) and the parallel mean-free path ($\lambda_{||}$) of 17 GV particles from 1957 to 1990 calculated from the North-South anisotropy and solar diurnal anisotropy observed by 5 high latitude neutron monitors and equation (5.6). The effects of perpendicular diffusion have been included in the calculations (see text) and the ratio of perpendicular to parallel diffusion is assumed to be 0.01.

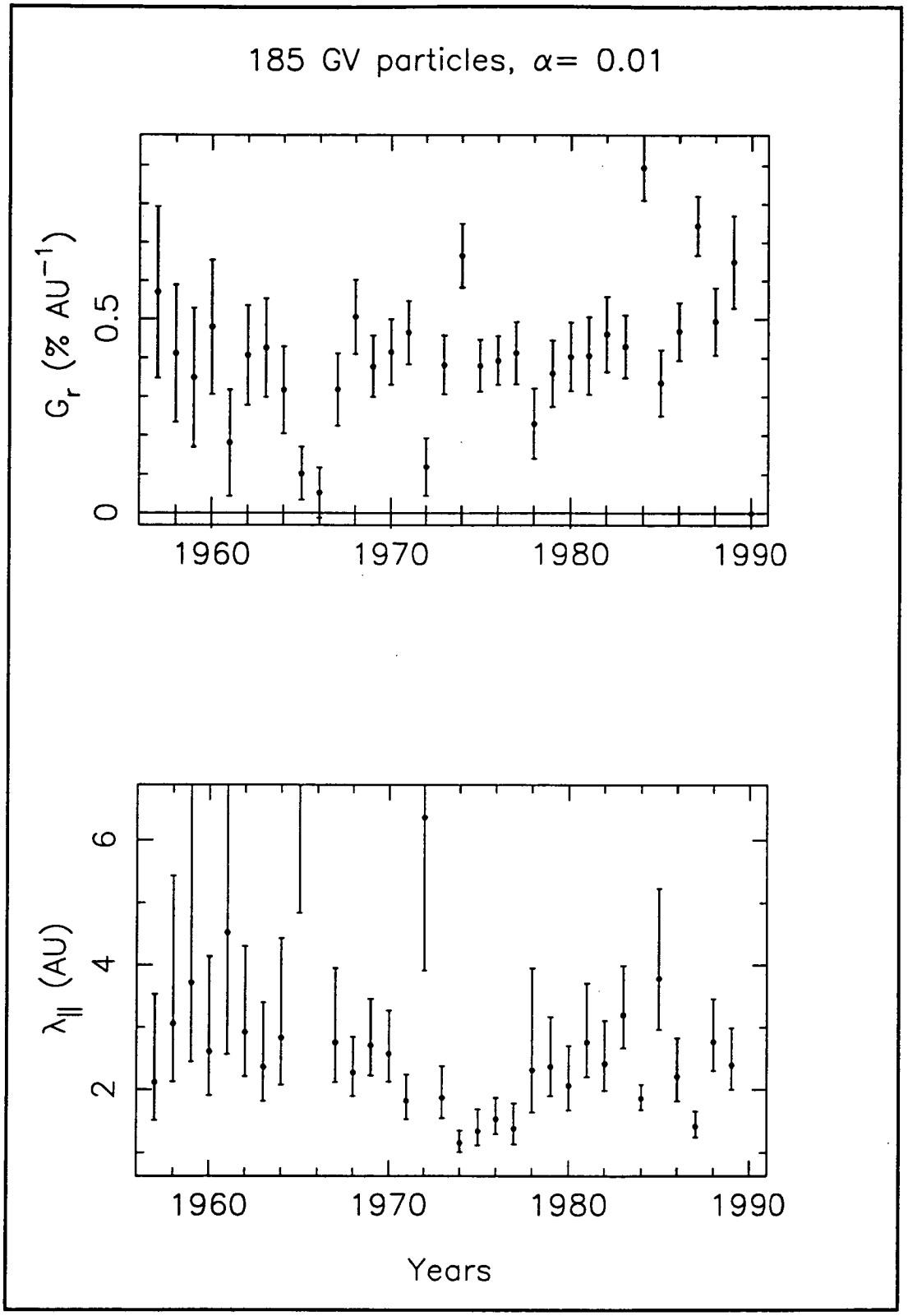

Figure 5.6 Same as Figure 5.5 except the values of G_r were calculated for 185 GV particles from observations by the Hobart underground muon telescope (HUV).

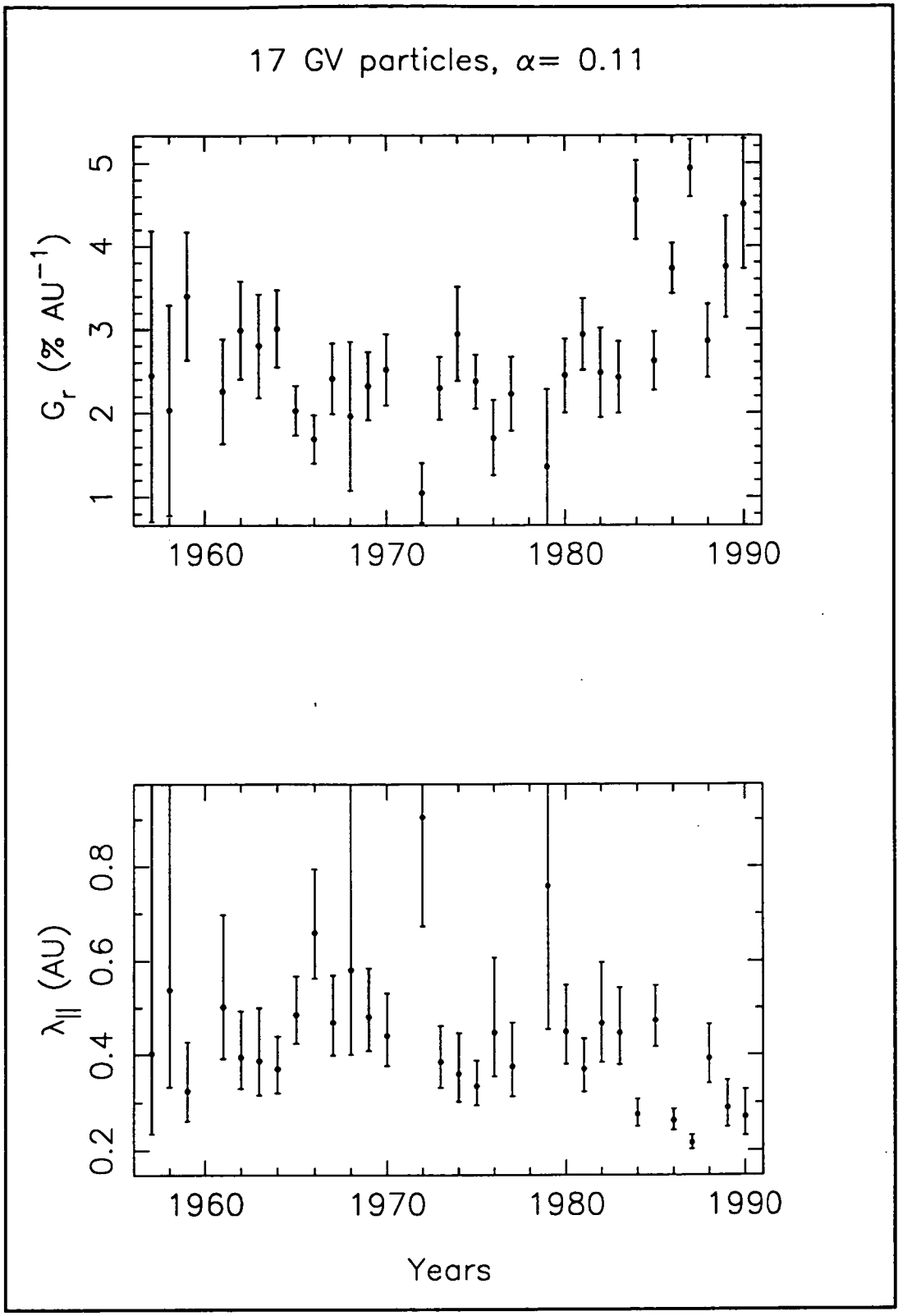

Figure 5.7 Same as Figure 5.5 except the ratio of perpendicular to parallel diffusion (α) is assumed to be 0.11.

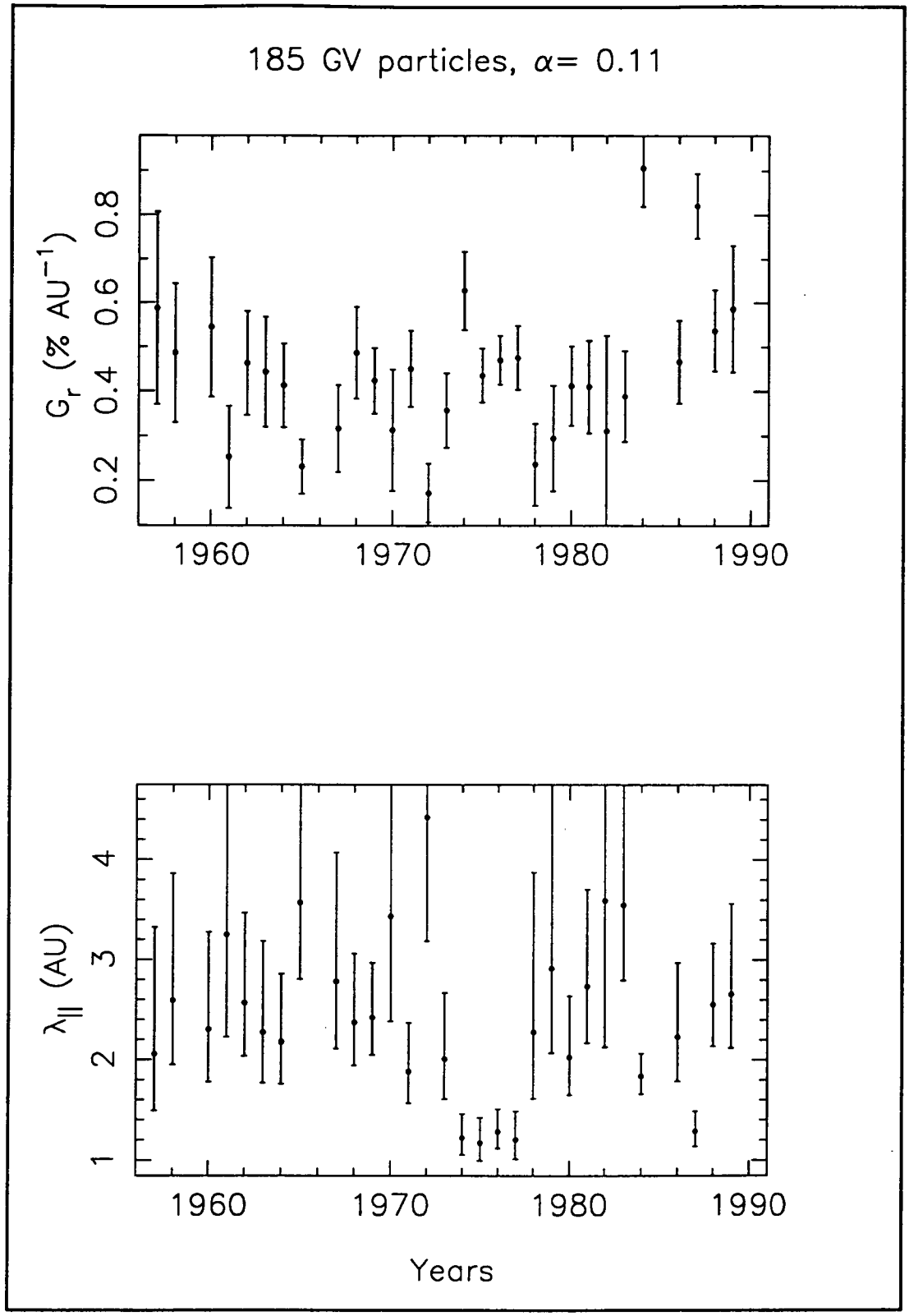

Figure 5.8 Same as Figure 5.6 except the ratio of perpendicular to parallel diffusion (α) is assumed to be 0.11.

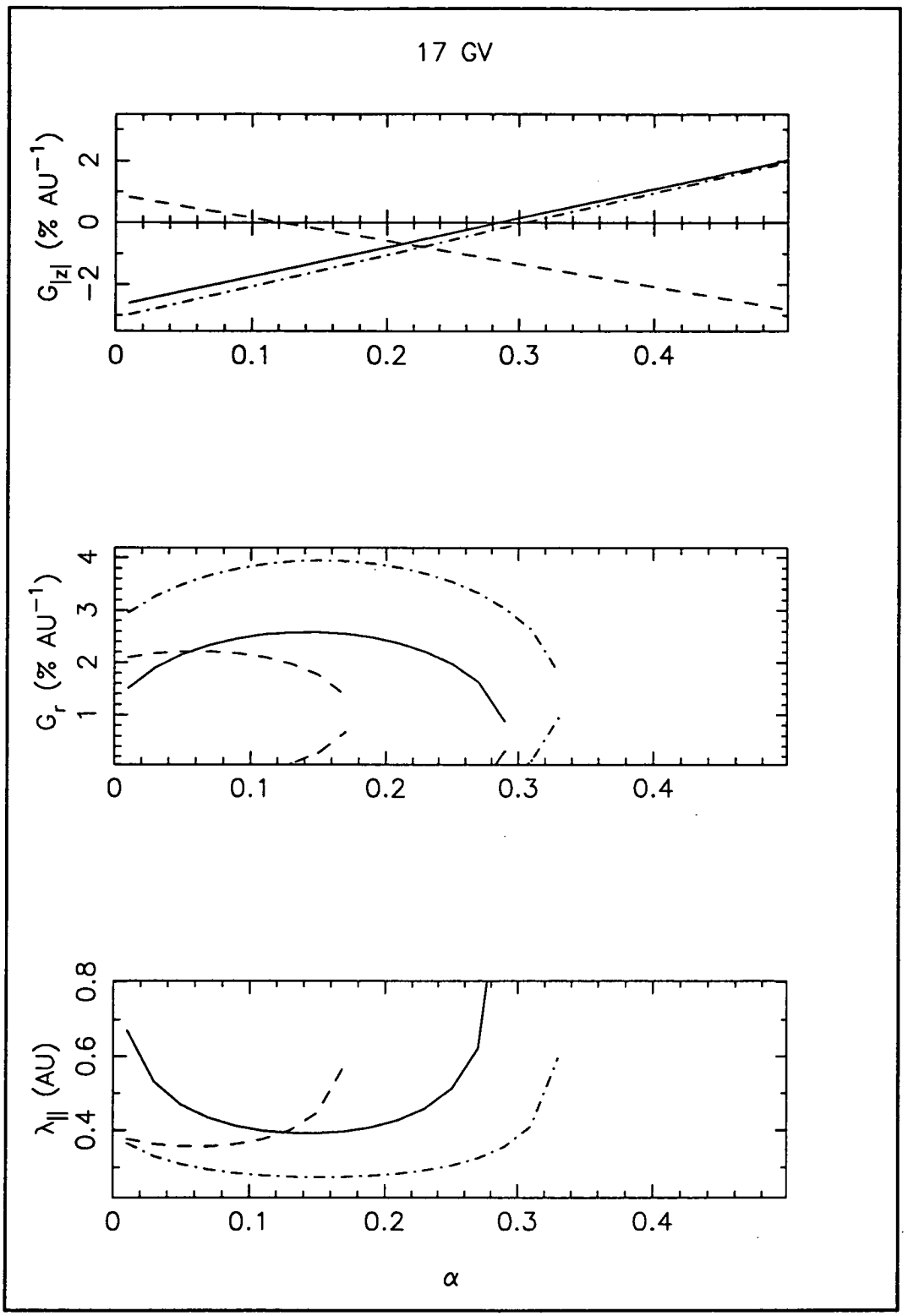

Figure 5.9 Functional dependence of the modulation parameters $G_{|z|}$, G_r and $\lambda_{||}$ on the ratio of perpendicular to parallel diffusion (α) for 17 GV particles. The dashed line represents the average results around the years of solar minimum during the A>0 magnetic polarity epoch, the solid line represents the results for the A<0 magnetic polarity epoch 1964 to 1966 and the dashed-dotted line represents the results averaged over the A<0 magnetic polarity epoch 1985 to 1987.

Note also that the values of $\lambda_{||}$ and G_r are not very sensitive to α except near the observational upper limits of α in all magnetic polarity epochs. The three functional forms of $\lambda_{||}$ (one for each magnetic polarity state of the heliosphere) in Figure 5.9 indicate very little magnetic polarity dependence of $\lambda_{||}$ except when α is very small ($\alpha < 0.03$). This is contrary to expectations from the observations of Section 5.2.1 and may be due to the high value of G_r causing a low $\lambda_{||}$ for 1987 and having considerable influence in the average value of $\lambda_{||}$ for the 1985 to 1987 period.

Figure 5.10 shows results of the same calculations performed on the $G_{|z|}$ and $\overline{\lambda_{||}G_r}$ results obtained from the ξ_{SD} observations by the HUV telescope and the ξ_{NS} results of 185 GV particles. Appendix 8 contains the results of calculating the functional form of $\lambda_{||}$ from the other instruments in Table 3.4. Two interesting characteristics can be observed in these results. First, during the $A<0$ magnetic polarity state most of the instruments indicate that $0.3 \leq \alpha \leq 0.4$ (MUN indicates that $\alpha \leq 0.47$ and DNM has an anomalous result $\alpha \leq 0.7$), i.e. the largest value of α allowable in the heliosphere (at least near the Earth) is between these values and is probably rigidity *independent*. Second, during the solar minimum years of the $A>0$ magnetic polarity state things are entirely different. Table 5.2 shows the observed values of the upper limit to α (α^{max}) at all rigidities for the $A>0$ magnetic polarity state.

Table 5.2 Values of the maximum allowable ratio of perpendicular to parallel diffusion (α^{max}) of cosmic ray particles as a function of rigidity during the $A>0$ magnetic polarity state.

P_{med} (GV)	α^{max}
17	0.17
135	0.75
165	0.59
185	0.85
195	0.91

At all rigidities, α^{max} is larger in the $A>0$ magnetic polarity epoch than in the $A<0$ epochs, except at 17 GV. There also seems to be a rigidity dependence to the observed α^{max} values during the $A>0$ magnetic polarity epoch.

Of course α^{max} is not necessarily the true value of α (in fact it is probably not), but it is surprising that in one polarity state α^{max} is rigidity dependent and in the other it is independent. This could mean that in the $A<0$ magnetic polarity states $\kappa_\perp/\kappa_{||}$ is never greater than 0.3, but in the $A>0$ state the relative amount of perpendicular diffusion becomes greater, especially at higher rigidities.

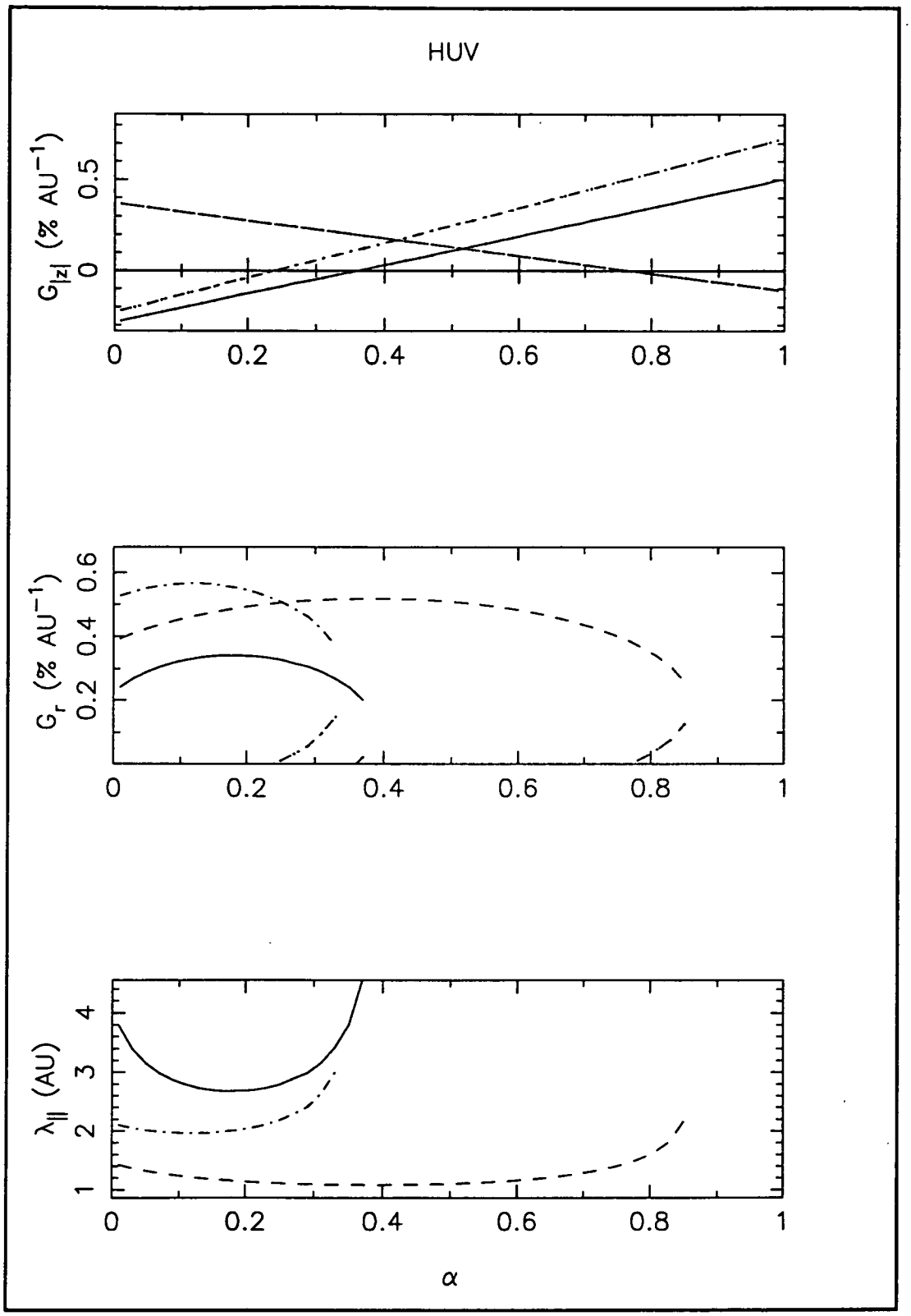

Figure 5.10 Functional dependence of the modulation parameters $G_{|z|}$, G_r and $\lambda_{||}$ on the ratio of perpendicular to parallel diffusion (α) for 185 GV particles. The curves represent the same epochs as in Figure 5.9.

Again the derived values of $\lambda_{||}$ and G_r are not very sensitive to α except near α^{max}, but at most rigidities where there are observations near solar minimum in more than one magnetic polarity state a definite polarity dependence of $\lambda_{||}$ is observed. The values of $\lambda_{||}$ at all rigidities (other than 17 GV particles) are significantly higher during the solar minimum epochs of $A<0$ magnetic polarity than the values of $\lambda_{||}$ during the solar minimum epoch of $A>0$ polarity. This polarity dependence is evidently greater at the highest rigidities studied here. Chen and Bieber (1993) explain this polarity dependence by invoking *magnetic helicity* of the magnetic irregularities which produce scattering of the particles in the heliosphere. It is not in the scope of this thesis (due primarily to time constraints) to discuss the effects of magnetic helicity on galactic cosmic ray particles with rigidities up to 200 GV. The discussion will be left here, with only a note that whatever mechanisms produce the $\lambda_{||}$ dependence on magnetic polarity at 17 GV observed by Chen and Bieber (1993) and here (in Section 5.2.1), could also affect higher rigidity particles in the heliosphere. The mechanism(s) seem to produce a greater dependence on the magnetic polarity at rigidities greater than 100 GV than at rigidities about 17 GV. Chen and Bieber (1993) state that the effects of magnetic helicity are greater on higher rigidity particles.

Summary

By analysing the yearly averaged sidereal and solar diurnal variation in data recorded by neutron monitors and muon telescopes the modulation parameters $\overline{\lambda_{||}G_r}$, $G_{|z|}$ and G_r have been determined. These results were presented in Chapters 3 and 4. By using these results, yearly and longer term average values of the parallel mean-free path $\lambda_{||}$ have been obtained from 1957 to 1990. This modulation parameter has been calculated for rigidities between 17 and 195 GV. From these calculations one may conclude that :

- the modulation parameter $\lambda_{||}$ of cosmic ray particles in the rigidity range 17 to 195 GV is polarity dependent. The value of $\lambda_{||}$ is generally larger during the $A<0$ magnetic polarity state than during the $A>0$ magnetic polarity state;
- the polarity dependence seems to be strongest at the highest rigidities examined;
- there is a linear relationship of $\lambda_{||}$ with rigidity. The value of $\lambda_{||}$ for 17 GV particles is generally less than 1 AU and for 185 GV particles it is generally less than 4 AU. This linear relationship is almost certainly different when the heliosphere is in opposite IMF polarity configurations; and
- around years of solar minimum the observed upper limit of the ratio of perpendicular to parallel diffusion is about 0.3 for all rigidities during the $A<0$ magnetic polarity states. During the $A>0$ polarity state this ratio depends on rigidity. At the highest rigidities studied here, perpendicular diffusion may be as high as 90% of parallel diffusion but does not significantly influence the modulation parameters $\lambda_{||}$ and G_r except around times of solar minimum.

CONCLUSION

The Sun's IMF and solar wind modulates the distribution of high energy galactic cosmic rays in the heliosphere. The modulation processes are characterised by diffusion, convection and drift velocities and produce streaming of particles in the heliosphere which manifests as anisotropic fluxes of particles. The solar diurnal anisotropy and the North-South anisotropy from 1957 to 1990 have been investigated in this thesis in an attempt to dispel some of the confusion surrounding their characteristics and to use these anisotropies as a tool for determining some of the important parameters pertaining to modulation theories. The rigidity spectra of the anisotropies have been derived; long term average spectra to investigate any magnetic polarity dependencies and the individual yearly spectra to study any shorter term temporal variations. The amplitudes and phases of the anisotropies were investigated over the same epochs. The modulation parameters - radial density gradient (G_r), bi-directional latitudinal gradient ($G_{|z|}$), the product of the parallel mean-free path and radial gradient ($\overline{\lambda_{||} G_r}$) and the parallel mean-free path ($\lambda_{||}$) have all been examined for temporal variations related to solar polarity reversals and any rigidity dependencies.

The rigidity spectrum of the solar diurnal anisotropy was determined in Chapter 3 to be essentially flat and to extend up to 100 GV on average. It is possible that this spectrum is dependent on the orientation of the Sun's magnetic dipole. This needs to be investigated in the future. The upper limiting rigidity to the solar diurnal anisotropy was found to have a correlation with the magnitude of the IMF. The form of the rigidity spectrum used in the analyses is adequate but future research should consider removing the abrupt cutoff from the formalism and including a more realistic steepening of the rigidity spectrum. This could alleviate the obvious paradox with the solar diurnal anisotropy existing in data obtained from particles with rigidities a factor of two or more higher than the derived formal upper limit. It may also allow a more accurate determination of modulation parameters in the heliosphere. The amplitude of the solar diurnal anisotropy has a variation related to solar activity and the phase is rigidity dependent and has a 22-year variation.

G_r at the Earth's orbit was shown to be about 2% AU^{-1} on average for 17 GV particles and about 0.4% AU^{-1} on average for 185 GV particles. These values are in reasonable agreement with previous determinations at similar rigidities (Kudo and Wada 1977, Yasue 1980, Bieber and Pomerantz 1986). The temporal variation was very small and not dependent on the magnetic polarity of the heliosphere. $\overline{\lambda_{||} G_r}$ is a parameter dependent on the magnetic polarity but interestingly, only has a rigidity dependence during the $A>0$ magnetic polarity state.

The determinations of the modulation parameters from the experimental results and theoretical description of the yearly averaged anisotropies suggest that the recent modulation models provide a good description of the long term modulation processes in the heliosphere. The results indicate that the latitudinal gradient has a component which is symmetric about the neutral sheet and that this component is dependent on the magnetic polarity of the Sun. The radial density gradient is not very sensitive to the magnetic polarity. Both of these results are predicted for particles with rigidities less than 10 GV by the latest theoretical models. The results here suggest that the same predictions are valid for cosmic rays with

rigidities an order of magnitude higher. It would be interesting to see the results of numerical models applied to particles with these higher rigidities.

The results have been obtained from data encompassing an epoch of 34 years; some of the instruments which recorded the data have been operating from 1957. It is fair to say that more modern instruments now have larger surface areas of collection and better counting capabilities. Some examples include the Hobart underground muon telescope which has been completely renovated during the past two years and has had its surface area increased by a factor of four. Since December 1994 the instrument has been completely fitted out with proportional counters, replacing the Geiger tubes which had been in operation since 1957. This instrument has been on-line since the beginning of 1995. The Mawson cosmic ray observatory has had continuous operation of a large surface area (proportional counter) surface muon telescope with multi-directional viewing capabilities since 1986. It would be advantageous to include the data collected by these instruments in the analyses of this thesis to improve the statistical reliability of the results. This would also be possible for the older data from the Deep River neutron monitor (1958 to 1964) which have only recently become available to the University of Tasmania and was included in Section 3.3.2. These data would be especially advantageous to the determination of the rigidity spectrum of the North-South anisotropy, since the rigidity spectrum derived in Chapter 4 was not statistically significant.

Further evidence that the Sun significantly modulates particles with rigidities much greater than usually modelled was obtained from the examination of the derived phase of the North-South anisotropy. The results were shown to be contaminated by a galactic anisotropy modulated asymmetrically with respect to above and below the neutral sheet. This effect had previously been predicted to exist (Nagashima et al. 1982). The results suggest that this effect exists in the rigidity range 17 to 200 GV and may extend up to 1400 GV. Again, more data could be included in the analysis to confirm these observations.

Finally, parallel and perpendicular diffusion were investigated for their effects on solar modulation. The $\lambda_{||}$ of cosmic rays near the Earth with rigidities up to 200 GV were determined to be magnetic polarity dependent in agreement with a study of $\lambda_{||}$ at 17 GV (Bieber and Chen 1991b, Chen and Bieber 1993). $\lambda_{||}$ has an average value of about 0.52 AU for 17 GV cosmic rays and an average value of 2.48 AU for 185 GV particles. The value determined for 17 GV cosmic rays is reasonably consistent with the average value determined by Chen and Bieber (1993). Around years of solar minimum during the $A<0$ magnetic polarity states the value of $\lambda_{||}$ appears to increase by about a factor of two or more at all rigidities. The effects of magnetic helicity on particles with such enormous rigidities are not known, but this study indicates that it would be extremely desirable to investigate this. A linear relationship between $\lambda_{||}$ and rigidity was also found to exist.

The most important extension to this work would be similar studies of data collected during the $A>0$ magnetic polarity state from 1991 to the present and future data collected up to the end of the magnetic cycle. Results from these data could then be compared with the results determined for the 1972 to 1979 epoch.

The analyses presented here indicate that the solar modulation of high energy cosmic rays remains significant at energies once considered to define the end of solar modulation.

REFERENCES

Ahluwalia, H. S., The regimes of the east-west and the radial anisotropies of cosmic rays in the heliosphere, *Planet. Space Sci, 36, 12,* 1451–1459, 1988a.

Ahluwalia, H. S., Is there a twenty year wave in the diurnal anisotropy of cosmic rays?, *Geophys. Res. Lett., 15, 4,* 287–290, 1988b.

Ahluwalia, H. S., The limiting primary rigidity for the cosmic ray diurnal anisotropy and the IMF, *Proc. Int. Conf. Cosmic Ray 22nd, 3,* 469–473, 1991.

Ahluwalia, H. S., Hale cycle effects in cosmic ray east-west anisotropy and interplanetary magnetic field, *J. Geophys. Res., 98,* 11513 – 11519, 1993.

Ahluwalia, H. S. and J. H. Ericksen, Solar diurnal variation of cosmic-ray intensity underground during solar activity cycle-20, *Proc. Int. Conf. Cosmic Ray 11th, 2,* 139–146, 1969.

Ahluwalia, H. S. and J. F. Riker, Secular changes in the upper cut-off rigidity of the solar diurnal anisotropy of cosmic rays, *Planet. Space Sci., 35,* 39–43, 1987.

Ahluwalia, H. S. and I. S. Sabbah, Cosmic ray diurnal anisotropy for a solar magnetic cycle, *Planet. Space Sci., 41,* 113–125, 1993.

Alania, M. V., R. G. Aslamazashvili, T. V. Djapiashvili and V. S. Tkemaladze, The effect of the particle drift in cosmic ray anisotropy, *Proc. Int. Conf. Cosmic Ray 18th, 10,* 19–94, 1983.

Antonucci, E., M. R. Attolini, S. Cecchini and M. Galli, On the heliolatitude distribution of galactic cosmic rays, *J. Geophys. Res., 90,* 7623–7627, 1985.

Baker, C. P., *Coupling coefficients for muon telescopes*, Honours thesis, Univ. of Tasmania, Tasmania, Australia, 1988.

Baker, C. P., Private communication, 1992.

Baker, C. P., *Cosmic ray modulation in the heliosphere*, Ph.D. thesis, Univ. of Tasmania, Tasmania, Australia, 1993.

Baker, C. P., J. E. Humble and M. L. Duldig, Effect of the magnetic field model on cosmic ray coupling coefficient calculations, *J. Geomag. Geoelectr., 42,* 1137–1144, 1990.

Baker, C. P., D. L. Hall, M. L. Duldig and J. E. Humble, North-South anisotropy and the radial gradient of cosmic-rays at 1 AU: 1982–1985, *Proc. Int. Conf. Cosmic Ray 23rd, 3,* 675–679, 1993a.

Baker, C.P., D. L. Hall, M. L. Duldig and J. E. Humble, Atmospheric correction analysis for the Mawson muon telescopes *Proc. Int. Conf. Cosmic Ray 23rd, 3*, 753–756, 1993b.

Bennett, R. D., J. C. Stearns and A. H. Compton, Diurnal variation of cosmic rays, *Physical Rev., 41*, 119–126, 1932.

Bercovitch, M., The response of the cosmic ray sidereal diurnal variation to reversal of solar magnetic field, in *Proceedings of International Symposium on Cosmic Ray Modulation in the Heliosphere*, pp. 329–336,. Iwate Univ., Morioka, Japan, 1984.

Bieber, J. W. and M. A. Pomerantz, Solar cycle variation of cosmic ray North-South anisotropy and radial gradient, *Astrophys. J., 303*, 843–848, 1986.

Bieber, J. W. and J. Chen, Cosmic ray diurnal anisotropy, 1936–1988: Implications for drift and modulation theories, *Astrophys. J., 372*, 301–313, 1991a.

Bieber, J. W. and J. Chen, Solar magnetic cycle variation of cosmic ray gradients and scattering mean free path, *Proc. Int. Conf. Cosmic Ray 22nd, 3*, 525–528, 1991b.

Chen, J., J. W. Bieber and M. A. Pomerantz, Cosmic ray uni-directional latitude gradient: Evidence for north-south asymmetric solar modulation, *J. Geophys. Res., 96*, 11,569–11,585, 1991.

Chen, J. and J. W. Bieber, Cosmic-ray anisotropies and gradients in three dimensions, *Astrophys. J., 405*, 375–389, 1993.

Christon, S. P., A. C. Cummings, E. C. Stone, K. W. Behannon, L. F. Burlaga, J. R. Jokipii and J. Kota, Differential measurement and model calculations of cosmic ray latitudinal gradient with respect to the heliospheric current sheet, *J. Geophys. Res, 91*, 2867–2877, 1986.

Coffey, H. E., Solar-Geophysical Data prompt reports, *Rep. 589(1)*. Natl. Geophys. Data Cent., Boulder, Colo., 1993.

Compton, A. H. and I. A. Getting, An apparent effect of galactic rotation on the intensity of cosmic rays, *Phys. Rev., 47*, 817–821, 1935.

Couzens, D. A. and J. H. King, Interplanetary medium data book, *suppl. 3A*, 1977–1985, Natl. Space Sci. Data Cent., NASA Goddard Space Flight Cent., Greenbelt, Md., 1986.

Cummings, A. C., E. C. Stone and W. R. Webber, Latitudinal and radial gradients of anomalous and galactic cosmic rays in the outer heliosphere, *Geophys. Res. Lett., 14(3)*, 174–177, 1987 .

Cutler, D. J., H. E. Bergeson, J. F. Davis and D. E. Groom, Measurement of the cosmic-ray sidereal anisotropy near 1500 GV, *Astrophys. J., 248*, 1166–1178, 1981.

Cutler, D. J. and D. E. Groom, Mayflower mine 1500 GV detector: Cosmic ray anisotropy and search for Cygnus X-3, *Astrophys. J., 376*, 322–334, 1991.

Duggal, S. P., M. A. Pomerantz and S. E. Forbush, Long-term variation in the magnitude of the diurnal anisotropy of cosmic rays, *Nature, 214,* 143–155, 1967.

Duggal, S. P., S. E. Forbush and M. A. Pomerantz, Variations of the diurnal anisotropy with periods of one and two solar cycles, *Proc. Int. Conf. Cosmic Ray 11th, 2,* 55–59, 1969.

Duggal, S. P. and M. A. Pomerantz, Long term changes in the solar diurnal anisotropy, *Proc. Int. Conf. Cosmic Ray 14th, 4,* 1209–1213, 1975.

Duggal, S. P. and M. A. Pomerantz, Relationship between sector boundaries and polar nucleonic intensity variations: The heliocentric gradient during solar cycle 20, *Proc. Int. Conf. Cosmic Ray 15th, 3,* 215–220, 1977.

Duldig, M. L., The Mawson automatic cosmic ray observatory (MACRO), *Proc. Int. Conf. Cosmic Ray 21st, 7,* 288 – 291, 1989.

Duldig, M. L., Underground observations of the sidereal diurnal variation at Mawson, *Proc. Int. Conf. Cosmic Ray 22nd, 3,* 422–425, 1991.

Duperier, A., The meson intensity at the surface of the earth and the temperature at the production level, *Proc. Phys. Soc., LXII, II,* 684–696, 1949.

Elliot, H. and D. W. N. Dolbear, Directional measurements of the diurnal variation of cosmic ray intensity, *J. Atmos. Terr. Phys., 1,* 205 – 214, 1951.

Erdös, G. and J. Kota, The spectrum of daily variations between 50 and 200 GV, *Proc. Int. Conf. Cosmic Ray 16th, 4,* 45–50, 1979.

Fenton, A. G., R. M. Jacklyn and R. B. Taylor, Cosmic ray observations at 42 m.w.e. underground at Hobart, *Nuovo Cimento, XXII(2),* 3985 – 3996, 1961.

Forbush, S. E., A variation, with a period of two solar cycles, in the cosmic-ray diurnal anisotropy, *J. Geophys.. Res, 72,19,* 4937–4939, 1967.

Forman, M. A., The Compton-Getting effect for cosmic-ray particles and photons and the Lorentz-invariance of distribution functions, *Planet. Space Sci., 18,* 25–31, 1970.

Forman, M. A. and L. J. Gleeson, Cosmic ray streaming and anisotropies, *Astrophys. Space Sci., 32,* 77–94, 1975.

Fujimoto, K., A. Inoue, K. Murakami and K. Nagashima, Coupling coefficients of cosmic ray daily variations for meson telescopes, *Rep. 9,* Cosmic Ray Res. Lab., Nagoya, Japan, 1984.

Gleeson, L. J., The equations describing the cosmic-ray gas in the interplanetary region, *Planet. Space Sci., 17,* 31–47, 1969.

Gussenhoven, M. S., Private communication, 1993.

Gussenhoven, M. S. and D. Madden, Monitoring the polar rain over a solar cycle: a polar rain index, *J. Geophys. Res.*, *95*, A7, 10399–10416, 1990.

Hall, D. L., M. L. Duldig and J. E. Humble, Speculation on the magnetic polarity dependence of the upper cutoff rigidity to the solar diurnal anisotropy, *Proc. Int. Conf. Cosmic Ray 23rd, 3*, 660-662, 1993.

Hall, D. L., J. E. Humble and M. L. Duldig, Modulation of high energy cosmic-rays in the heliosphere. *J. Geophys. Res.*, *99* (11), 1443-1457, 1994.

Hashim, A. and M. Bercovitch, A cosmic ray density gradient perpendicular to the ecliptic plane, *Planet. Space Sci., 20,* 791–801, 1972.

Hatton, C. J., *Progress in elementary particles and cosmic ray physics, 20*, North Holland publishing company, pp. 1-100, 1971.

Humble, J. E., *Diurnal and transient cosmic ray variations*. Ph.D. Thesis, University of Tasmania, 1971.

Isenberg, P. A. and J. R. Jokipii, Effects of particle drift on cosmic ray transport. II. Analytical solution to the modulation problem with no latitudinal diffusion, *Astrophys. J., 219,* 74–749, 1978.

Isenberg, P. A. and J. R. Jokipii, Gradient and curvature drifts in magnetic fields with arbitrary spatial variation, *Astrophys. J., 234*, 746–752, 1979.

Ip, W.-H., W. Fillius, A. Mogro-Campero, L. J. Gleeson and W. I. Axford, Quiet time interplanetary cosmic ray anisotropies observed from Pioneer 10 and 11, *J. Geophys. Res., 83 (A4)*, 1633-1640, 1978.

Jacklyn, R. M., Evidence for a two-way sidereal anisotropy in the charged primary cosmic radiation, *Nature, 211,* 690–693, 1966.

Jacklyn, R.M., Studies of the sidereal daily variation of cosmic ray intensity with particlular reference to observations at 40 m.w.e. underground. *ANARE Scientific Reports. Series C(II), publication No.114, Australian Antarctic Division*, 1970.

Jacklyn, R. M. and J. E. Humble, The upper limiting primary rigidity of the cosmic ray solar anisotropy, *Aust. J. Phys., 18,* 451–471, 1965.

Jacklyn, R. M., S. P. Duggal and M. A. Pomerantz, The spectrum of the cosmic ray solar diurnal modulation, *Proc. Int. Conf. Cosmic Ray 11th, 2,* 47–54, 1969.

Jacklyn, R. M. and M. L. Duldig, The determination of the accidental rate in the output of a 2-tray gas counter telescope, *Proc. Int. Conf. Cosmic Ray 20th , 4*, 380–383, 1987.

Jokipii, J. R., The effects of heliospheric magnetic structure on the modulation of galactic cosmic rays, in *Proceedings of International Symposium on Cosmic Ray Modulation in the Heliosphere,* pp. 27–38, Iwate Univ., Morioka, Japan, 1984.

Jokipii, J. R., The physics of cosmic-ray modulation, *Adv. Space Res., 9(12),* 105–119, 1989.

Jokipii, J. R. and D. A. Kopriva, Effects of particle drift on the transport of cosmic rays. III., Numerical models of galactic cosmic-ray modulation, *Astrophys. J., 234,* 384–392, 1979.

Jokipii, J. R. and J. M. Davila, Effects of particle drift on the transport of cosmic rays. V. More realistic diffusion coefficients, *Astrophys. J., 248,* 1156–1161, 1981.

Jokipii, J. R. and B. Thomas, Effects of drift on the transport of cosmic rays. IV. Modulation by a wavy interplanetary current sheet, *Astrophys. J., 243,* 1115–1122, 1981.

Jokipii, J. R. and J. Kota, The polar heliospheric magnetic field, *Geophys. Res. Lett., 16,* 1–4, 1989.

Jokipii, J. R., E. H. Levy and W. B. Hubbard, Effects of particle drift on cosmic ray transport. I. General properties, application to solar modulation, *Astrophys. J., 213,* 861–868, 1977.

King, J. H., Interplanetary medium data book, *suppl. 4,* 1985–1988, Natl. Space Sci. Data Cent., NASA Goddard Space Flight Cent., Greenbelt, Md., 1989.

Kota, J., Drift – The essential process in losing energy, *Proc. Int. Conf. Cosmic Ray 16th, 3,* 13–18, 1979.

Kota, J. and J. R. Jokipii, Effects of drift on the transport of cosmic rays. VI. A three-dimensional model including diffusion, *Astrophys. J., 265,* 573–581, 1983.

Kudo, S. and M. Wada, Field dependent north-south anisotropy of cosmic rays in rigidities from 10 GV to 300 GV, *Proc. Int. Conf. Cosmic Ray 15th, 3,* 158–163, 1977.

Levy, E. H., Theory of the solar magnetic cycle wave in the diurnal variation of energetic cosmic Rays: Physical basis of the anisotropy, *J. Geophys. Res., 18, 13,* 2082–2088, 1976.

Lindholm, F., *Gerlands Beitrage zur Geophysik., 22,* 141, 1929.

McDonald, F. B., H. Moraal, J. P. L. Reinecke, N. Lal and R. E. McGuire, The cosmic radiation in the heliosphere at successive solar minima, *J. Geophys. Res, 97,* 1557–1570, 1992.

McKibben, R. B., Reanalysis and confirmation of positive latitude gradients for anomalous helium and galactic cosmic rays measured in 1975–1976 with Pioneer 11, *J. Geophys. Res., 94,* 17021–17033, 1989.

McKibben, R. B., K. R. Pyle and J. A. Simpson, The solar latitude and radial dependence of the anomalous cosmic ray helium component, *J. Geophys. Res., 94,* 17021–17033, 1979.

Moraal, H., Proton modulation near solar minimum periods in consecutive solar cycles, *Proc. Int. Conf. Cosmic Ray 21st, 6,* 140–143, 1990.

Mori, S. and K. Nagashima, Inference of sector polarity of the inter-planetary magnetic field from the cosmic ray north-south asymmetry, *Planet. Space Sci., 27,* 39–46, 1979.

Mori, S., S. Yasue, S. Sagisaka, M. Ichinose, K. Chino, S. Akahane and T. Higuchi, Matsushiro underground cosmic-ray observatory (220 m.w.e. depth) and the observation of high energy ($<10^{12}$ eV) cosmic ray intensity variation, *J. Fac. Sci., Shinshu Univ., 24,* 1–46, 1989.

Mori, S., S. Yasue, M. Munakata, A. A. Darwish and A. A. Bishara, Observation of Earth's orbital motion using cosmic-ray Compton-Getting effect at Matsushiro underground station, *Proc. Int. Conf. Cosmic Ray 22nd (3),* 445–449, 1991.

Nagashima, K., Three-dimensional cosmic ray anisotropy in interplanetary space. Part *I., Rep. Ionos. Res. Jpn., 25(3),* 189–211, 1971.

Nagashima, K. and H. Ueno, Three-dimensional cosmic ray anisotropy in interplanetary space. Part *II., Rep. Ionos. Res. Jpn., 25(3),* 212–241, 1971.

Nagashima, K., I. Morishita and S. Yasue, Modulation of galactic cosmic ray anisotropy in heliomagnetosphere: average sidereal daily variation, *Planet. Space Sci., 30,* 879–896, 1982.

Nagashima, K., R. Tatsuoka and S. Matsuzaki, Spurious sidereal daily variation of cosmic rays produced from stationary anisotropy of solar origin, *Nuovo Cimento Soc. Ital. Fis. C, 6,* 550–565, 1983a.

Nagashima, K., Y. Ishida, S. Mori and I. Morishita, Cosmic ray sidereal diurnal variation of galactic origin observed by neutron monitors, *Planet. Space Sci., 31,* 1269–1278, 1983b.

Nagashima, K., S. Sakakibara, A. G. Fenton and J. E. Humble, The insensitivity of the cosmic ray galactic anisotropy to heliomagnetic polarity reversals, *Planet. Space Sci., 33,* 395–405, 1985.

Nagashima, K., H. Ueno and K. Fujimoto, Heliomagnetic dipole moment and daily variation of cosmic rays underground, *Nature, 328,* 600–601, 1987.

Nagashima, K., K. Fujimoto and R. M. Jacklyn, The excess influx of galactic cosmic rays from the tailend side of the heliomagnetosphere, inferred from their sidereal daily variation, *Mini International Conference on Cosmic Rays Towards the Sun and their Propagation,* Nagoya Uni., Nagoya, Japan, 1994.

Newkirk Jr., G., J. Asbridge, J. A. Lockwood, M. Garcia-Munoz and J. A. Simpson, Variation of cosmic rays and solar wind properties with respect to the heliospheric current sheet. 2. Rigidity dependence of the latitudinal gradient of cosmic rays at 1 AU, *J. Geophys. Res., 91,* 2879–2884, 1986.

Palmer, I. D., Transport coefficients of low energy cosmic rays in interplanetary space, *Revs. Geophys. Space. Phys., 20(2),* 335–351, 1982.

Parker, E. N., Theory of streaming of cosmic rays and the diurnal variation, *Planet. Space Sci., 12,* 735–749, 1964.

Parsons, N. R., *Cosmic ray studies at high southern latitudes with special reference to the daily intensity variation,* Ph.D. thesis, Univ. of Tasmania, Tasmania, Aust., 1959.

Peacock, D. S. and T. Thambyahpillai, Muon solar daily variation at a depth of 60 metres water equivalent, *Nature, 215,* 146–147, 1967.

Peacock, D. S., J. C. Dutt and T. Thambyahpillai, Directional measurements of the cosmic-ray daily variation at a vertical depth of 60 m.w.e. in London, *Canadian J. Phys., 46,* 787–793, 1968.

Potgieter, M. S. and H. Moraal, A drift model for the modulation of galactic cosmic-rays, *Astrophys. J., 294,* 425–440, 1985.

Rao, U. R., K. G. McCracken and D. Venkatesan, Asymptotic cones of acceptance and their use in the study of the daily variation of cosmic radiation, *J. Geophys. Res., 68,* 345–369, 1963.

Sandstrom, A. E., *Cosmic Ray Physics,* North Holland publishing company, 1965.

Svalgaard, L., Interplanetary sector structure 1947–1975., *SUIPR Rep. 648,* Inst. for Plasma Res., Stanford, Calif., 1976.

Swinson, D. B., Sidereal cosmic ray diurnal variations, *J. Geophys. Res., 74,* 5591 – 5598, 1969.

Swinson, D. B., Cosmic ray density gradient perpendicular to the ecliptic plane, *J. Geophys. Res., 75,* 7303–7306, 1970.

Swinson, D. B., Solar modulation origin of 'sidereal' cosmic ray anisotropies, *J. Geophys. Res., 76,* 4217–4223, 1971.

Swinson, D. B., Field dependent cosmic ray streaming at high rigidities, *J. Geophys. Res., 81, 13,* 2075–2081, 1976.

Swinson, D. B., Long term variations of the cosmic ray north-south anisotropy and the radial cosmic ray gradient at high rigidity, *J. Geophys. Res., 93,* 5890–5896, 1988.

Swinson, D. B. and H. Kananen, Reversal of the cosmic ray density gradient perpendicular to the ecliptic plane, *J. Geophys. Res., 87,* 1685–1687, 1982.

Swinson, D. B. and S. I. Yasue, Long-term waves in the cosmic ray North-South anisotropy: II: 1 year and 11 year waves, *Proc. Int. Conf. Cosmic Ray 22nd, (3),* 485–489, 1991.

Swinson, D. B., J. E. Humble, M. A. Shea and D. F. Smart, Solar activity asymmetries and their possible effect on the high energy cosmic ray perpendicular gradient, *Adv. Space Res.*, *9(4)*, 221 – 224, 1986.

Swinson, D. B., V. H. Regener and R. H. St.John, Correlation of cosmic ray diurnal anisotropies with the interplanetary magnetic field over 21 years, *Planet. Space Sci., 38, 11,* 1387–1398, 1990.

Swinson, D. B., J. E. Humble, M. A. Shea and D. F. Smart, Latitudinal cosmic ray gradients: their relation to solar activity asymmetry, *J. Geophys. Res., 96*:1757 – 1765, 1991.

Ueno, H., Z. Fujii, S. Mori, S. Yasue and K. Nagashima, Sidereal diurnal variations observed at Nagoya, Misato and Sakashita stations (NAMS), in *Proceedings of International Symposium on Cosmic Ray Modulation in the Heliosphere,* pp.349–354, Iwate Univ., Morioka, Japan, 1984.

Venkatesan, D. and Badruddin, Cosmic-ray intensity variations in the 3-dimensional heliosphere, *Space Sci. Rev., 52,* 121–194, 1990.

Webber, W. R. and J. A. Lockwood, An observation of a heliospheric magnetic cycle dependence for the integral radial gradient of E>60 MEV cosmic rays, *J. Geophys. Res., 96,* 15899–15905, 1991.

Webber, W. R. and J. A. Lockwood, On the interplanetary cosmic ray latitudinal gradient, *J. Geophys. Res., 97,* 8221–8230, 1992.

Wilcox, J. M., The interplanetary magnetic field. Solar origin and terrestrial effects, *Space Sci. Rev., 8,* 258–328, 1968.

Yasue, S., North-south anisotropy and radial density gradient of galactic cosmic rays, *J. Geomag. Geoelectr., 32,* 617–635, 1980.

Yasue, S., S. Mori, S. Sakakibara and K. Nagashima, Coupling coefficients of cosmic ray daily variations for neutron monitor stations, *Rep. 7,* Cosmic Ray Res. Lab., Nagoya, Japan, 1982.

Yasue, S., S. Mori and S. Sagisaka, Sidereal diurnal variation observed at Matsushiro, in *Proceedings of International Symposium of Cosmic Ray Modulation in the Heliosphere,* pp. 355–359, Iwate Univ., Morioka, Japan, 1984.

APPENDIX 1

SOLAR DIURNAL ANISOTROPY

This appendix proves that the amplitude of the solar diurnal anisotopy can be a function of the relative importance of parallel and perpendicular diffusion. See Chapter 1 for details.

Using Forman and Gleeson's model (1975) the true corotation anisotropy is obtained from assuming that there is no net radial streaming, $\kappa_\perp$ is negligible and drifts are also negligible. From equation (1.2), if we assume that the solar wind speed is 400 km sec^{-1} then

$$\xi = \left(\frac{3CV}{v}\right)\hat{e}_\phi$$
$$= 0.6\%$$

If $\kappa_\perp$ is non-negligible then

$$\xi = \left(\frac{3CV}{v}\right)\frac{(\kappa_\parallel - \kappa_\perp)\sin\chi\cos\chi}{\kappa_\parallel\cos^2\chi + \kappa_\perp\sin^2\chi}\hat{e}_\phi$$

By defining α as the ratio of perpendicular to parallel diffusion (i.e. $\alpha = \kappa_\perp/\kappa_\parallel$), if the angle between the IMF and Earth-Sun line, χ is 45° then

$$\xi = \left(\frac{3CV}{v}\right)\frac{(1-\alpha)0.5\kappa_\parallel}{0.5(\kappa_\parallel + \kappa_\perp)}\hat{e}_\phi$$
$$= \left(\frac{3CV}{v}\right)\frac{(1-\alpha)\kappa_\parallel}{(1+\alpha)\kappa_\parallel}\hat{e}_\phi$$
$$= 0.6\frac{(1-\alpha)}{(1+\alpha)}\hat{e}_\phi$$

When $\alpha = 0.01$, $\xi = 0.58\%$. When $\alpha = 0.1$, $\xi = 0.49\%$.

APPENDIX 2

HARMONIC DIALS IN SOLAR TIME

This appendix contains the results of Fourier analysing the data recorded by the instruments used in Chapter 3 for the first harmonics in solar time. The yearly averaged results are presented as harmonic dial diagrams.

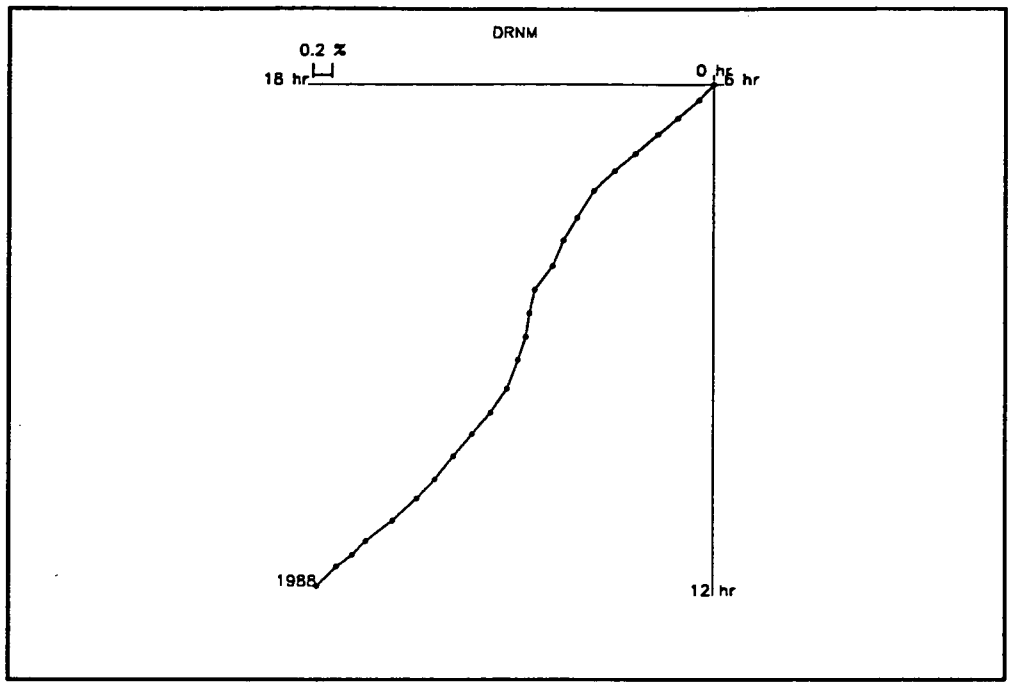

Figure A2.1 Vector sum diagram (harmonic dial) of the yearly averaged solar diurnal variation in Deep River neutron monitor (DRNM) data from 1965 to 1988. The median rigidity of DRNM is 17 GV.

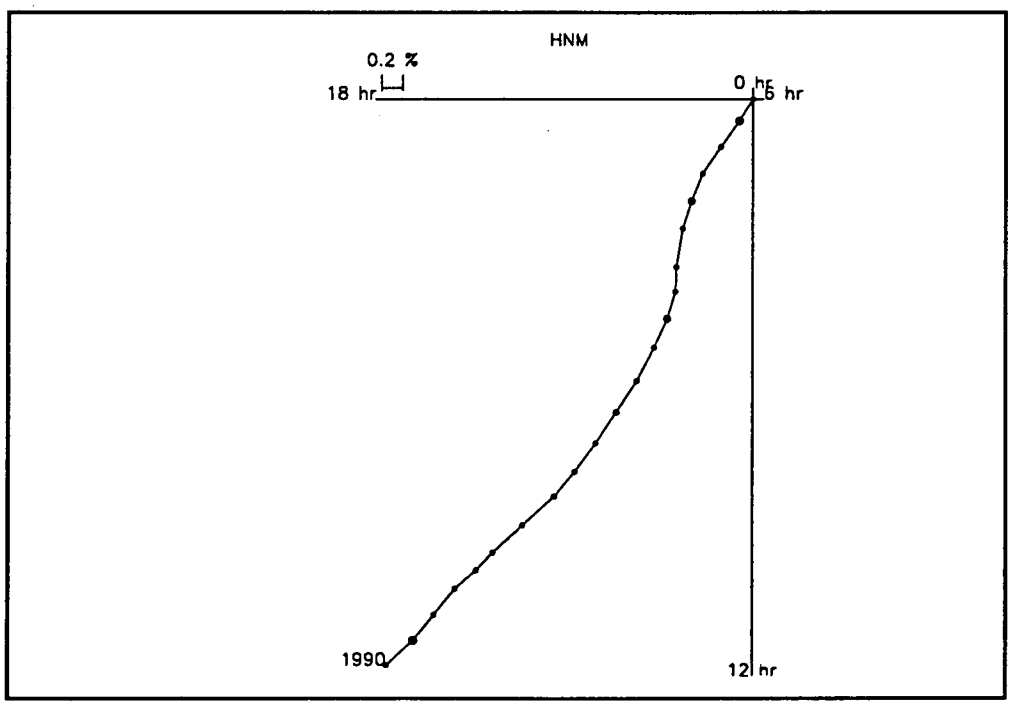

Figure A2.2 Vector sum diagram of the yearly averaged solar diurnal variation in Hobart neutron monitor (HNM) data from 1968 to 1990. The median rigidity of HNM is 17 GV.

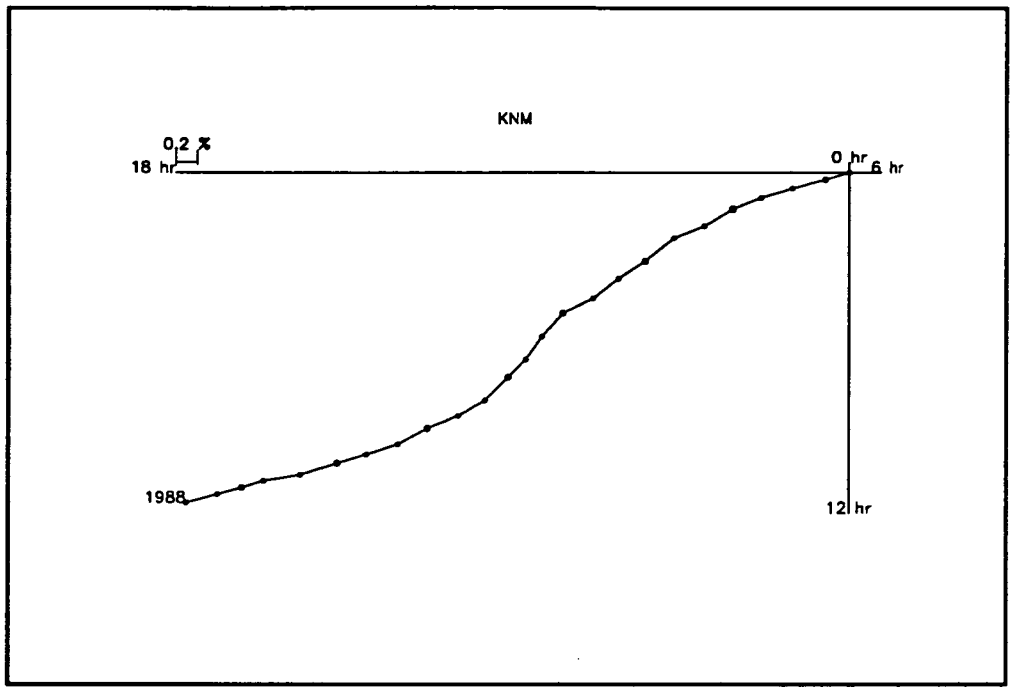

Figure A2.3 Vector sum diagram of the yearly averaged solar diurnal variation in Kerguelen neutron monitor (KNM) data from 1965 to 1988. The median rigidity of KNM is 17 GV.

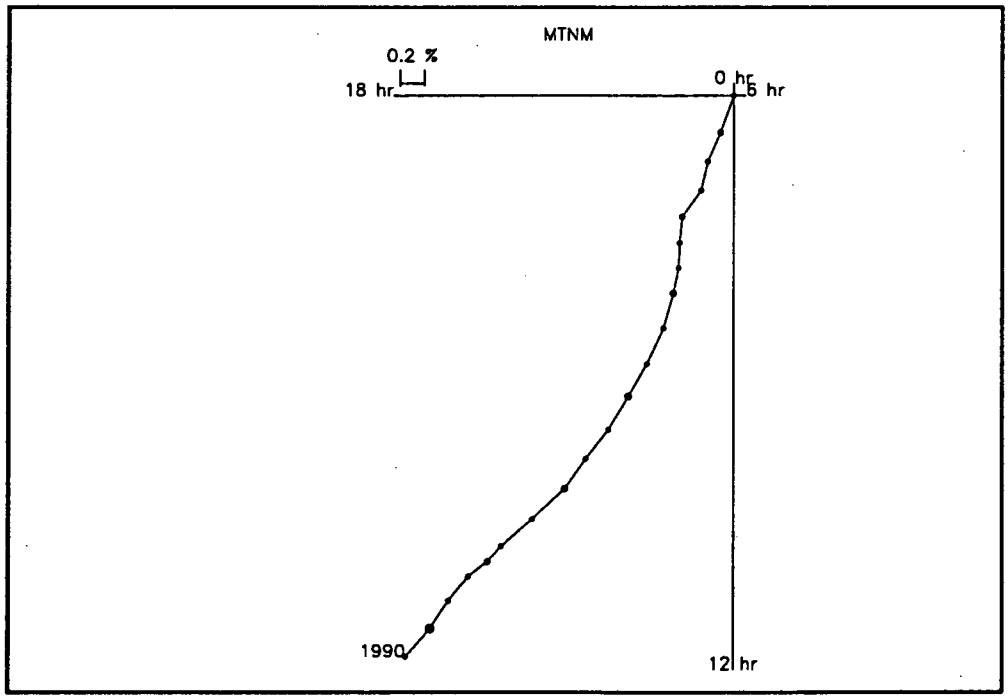

Figure A2.4 Vector sum diagram of the yearly averaged solar diurnal variation in Mount Wellington neutron monitor (MTNM) data from 1971 to 1990. The median rigidity of MTNM is 17 GV.

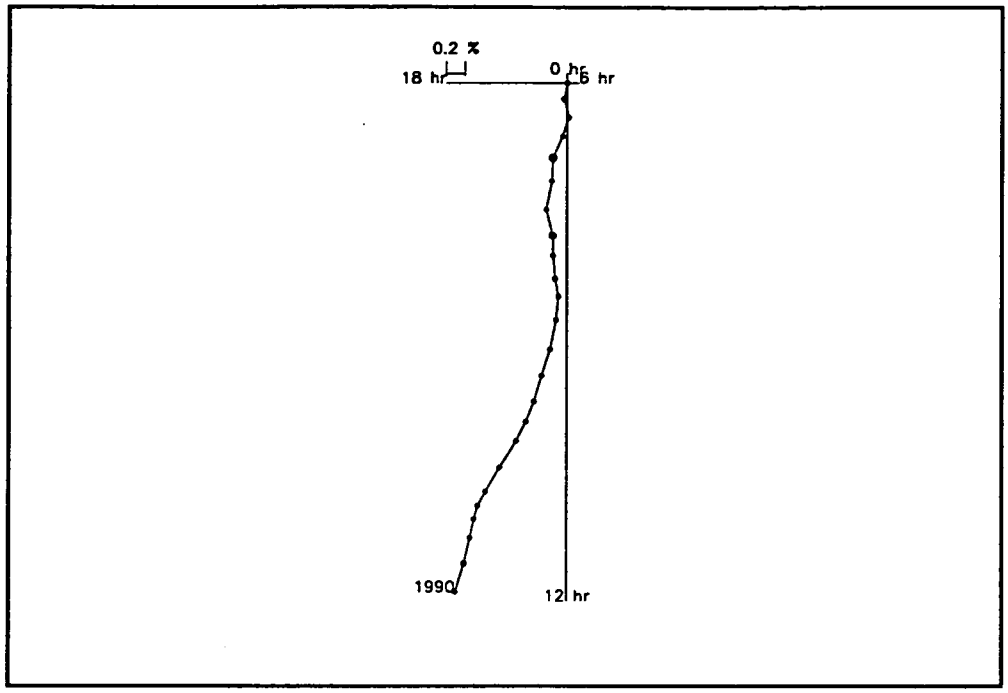

Figure A2.5 Vector sum diagram (harmonic dial) of the yearly averaged solar diurnal variation in Brisbane neutron monitor (BNM) data from 1965 to 1990. The median rigidity of BNM is 28 GV.

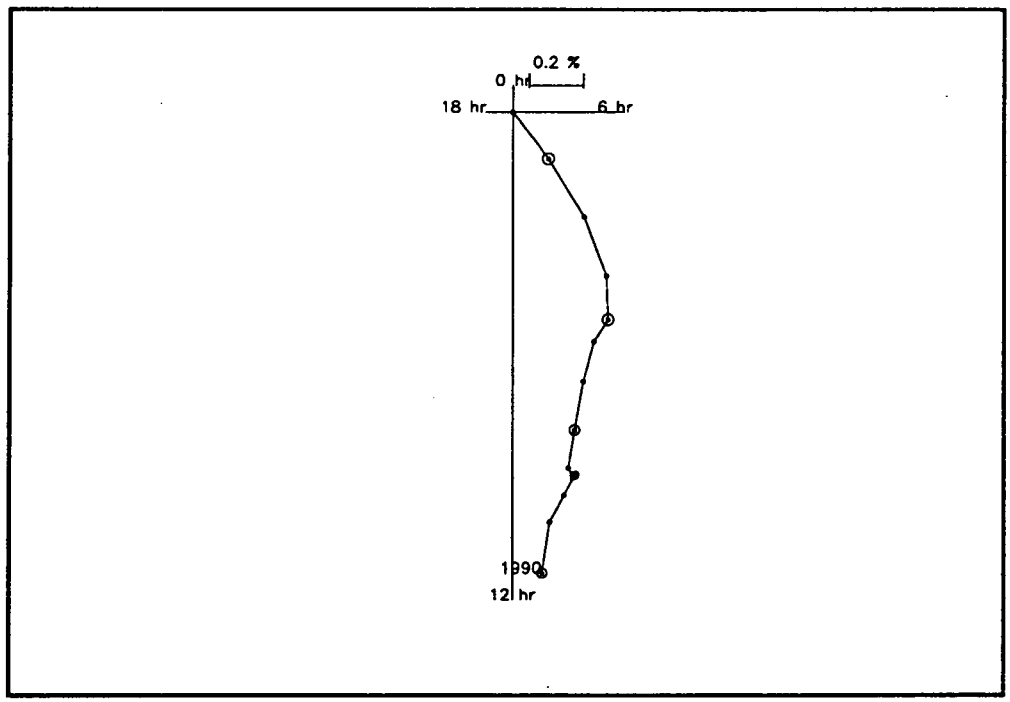

Figure A2.6 Vector sum diagram (harmonic dial) of the yearly averaged solar diurnal variation in Darwin neutron monitor (DNM) data from 1978 to 1990. The median rigidity of DNM is 50 GV.

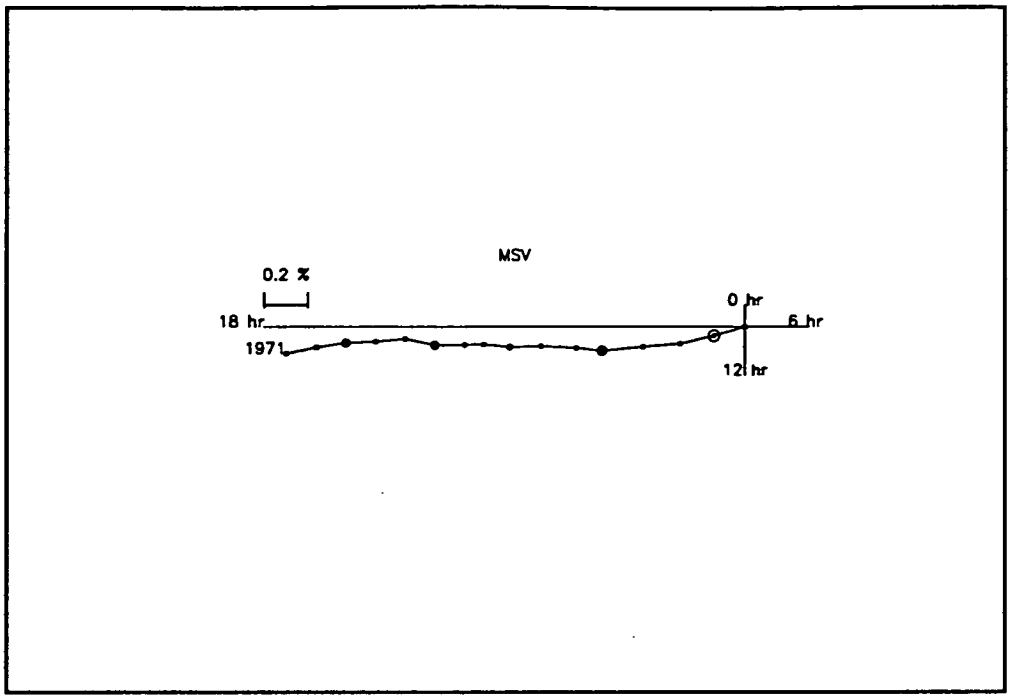

Figure A2.7 Vector sum diagram of the yearly averaged solar diurnal variation in Mawson surface muon telescope (MSV) data from 1957 to 1971. The median rigidity of MSV is 50 GV.

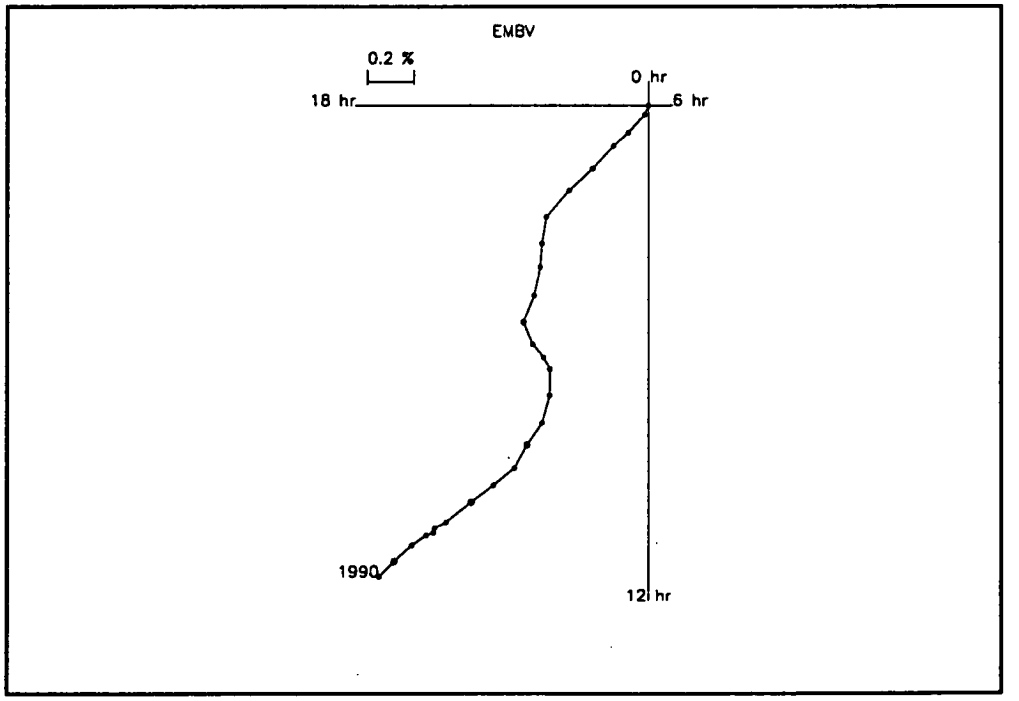

Figure A2.8 Vector sum diagram of the yearly averaged solar diurnal variation in Embudo vertical underground muon telescope (EMBV) data from 1966 to 1990. The median rigidity of EMBV is 135 GV.

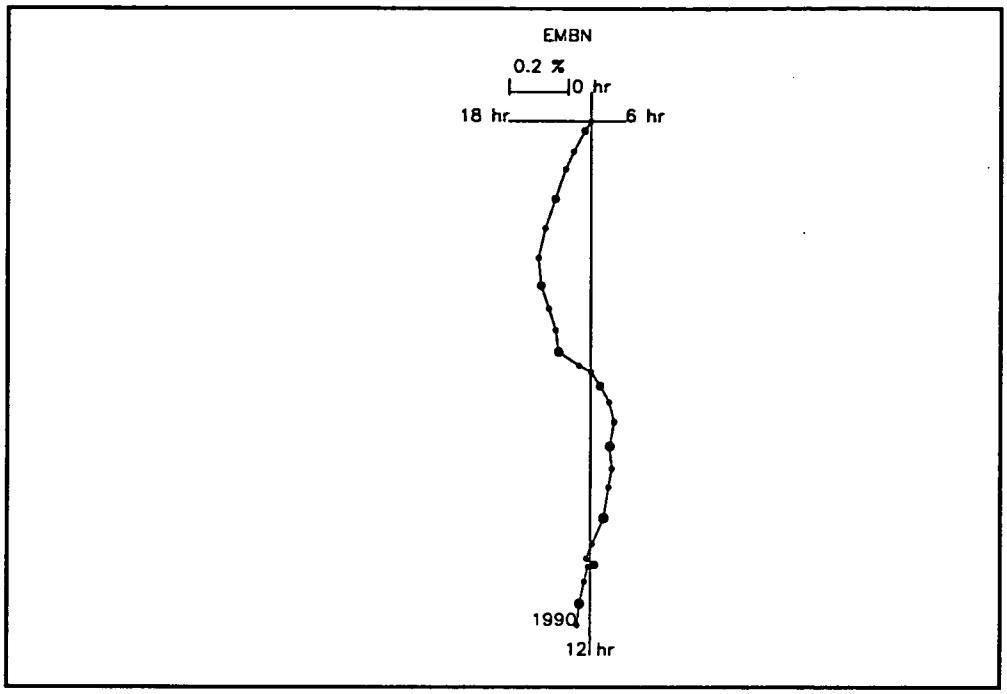

Figure A2.9 Vector sum diagram of the yearly averaged solar diurnal variation in Embudo north underground muon telescope (EMBN) data from 1965 to 1990. The median rigidity of EMBN is 140 GV.

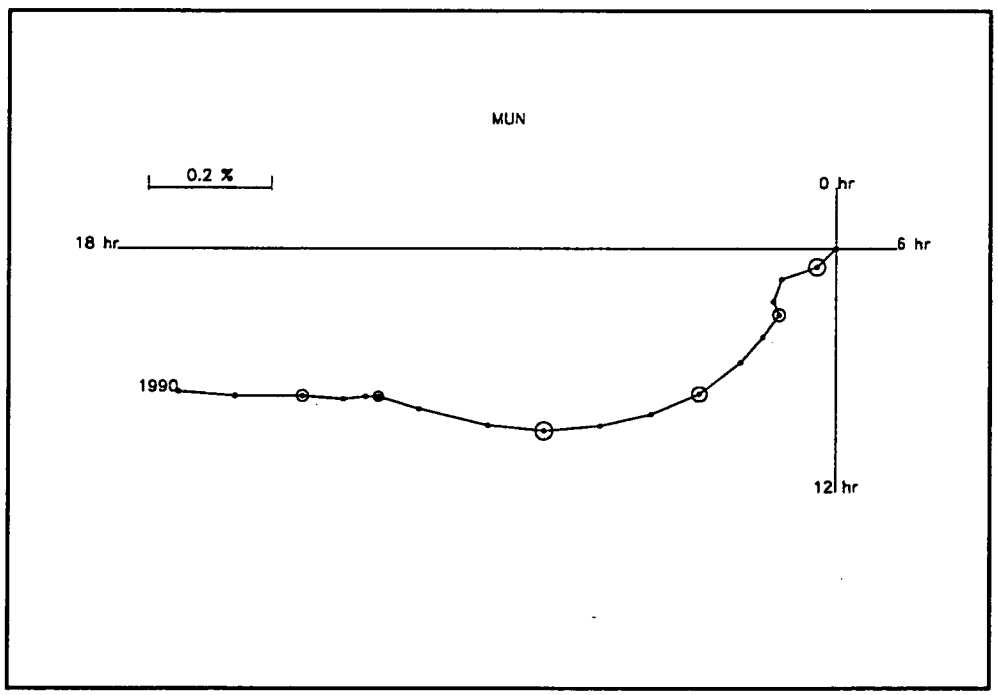

Figure A2.10 Vector sum diagram of the yearly averaged solar diurnal variation in Mawson north underground muon telescope (MUN) data from 1973 to 1990. The median rigidity of MUN is 165 GV.

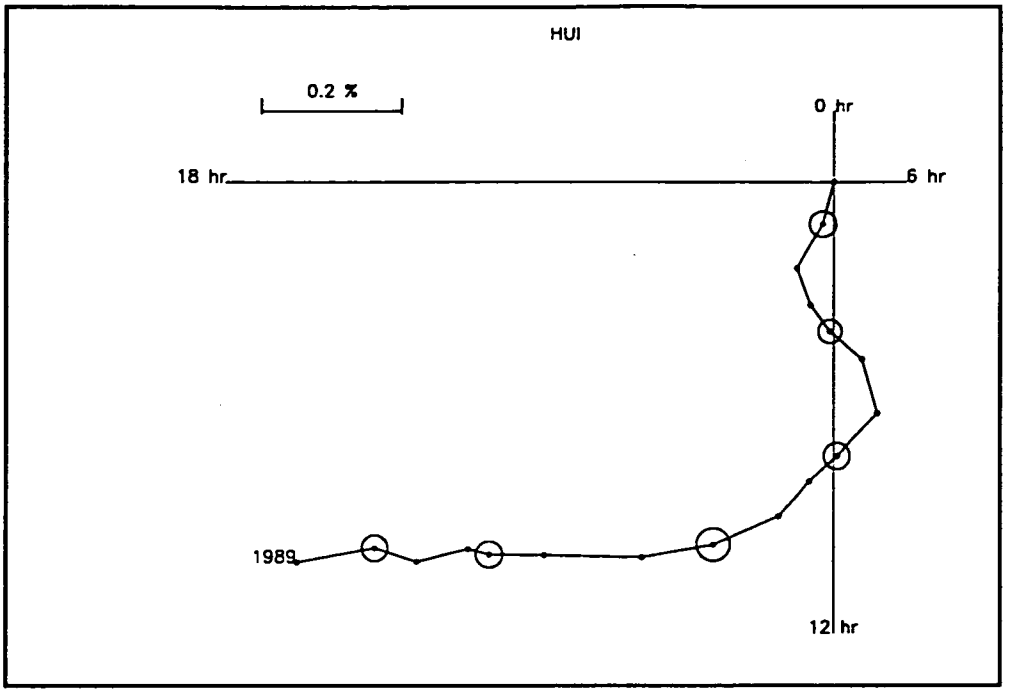

Figure A2.11 Vector sum diagram of the yearly averaged solar diurnal variation in Hobart north underground muon telescope (HUI) data from 1973 to 1990. The median rigidity of HUI is 195 GV.

APPENDIX 3

UPPER LIMITING RIGIDITY TO THE SOLAR DIURNAL ANISOTROPY

Upper limiting rigidity (P_u) of the solar diurnal anisotropy derived from each pair of neutron monitor - underground muon telescope observation of the solar diurnal variation. P_u is determined from the calculation of the free-space amplitude constant of the solar diurnal anisotropy for an assumed spectral index (γ). The calculations have been performed for $\gamma \in$ (-0.2, 0.3). In each plot the two instruments from which the results were obtained are labelled at the top by their mnemonics, e.g. results obtained from comparing the free-space amplitudes calculated from Hobart vertical underground muon telescope data with those calculated from Mawson neutron monitor data are labelled HUV vs MNM.

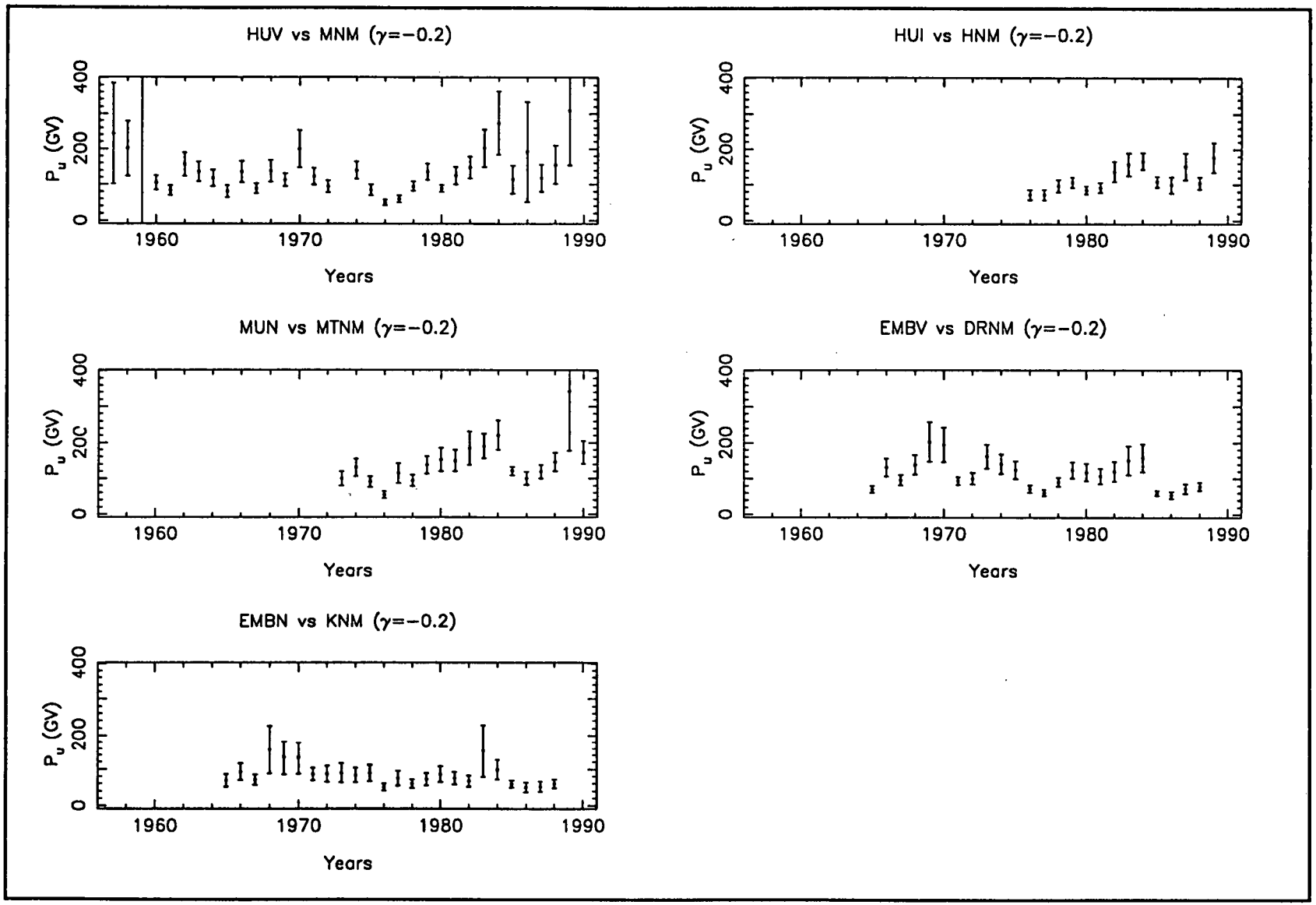
HUV vs MNM (γ=−0.2)
HUI vs HNM (γ=−0.2)
MUN vs MTNM (γ=−0.2)
EMBV vs DRNM (γ=−0.2)
EMBN vs KNM (γ=−0.2)
P_u (GV)
0
200
400
1960
1970
1980
1990
Years

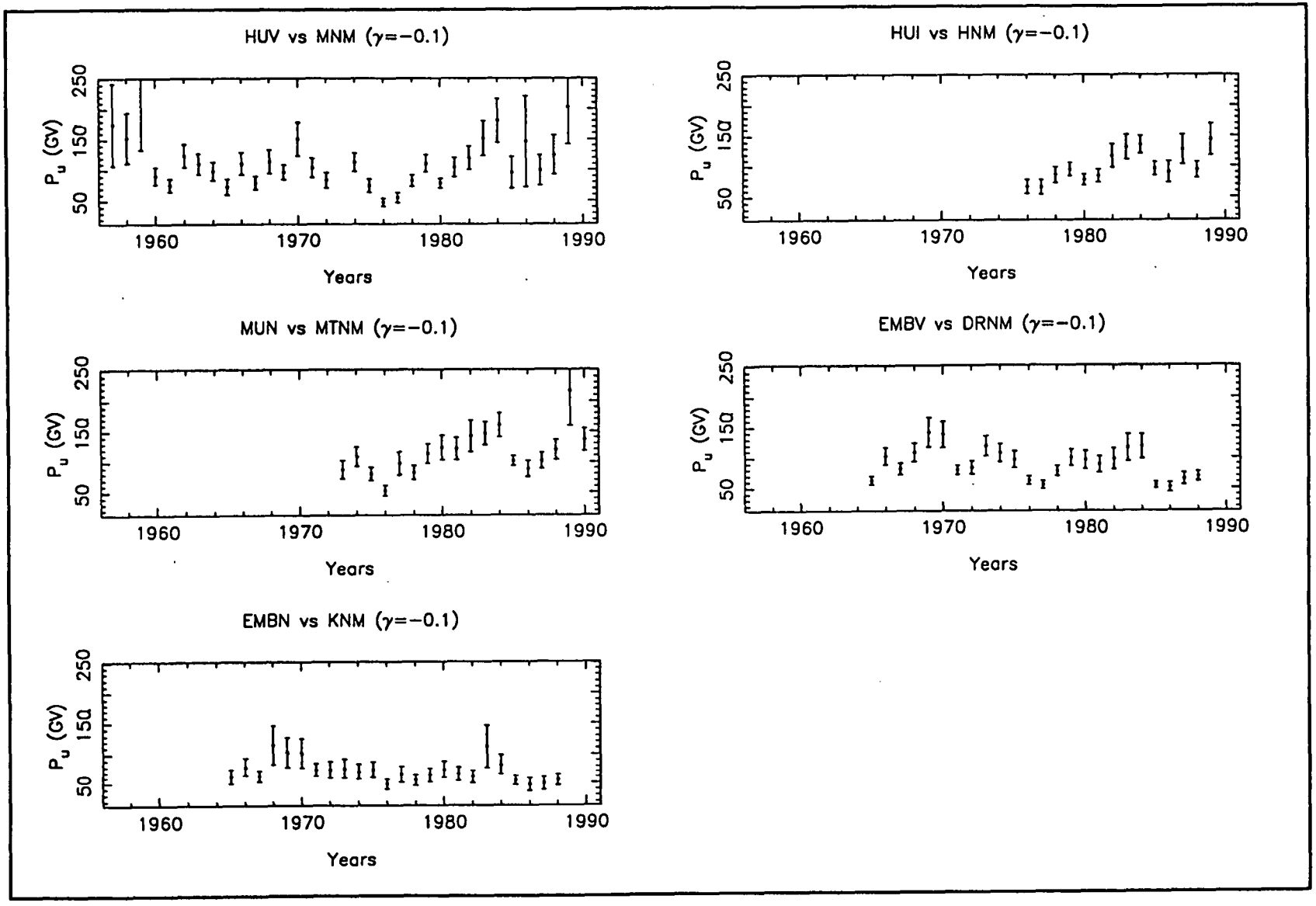
HUV vs MNM (γ=−0.1)
HUI vs HNM (γ=−0.1)
MUN vs MTNM (γ=−0.1)
EMBV vs DRNM (γ=−0.1)
EMBN vs KNM (γ=−0.1)
P_u (GV)
50
150
250
1960
1970
1980
1990
Years

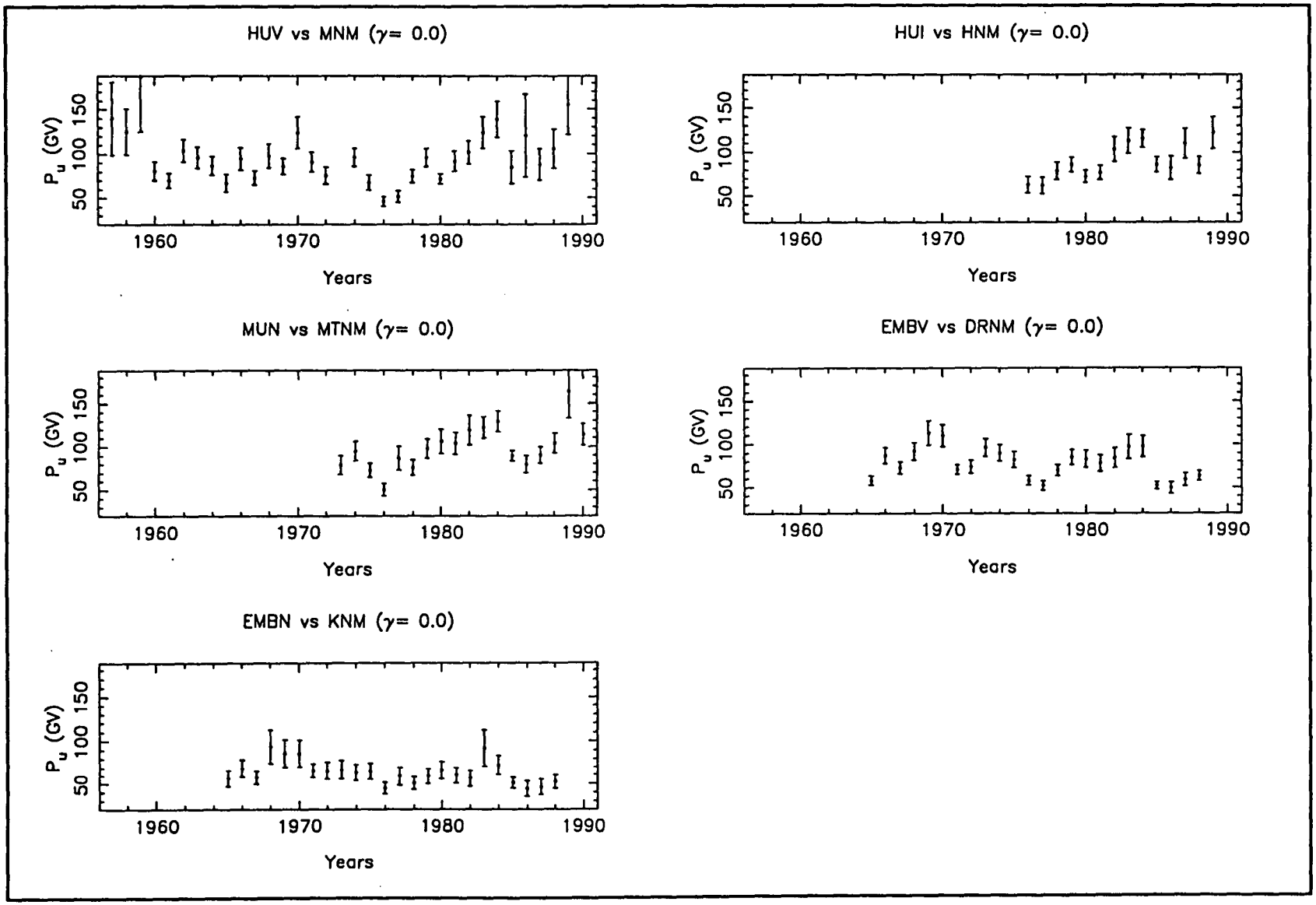
HUV vs MNM (γ= 0.0)
HUI vs HNM (γ= 0.0)
MUN vs MTNM (γ= 0.0)
EMBV vs DRNM (γ= 0.0)
EMBN vs KNM (γ= 0.0)
P_u (GV)
50 100 150
1960
1970
1980
1990
Years

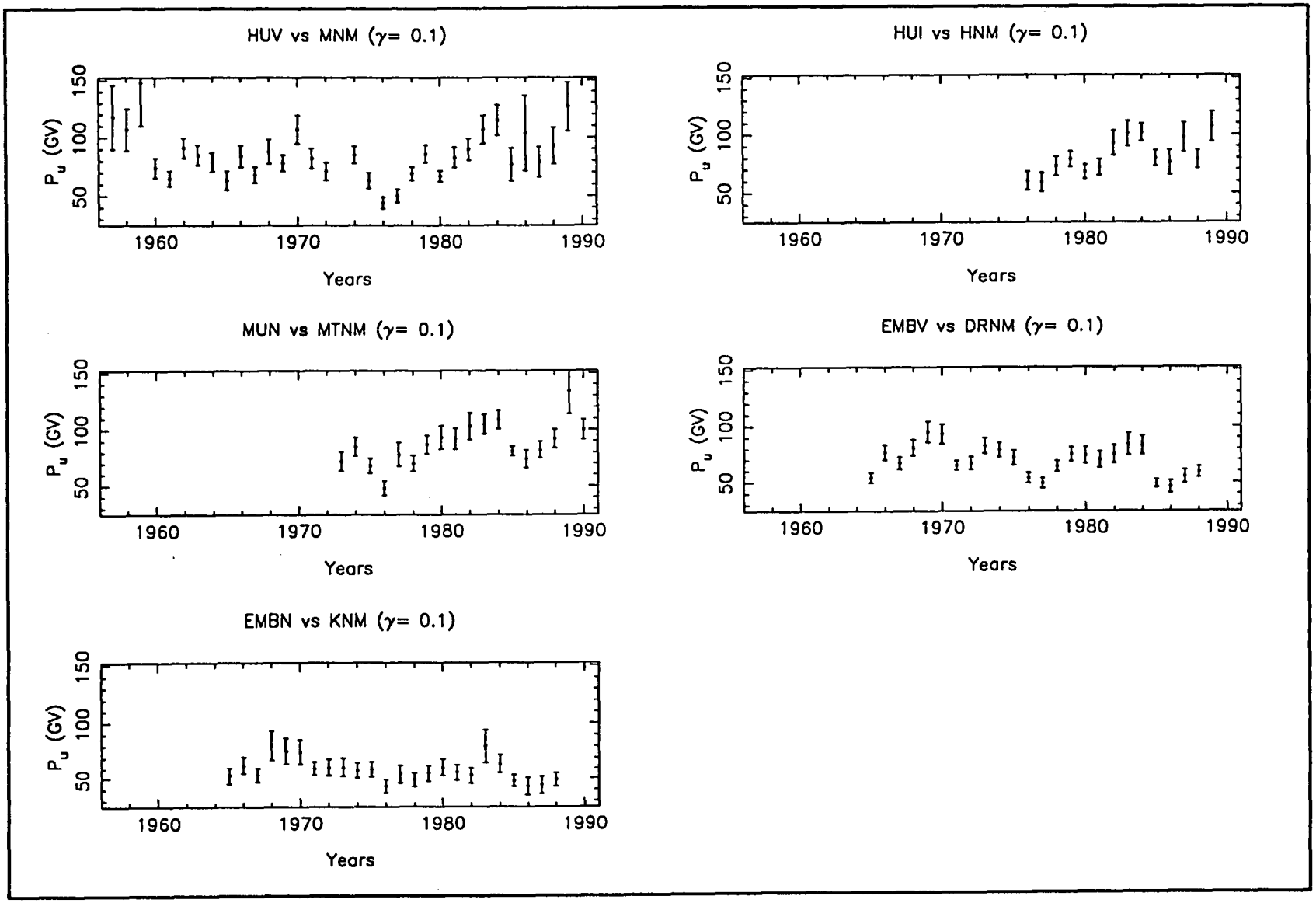
HUV vs MNM (γ= 0.1)
HUI vs HNM (γ= 0.1)
MUN vs MTNM (γ= 0.1)
EMBV vs DRNM (γ= 0.1)
EMBN vs KNM (γ= 0.1)
P_u (GV)
50
100
150
1960
1970
1980
1990
Years

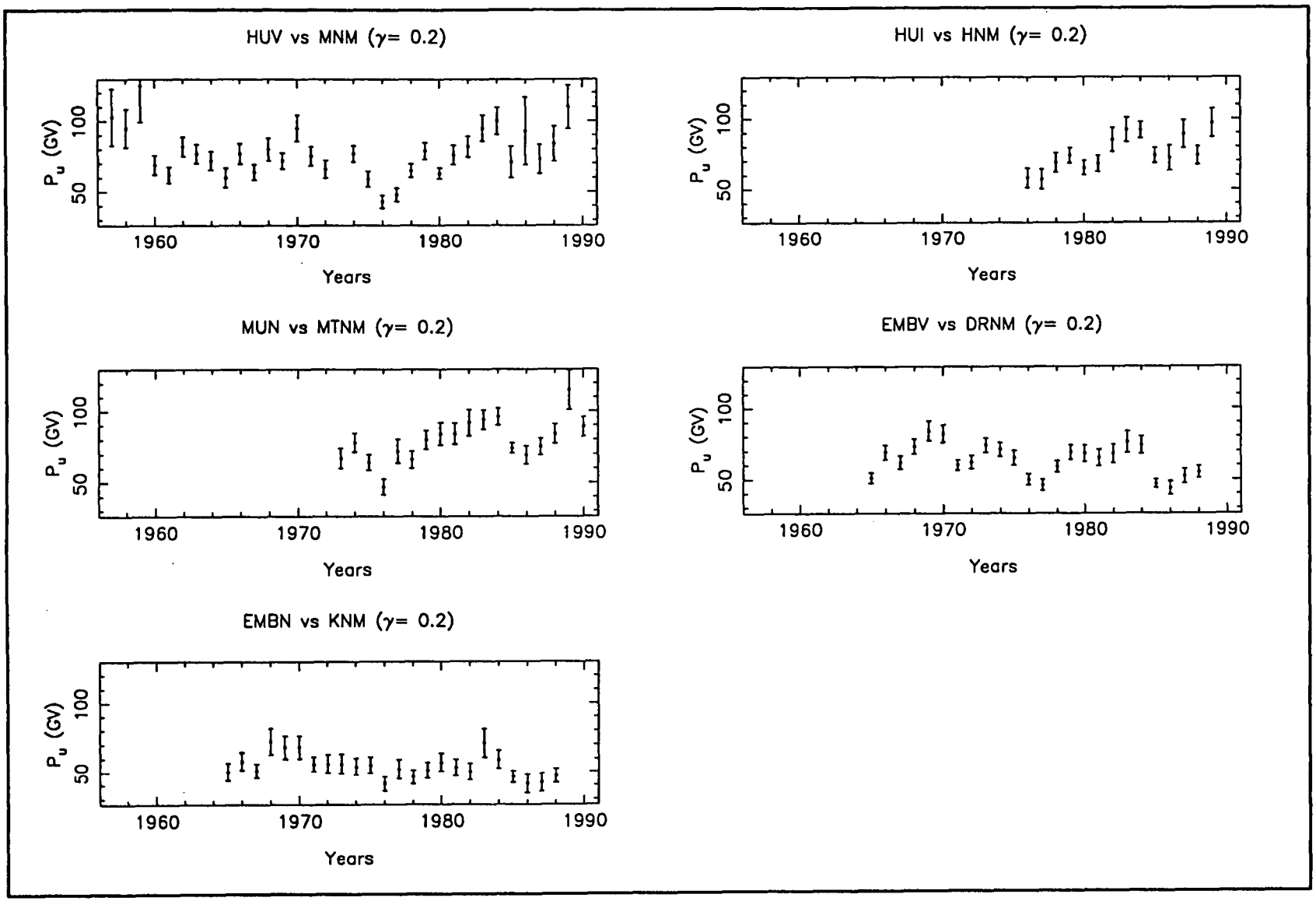
HUV vs MNM (γ= 0.2)
HUI vs HNM (γ= 0.2)
MUN vs MTNM (γ= 0.2)
EMBV vs DRNM (γ= 0.2)
EMBN vs KNM (γ= 0.2)
P_u (GV)
50
100
1960
1970
1980
1990
Years

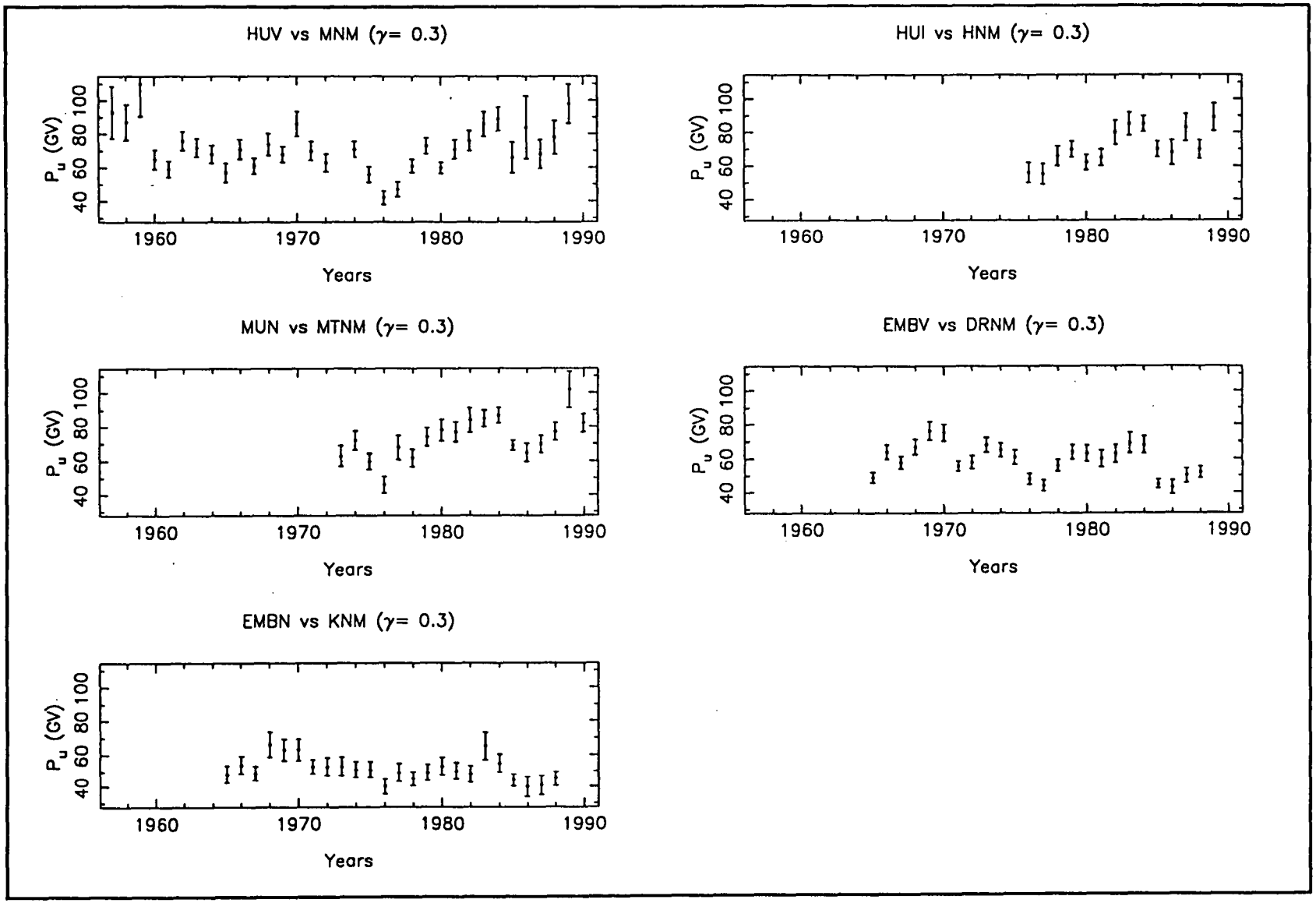
HUV vs MNM (γ= 0.3)
HUI vs HNM (γ= 0.3)
MUN vs MTNM (γ= 0.3)
EMBV vs DRNM (γ= 0.3)
EMBN vs KNM (γ= 0.3)
P_u (GV)
40 60 80 100
1960 1970 1980 1990
Years

APPENDIX 4

SOLAR DIURNAL ANISOTROPY - BEST FIT RIGIDITY SPECTRA CONTOUR DIAGRAMS

Contour plots of the χ^2 values obtained from each years' solar diurnal variation. The values of χ^2 are calculated from equation (3.23) and the method described in Section 3.2.2. The best-fit rigidity spectrum for each year is plotted as an asterisk. The 68% and 90% confidence regions are plotted as dashed lines. Table A1 contains the χ^2 values of the 7 solid contour lines in each plot starting from the outer-most contour line to the minimum value.

Table A1 Values of χ^2 contour regions.

Year	Outer contour χ^2	2nd most outer	3rd most outer	4th most outer	5th most outer	6th most outer	minimum χ^2	Number of data
1957	78	40	20	10	5	2.5	0.01	3
1958	130	66	33	16	8	4	0.06	3
1959	182	91	45	23	12	6	0.01	3
1960	164	83	41	20	10	5	0.01	3
1961	154	78	39	19	10	5	0.01	3
1962	425	214	107	54	27	14	0.2	3
1963	339	171	86	43	22	11	0.1	3
1964	286	144	72	36	18	9	0.02	3
1965	854	433	219	112	59	32	5	7
1966	689	349	176	89	46	24	2	7
1967	571	290	147	75	39	21	3	7
1968	708	364	189	101	58	36	13	8
1969	860	444	232	125	73	46	19	8
1970	861	453	244	140	88	62	36	8
1971	1436	736	380	201	112	68	23	9
1972	1099	558	281	143	75	40	1	8
1973	1374	707	367	197	112	70	26	9
1974	1247	634	322	166	89	50	10	8
1975	1042	536	278	148	84	52	19	8
1976	1123	574	294	155	85	51	15	9
1977	948	487	252	134	76	46	16	10
1978	1205	615	314	163	88	51	12	11
1979	1405	722	374	199	113	70	25	11
1980	1756	898	461	242	133	79	23	11
1981	1270	654	340	183	105	66	26	11
1982	1022	527	274	147	85	53	21	11
1983	1376	701	357	185	99	56	12	11
1984	2157	1122	595	331	200	135	67	11
1985	2753	1430	755	417	250	166	79	11
1986	1076	569	310	181	117	85	52	11
1987	1306	697	386	231	154	115	75	11
1988	1269	655	342	185	108	69	29	11
1989	469	257	149	95	69	55	41	9
1990	933	495	271	159	104	76	7	7

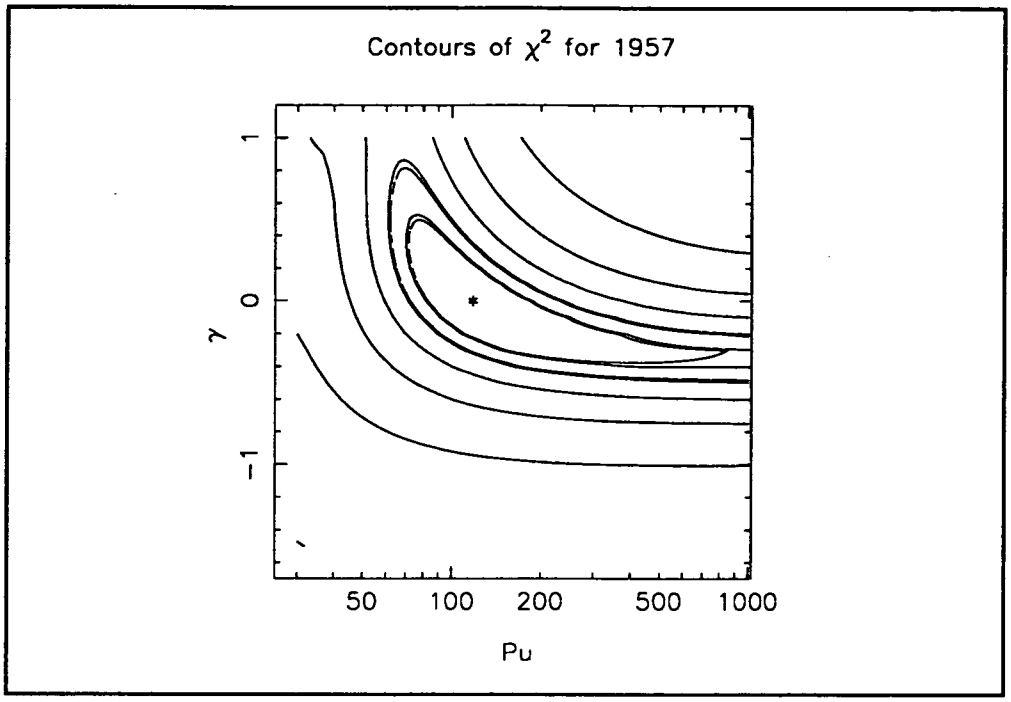
Contours of χ^2 for 1957
1
0
−1
γ
50
100
200
500
1000
Pu

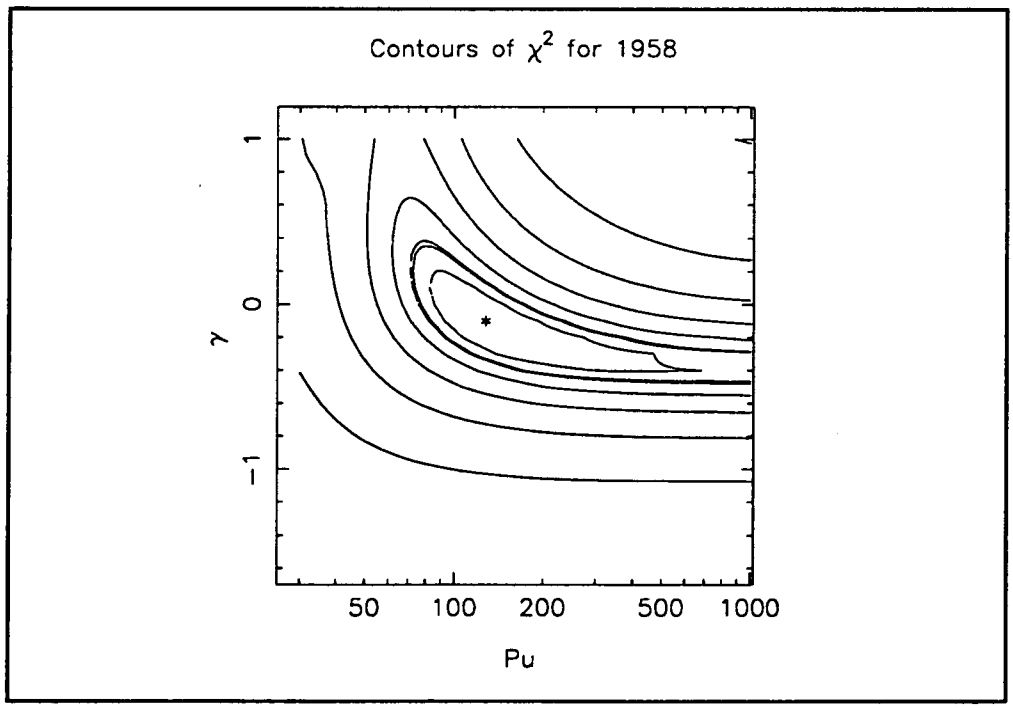
Contours of χ^2 for 1958
1
0
−1
γ
50
100
200
500
1000
Pu

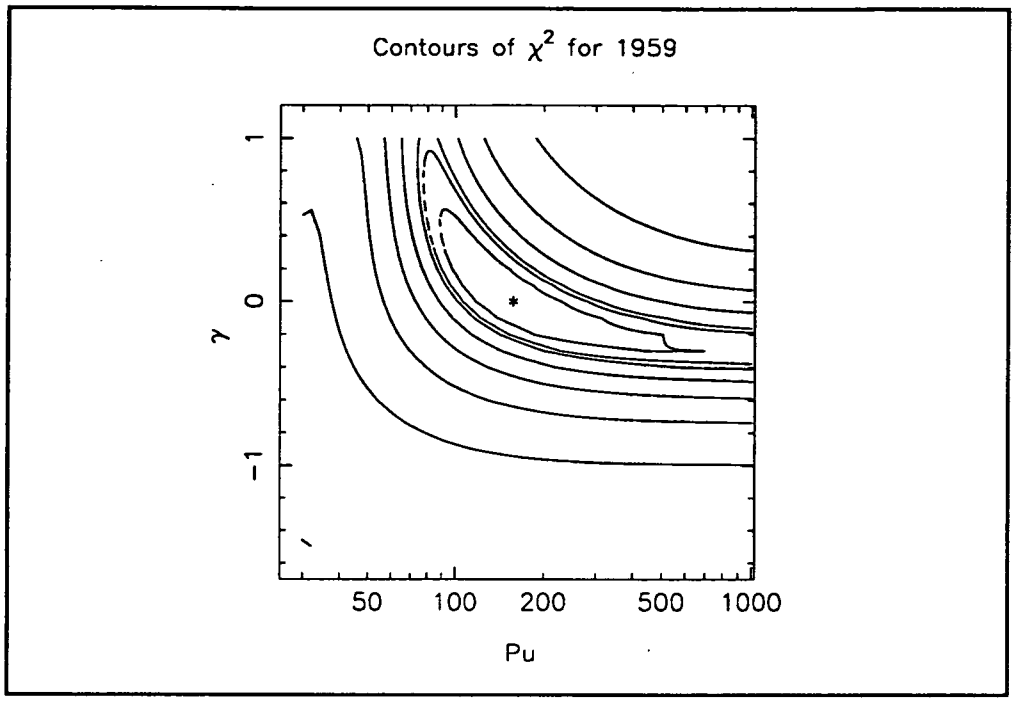
Contours of χ^2 for 1959
1
0
−1
γ
50
100
200
500
1000
Pu

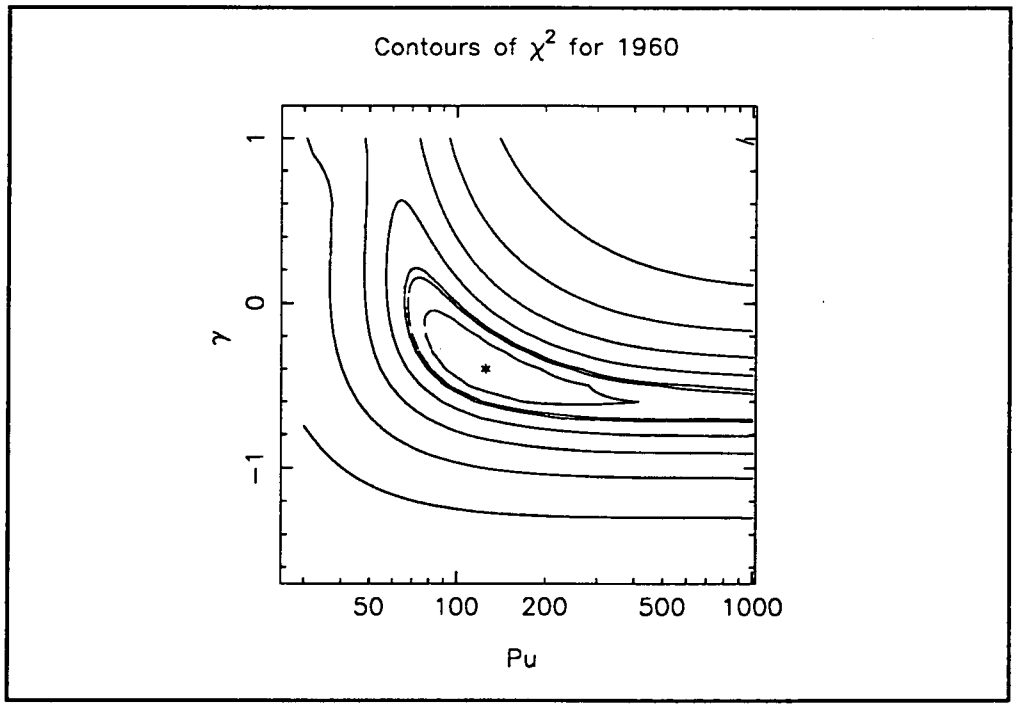
Contours of χ^2 for 1960
1
0
−1
γ
50
100
200
500
1000
Pu

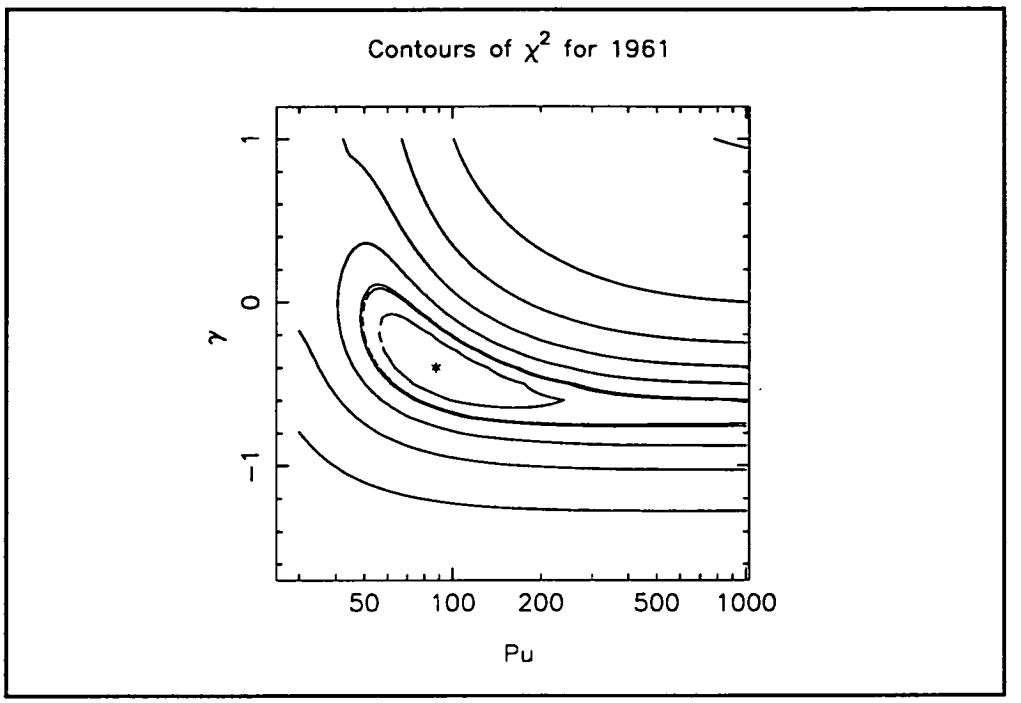
Contours of χ^2 for 1961
γ
1
0
−1
50
100
200
500
1000
Pu

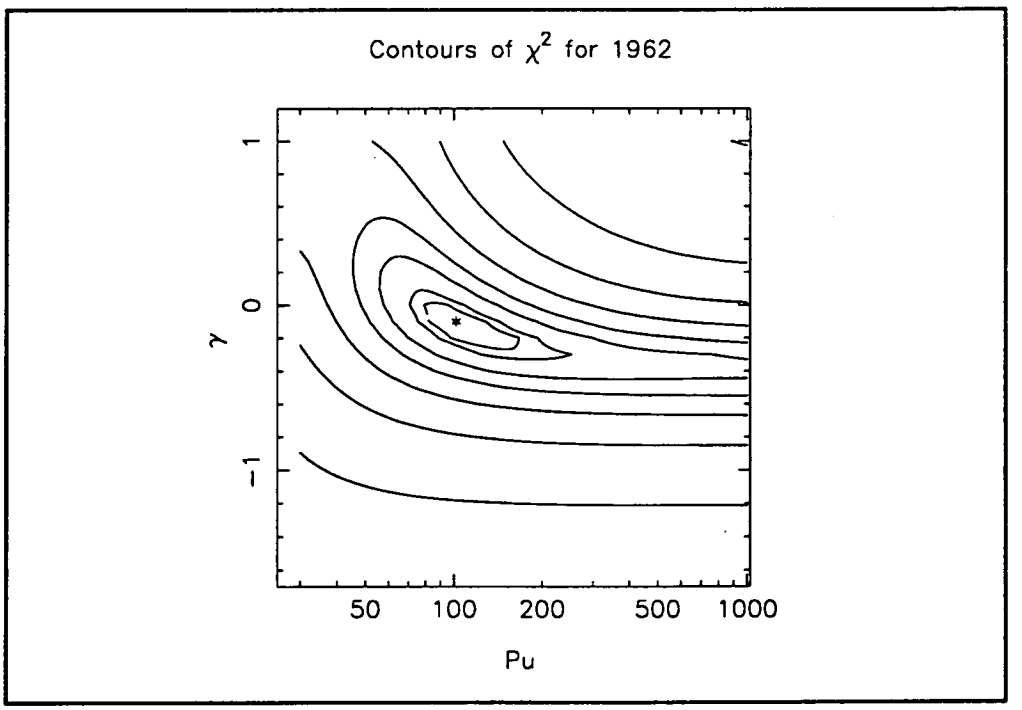
Contours of χ^2 for 1962
γ
1
0
−1
50
100
200
500
1000
Pu

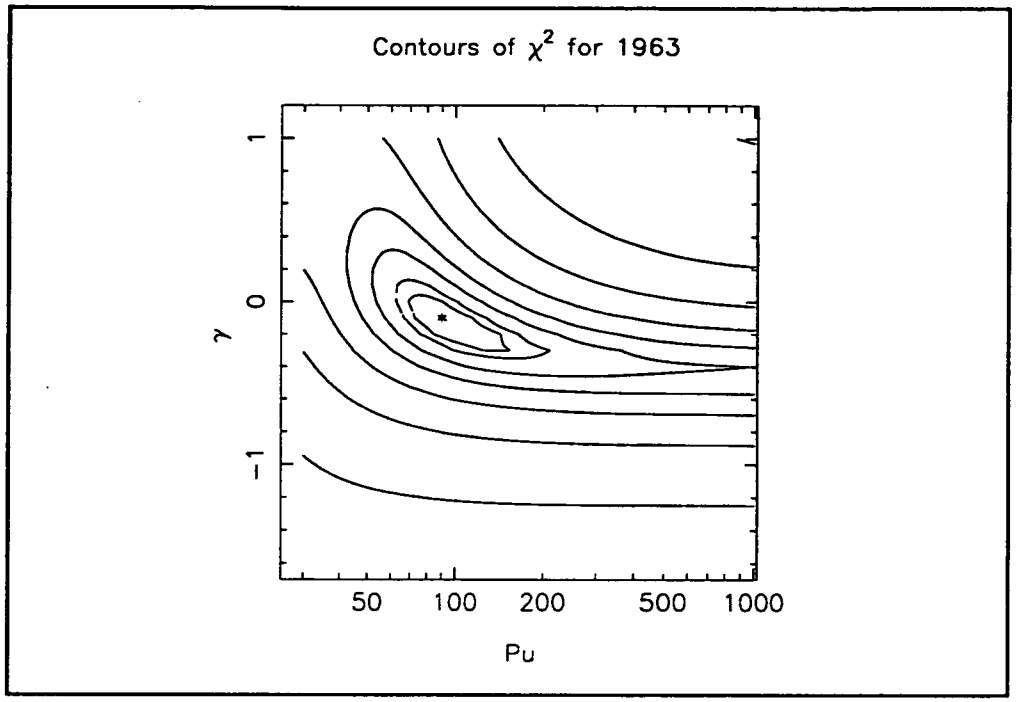
Contours of χ^2 for 1963
γ
1
0
−1
50
100
200
500
1000
Pu

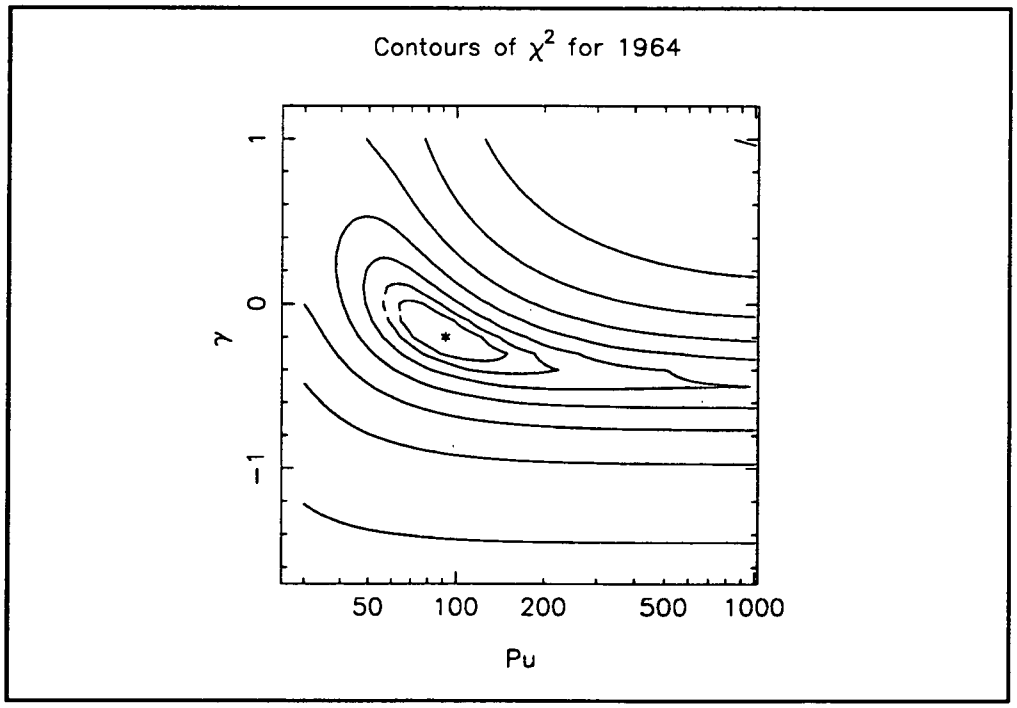
Contours of χ^2 for 1964
γ
1
0
−1
50
100
200
500
1000
Pu

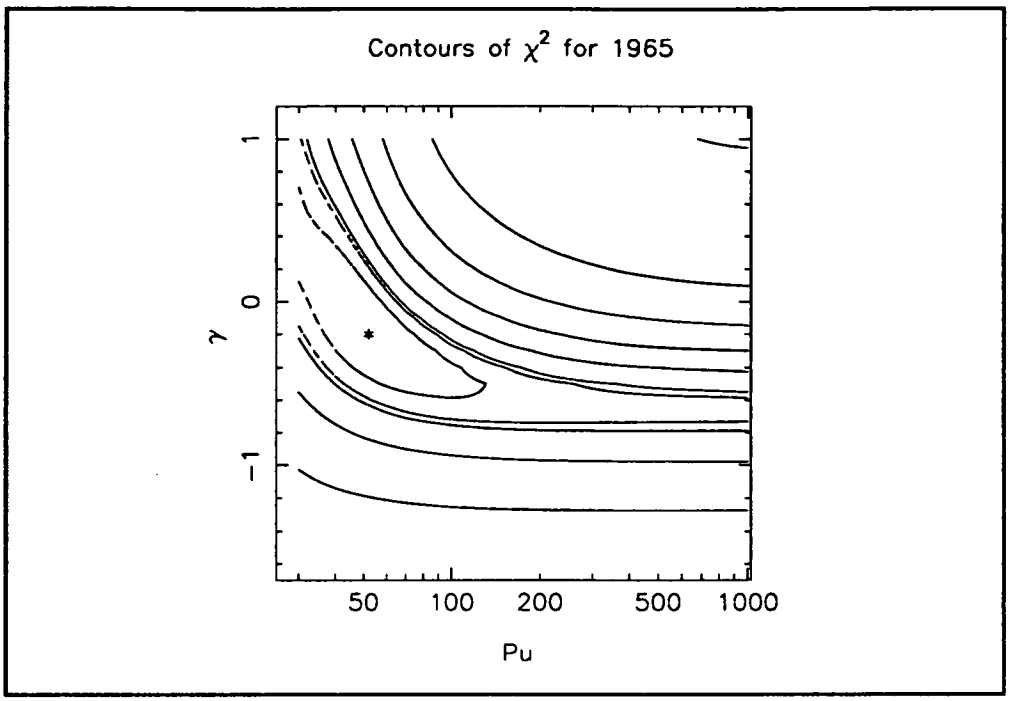
Contours of χ^2 for 1965
1
0
−1
γ
50
100
200
500
1000
Pu

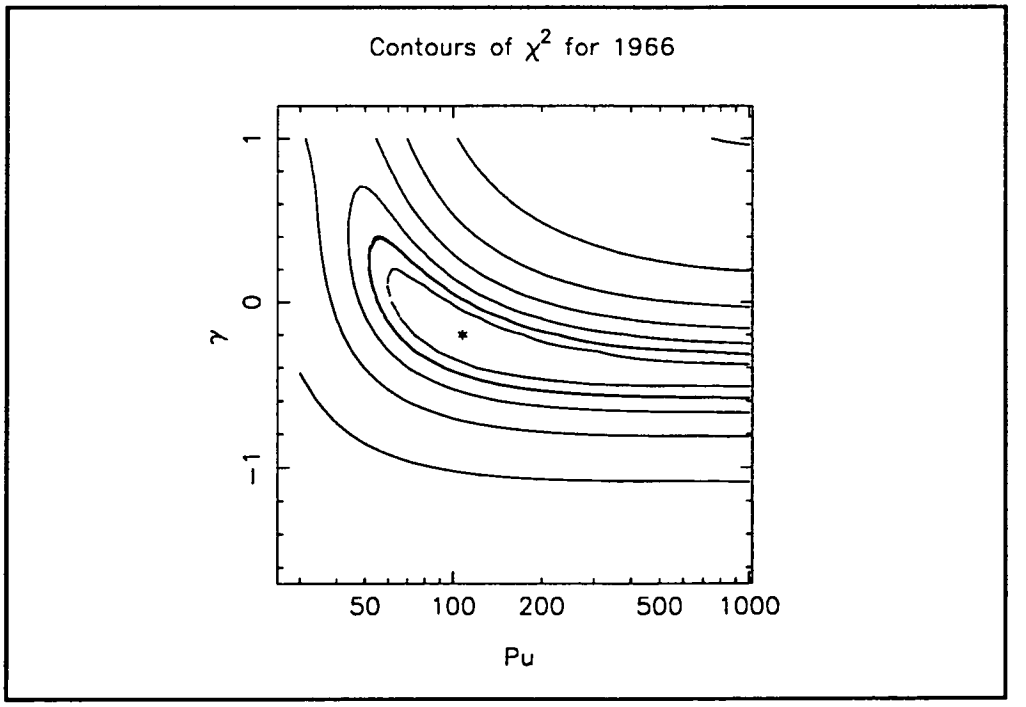
Contours of χ^2 for 1966
1
0
−1
γ
50
100
200
500
1000
Pu

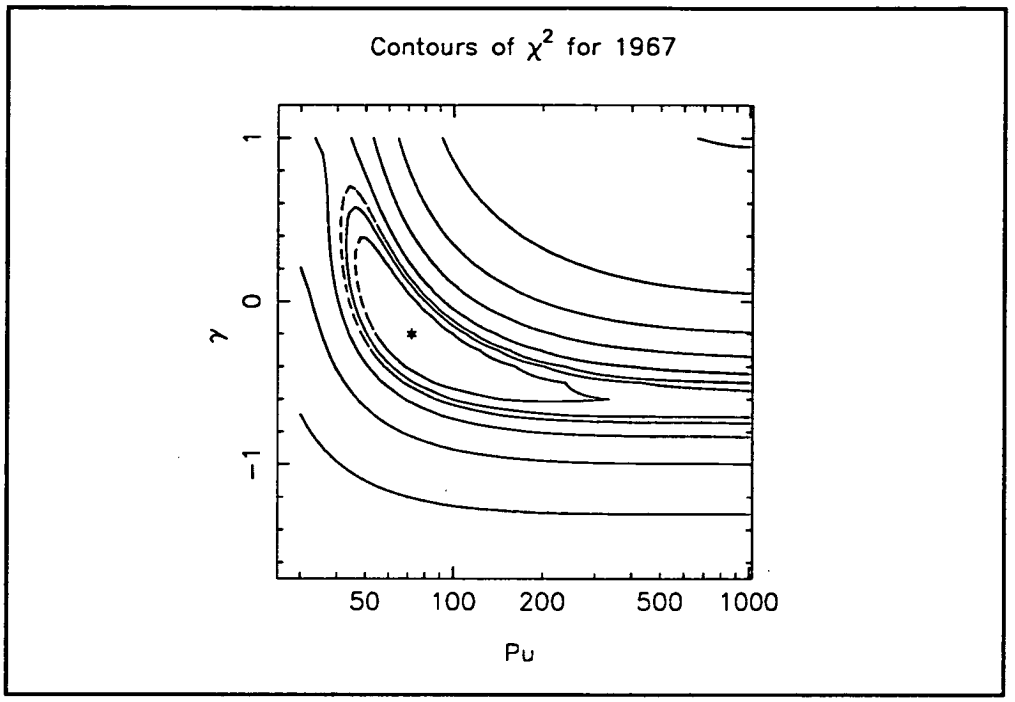
Contours of χ^2 for 1967
1
0
−1
γ
50
100
200
500
1000
Pu

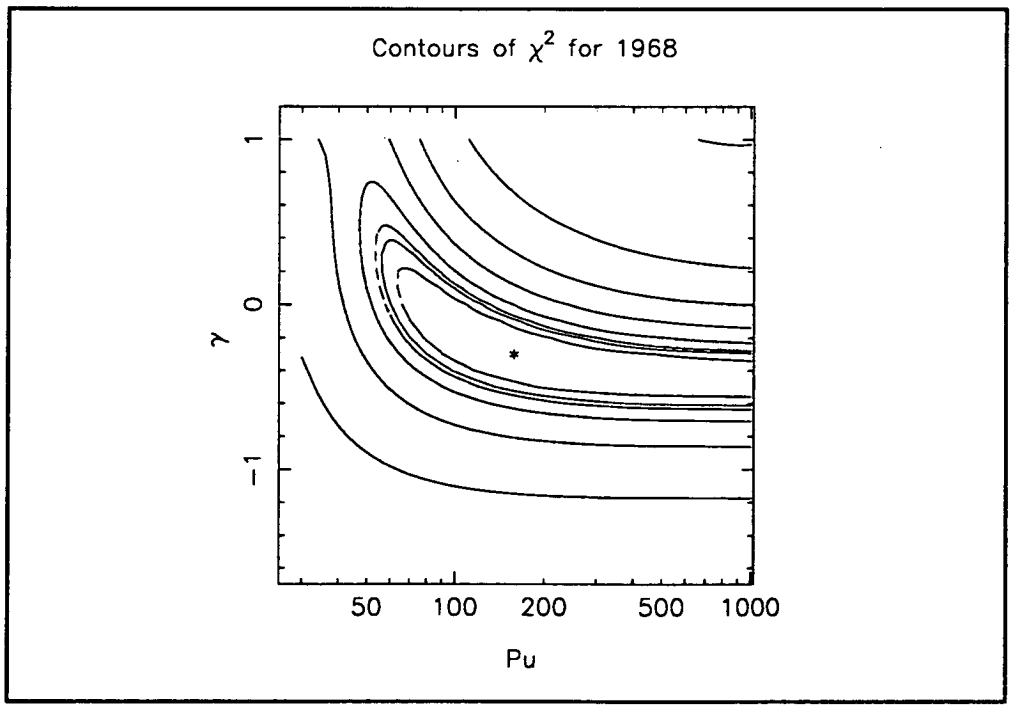
Contours of χ^2 for 1968
1
0
−1
γ
50
100
200
500
1000
Pu

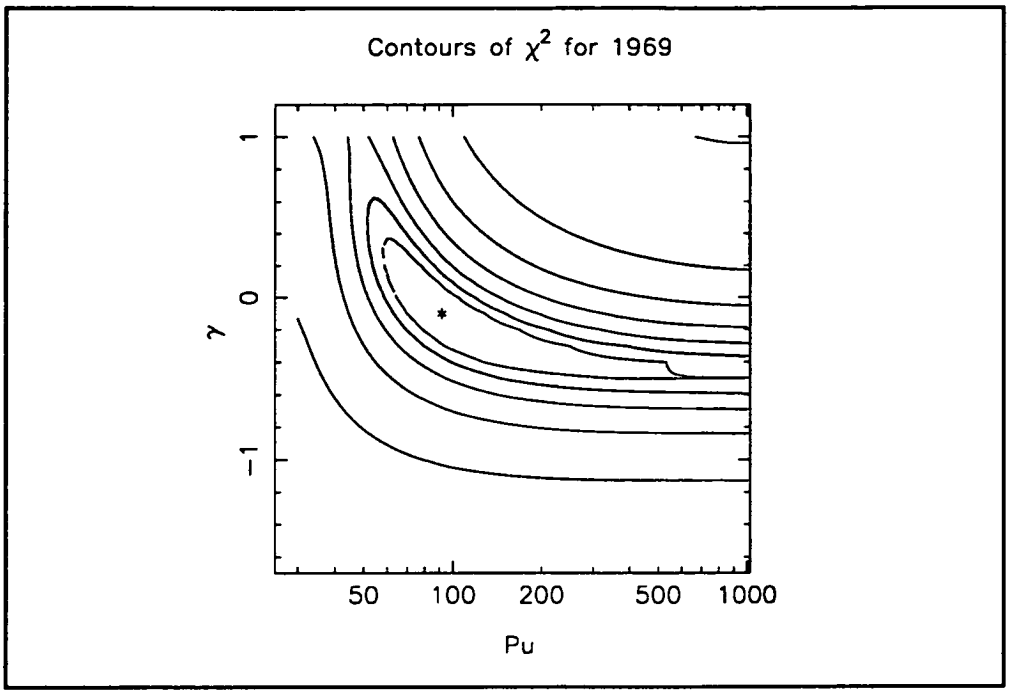
Contours of χ^2 for 1969
1
0
−1
γ
50
100
200
500
1000
Pu

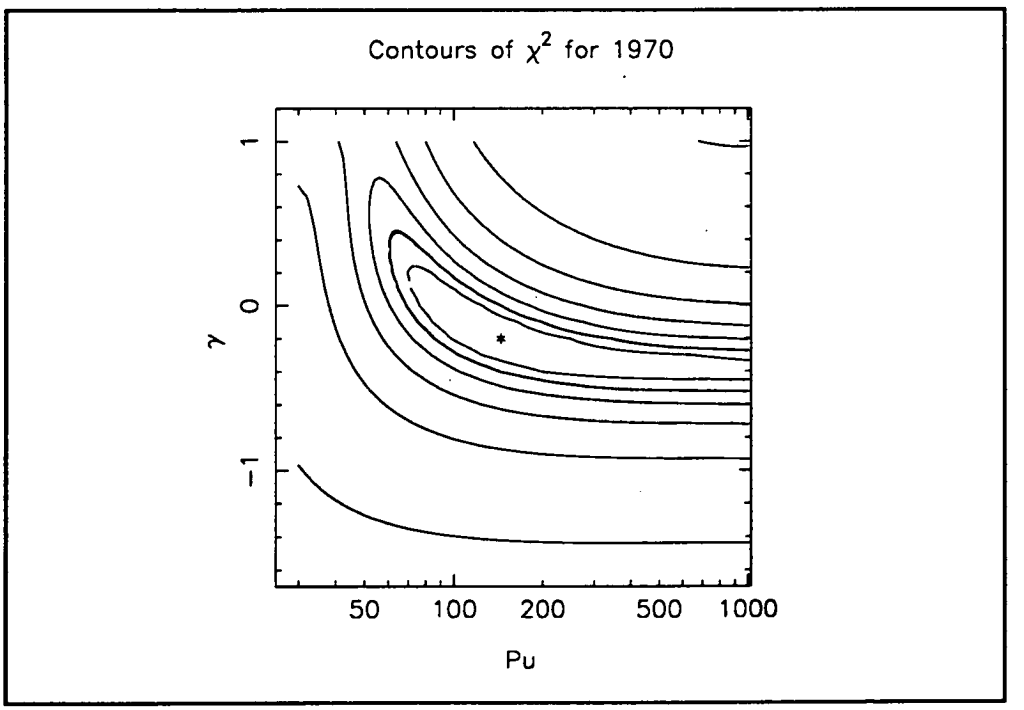
Contours of χ^2 for 1970
1
0
−1
γ
50
100
200
500
1000
Pu

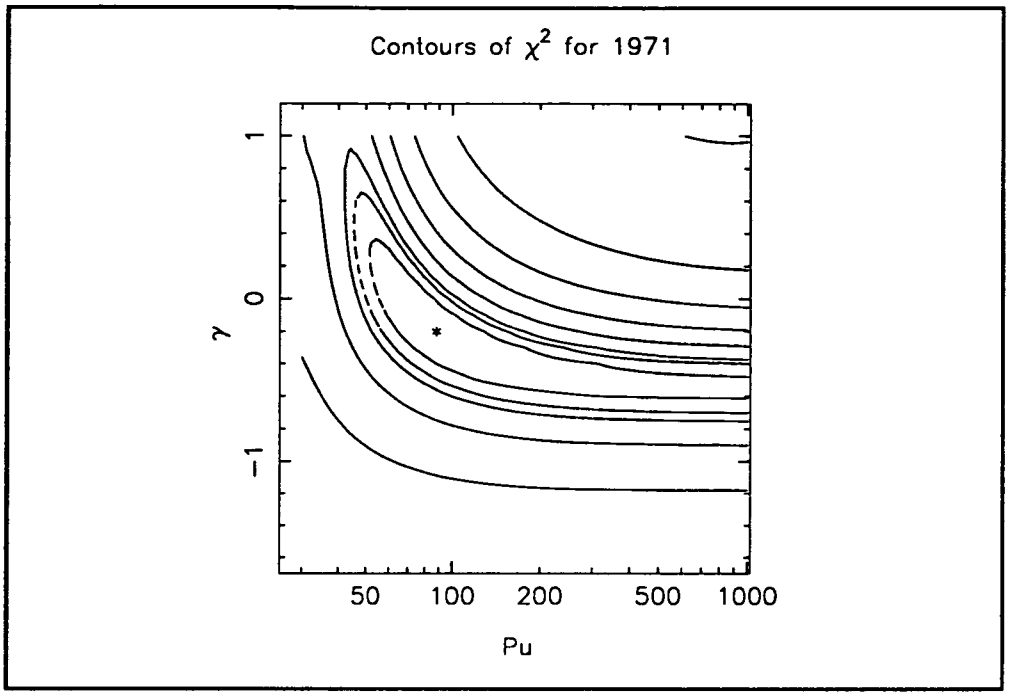
Contours of χ^2 for 1971
1
0
−1
γ
50
100
200
500
1000
Pu

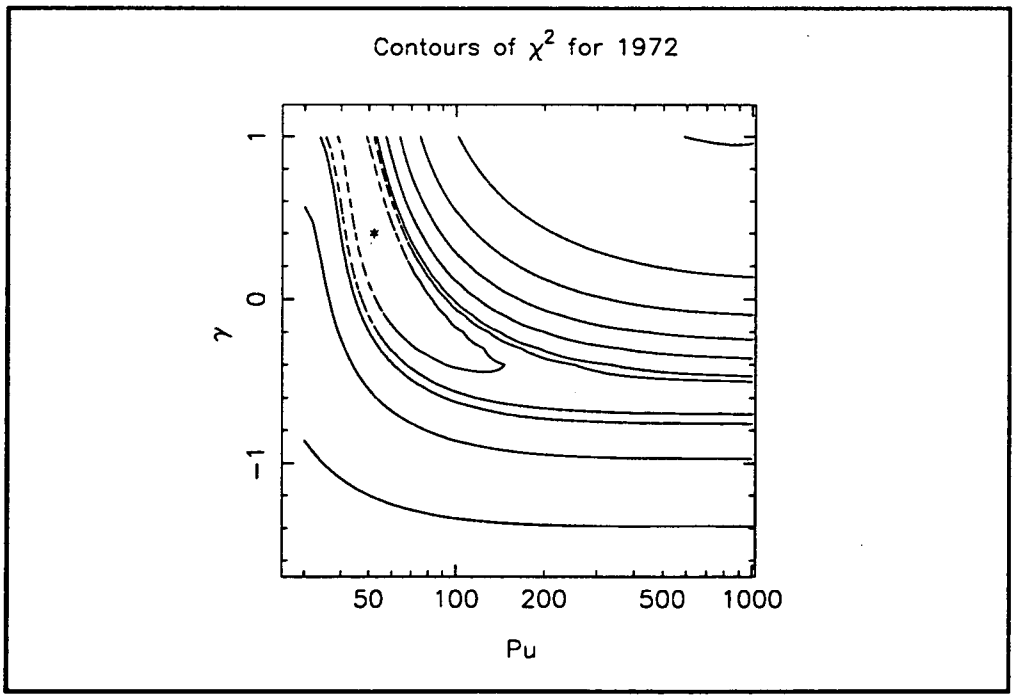
Contours of χ^2 for 1972
1
0
−1
γ
50
100
200
500
1000
Pu

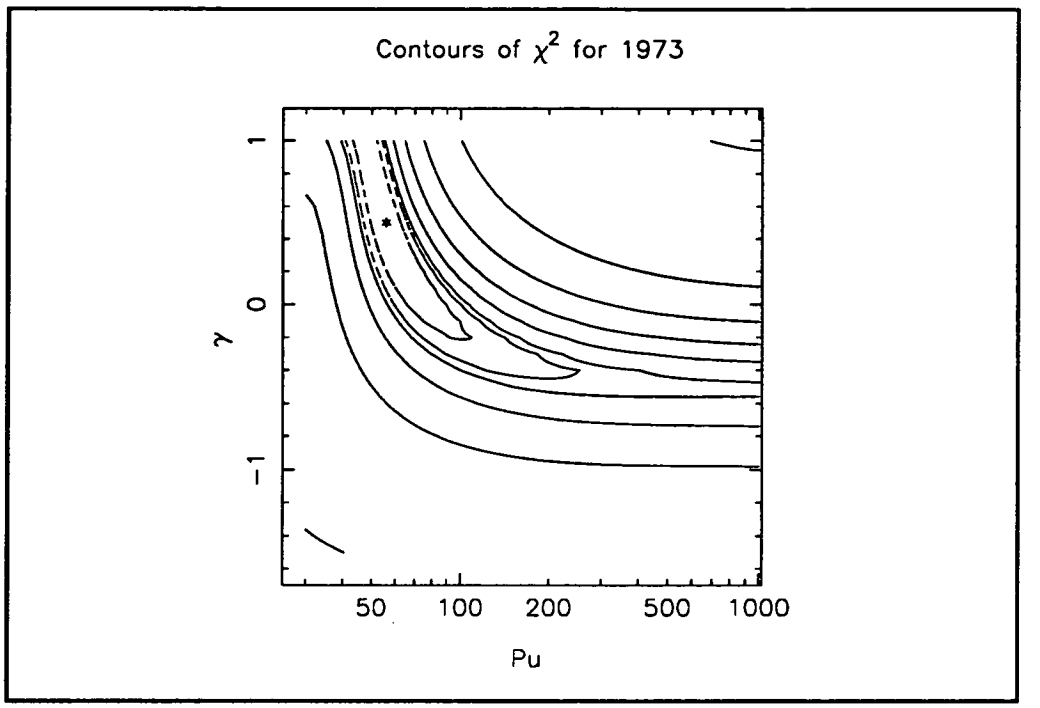
Contours of χ^2 for 1973
1
0
−1
γ
50
100
200
500
1000
Pu

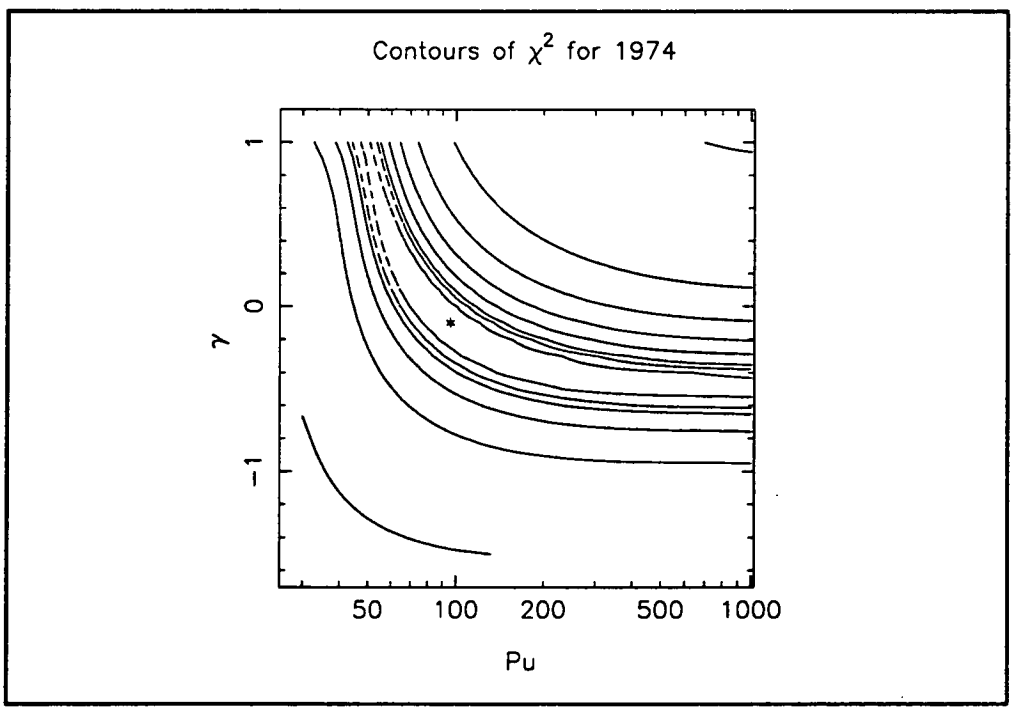
Contours of χ^2 for 1974
1
0
−1
γ
50
100
200
500
1000
Pu

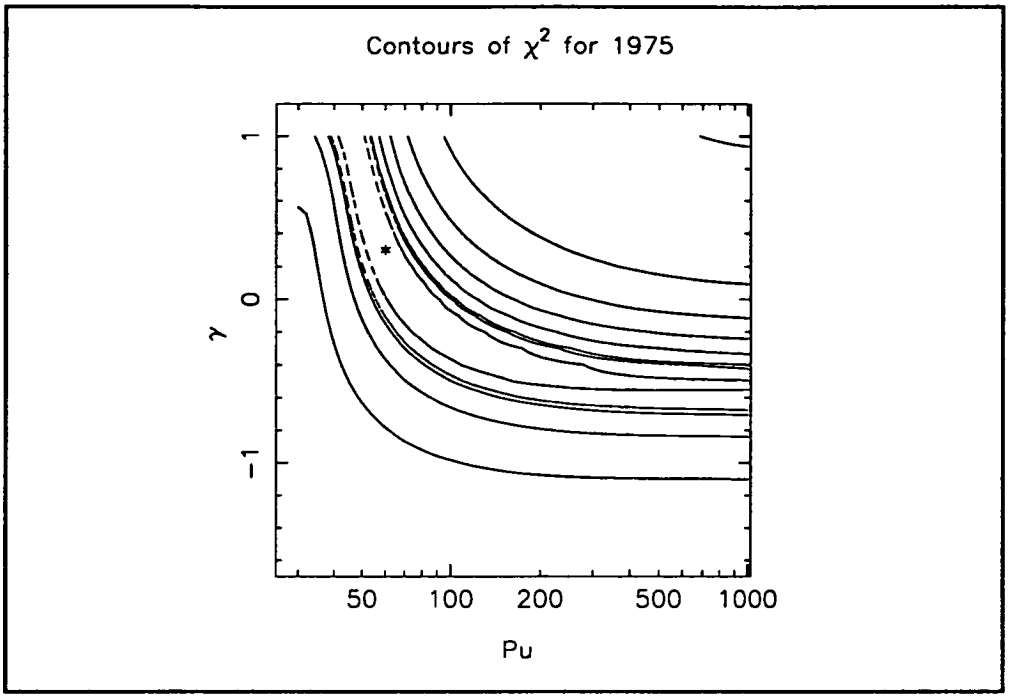
Contours of χ^2 for 1975
γ
1
0
−1
50
100
200
500
1000
Pu

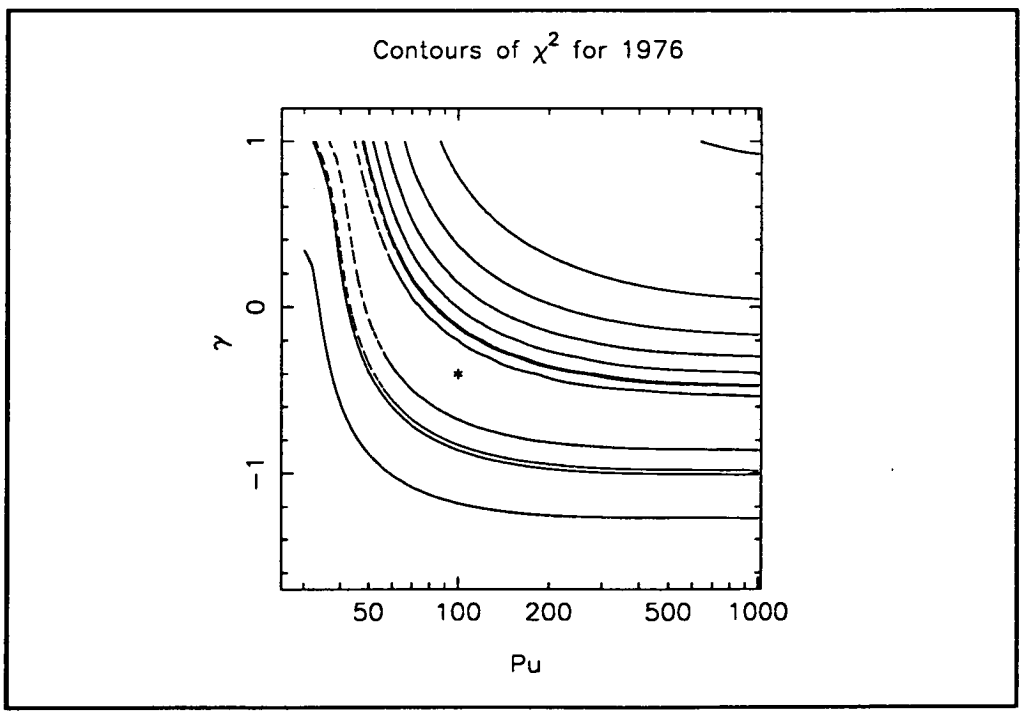
Contours of χ^2 for 1976
γ
1
0
−1
50
100
200
500
1000
Pu

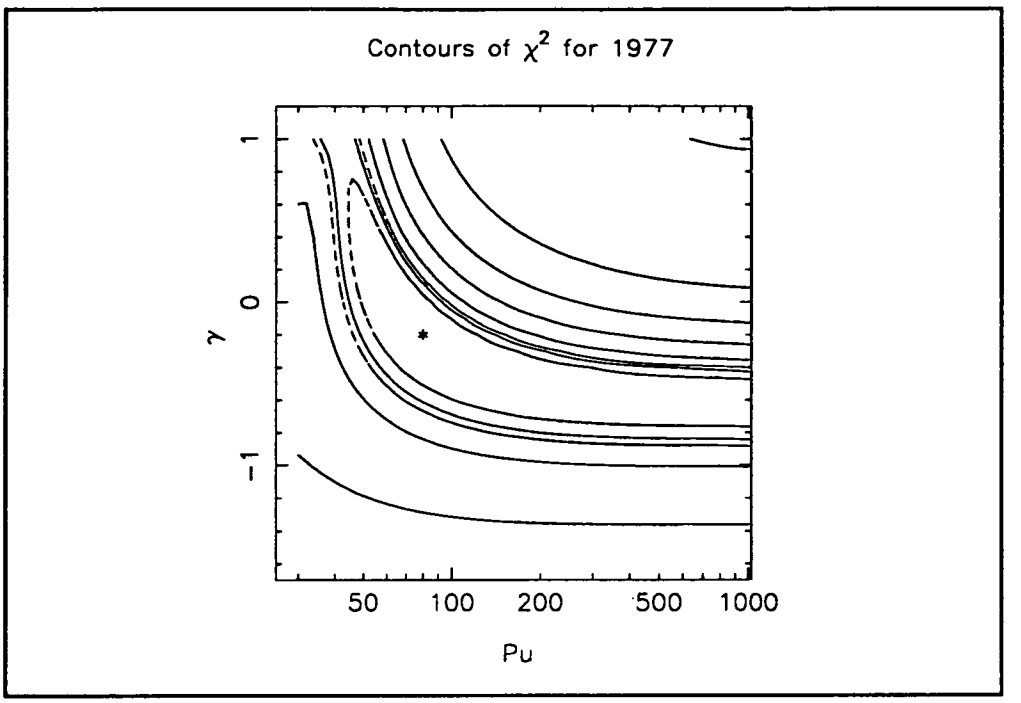
Contours of χ^2 for 1977
1
0
−1
γ
50
100
200
500
1000
Pu

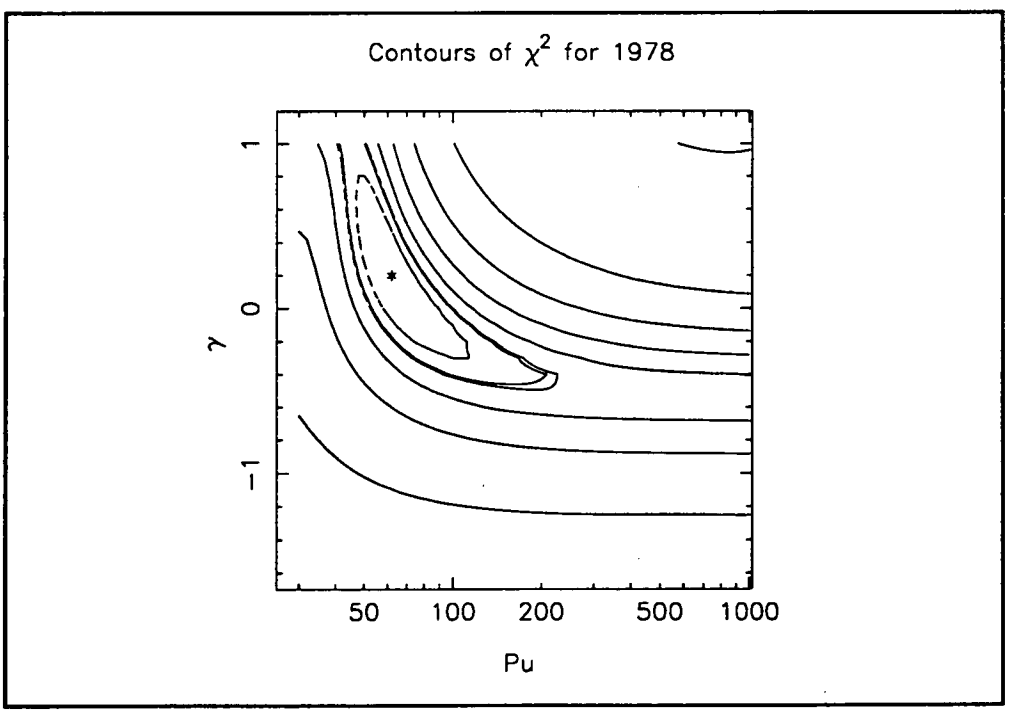
Contours of χ^2 for 1978
1
0
−1
γ
50
100
200
500
1000
Pu

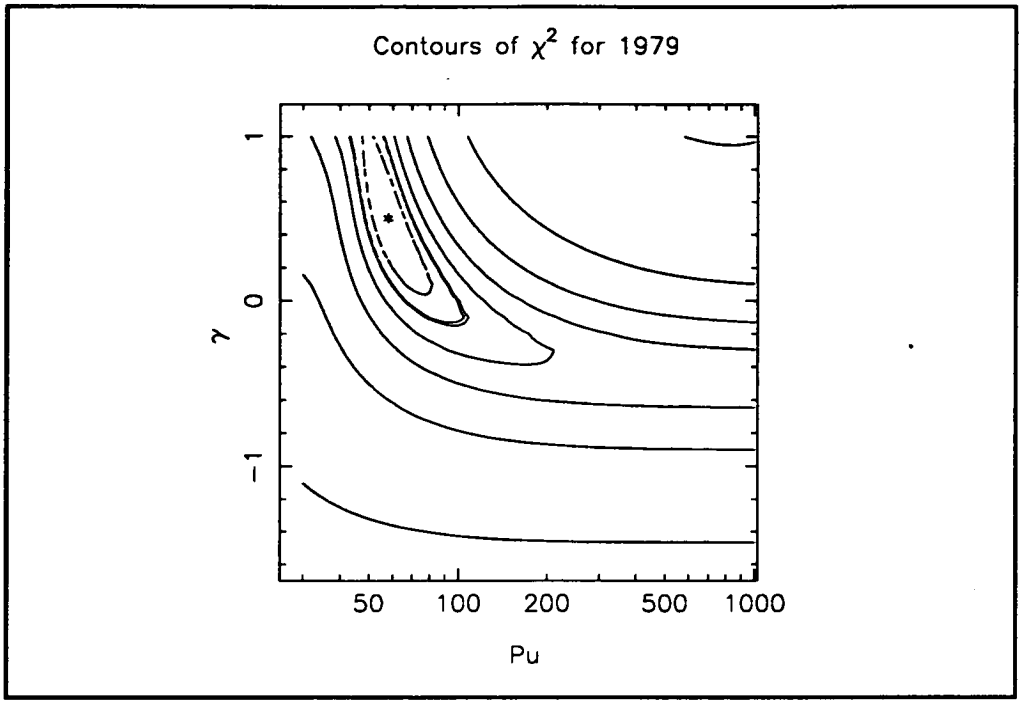
Contours of χ^2 for 1979
1
0
−1
γ
50
100
200
500
1000
Pu

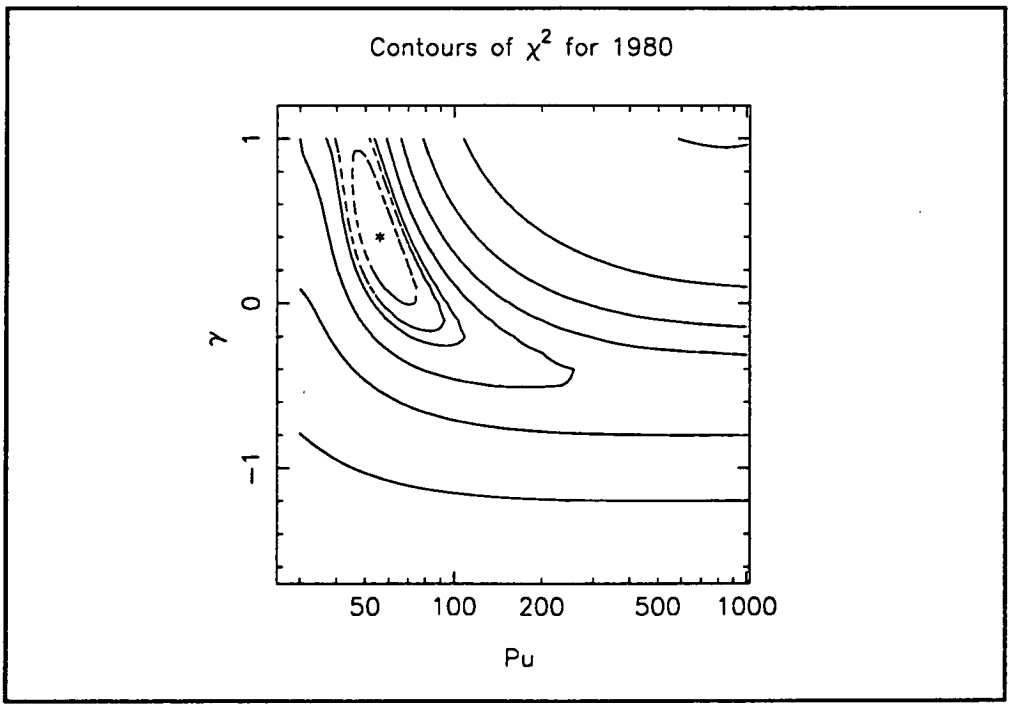
Contours of χ^2 for 1980
1
0
−1
γ
50
100
200
500
1000
Pu

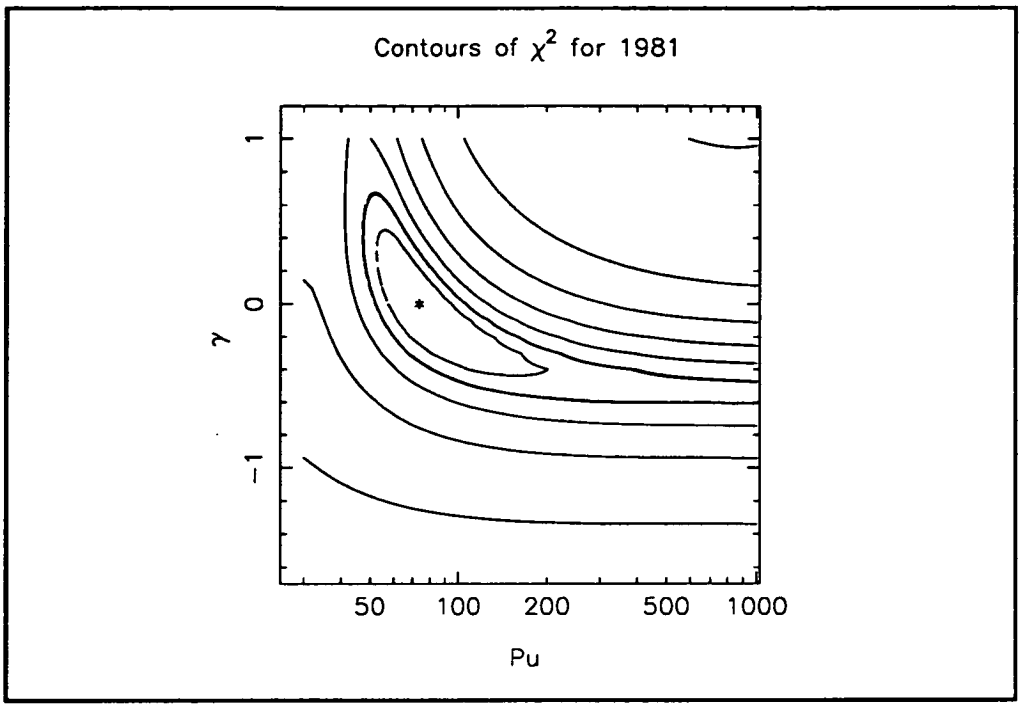
Contours of χ^2 for 1981
1
0
−1
γ
50
100
200
500
1000
Pu

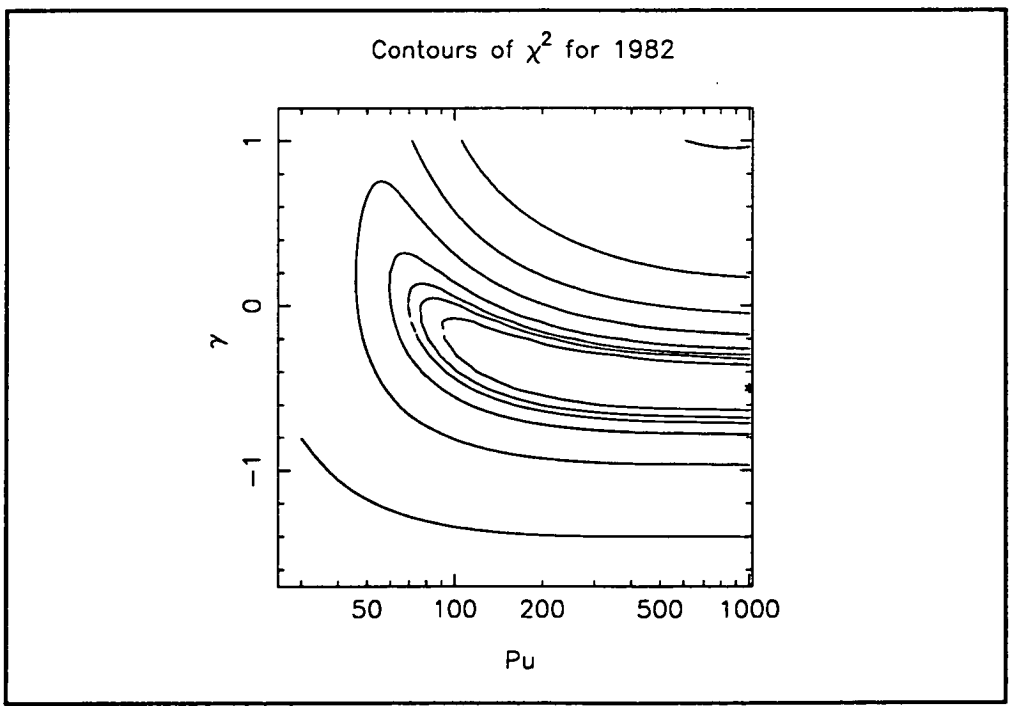
Contours of χ^2 for 1982
1
0
−1
γ
50
100
200
500
1000
Pu

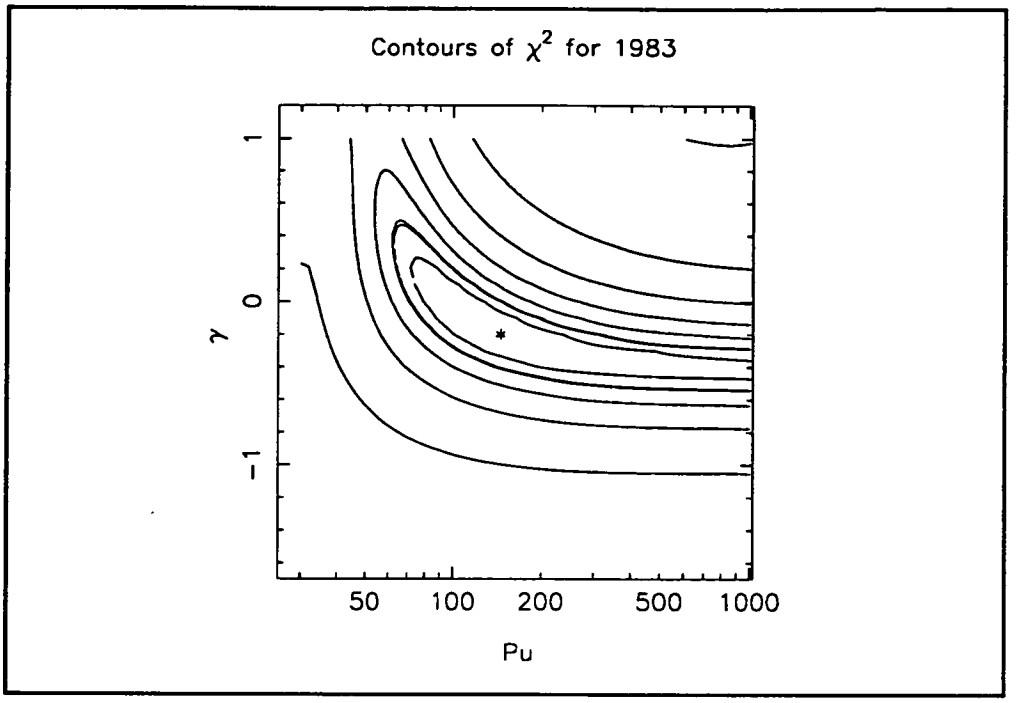
Contours of χ^2 for 1983
1
0
−1
γ
50
100
200
500
1000
Pu

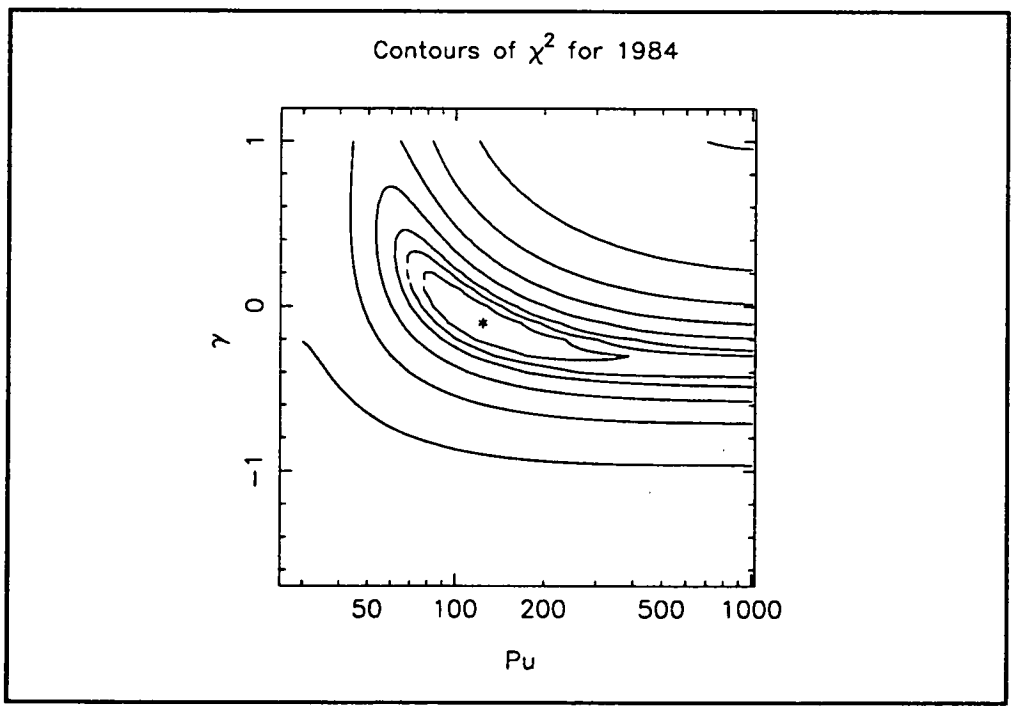
Contours of χ^2 for 1984
1
0
−1
γ
50
100
200
500
1000
Pu

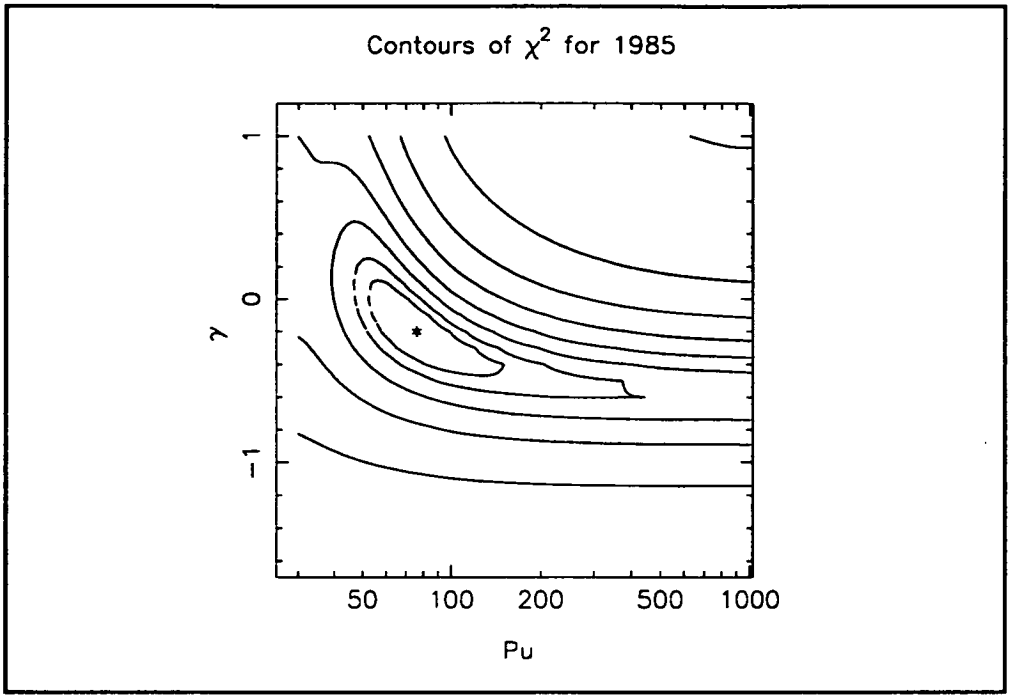
Contours of χ^2 for 1985
γ
1
0
−1
50
100
200
500
1000
Pu

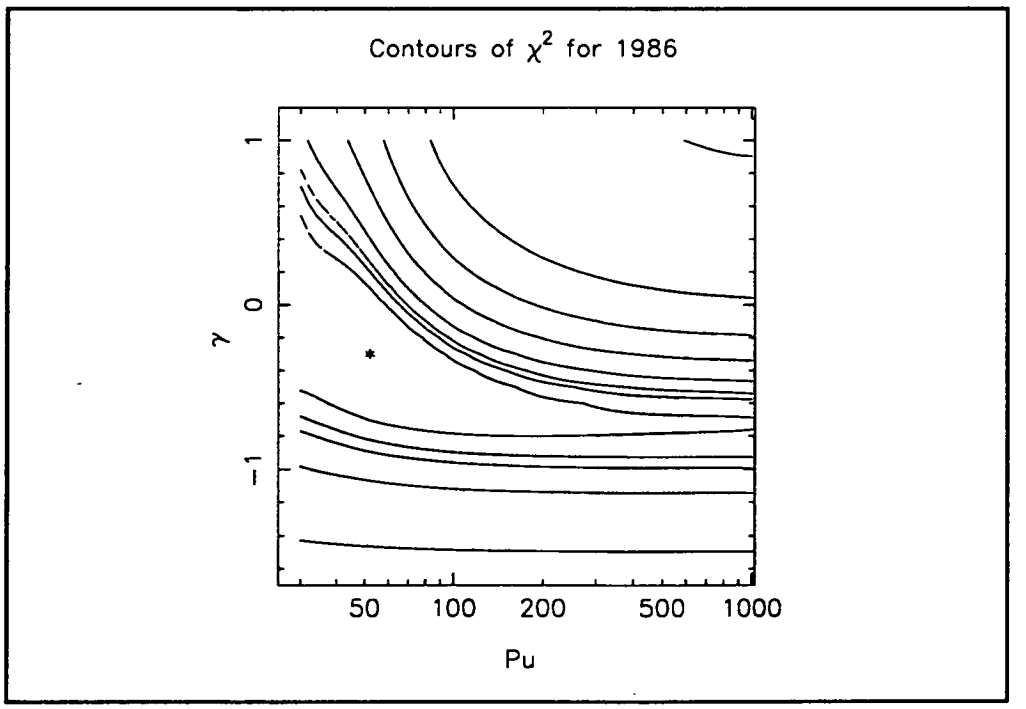
Contours of χ^2 for 1986
γ
1
0
−1
50
100
200
500
1000
Pu

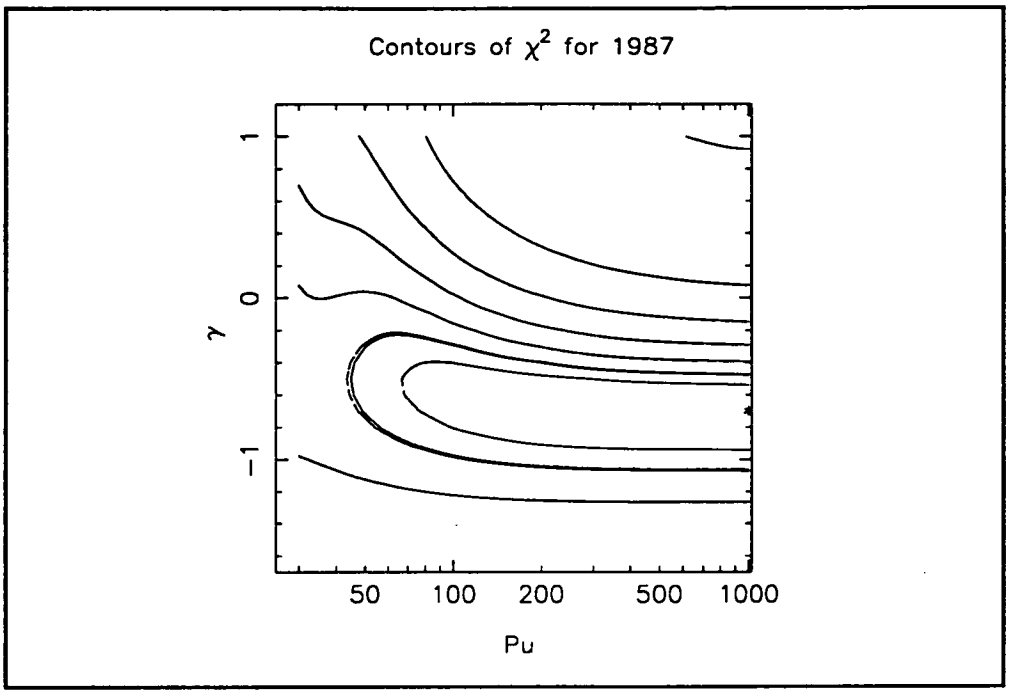
Contours of χ^2 for 1987
1
0
−1
γ
50
100
200
500
1000
Pu

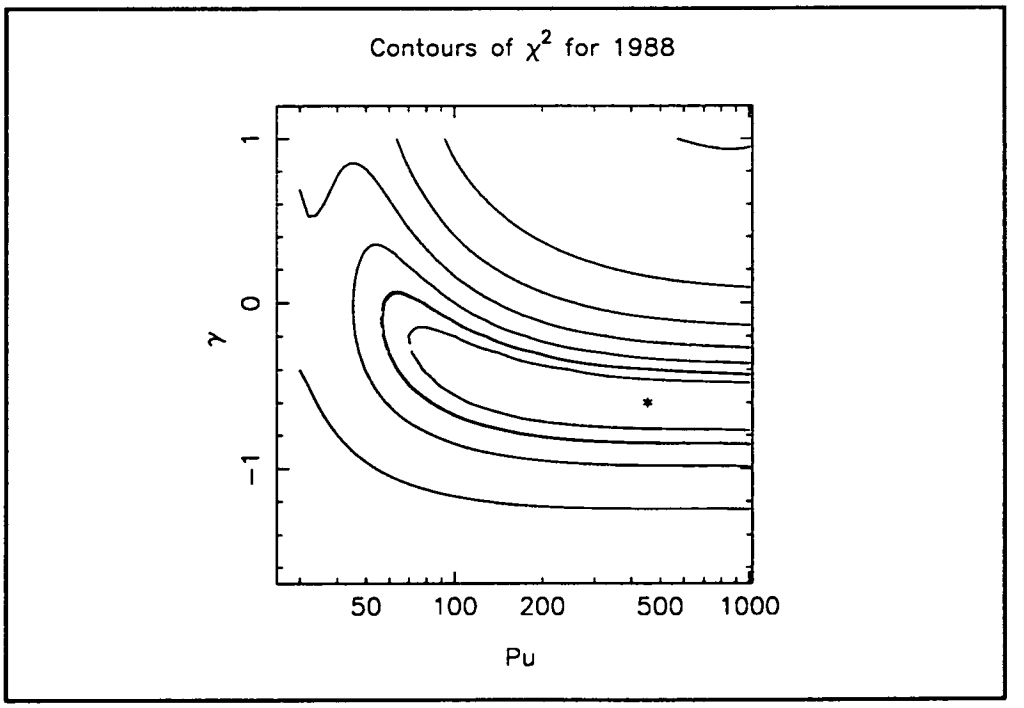
Contours of χ^2 for 1988
1
0
−1
γ
50
100
200
500
1000
Pu

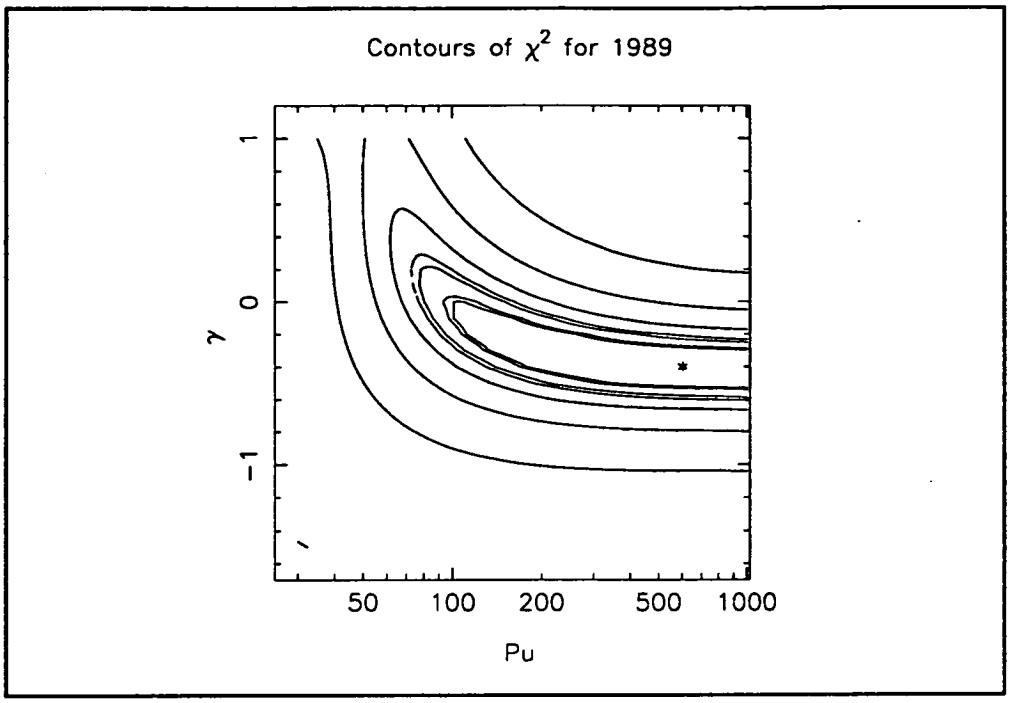
Contours of χ^2 for 1989
γ
1
0
−1
50
100
200
500
1000
Pu

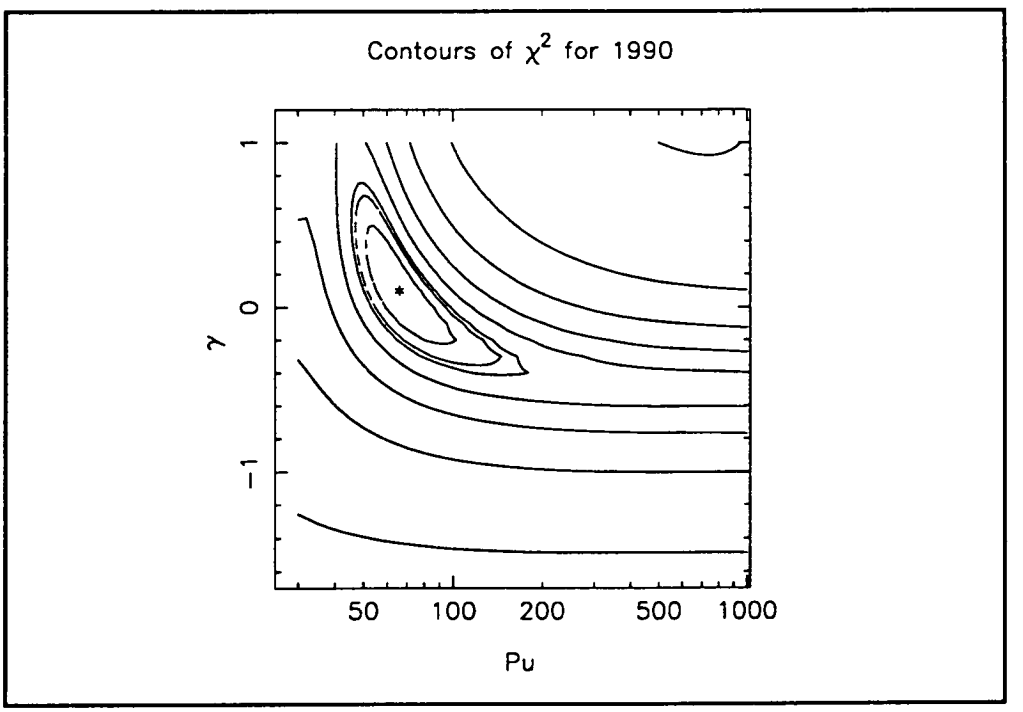
Contours of χ^2 for 1990
γ
1
0
−1
50
100
200
500
1000
Pu

APPENDIX 5

MODULATION PARAMETERS $\overline{\lambda_{||}G_r}$ AND $G_{|Z|}$

This appendix contains plots of the modulation parameters $\overline{\lambda_{||}G_r}$ and $G_{|Z|}$ calculated from measurements of the solar diurnal variation from 1957 to 1990. See equations (3.16) and (3.20) and Section 3.1 for the description of the method of calculating these quantities. The rigidity spectrum assumed for the solar diurnal anisotropy when calculating these parameters was ($\gamma = 0$, $P_u = 100$ GV).

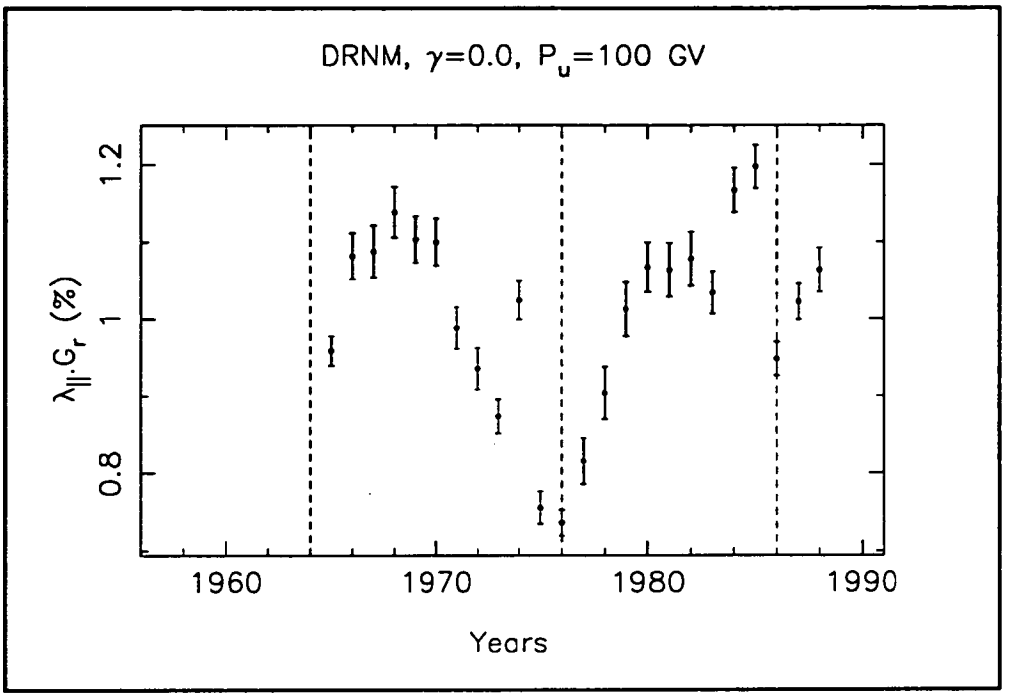
DRNM, γ=0.0, P_u=100 GV
λ_||·G_r (%)
0.8
1
1.2
1960
1970
1980
1990
Years

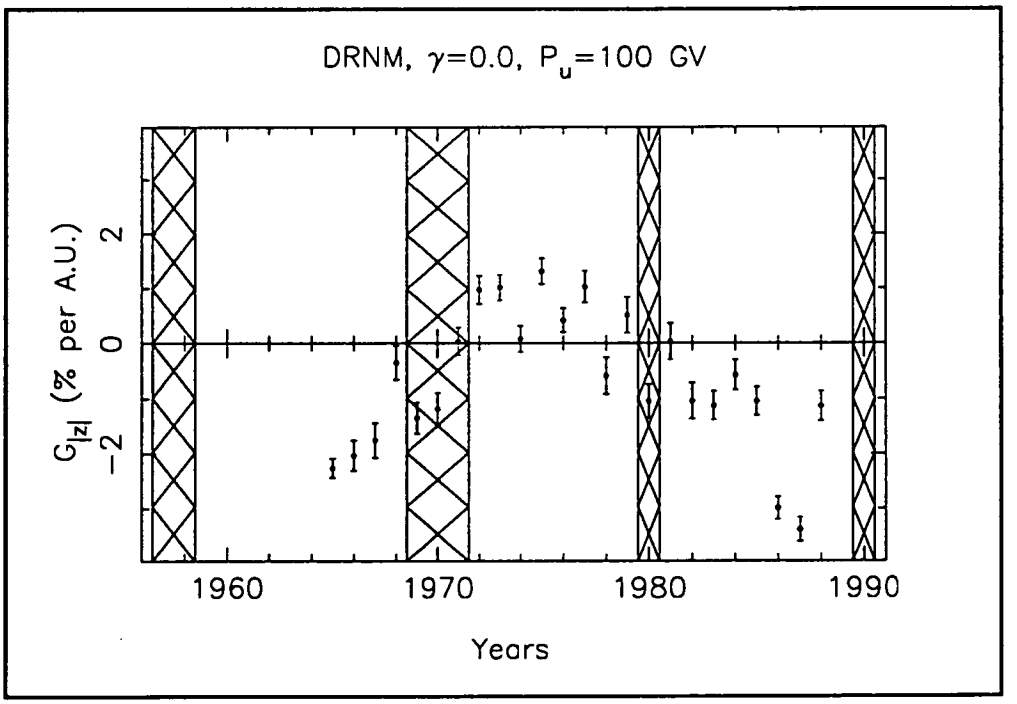
DRNM, γ=0.0, P_u=100 GV
G_|z| (% per A.U.)
−2
0
2
1960
1970
1980
1990
Years

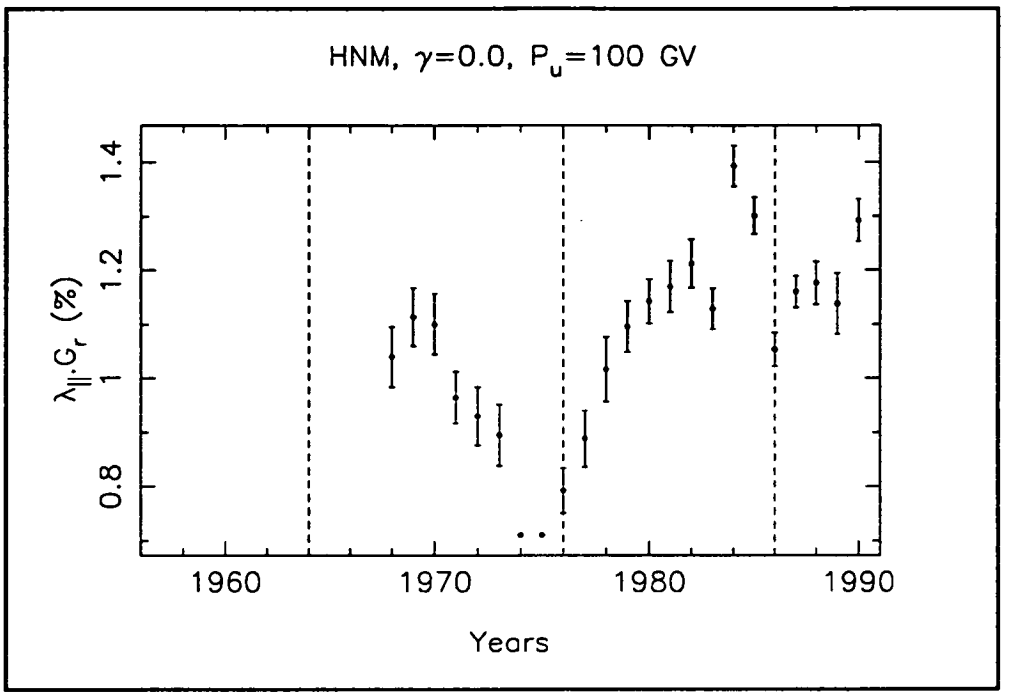
HNM, γ=0.0, P_u=100 GV
λ_||.G_r (%)
0.8
1
1.2
1.4
1960
1970
1980
1990
Years

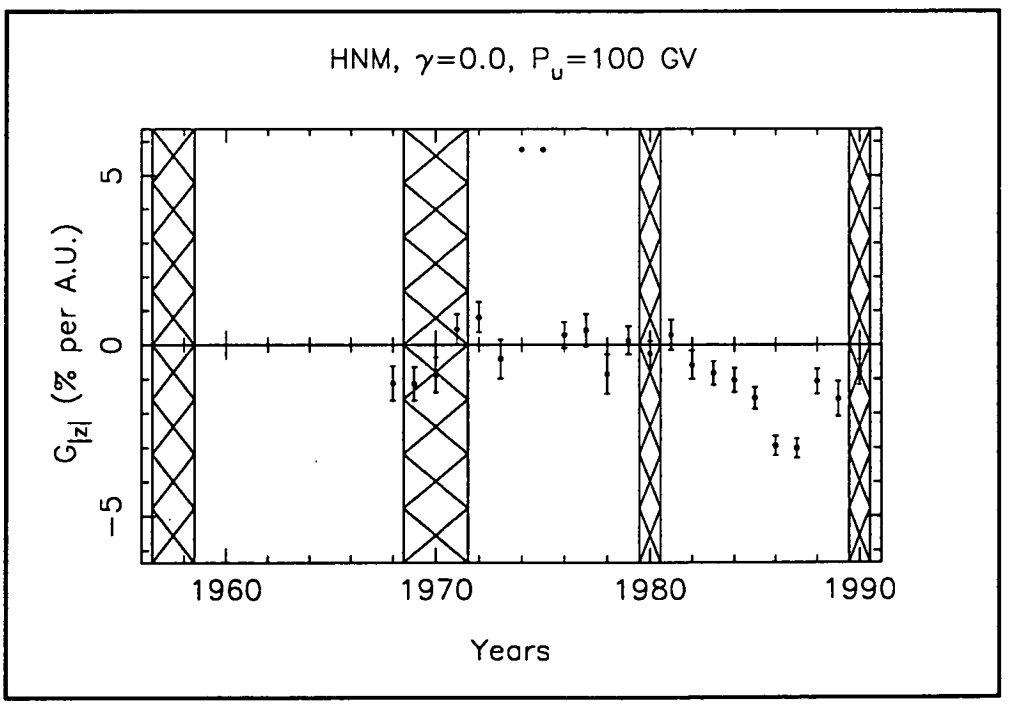
HNM, γ=0.0, P_u=100 GV
G_|z| (% per A.U.)
−5
0
5
1960
1970
1980
1990
Years

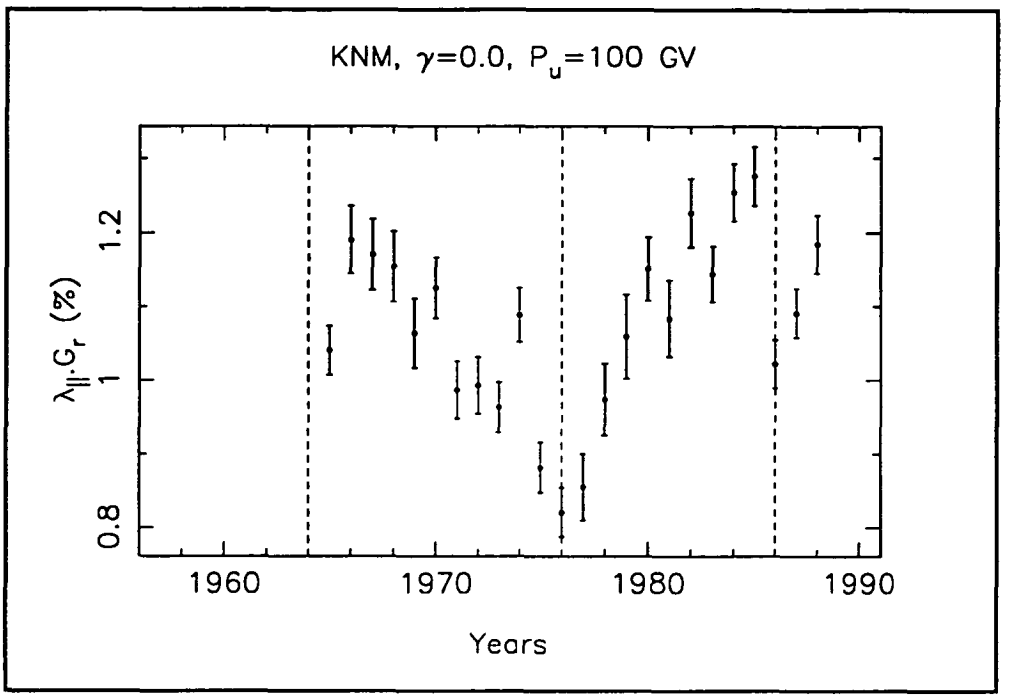
KNM, γ=0.0, P_u=100 GV
λ_||.G_r (%)
0.8
1
1.2
1960
1970
1980
1990
Years

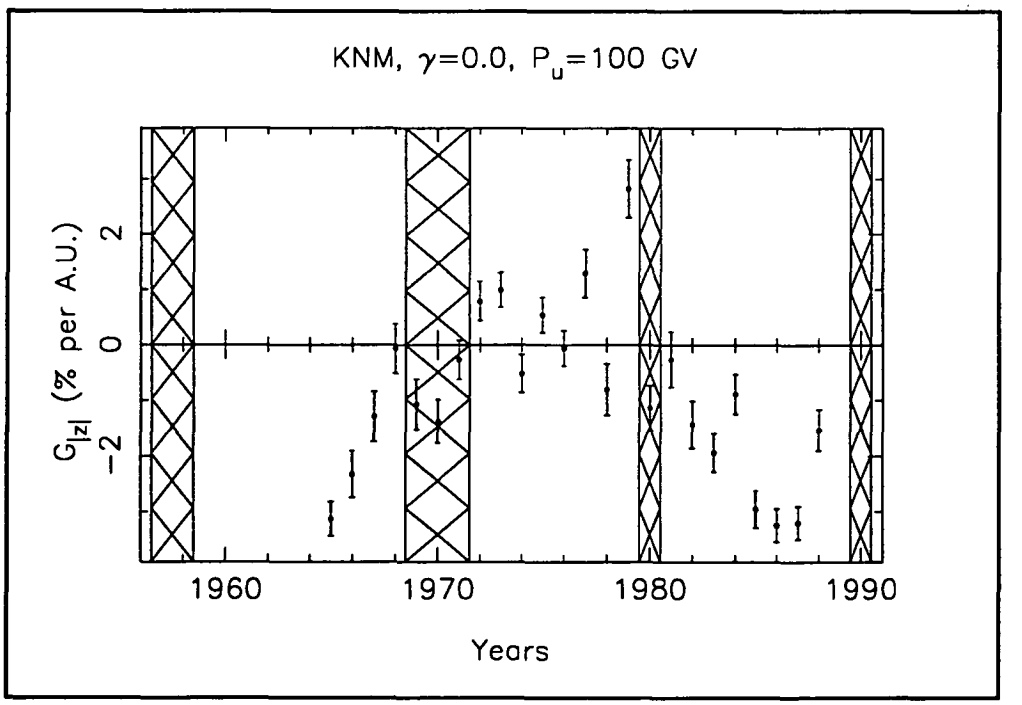
KNM, γ=0.0, P_u=100 GV
G_|z| (% per A.U.)
−2
0
2
1960
1970
1980
1990
Years

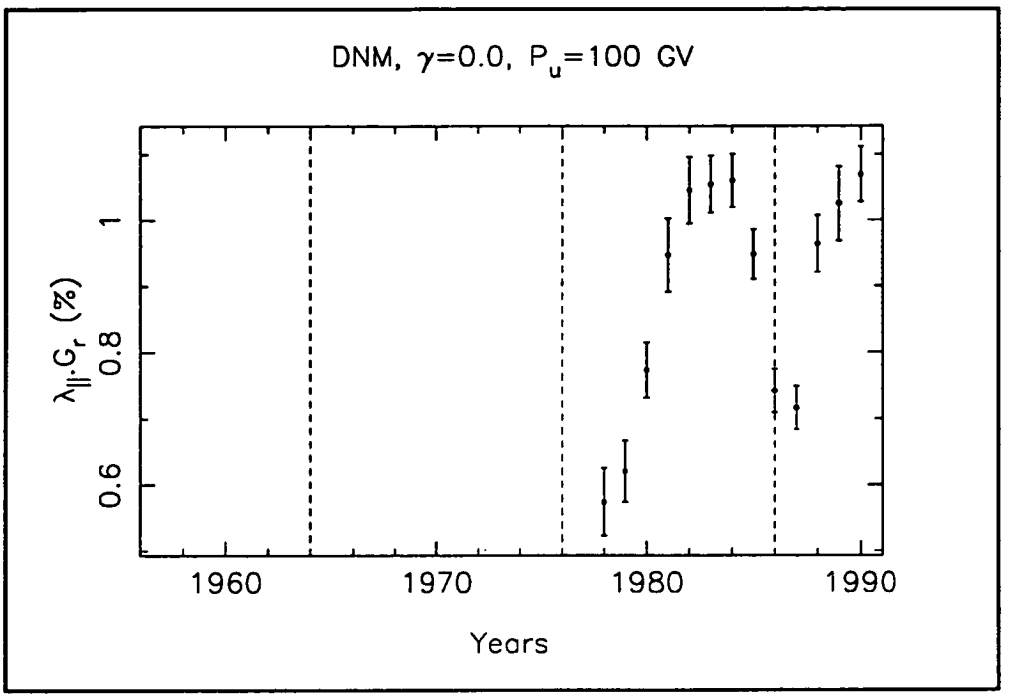
DNM, γ=0.0, P_u=100 GV
λ_||.G_r (%)
0.6
0.8
1
1960
1970
1980
1990
Years

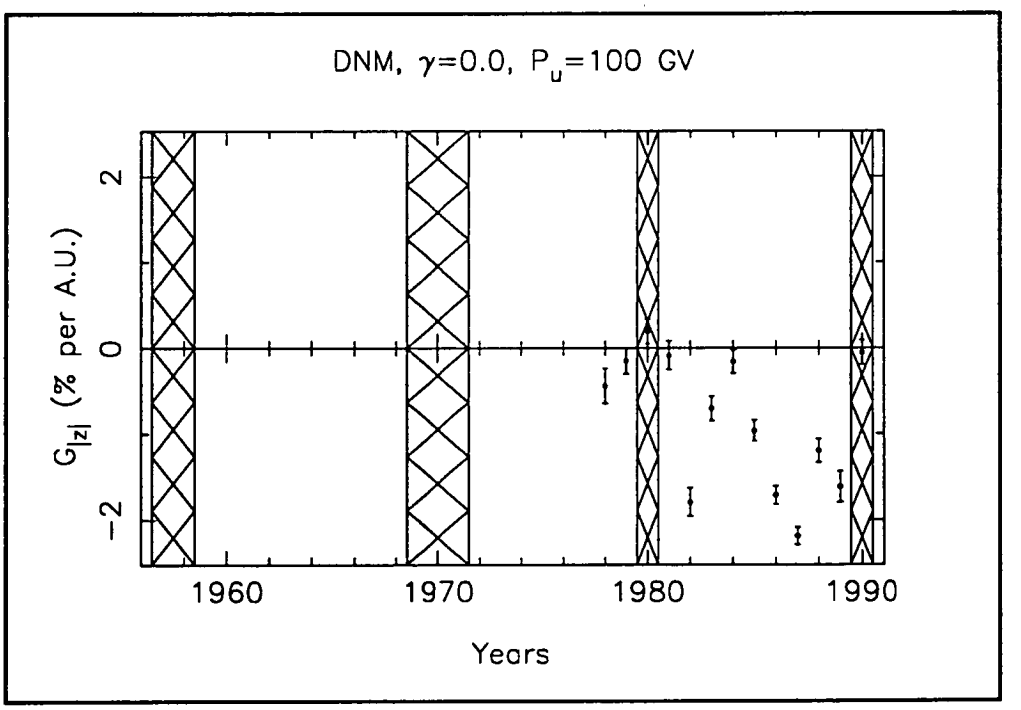
DNM, γ=0.0, P_u=100 GV
G_|z| (% per A.U.)
−2
0
2
1960
1970
1980
1990
Years

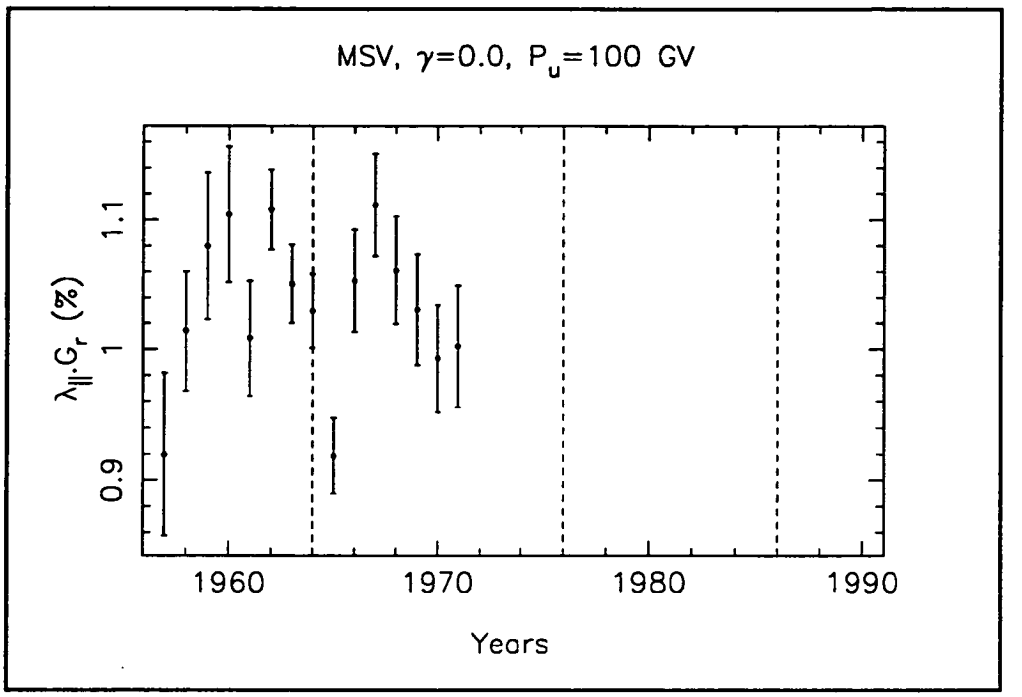
MSV, γ=0.0, P_u=100 GV
λ_∥.G_r (%)
0.9
1
1.1
1960
1970
1980
1990
Years

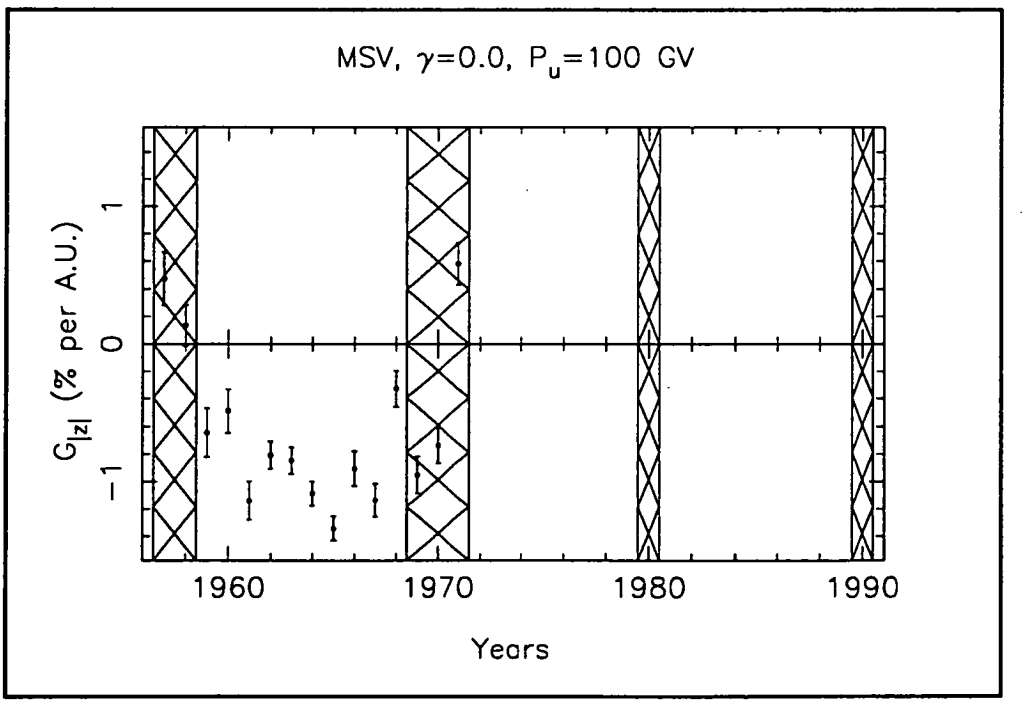
MSV, γ=0.0, P_u=100 GV
G_|z| (% per A.U.)
−1
0
1
1960
1970
1980
1990
Years

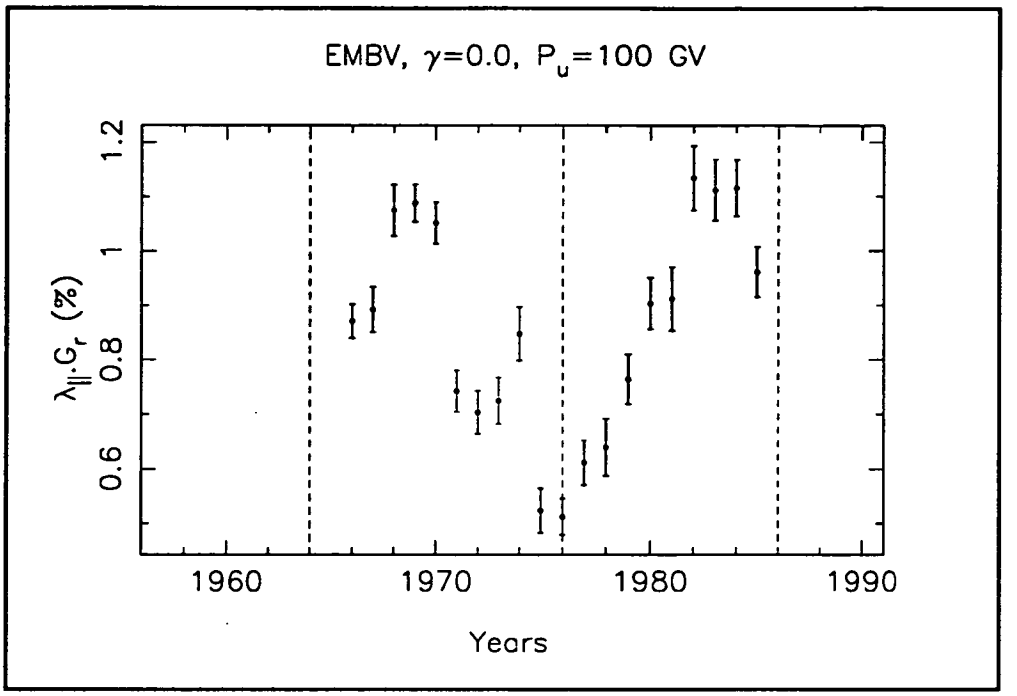
EMBV, γ=0.0, P_u=100 GV
λ_∥.G_r (%)
0.6
0.8
1
1.2
1960
1970
1980
1990
Years

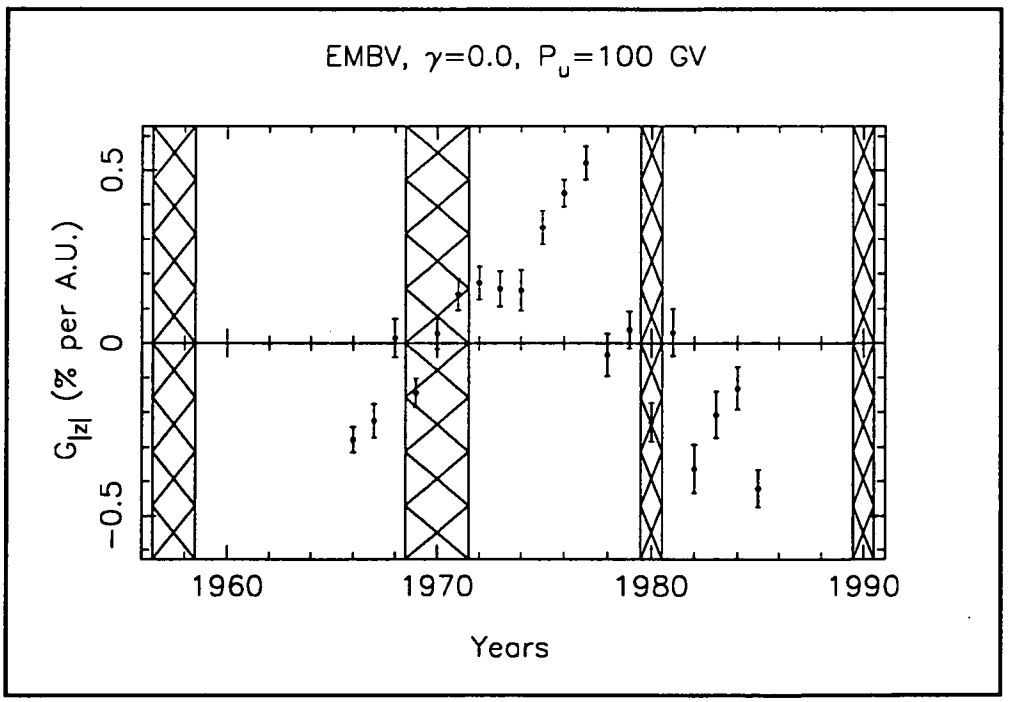
EMBV, γ=0.0, P_u=100 GV
G_|z| (% per A.U.)
−0.5
0
0.5
1960
1970
1980
1990
Years

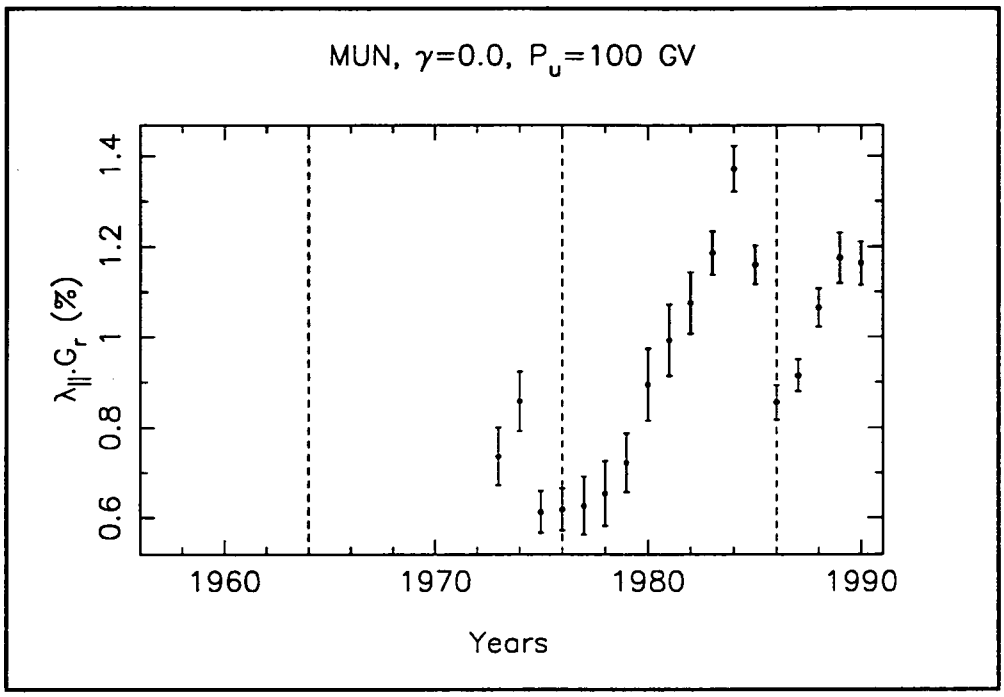
MUN, γ=0.0, P_u=100 GV
λ_||.G_r (%)
0.6
0.8
1
1.2
1.4
1960
1970
1980
1990
Years

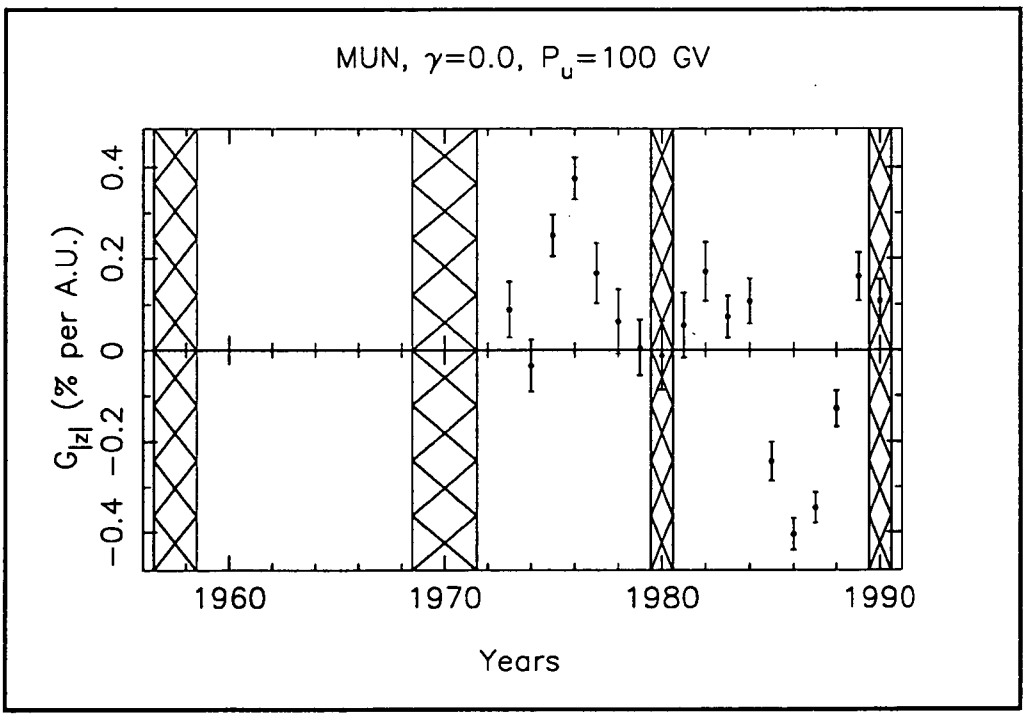
MUN, γ=0.0, P_u=100 GV
G_|z| (% per A.U.)
−0.4
−0.2
0
0.2
0.4
1960
1970
1980
1990
Years

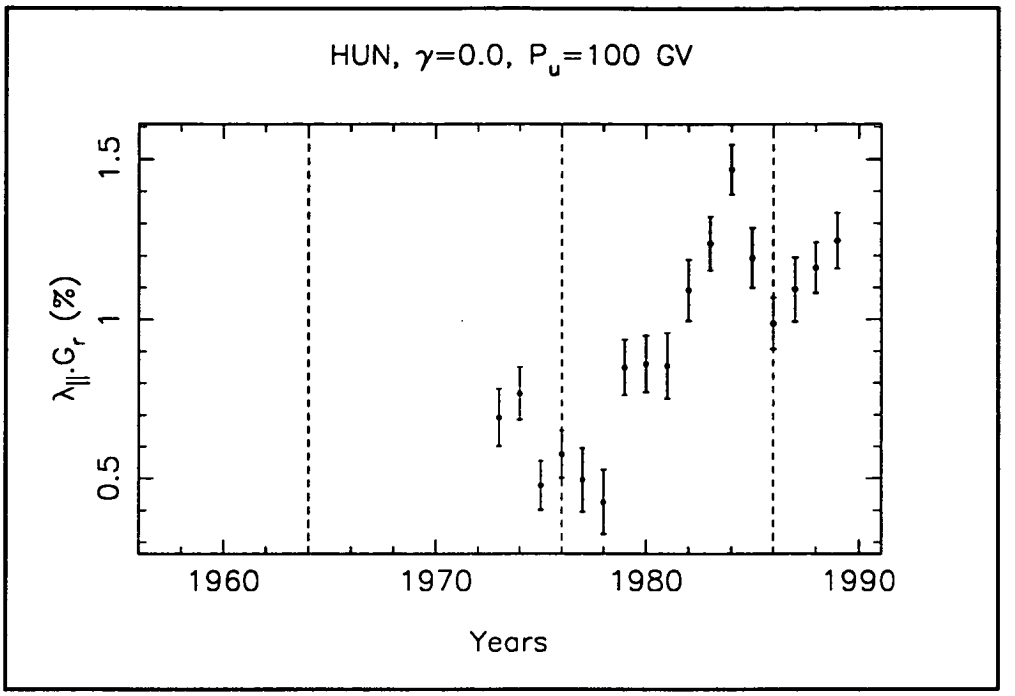
HUN, γ=0.0, P_u=100 GV
λ||.G_r (%)
0.5
1
1.5
1960
1970
1980
1990
Years

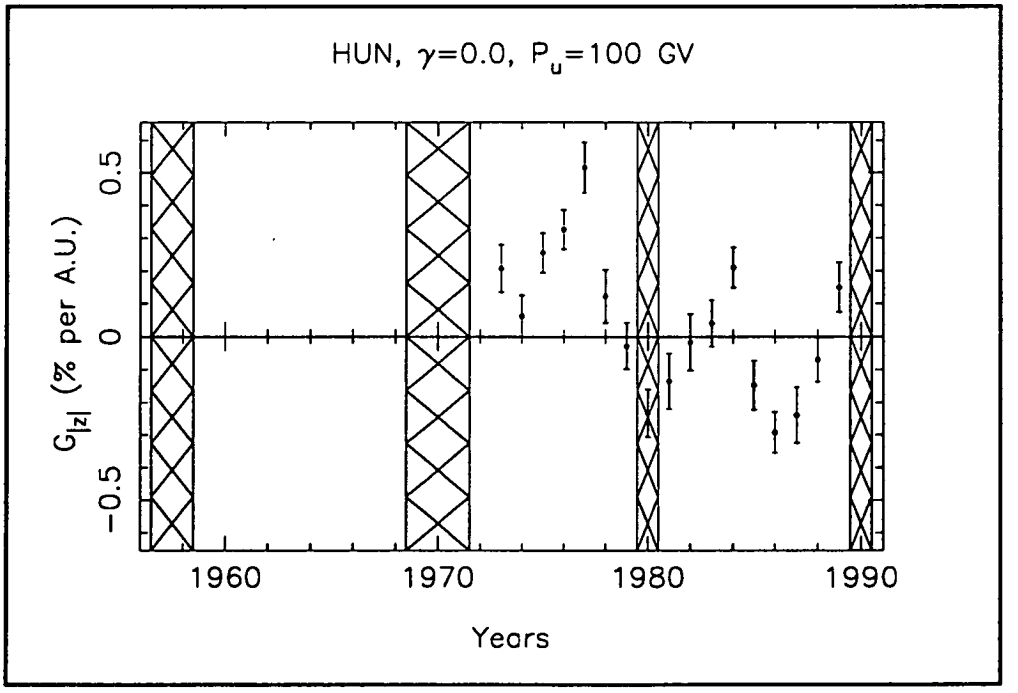
HUN, γ=0.0, P_u=100 GV
G|z| (% per A.U.)
−0.5
0
0.5
1960
1970
1980
1990
Years

APPENDIX 6

SOLUTIONS TO EQUATION (4.14)

This appendix contains the derivation of the solutions to equation (4.14).

We define (equation 4.14) as

$$\chi^2 = \sum_{i=1}^{N} w_i \left[\left(a_{NS,i} - a_{NS} \right)^2 + \left(b_{NS,i} - b_{NS} \right)^2 \right]$$

$$= \sum_{i=1}^{N} w_i \left[\left(a_{NS,i} - \left(c^1_{1,i} \xi^{NS}_x + s^1_{1,i} \xi^{NS}_y \right) \right)^2 + \left(b_{NS,i} - \left(-s^1_{1,i} \xi^{NS}_x + c^1_{1,i} \xi^{NS}_y \right) \right)^2 \right]$$

where :

$$\eta_{NS} \sin\theta_R = \sqrt{\left(\xi^{NS}_x \right)^2 + \left(\xi^{NS}_y \right)^2}$$

$$\phi_{NS} = \frac{24}{2\pi} \arctan\left(\frac{\xi^{NS}_y}{\xi^{NS}_x} \right)$$

$$D^G(t) = a_{NS} \cos\frac{2\pi t}{24} + b_{NS} \sin\frac{2\pi t}{24}$$

and $$a_{NS} = c^1_1 \xi^{NS}_x + s^1_1 \xi^{NS}_y$$

$$b_{NS} = -s^1_1 \xi^{NS}_x + c^1_1 \xi^{NS}_y$$

To analytically derive the best-fit (ξ^{NS}_x, ξ^{NS}_y) one notes that any minimum in the χ^2 function (as a function of varying ξ^{NS}_x or ξ^{NS}_y) will mean :

$$\frac{\partial}{\partial \xi^{NS}_x} \left(\chi^2 \right) = 0$$

and $$\frac{\partial}{\partial \xi^{NS}_y} \left(\chi^2 \right) = 0$$

Therefore :

$$\frac{\partial}{\partial \xi_x^{NS}}\left(\chi^2\right) = \sum_{i=1}^{N} w_i 2\left[a_{NS,i} - \left(c_{1,i}^1 \xi_x^{NS} + s_{1,i}^1 \xi_y^{NS}\right)\right]\left(-c_{1,i}^1\right)$$

$$+ \sum_{i=1}^{N} w_i 2\left[b_{NS,i} - \left(-s_{1,i}^1 \xi_x^{NS} + c_{1,i}^1 \xi_y^{NS}\right)\right]\left(s_{1,i}^1\right)$$

$$= 2\xi_x^{NS} \sum_{i=1}^{N} w_i \left(\left(c_{1,i}^1\right)^2 + \left(s_{1,i}^1\right)^2\right)$$

$$+ 2\sum_{i=1}^{N} w_i b_{NS,i} s_{1,i}^1$$

$$- 2\sum_{i=1}^{N} w_i a_{NS,i} c_{1,i}^1$$

$$= 0$$

Which implies :

$$\xi_x^{NS} \sum_{i=1}^{N} w_i \left(\left(c_{1,i}^1\right)^2 + \left(s_{1,i}^1\right)^2\right) = \sum_{i=1}^{N} w_i a_{NS,i} c_{1,i}^1 - \sum_{i=1}^{N} w_i b_{NS,i} s_{1,i}^1$$

and

$$\xi_x^{NS} = \frac{\sum_{i=1}^{N} w_i \left(a_{NS,i} c_{1,i}^1 - b_{NS,i} s_{1,i}^1\right)}{\sum_{i=1}^{N} w_i \left(\left(c_{1,i}^1\right)^2 + \left(s_{1,i}^1\right)^2\right)}$$

Similarly

$$\frac{\partial}{\partial \xi_y^{NS}}\left(\chi^2\right) = 2\xi_y^{NS} \sum_{i=1}^{N} w_i \left(\left(c_{1,i}^1\right)^2 + \left(s_{1,i}^1\right)^2\right)$$

$$- 2\sum_{i=1}^{N} w_i a_{NS,i} s_{1,i}^1$$

$$- 2\sum_{i=1}^{N} w_i b_{NS,i} c_{1,i}^1$$

$$= 0$$

when :

$$\xi_y^{NS} = \frac{\sum_{i=1}^{N} w_i \left(a_{NS,i} s_{1,i}^1 + b_{NS,i} c_{1,i}^1 \right)}{\sum_{i=1}^{N} w_i \left(\left(c_{1,i}^1 \right)^2 + \left(s_{1,i}^1 \right)^2 \right)}$$

APPENDIX 7

MODULATION PARAMETERS - $\lambda_{||}$

This appendix contains the yearly average values of $\lambda_{||}$ determined from the solar diurnal anisotropy and the North-South anisotropy in Section 5.2.1.

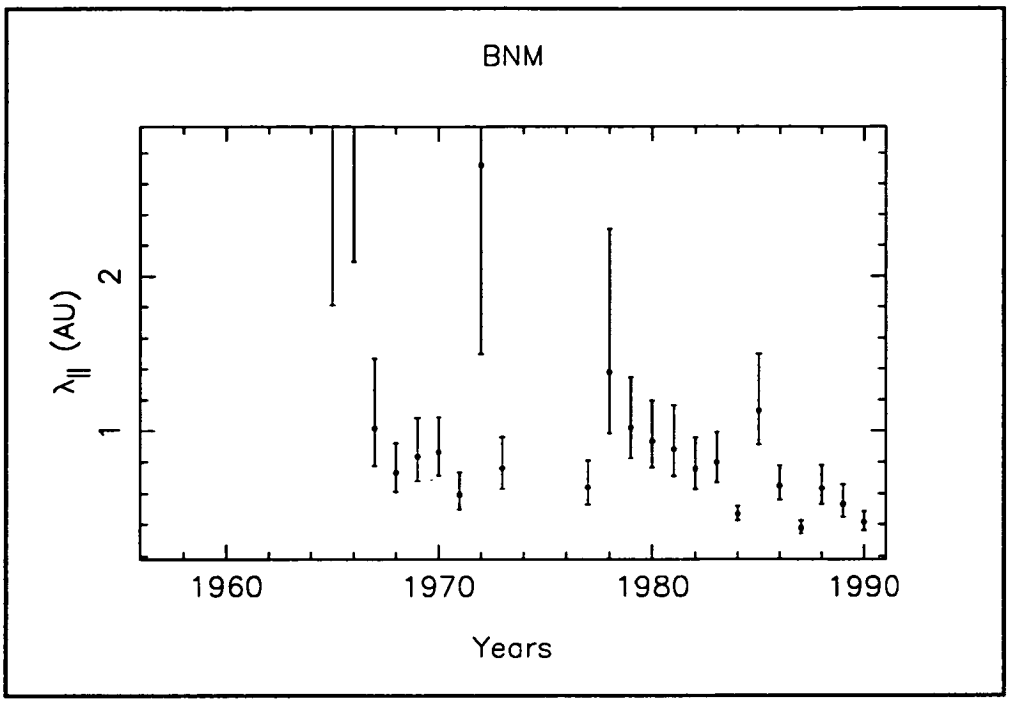

Brisbane neutron monitor. Median rigidity is 28 GV.

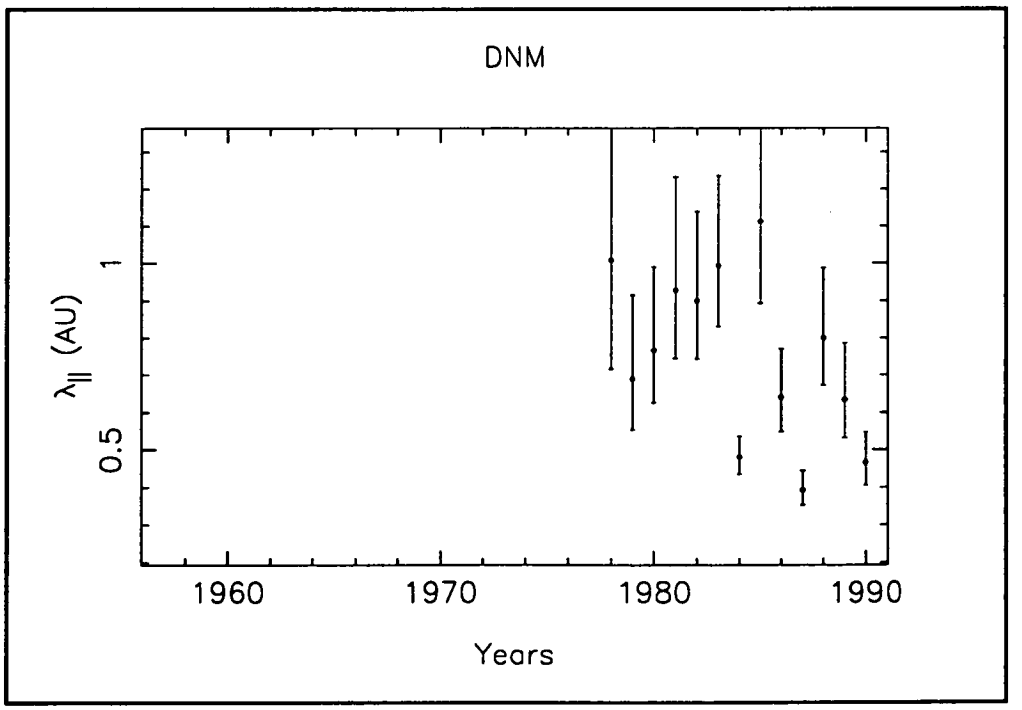

Darwin neutron monitor. Median rigidity is 50 GV.

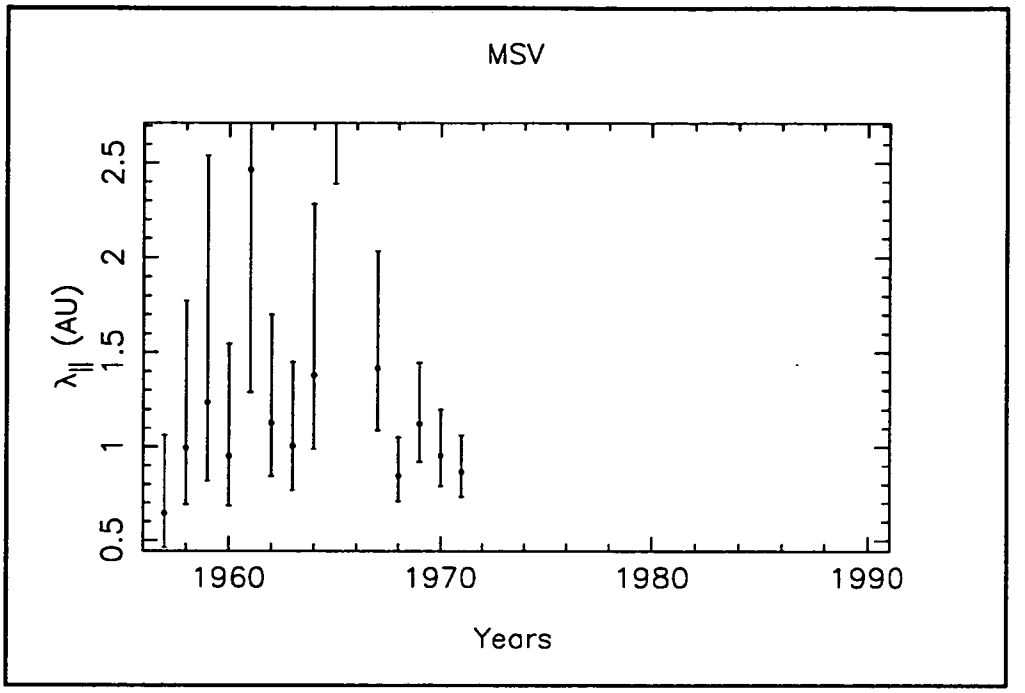

Mawson surface muon telescope. Median rigidity is 50 GV.

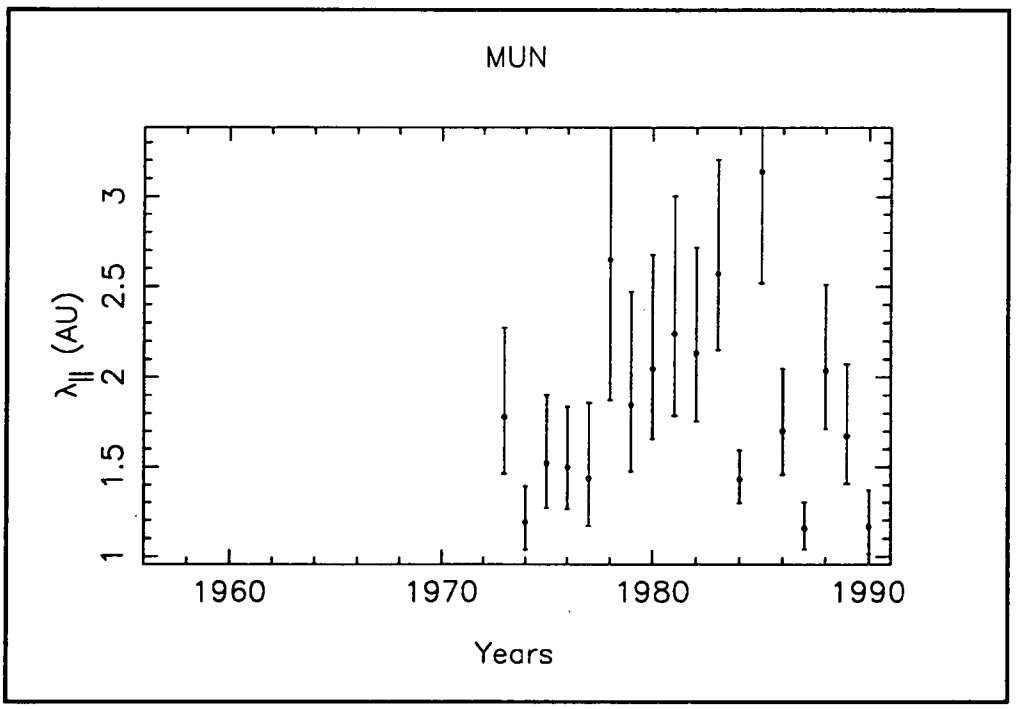

Mawson underground (north) muon telescope. Median rigidity is 165 GV.

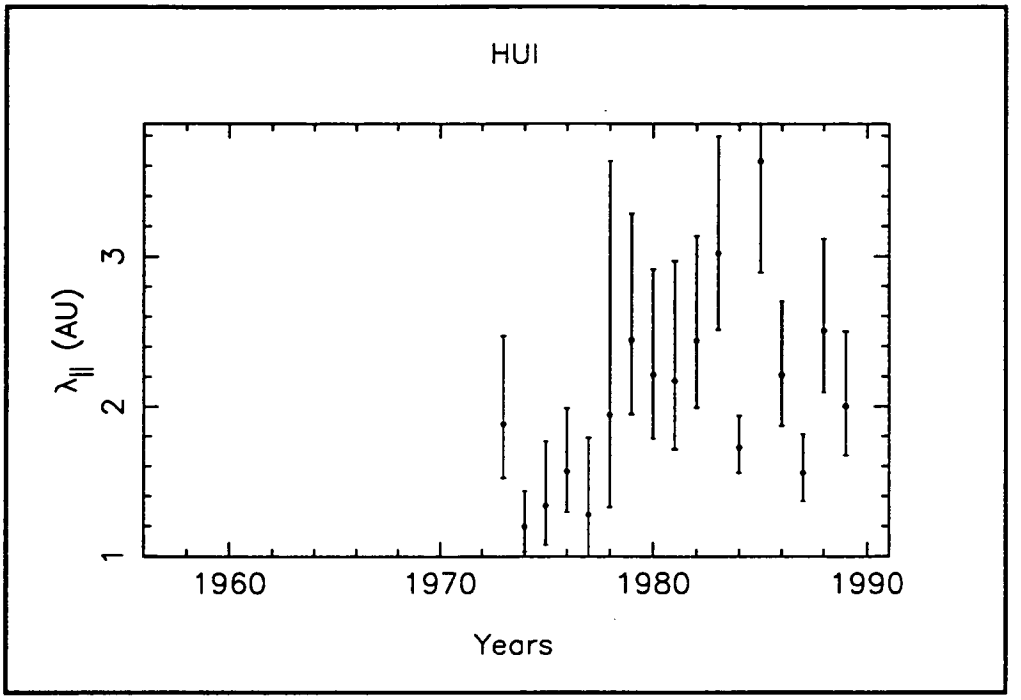

Hobart underground (inclined) muon telescope. Median rigidity is 195 GV.

APPENDIX 8

DEPENDENCE OF MODULATION PARAMETERS ON PERPENDICULAR DIFFUSION

This appendix contains the function dependence of the average values of $\lambda_{||}$, the radial density gradient (G_r) and the bi-directional latitudinal gradient indicator ($G_{|z|}$) around years of solar minimum on the ratio of perpendicular to parallel diffusion (α) of cosmic ray particles in the rigidity range 50 GV to 195 GV. The dependence of the modulation parameters $\lambda_{||}$ and G_r was calculated from the solar diurnal anisotropy and the North-South anisotropy. The method used to do the calculations is presented in Section 5.1.2. The dashed line represents the average results around the years of solar minimum during the A >0 magnetic polarity epoch, the solid line represents the results for the A <0 magnetic polarity epoch 1964 to 1966 and the dashed-dotted line represents the results averaged over the A <0 magnetic polarity epoch 1985 to 1987.

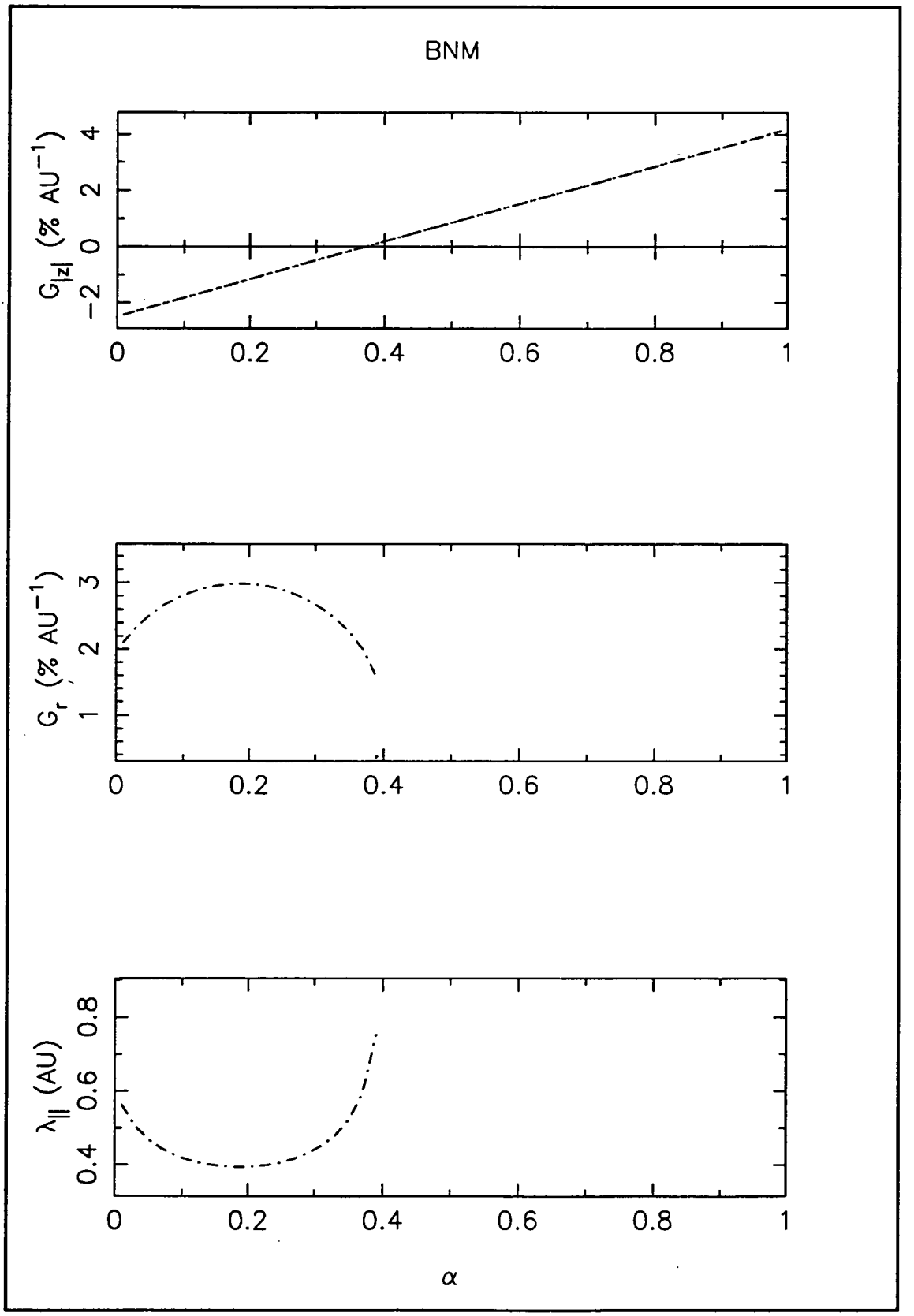

Brisbane neutron monitor. Median rigidity is 28 GV.

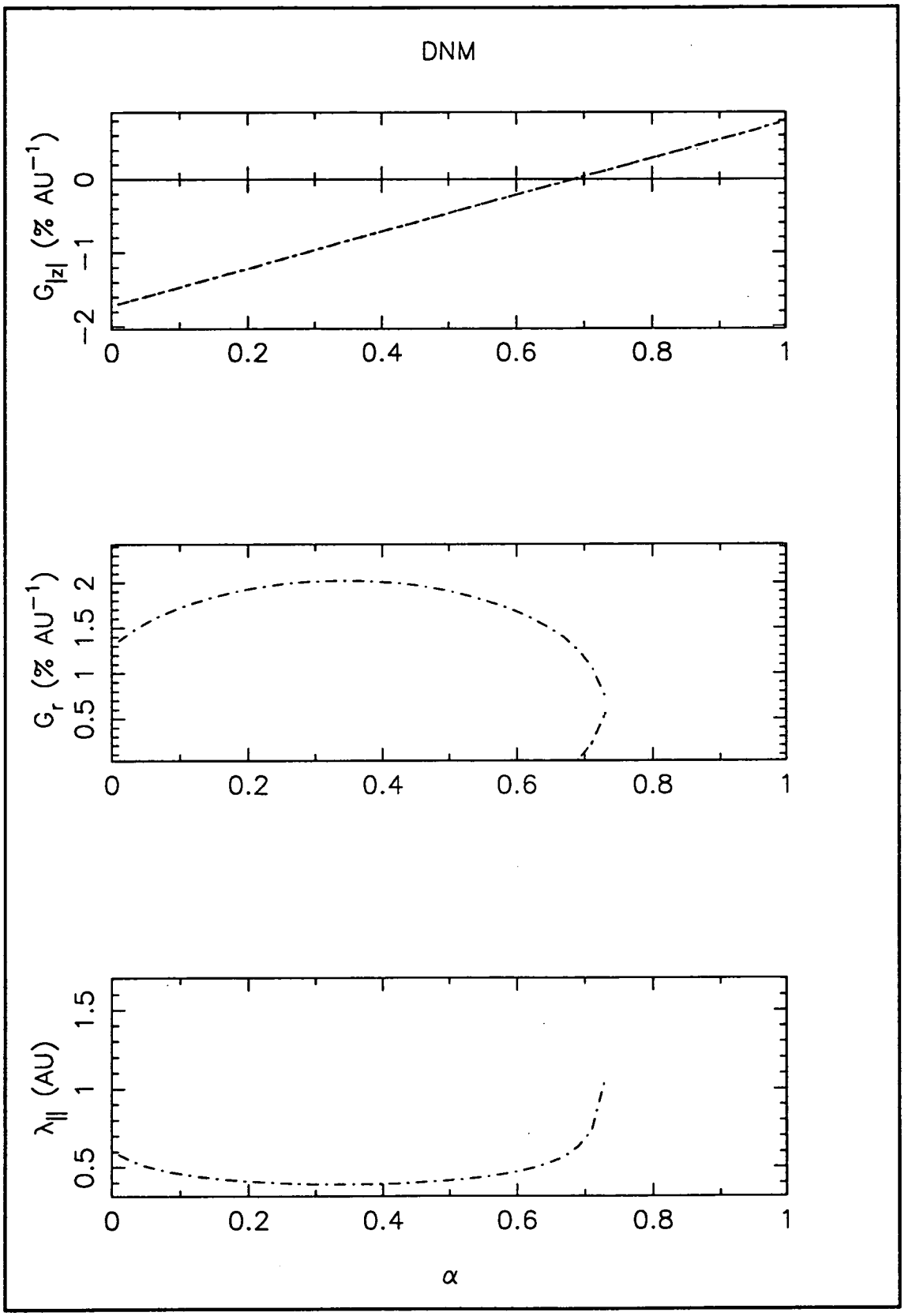

Darwin neutron monitor. Median rigidity is 50 GV.

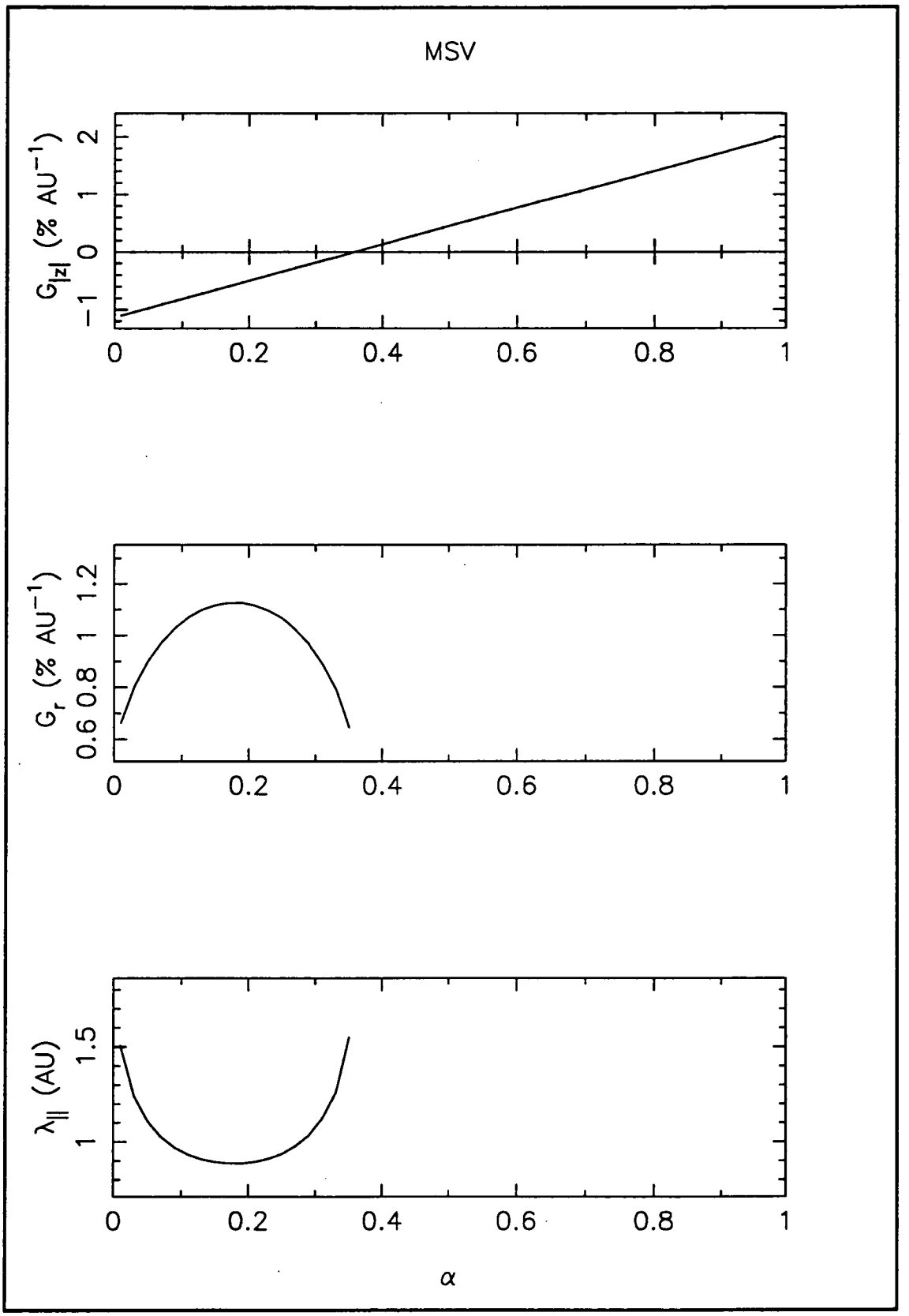

Mawson surface muon telescope. Median rigidity is 50 GV.

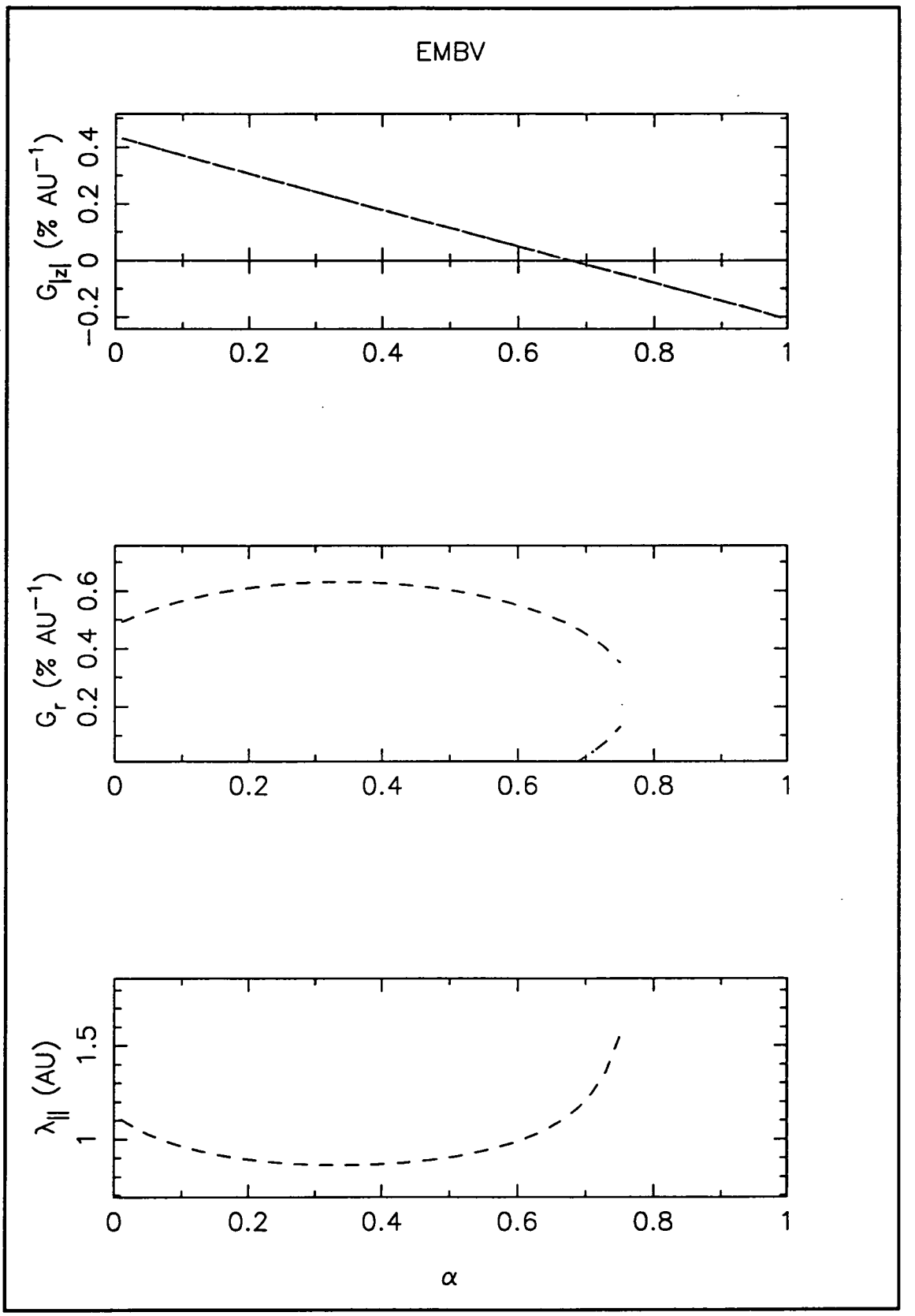

Embudo underground (vertical) muon telescope. Median rigidity is 135 GV.

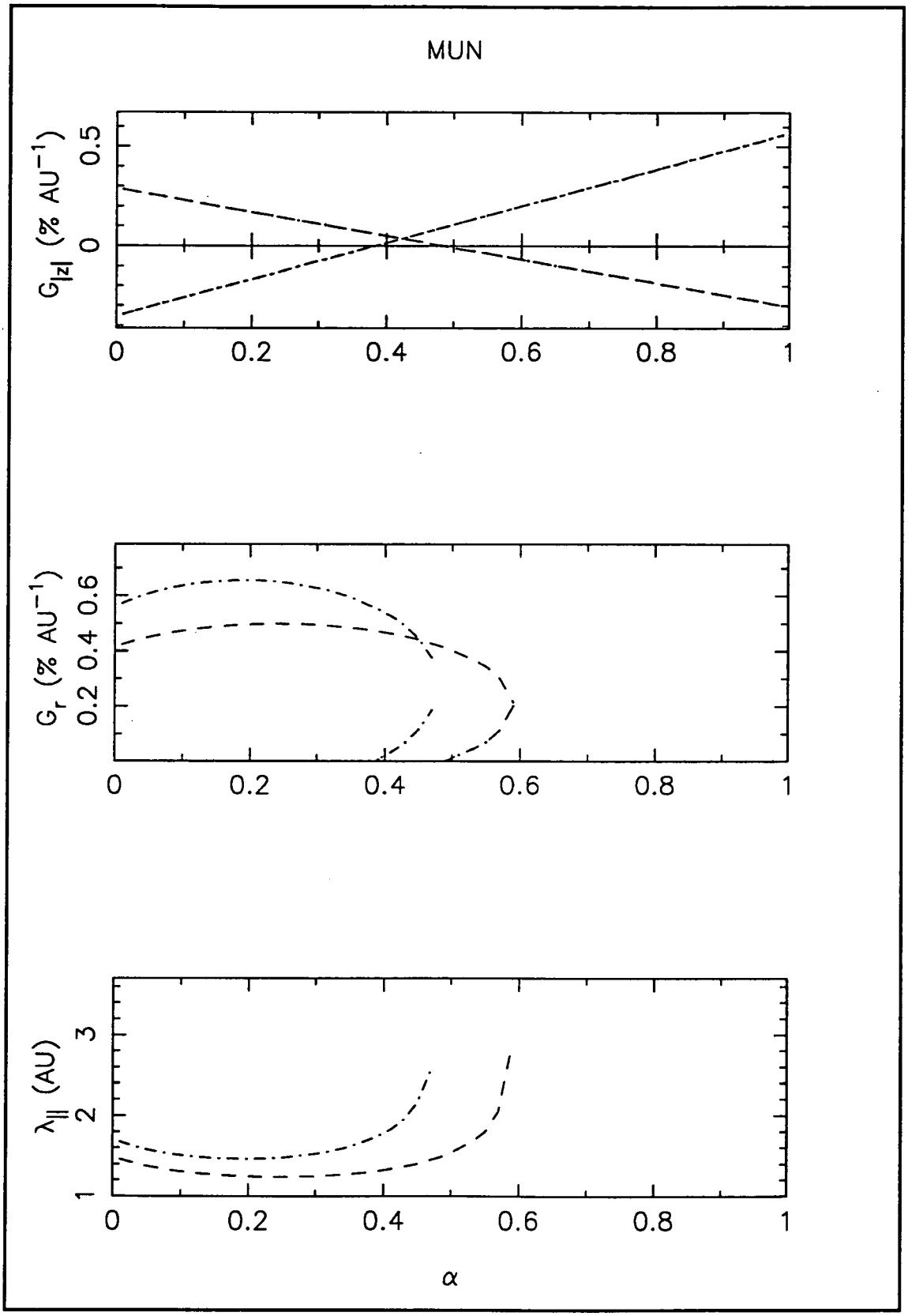

Mawson underground (north) muon telescope. Median rigidity is 165 GV.

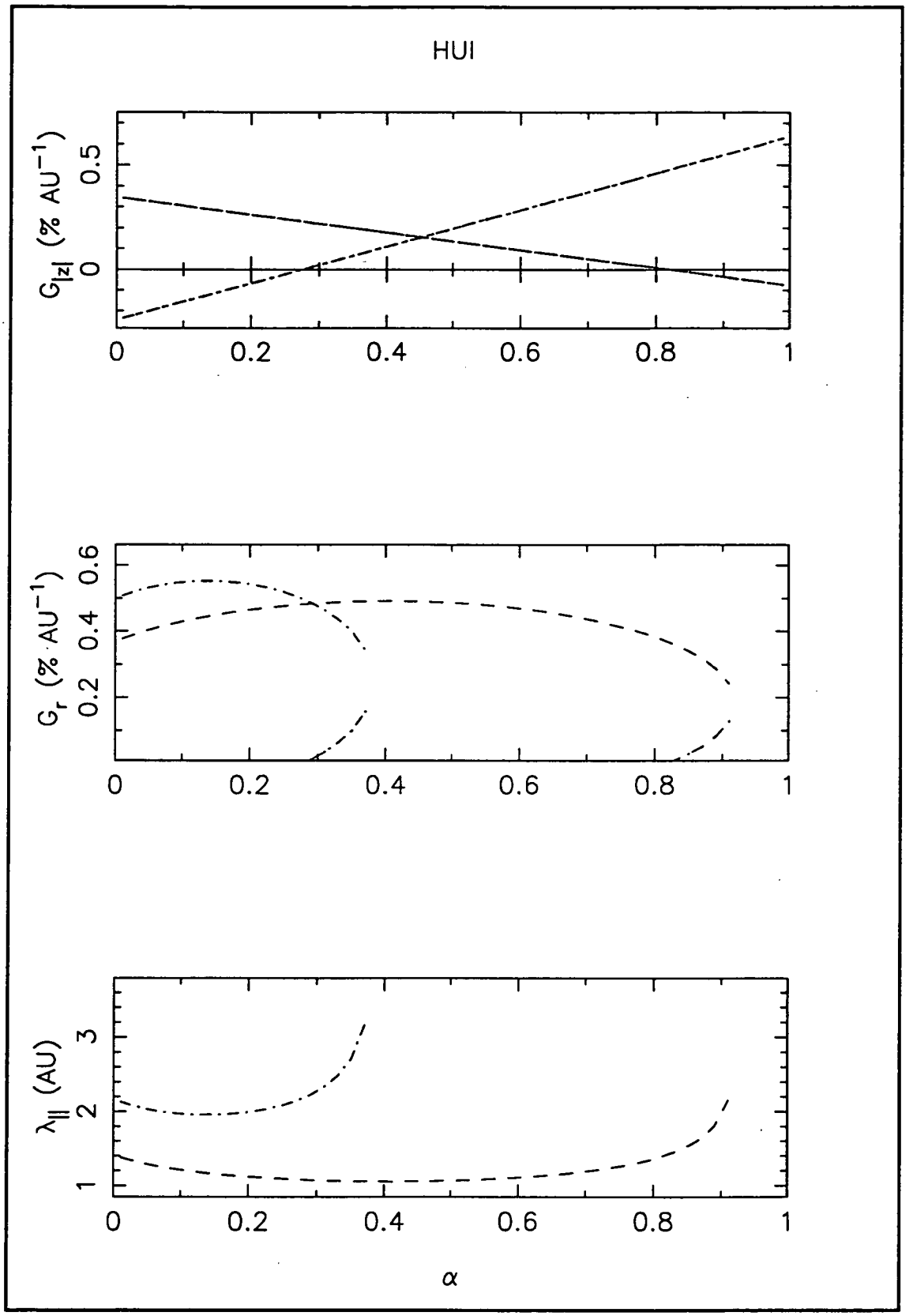

Hobart underground (inclined) muon telescope. Median rigidity is 195 GV.

APPENDIX 9

PUBLICATIONS

Publications which appeared in journals and conference proceedings while undertaking this degree are listed below.

Hall, D. L., J. E. Humble and M. L. Duldig, A comparitive study of solar modulation processes as recorded by southern latitude cosmic ray telescopes, *ANARE Research Notes, Australian Antarctic Division, 88*, 264-278, 1992.

Hall, D. L., J. E. Humble and M. L. Duldig, New measurements of the upper limiting rigidity to the solar diurnal variation, *Proc. Int. Conf. Cosmic Ray 23rd, 3*, 648-651, 1993.

Hall, D. L., J. E. Humble and M. L. Duldig, Radial and latitudinal density gradients in cosmic-rays derived from the solar diurnal variation, *Proc. Int. Conf. Cosmic Ray 23rd, 3*, 679-682, 1993

Hall, D. L., J. E. Humble and M. L. Duldig, Speculation on the magnetic polarity dependence of the upper cutoff rigidity to the solar diurnal anisotropy, *Proc. Int. Conf. Cosmic Ray 23rd, 3*, 660-662, 1993.

Baker, C. P., D. L. Hall, J. E. Humble and M. L. Duldig, North-South anisotropy and the radial gradient of cosmic-rays at 1 AU: 1982–1985, *Proc. Int. Conf. Cosmic Ray 23rd, 3*, 675–679, 1993.

Baker, C. P., D. L. Hall, J. E. Humble and M. L. Duldig, Atmospheric correction analysis for the Mawson muon telescopes, *Proc. Int. Conf. Cosmic Ray 23rd, 3*, 753–756, 1993.

Hall, D. L., J. E. Humble and M. L. Duldig, Modulation of high energy cosmic-rays in the heliosphere, *J. Geophys. Res., 99* (11), 1443-1457, 1994.

Hall, D. L., J. E. Humble and M. L. Duldig, Radial and latitudinal density gradients in galactic cosmic rays, *Proc. Astron. Soc. Aust., 11(2)*, 170-174, 1994.

Hall, D. L., M. L. Duldig and J. E. Humble, The north-south anisotropy and the radial density gradient of galactic cosmic rays at 1 A.U, *Proc. Astron. Soc. Aust.*, submitted.

Hall, D. L., M. L. Duldig and J. E. Humble The mean-free path of galactic cosmic rays at 1 A.U., *Proc. Astron. Soc. Aust.*, submitted.

Hall, D. L., M. L. Duldig and J. E. Humble, Asymmetric heliospheric modulation of a galactic anisotropy, *Proc. Int. Conf. Cosmic Ray 24th*, submitted.

Hall, D.L., M. L. Duldig and J. E. Humble, The mean-free path of galactic cosmic rays at 1 A.U., *Proc. Int. Conf. Cosmic Ray 24th,* submitted.

Bieber, J. W., P. Evenson, J. E. Humble, M. L. Duldig and D. L. Hall, Neutron monitor survey of the Southern Ocean, *Proc. Int. Conf. Cosmic Ray 24th,* submitted.